

DIGITAL COMMUNICATION

Second Edition

Edward A. Lee
University of California at Berkeley

David G. Messerschmitt
University of California at Berkeley



Kluwer Academic Publishers
Boston/Dordrecht/London

Distributors for North America:

Kluwer Academic Publishers
101 Philip Drive
Assinippi Park
Norwell, Massachusetts 02061 USA

Distributors for all other countries:

Kluwer Academic Publishers Group
Distribution Centre
Post Office Box 322
3300 AH Dordrecht, THE NETHERLANDS

Library of Congress Cataloging-in-Publication Data

Lee, Edward A., 1957-

Digital communication / Edward A. Lee and David G. Messerschmitt.

-- 2nd ed.

p. cm.

Includes bibliographical references and index.

ISBN 0-7923-9391-0 (acid-free paper)

I. Digital communications. II. Messerschmitt, David G.

II. Title.

TK5103.7.L44 1994

521.382--dc20

93-26197

CIP

Copyright © 1994 by Kluwer Academic Publishers. Fourth Printing 1998.

All rights reserved. No part of this publication may be reproduced, stored in a retrieval system or transmitted in any form or by any means, mechanical, photo-copying, recording, or otherwise, without the prior written permission of the publisher, Kluwer Academic Publishers, 101 Philip Drive, Assinippi Park, Norwell, Massachusetts 02061.

Printed on acid-free paper.

Printed in the United States of America

**To our parents,
and to Dody, Laura, and Rhonda**

CONTENTS

PREFACE
NOTES TO THE INSTRUCTOR

PART I: THE BASICS

1	INTRODUCTION	1
1.1	APPLICATIONS OF DIGITAL COMMUNICATION	2
1.2	DIGITAL vs. ANALOG COMMUNICATIONS	5
1.3	PLAN OF THE BOOK	7
1.4	FURTHER READING	8
2	DETERMINISTIC SIGNAL PROCESSING	11
2.1	SIGNALS	11
2.2	LTI SYSTEMS AND FOURIER TRANSFORMS	13
2.3	THE NYQUIST SAMPLING THEOREM	15
2.4	PASSBAND SIGNALS and MODULATION	17
2.5	Z TRANSFORMS AND RATIONAL TRANSFER FUNCTIONS	21
2.6	SIGNAL SPACE REPRESENTATIONS	31
2.7	FURTHER READING	39
2-A	SUMMARY OF FOURIER TRANSFORM PROPERTIES	39
2-B	SPECTRAL FACTORIZATION	41
3	STOCHASTIC SIGNAL PROCESSING	48
3.1	RANDOM VARIABLES	48
3.2	RANDOM PROCESSES	57
3.3	MARKOV CHAINS	68
3.4	THE POISSON PROCESS AND QUEUEING	75
3.5	FURTHER READING	85

3-A	POWER SPECTRUM OF A CYCLOSTATIONARY PROCESS	86
3-B	POWER SPECTRUM OF A MARKOV CHAIN	87
3-C	DERIVATION OF POISSON PROCESS	90
3-D	MOMENT GENERATING FUNCTION OF SHOT NOISE	91

4 LIMITS OF COMMUNICATION 97

4.1	JUST ENOUGH INFORMATION ABOUT ENTROPY	99
4.2	CAPACITY OF DISCRETE-TIME CHANNELS	102
4.3	FURTHER READING	110
4-A	ASYMPTOTIC EQUIPARTITION THEOREM	110

5 PHYSICAL MEDIA AND CHANNELS 115

5.1	COMPOSITE CHANNELS	116
5.2	TRANSMISSION LINES	119
5.3	OPTICAL FIBER	127
5.4	MICROWAVE RADIO	142
5.5	TELEPHONE CHANNELS	160
5.6	MAGNETIC RECORDING CHANNELS	167
5.7	FURTHER READING	171

PART II: MODULATION AND DETECTION

6 MODULATION 178

6.1	AN OVERVIEW OF BASIC PAM TECHNIQUES	179
6.2	PULSE SHAPES	187
6.3	BASEBAND PAM	191
6.4	PASSBAND PAM	199
6.5	ALPHABET DESIGN	213
6.6	THE MATCHED FILTER — ISOLATED PULSE CASE	224
6.7	SPREAD SPECTRUM	229
6.8	ORTHOGONAL MULTIPULSE MODULATION	230
6.9	COMBINED PAM AND MULTIPULSE MODULATION	249
6.10	OPTICAL FIBER RECEPTION	261
6.11	MAGNETIC RECORDING	262
6.12	FURTHER READING	263
6-A	MODULATING RANDOM PROCESSES	263
6-B	THE GENERALIZED NYQUIST CRITERION	266

7 SIGNAL and RECEIVER DESIGN 279

- 7.1 SIGNAL MODEL 282
- 7.2 SPECIFIC MODULATION TECHNIQUES 286
- 7.3 PAM WITH INTERSYMBOL INTERFERENCE 294
- 7.4 BANDWIDTH and SIGNAL DIMENSIONALITY 304
- 7.5 FURTHER READING 307

8 NOISE 311

- 8.1 COMPLEX-VALUED GAUSSIAN PROCESSES 311
- 8.2 FUNDAMENTAL RESULTS 316
- 8.3 PERFORMANCE of PAM 320
- 8.4 PERFORMANCE of MINIMUM-DISTANCE RECEIVERS 329
- 8.5 PAM with ISI 334
- 8.6 SPREAD SPECTRUM 337
- 8.7 CAPACITY AND MODULATION 344
- 8.8 QUANTUM NOISE in OPTICAL SYSTEMS 360
- 8.9 FURTHER READING 371

9 DETECTION 378

- 9.1 DETECTION OF A SINGLE REAL-VALUED SYMBOL 380
- 9.2 DETECTION OF A SIGNAL VECTOR 385
- 9.3 KNOWN SIGNALS IN GAUSSIAN NOISE 390
- 9.4 OPTIMAL INCOHERENT DETECTION 402
- 9.5 OPTIMAL DETECTORS for PAM WITH ISI 406
- 9.6 SEQUENCE DETECTION: THE VITERBI ALGORITHM 409
- 9.7 SHOT NOISE SIGNAL WITH KNOWN INTENSITY 424
- 9.8 FURTHER READING 427
 - 9-A KARHUNEN-LOÈVE EXPANSION 428
 - 9-B GENERAL ML AND MAP SEQUENCE DETECTORS 430
 - 9-C BIT ERROR PROBABILITY FOR SEQUENCE DETECTORS 432

10 EQUALIZATION 442

- 10.1 OPTIMAL ZERO-FORCING EQUALIZATION 445
- 10.2 GENERALIZED EQUALIZATION METHODS 464
- 10.3 FRACTIONALLY SPACED EQUALIZER 482
- 10.4 TRANSVERSAL FILTER EQUALIZERS 486
- 10.5 ISI and CHANNEL CAPACITY 487
- 10.6 FURTHER READING 511
 - 10-A DFE ERROR PROPAGATION 511

11 ADAPTIVE EQUALIZATION **517**

11.1	CONSTRAINED-COMPLEXITY EQUALIZERS	519
11.2	ADAPTIVE LINEAR EQUALIZER	532
11.3	ADAPTIVE DFE	541
11.4	FRACTIONALLY SPACED EQUALIZER	543
11.5	PASSBAND EQUALIZATION	546
11.6	FURTHER READING	549
11-A	SG ALGORITHM ERROR VECTOR NORM	549

PART III: CODING

12 SPECTRUM CONTROL **555**

12.1	GOALS OF LINE CODES	556
12.2	LINE CODE OPTIONS	558
12.3	FILTERING FOR SPECTRUM CONTROL	573
12.4	CONTINUOUS-PHASE MODULATION	589
12.5	SCRAMBLING	591
12.6	FURTHER READING	597
12-A	MAXIMAL-LENGTH FEEDBACK SHIFT REGISTERS	598

13 ERROR CONTROL **609**

13.1	BLOCK CODES	613
13.2	CONVOLUTIONAL CODES	626
13.3	HISTORICAL NOTES AND FURTHER READING	636
13-A	LINEARITY OF CODES	637
13-B	PATH ENUMERATORS	642

14 SIGNAL-SPACE CODING **650**

14.1	MULTIDIMENSIONAL SIGNAL CONSTELLATIONS	652
14.2	TRELLIS CODES	668
14.3	COSET CODES	684
14.4	SIGNAL-SPACE CODING AND ISI	688
14.5	FURTHER READING	694

PART IV: SYNCHRONIZATION

15 PHASE-LOCKED LOOPS 700

- 15.1 IDEAL CONTINUOUS-TIME PLL 702
- 15.2 DISCRETE-TIME PLLs 709
- 15.3 PHASE DETECTORS 713
- 15.4 VARIATIONS ON A THEME: VCOS 718
- 15.5 FURTHER READING 720

16 CARRIER RECOVERY 725

- 16.1 DECISION-DIRECTED CARRIER RECOVERY 726
- 16.2 POWER OF N CARRIER RECOVERY 733
- 16.3 FURTHER READING 734

17 TIMING RECOVERY 737

- 17.1 TIMING RECOVERY PERFORMANCE 739
- 17.2 SPECTRAL-LINE METHODS 741
- 17.3 MMSE TIMING RECOVERY AND APPROXIMATIONS 748
- 17.4 BAUD-RATE TIMING RECOVERY 754
- 17.5 ACCUMULATION OF TIMING JITTER 756
- 17.6 FURTHER READING 759
- 17-A THE POISSON SUM FORMULA 759
- 17-B DISCRETE-TIME DERIVATIVE 760

PART V: MULTIPLE ACCESS

18 MULTIPLE ACCESS ALTERNATIVES 765

- 18.1 MEDIUM TOPOLOGY FOR MULTIPLE ACCESS 767
- 18.2 MULTIPLE ACCESS BY TIME DIVISION 770
- 18.3 MULTIPLE ACCESS BY FREQUENCY DIVISION 787
- 18.4 MULTIPLE ACCESS BY CODE DIVISION 789
- 18.5 THE CELLULAR CONCEPT 792

19 ECHO CANCELLATION

797

19.1	PRINCIPLE OF THE ECHO CANCELER	798
19.2	BASEBAND CHANNEL	801
19.3	PASSBAND CHANNEL	804
19.4	ADAPTATION	809
19.5	FAR-END ECHO	815
19.6	FURTHER READING	818
19-A	REAL-ERROR CANCELER CONVERGENCE	819

EXERCISE SOLUTIONS 825

PERMUTED INDEX 865

PREFACE

This book concerns digital communication. Specifically, we treat the transport of bit streams from one geographical location to another over various physical media, such as wire pairs, coaxial cable, optical fiber, and radio waves. Further, we cover the multiple access and synchronization issues relevant to constructing communication networks that simultaneously transport bit streams from many users. The material in this book is thus directly relevant to the design of a multitude of digital communication systems, including for example local and metropolitan area data networks, voice and video telephony systems, digital CATV distribution, digital cellular and radio systems, the narrowband and broadband integrated services digital network (ISDN), computer communication systems, voiceband data modems, and satellite communication systems. We extract the common principles underlying these and other applications and present them in a unified framework.

This book is intended for *designers* and *would-be designers* of digital communication systems. To limit the scope to manageable proportions we have had to be selective in the topics covered and in the depth of coverage. In the case of advanced information, coding, and detection theory, for example, we have not tried to duplicate the in-depth coverage of many advanced textbooks, but rather have tried to cover those aspects directly relevant to the design of digital communication systems. For example, in our view it would be unfortunate to defer many of the insights of information theory to an advanced course on that topic, since the bounds they provide are directly relevant to the design of systems. Thus, we discuss the channel capacity results of information theory, as well as elementary derivations and justification of those results, without getting into the detail or rigor that the students will encounter in an advanced course on information theory. As another example, we restrict our coverage of detection theory to that portion especially relevant to the design of digital communication systems, such as the detection of known signals with additive Gaussian or quantum noise or after transmission over a binary-symmetric channel.

Our emphasis on topics important to designers leads us to more detailed treatment of some topics than is traditional in academic textbooks, for example in our coverage of synchronization. We devote several chapters to synchronization, including PLL's, timing recovery, and carrier recovery. Another example of a non-traditional topic is a description of the properties of the most important communication media, including radio, cable, and fiber. We then relate the modulation, detection, and coding techniques back to these properties. The book is also modern in its treatment of signal-space and trellis coding.

In the Second Edition, we have both tried to improve on some of the existing material, as well as add new material. Two major topics that we have concentrated on are the combination of coding with intersymbol interference, and fading channels and wireless communication. Both of these topics have been very active both in the literature and in commercial application since the First Edition. In terms of improving on the old development, we have completely rewritten Chapters 6-8 of the First Edition, turning them into Chapters 6-10 in the Second Edition. In addressing a perceived shortcoming of the First Edition, we have included solutions to the exercises at the end of the book. What follows is a chapter-by-chapter summary of the changes.

Chapter 2. We added a lot of new material on rational transfer functions, including spectral factorizations. Later, when equalization is covered, we concentrate on the rational case, since many concrete statements can be made with mathematical ease. Also added is a derivation of the basic modulation and demodulation, which is later used in Chapter 6.

Chapter 3. A small amount of material on innovations and linear prediction theory has been added. Linear prediction later plays a major role in Chapter 10 in the context of decision-feedback equalization.

Chapter 4. The capacity of the Gaussian vector channel is derived.

Chapter 5. The description of fading channels has been significantly upgraded, including derivation of standard channel models for narrowband and wideband Rayleigh fading channels. A short description of optical amplifiers has also been added.

Chapter 6. The probability of error derivations has been deferred to Chapter 8, and rather this chapter concentrates on signal-to-noise ratio derivations. Some topics of recent importance have been added, including spread spectrum (preceded by a derivation of the matched filter), code-division multiple access, and multicarrier modulation. A new generalized Nyquist criterion, that extends the Nyquist criterion to various types of orthogonal signaling, is derived and used to compare spectral efficiencies of the modulation techniques.

Chapter 7. This is a completely new chapter that follows a new approach for texts on digital communication. A simple signal space minimum-distance criterion is defined, and used to derive receiver structures for a variety of modulation techniques. By avoiding bringing in noise and optimality considerations, this chapter is able to derive all the standard receiver structures very quickly, and compare them. Surprisingly, this includes even the "whitened matched filter", normally derived from noise whitening considerations, but derived here solely from signal space considerations.

Chapter 8. This new chapter analyzes the probability of error of various receiver structures, including the receiver designs derived in Chapter 6 on the basis of intuitive and SNR considerations, as well as the minimum-distance receiver designs of Chapter 7. We begin by specifically treating complex-valued Gaussian noise, which is the subject of a lot of misconceptions in many textbooks. Many books, including our First Edition, seem to imply that complex Gaussian processes are characterized by their power spectrum, are stationary if they are wide-sense stationary, etc., statements that are all incorrect or incomplete. We attempt to clear this up by doing a more

complete treatment, and defining a desirable property called "circular symmetry" which guarantees the nice properties and which seems to be widely satisfied in digital communication systems. This chapter then proceeds to compare the modulation techniques by first deriving the capacity of an ideal white Gaussian noise channel, and then comparing the performance of each modulation technique to the capacity ideal. The particular approach used is to define a rate-normalized SNR and a "SNR gap to capacity", an approach used recently by Forney and Eyuboglu.

Chapter 9. This chapter, which is a revision of Chapter 7 of the First Edition, derives the optimal receiver structures based on probability of error criterion (ML and MAP). Basicly, this chapter justifies the minimum-distance receiver designs already derived earlier in Chapter 7, and further extends them to colored noise. Rather than rely on whitening filter arguments as in the First Edition, we have done a full Karhunen-Loeve expansion approach. Chapter 10. This is a major revision of Chapter 8 of the First Edition, which now considers only intersymbol interference and equalization, rather than also doing receiver optimization as before. We start by finding optimal equalizer structures, which leads to matched-filter front ends. Then in contrast to the First Edition, as well as other texts, we remove the assumption of a matched filter front end, and re-optimize the equalizers. Our motivation here is based on two related facts: Matched filtering is often impossible to implement theoretically for non-minimum phase channels, and is seldom used in practice for unknown or time-varying channels. In our view, the traditional treatments of optimal equalization based on matched filtering obscure many practically-important issues, such as the quite different characteristics of minimum-phase and non-minimum phase channels. Our treatment maintains relative mathematical simplicity by concentrating on rational spectra. Also added to this chapter is substantial treatment of the capacity of channels with ISI (based on water pouring), and the effect of ISI on capacity. We also generalize the rate-normalized SNR to channels with ISI, and characterize thereby the "SNR gap to capacity" for different equalization techniques, establishing "Price's results" that the gap to capacity is often independent of the ISI when decision-feedback equalization is used.

In addition to those folks mentioned in the Preface to the First Edition, we owe a debt of gratitude to a number of additional friends and colleagues who assisted us by reading and commenting on selected Chapters in the second edition, or by providing useful reference material.

This book is suitable as a first-year graduate textbook, and should also be of interest to many professionals in industry. We have attempted to make the book more attractive to both audiences through the inclusion of many practical examples and a practical flavor in the choice of topics. In addition, we have increased the readability by relegating many of the more detailed derivations to appendices and exercises, both of which are included in the book. The inclusion of exercise solutions at the end of the book is new to the Second Edition. A solutions manual for the problems is available from the publisher.

We owe a debt of gratitude to a number of our friends and colleagues who have assisted us by reading and commenting on selected chapters. For the first edition,

these include Bob Aaron, Jeff Bier, John Barry, Graham Brand, Thomas Chen, Paul Frieburg, Biswa Ghosh, Vijay Madisetti, Teresa Meng, Sara Miller, Rhonda Righter, Ruth Schaefer, Gil Sih, Mehmet Soyuer, Aram Thomasian, Ho-Ping Tseng, and Greg Uehara, as well as the students in EECS 225 in the Spring of 1987. The assistance of several anonymous reviewers in making sure all the essential topics are covered is gratefully acknowledged. The diligent and artistic effort of Pei Ku in generating many of the figures is appreciated. For the Second Edition, additional colleagues provided proofreading assistance, including Shuvra Bhattacharyya, Shih-fu Chang, Wan-the Chang, Soonhoi Ha, Paul Haskell, Chih-Tsung Huang, Joseph Kahn, William Li, Jean-Paul Linnartz, Vijay Madisetti, Praveen Murthy, Sun-Inn Shih, S. Sriram, and Louis Yun, as well as the students in EECS 224 in the Fall of 1992. Special thanks goes to G.David Forney, Jr. and John Barry, who each devoted many hours to proofreading the manuscript and suggesting added material or improved derivations. While many of these colleagues have pointed out many errors and omissions, any remaining errors are of course the full responsibility of the authors.

We hope the result is a readable and useful book, and always appreciate comments and suggestions from the readers.

*Edward A. Lee
David G. Messerschmitt*

Berkeley, California
June 12, 1993

NOTES TO THE INSTRUCTOR

This book can be used as a textbook for advanced undergraduates, or for a first course in digital communication for graduate students. We presume a working knowledge of transforms, linear systems, and random processes, and review these topics in chapters 2 and 3 at a depth suitable only for establishing notation. This treatment also serves to delimit the background assumed in the remainder of the book. We include a more detailed treatment of basic topics important to digital communication but which may not be familiar to a first-year graduate student, including signal space (chapter 2), Markov chains and their analysis (chapter 3), Poisson processes and shot noise (chapter 3), the basic boundaries of communication from information theory (chapter 4), and maximum likelihood detection and the Viterbi algorithm (chapter 9). These treatments are self-contained and assume only the basic background mentioned earlier. These basic topics can be covered at the beginning of the course, or can wait until the first time they are used. Our own preference is the latter, since the immediate application of the techniques serves as useful reinforcement.

The core of book is the treatment of communications media (chapter 5), modulation (chapter 6), detection and equalization (chapters 7 through 11), coding (chapters 12 through 14), and synchronization (chapters 15 through 17). These topics are covered in considerable depth. After completing a course based on this book, students should be highly motivated to take advanced courses in information theory, algebraic coding, detection and estimation theory, and communication networks, and will have a prior appreciation of the utility of these topics.

There is sufficient material in this book for two semesters of instruction, although it can easily be used for a single-semester course by selectively covering topics. At Berkeley we use this book for a one-semester graduate course that has as prerequisites undergraduate courses in systems and transforms and probability and random processes. We do not presume any prior exposure to signal space, Markov chains, or the Poisson process. In this course we rely on the students to review Chapters 1 through 4 themselves, and we cover Chapters 5 through 10 and Chapter 13 and 14 in lecture. Chapter 11 is skipped because adaptive filtering techniques are covered in another signal processing course.

1

INTRODUCTION

*But let your communication be, Yea, yea; Nay, nay:
for whatever is more than these, cometh of evil.*

— The Gospel According to St. Matthew (5:37)

Digital transmission of information has sufficiently overwhelming advantages that it increasingly dominates communication systems. In computer-to-computer communication, the information to be transported is inherently digital, so digital transmission is the only practical alternative. But computer communication is still a small fraction of all digital communications. A much larger fraction is devoted to transmitting inherently analog signals, particularly speech and images. Such signals can be (and traditionally have been) transmitted in analog form. Why would they be transmitted digitally? Not so long ago, digital transmission of voice and video was considered wasteful of bandwidth, and the cost of converting from analog to digital and back was of concern. But four things have happened to change all that:

- The encoding of analog signals in digital form has benefited from advances in compression algorithms, which reduce dramatically the bit rate required to represent a voice or video signal with high subjective quality.

- Signal processing and coding techniques have dramatically increased the bit rate that can be supported through a given physical channel.
- Integrated circuits have greatly reduced the cost of realizing complex signal processing and coding functions inherent in digital transmission.
- Optical fiber has reduced the cost of transmitting high bit rates over long distances.

The result of these developments is a complete turnaround in thinking. Today the greatest impetus for digital transmission is often the *reduced* bandwidth, or equivalently the greater overall system capacity that can be achieved with digital transmission. For example, both cellular telephone and cable television are in the process of converting to digital transmission, in part on the basis of the greater system capacity. In fact, today virtually all communication is either already digital, in the process of being converted to digital, or under consideration for conversion.

An essential element in this digital revolution is the transmission of a higher and higher bit rates over a given physical transmission medium. That is the subject of this book.

1.1. APPLICATIONS OF DIGITAL COMMUNICATION

Digital communication is used for signals that are inherently analog and continuous-time, such as speech and images, and signals that are inherently digital, such as text files. The demands placed on a communication system are different in each case. Furthermore, modern communication networks provide a mixture of services, and hence must take into account the demands of each.

1.1.1. Digital Transmission of Speech and Video

It is common in modern practice to convert analog continuous-time signals to digital form for transmission. A technique commonly used for transmission of speech and video is *pulse code modulation (PCM)*, shown in Figure 1-1. The continuous-time speech or video signal is first *sampled* at a rate f_s Hz (or samples/sec), which must be greater than twice the highest frequency component in the signal (see Section

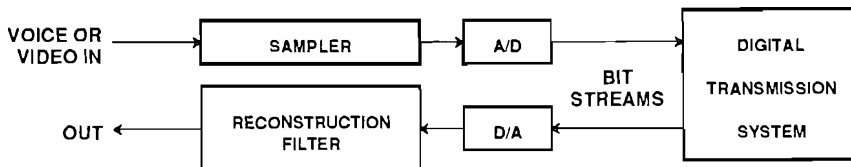


Figure 1-1. A digital transmission system used for PCM transmission.

2.3). Often this sampling operation is preceded by a lowpass filter, not shown, which ensures that the signal is properly bandlimited. Each sample is then converted to an n -bit binary word by an analog-to-digital converter (A/D). The output is a bit stream with a bit rate of nf_s bits per sec (often written bps or b/s). The bit stream is then transmitted over a digital transmission system, and the voice or video signal is reconstructed with a digital-to-analog converter (D/A) and a reconstruction low-pass filter. PCM was patented in France by Reeves in the late 1930's, and was first used during World War II.

Example 1-1.

The first commercial PCM system was *T1-carrier*, shown in Figure 1-2. The design was completed at Bell Laboratories in 1962. It is still widely used for relatively short-distance transmission between central offices in metropolitan areas. The T1-carrier system transmits a bit stream at 1.544 Mb/s (1.544×10^6 b/s) over two wire-pairs, one for each direction of transmission. Of this capacity, 1.536 Mb/s is available for the transmission of 24 voice channels with the rest used for supervisory functions (Chapter 18). Each voice channel is sampled 8000 times per second and is quantized to eight bits per sample, for a total bit rate of 64 kb/s (64×10^3 b/s) per voice channel. The channel bank also *multiplexes* or combines the 24 bit streams together into the 1.536 Mb/s stream. \square

The internal implementation of such a digital transmission system can be intricate, and is the subject of this book. However, from the viewpoint of voice and video transmission, the digital transmission system is simple in that it can be fully characterized by only four parameters:

- the *bit rate*,
- the *propagation and processing delay*,
- the *probability of error* (Chapter 8), which indicates how likely the bits arriving at the destination are to differ from the transmitted bits, and
- the *timing jitter* in the arriving bit stream (Chapter 17).

Both bit errors and timing jitter can cause some degradation in the quality of the recovered voice or video signal, and excessive delay can impair a conversation, so the designer of the digital communication system must control these impairments. They are, however, far less complicated than the types of distortion commonly encountered

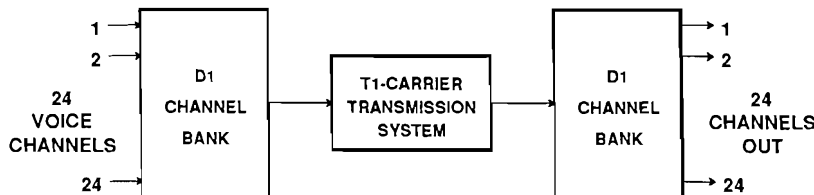


Figure 1-2. The T1-carrier transmission system with associated D1 channel bank for sampling, A/D conversion, and multiplexing.

in analog transmission.

Another application of digital communication techniques is *storage systems* using *magnetic* or *optical media*. In this case the objective is not transmission "from here to there" but rather "from now to then." These media have unique impairments, different from those in transmission media, but many of the same basic techniques apply.

1.1.2. Computer Communication

The data generated by computers for transmission to other computers or terminals does not require the conversion shown in Figure 1-1. For computer communication it is common to use the term *data transmission* rather than *digital transmission*. But we should emphasize that the same transmission system can be used for PCM transmission and for data transmission. In fact, a major goal of many current design activities is to combine voice, video, and data within an *integrated* transmission environment (Chapter 22). For this reason, in this book we lump the two categories under the common heading *digital communication*.

A digital communication system used for data transmission is characterized by its bit rate, delay, error rate, and jitter, just like a system used for PCM transmission. The relative importance of these impairments is different, however. Data transmission is usually much more sensitive to bit errors than speech and video signals, but on the other hand is usually unaffected by jitter. Also, data often requires only sporadic rather than continuous communication. For example, a user sitting at a terminal may desire that the individual characters be transmitted at 9.6 kb/s, but the infrequently generated characters may require an actual average bit rate of only 50 b/s. We can characterize this property more formally as a big difference between peak and average bit rates. Special techniques have therefore been developed for data (Chapter 21). These often introduce additional impairments like delay variation with time and lost bits.

1.1.3. Telecommunication Networks

Practical applications require more than a single point-to-point digital communication link. A *digital communication network* simultaneously connects many users to one another, and often includes *switching*, which allows the users to initiate connections to specific other users. For historical reasons, networks designed for these different purposes are often assigned different terminology: a *telephone* or *telephony network* is designed to handle PCM transmission, and a *data network* or *computer network* is designed to transmit data. However, the terminology is rapidly becoming obsolete through the introduction of networks designed for all sources. Such networks we will call *telecommunication networks*. A good example is the *integrated services digital network (ISDN)* that is currently being deployed worldwide.

Telecommunication networks are often classified according to geographical extent. *Local area networks* are designed to communicate at very high bit rates over a small geographical area (on the order of one km in extent). Most existing local area networks are designed primarily for computer communication. *Metropolitan area networks* are currently being conceptualized as a wider area counterpart to the local

area network, and can cover an area extending approximately 50 kilometers using optical fiber. *Wide area networks*, encompassing as much as a country or the world, use a combination of cable, terrestrial microwave radio, underwater cable and fiber, and satellite, to cover large distances. The world-wide telephony network is an example of such a network. Another example is the *internet*, which is used primarily for computer communications.

Networks that transport multiple bit streams also include some form of switching. Switching enables reconfiguration of point-to-point connections in the network, and usually takes one of two basic forms — *circuit switching* or *packet switching* (Chapter 18). In circuit switching, the network connects a constant-rate bit stream to the destination for a relatively long period of time (of the order of minutes or longer). This mode arose in the context of voice networks, where the circuit is formed for the duration of one telephone call. In packet switching, the data is encapsulated into relatively short bundles of bits called packets, and a destination address is appended. The packet can then be routed through the network. One advantage of packet switching is that the bit stream between source and destination can have a variable bit rate — this is accomplished by generating only the needed packets. This leads to greater efficiency for sources of data that have a large ratio of peak to average bit rate.

1.2. DIGITAL vs. ANALOG COMMUNICATIONS

For data communication, there is no practical alternative to digital transmission. For voice and video signals, however, there are important advantages and disadvantages to digital transmission.

Interface Abstraction

The relatively simple characterization of a digital communication system is an important advantage over analog communication, where there are many more ways in which a transmission can be degraded. For example, the signal-to-noise ratio may be poor, or the signal may suffer second or third order intermodulation distortion, or crosstalk from one user to another, or the system may clip the input signal. By contrast a digital communication system has only three parameters: bit rate, probability of error, and timing jitter. The impairments of the physical medium, which may be quite severe, are largely hidden from the user. Also hidden are the implementation details of the digital communication system itself. This property we call the *interface abstraction* of the transmission system. The power of this abstraction was perhaps first appreciated by Claude Shannon in his classic 1948 paper which started the field of information theory (Chapter 4). He showed that theoretically there is nothing lost by defining the interface between the signal to be transmitted and the transmission system to be a bit stream, regardless of whether the signal is analog or digital.

The Regenerative Effect

Consider the problem of transporting a bit stream over a long distance. The degradation of an uninterrupted physical medium, such as a cable or optical fiber, may be unacceptable. The digital solution is to place *regenerative repeaters* at periodic intervals in the physical medium, as shown in Figure 1-3. Each of these repeaters includes a receiver, which detects the bit stream just as is done at the eventual destination, and a re-transmitter similar to the one at the origination. In the absence of transmission bit errors, the bit stream that is regenerated in this repeater is *identical* to the one that was originally transmitted. Any effects due to noise and distortion on the physical medium have been *completely removed* by the regenerative repeater (except insofar as they cause occasional bit errors). Contrast this to analog transmission, where the equivalent repeaters consist basically of amplifiers, and the noise and distortion accumulates as the distance increases.

In practice, the digital communication system will introduce some errors in the detection of the bit stream. When the probability of error at each repeater is low, the total probability of error for m repeaters is approximately m times the probability of error for a single repeater. Assuming a maximum number of repeaters, we can derive from an overall probability of error objective a performance requirement for a single repeater. We can then meet that objective by adjusting the design of the repeater, the design of the signal, and the spacing between repeaters (closer spacing will result in a lower error rate for a given physical medium of transmission).

The same regenerative effect applies to the storage of signals. Consider for example the high quality possible with digital audio. Part of the reason for this is that each time the audio signal is copied onto a new medium (for example from a magnetic tape to a laser disk), the signal is regenerated, and degradations peculiar to the original medium are removed.

Economics

We have seen that digital communication has some powerful technical advantages. What are the relative *economics* of digital and analog communication? There is a price to be paid for the technical advantages. Without getting into detail, a qualitative comparison can be made as follows.

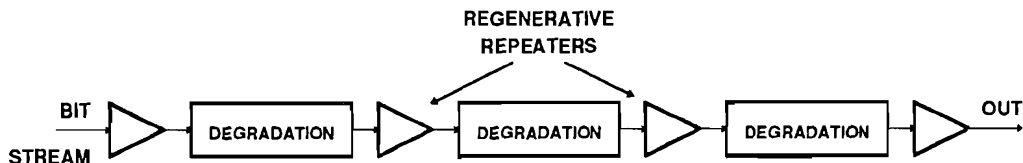


Figure 1-3. A chain of regenerative repeaters reduces the effect of cascaded degradations by regenerating the digital signal at intermediate points in the transmission.

- The multiplexing and switching of digital signals is much lower in cost than for analog signals. This is particularly true for multiplexing, because frequency-division multiplexing of analog signals requires complicated filters (Chapter 18).
- Some economical media, such as optical fiber and laser disks, are better suited to digital transmission than analog.
- Digital communication of analog waveforms such as voice and video requires an additional step of sampling and analog-to-digital conversion. The cost of this conversion was initially an impediment to the widespread use of digital communication, but with integrated circuit technology this cost is rapidly becoming insignificant, particularly for voiceband signals.
- Regenerative repeaters for digital communication are considerably more complicated than their analog counterparts (which are just amplifiers). However, the capacity of these systems is so large that this added cost is insignificant to individual users.
- With modern compression and transmission technology (the latter being the subject of this book), PCM transmission of analog signals can be accomplished with less bandwidth than analog transmission of the same signal. This characteristic is critical in radio transmission, because the radio spectrum is in short supply. It can also have important economic advantages for other media, such as the telephone subscriber loop and coaxial cable television.
- Digital communication raises complicated synchronization issues (Chapters 15-19) that are largely avoided in analog communication.

The bottom line is that it took a while, about 20 years, for digital communication to almost completely supplant its analog competitors, but that revolution is now nearly complete. This is a result of a combination of economic factors, technological advances, and demands for new services.

1.3. PLAN OF THE BOOK

This book concentrates on the techniques that are used to design a digital communication system starting with any of the common physical media. Our concern is thus with how to get a bit stream from one location to another, and not so much with how this bit stream is used. In the particular context of a computer network, this aspect of the system is called the *physical layer*. We also address the problems of multiple bit streams sharing a common medium, called *multiple-access*.

In Chapters 2-4 some basics required for the understanding of later material are covered. Many readers will have a prior background in many of these basics, in which case only a superficial reading to pick up notation is required. We have also covered some basic topics with which the reader may not be so familiar. These include spectral factorization of rational transfer functions (Chapter 2), signal space (Chapter 2), Markov chains and Poisson processes (Chapter 3), and information theoretic bounds (Chapter 4). The characteristics of the physical media commonly encountered are covered in Chapter 5.

Chapters 6-14 cover the theory of modulation, detection, and coding that is necessary to understand how a single bit stream is transported over a physical medium. The need for this theory arises because all physical media are analog and continuous-time in nature. It is ironic that much of the design of a digital communication system is inevitably related to the analog and continuous-time nature of the medium, even though this is not evident at the abstracted interface to the user.

The design of a digital communication system or network raises many difficult *synchronization* issues that are covered in Chapters 15-17. Often a large part of the effort in the design of a digital communication system involves phase-locked loops, timing, and carrier recovery.

A complete telecommunication network requires that many bit streams originating with many different users be transported simultaneously while sharing facilities and media. This leads to the important topic of *multiple access* of more than one user to a single physical medium for transmission. This is covered in Chapters 18-19.

1.4. FURTHER READING

There are a number of excellent books on digital communication. While these books have a somewhat different emphasis from this one, they provide very useful supplementary material. The books by Roden [1], Benedetto, Biglieri, and Castellani [2], and Gitlin, Hayes, and Weinstein [3] cover similar material to this one, perhaps with a bit less practical emphasis. The books by Blahut [4] and Bingham [5] are valued for their practical orientation. Two texts provide additional detail on topics in this book: the recent book by Proakis [6] is an excellent treatise on applied information theory and advanced topics such as coding, spread spectrum, and multipath channels; the book by Viterbi and Omura [7] gives a detailed treatment of source and channel coding as applied to digital communication, as does Biglieri, Divsalar, McLane, and Simon [8]. An excellent treatment of the statistical communication theory as applied to digital communication is given by Schwartz [9]. On the topics of modulation, equalization, and coding the book by Lucky, Salz, and Weldon is somewhat dated but still recommended reading [10]. The same applies to the book by Wozen-craft and Jacobs, which emphasizes principles of detection [11]. Books by Keiser and Strange [12] and Bellamy [13] give broad coverage of digital transmission at a descriptive level. Practical details of digital transmission can be found in a book published by AT&T Technologies [14], in the book by Bylanski and Ingram [15], and for the particular case of PCM encoding, in the book by Cattermole [16]. A couple of books expand on our brief description of digital switching, including McDonald [17] and Pearce [18]. For the information theory background that gives a solid theoretical foundation for digital communication, the books by Gallager [19], Cover and Thomas [20], Blahut [21], and McEliece [22] are recommended. Schwartz [23] and Bertsekas and Gallager [24] are recommended comprehensive texts on computer networks. There are also many elementary texts that cover both digital and analog communication, as well as the basic systems, transforms, and random process theory. Simulation techniques for communication systems are covered comprehensively in Jeruchim,

Balaban, Shanmugan [25].

PROBLEMS

- 1-1. For an A/D converter, define a signal-to-error ratio as the signal power divided by the quantization error power, expressed in dB. A uniform quantizer, which has equally-spaced thresholds, has two parameters: the number of bits n and the step size Δ .
 - (a) If we were to increase n by one, to $n+1$, for the same input signal, what would be the appropriate change to Δ ?
 - (b) Without doing a detailed analysis, what do you suppose would be the effect on signal-to-error ratio of increasing from n to $n+1$ bits/sample?
 - (c) What effect will this same change have on the bit rate?
 - (d) Using the prior results, what is the *form* of the relationship between signal-to-error ratio and the bit rate? (You may have unknown constants in your equation.)
- 1-2. An analog signal is transmitted using a PCM system. Discuss qualitatively the effects of bit errors on the recovered analog signal.
- 1-3. Discuss qualitatively the sources of delay that you would expect in a PCM system.
- 1-4. Suppose you have a source of data that outputs a bit stream with a bit rate that varies with time, but also has a peak or maximum bit rate. Describe qualitatively how you might transmit this bit stream over a link that provides a constant bit rate.

REFERENCES

1. M. S. Roden, *Digital And Data Communication Systems*, Prentice-Hall, Englewood Cliffs, N.J. (1982).
2. S. Benedetto, E. Biglieri, and V. Castellani, *Digital Transmission Theory*, Prentice-Hall, Inc., Englewood Cliffs, NJ (1987).
3. R. D. Gitlin, J. F. Hayes, and S. B. Weinstein, *Data Communications Principles*, Plenum Press, New York and London (1992).
4. R. E. Blahut, "Digital Transmission of Information," *Addison-Wesley*, (1990).
5. J. A. C. Bingham, *The Theory and Practice of Modem Design*, John Wiley & Sons, New York (1988).
6. J. G. Proakis, *Digital Communications, Second Edition*, McGraw-Hill Book Co., New York (1989).
7. A. J. Viterbi and J. K. Omura, *Principles of Digital Communication and Coding*, McGraw-Hill (1979).
8. E. Biglieri, D. Divsalar, P. J. McLane, and M. K. Simon, *Introduction to Trellis-Coded Modulation with Applications*, Macmillan, New York (1991).
9. M. Schwartz, *Information Transmission, Modulation, and Noise*, McGraw-Hill, New York (1980).
10. R. W. Lucky, J. Salz, and E. J. Weldon, Jr., *Principles of Data Communication*, McGraw-Hill Book Co., New York (1968).

11. J. M. Wozencraft and I. M. Jacobs, *Principles of Communication Engineering*, Wiley, New York (1965).
12. B. E. Keiser and E. Strange, *Digital Telephony and Network Integration*, Van Nostrand Reinhold, New York (1985).
13. J. Bellamy, *Digital Telephony*, John Wiley, New York (1982).
14. Bell Laboratories Members of Technical Staff, *Transmission Systems for Communications*, Western Electric Co., Winston-Salem N.C. (1970).
15. P. Bylanski and D. G. W. Ingram, *Digital Transmission Systems*, Peter Peregrinus Ltd., Stevenage England (1976).
16. K. W. Cattermole, *Principles of Pulse Code Modulation*, Iliffe Books Ltd., London England (1969).
17. J. C. McDonald, *Fundamentals of Digital Switching*, Plenum Press, New York (1983).
18. J. G. Pearce, *Telecommunications Switching*, Plenum, New York (1981).
19. R. Gallager, *Information Theory and Reliable Communication*, John Wiley and Sons, Inc., New York (1968).
20. T. M. Cover and J. A. Thomas, "Elements of Information Theory," Wiley, (1991).
21. R. E. Blahut, "Principles and Practice of Information Theory," Addison-Wesley, (1987).
22. R. J. McEliece, *The Theory of Information and Coding*, Addison Wesley Pub. Co. (1977).
23. M. Schwartz, *Telecommunication Networks: Protocols, Modeling, and Analysis*, Addison-Wesley, Reading, Mass. (1987).
24. D. Bertsekas and R. Gallager, "Data Networks," Prentice-Hall, (1987).
25. M. C. Jeruchim, P. Balaban, and K. S. Shanmugan, *Simulation of Communication Systems*, Plenum Press, New York (1992).

2

DETERMINISTIC SIGNAL PROCESSING

In this chapter we review some basic concepts in order to establish the notation used in the remainder of the book. In addition, we cover in more detail several specific topics that some readers may not be familiar with, including complex signals and systems, the convergence of bilateral Z-transforms, and signal space geometry. The latter allows simple geometric interpretation of many signal processing operations, and demonstrates relationships among many seemingly disparate topics.

2.1. SIGNALS

A *continuous-time signal* is a function $x(t)$ of the real valued variable t , usually denoting time. A *discrete-time signal* is a sequence $\{x_k\}$, where k usually indexes a discrete progression in time. Throughout this book we will see systems containing both continuous-time and discrete-time signals. Often a discrete-time signal results from *sampling* a continuous-time signal; this is written $x_k = x(kT)$, where T is the *sampling interval*, and $2\pi/T$ is the sampling frequency, in radians per second. The sampling operation can be represented as

$$x_k = x(kT) = \int_{-\infty}^{\infty} x(\tau) \delta(\tau - kT) d\tau, \quad (2.1)$$

where $\delta(\tau)$ is the *Dirac delta function* or *continuous-time impulse*. The discrete-time

signal x_k has a continuous-time *pulse amplitude modulation (PAM)* representation

$$\hat{x}(t) = \sum_{k=-\infty}^{\infty} x_k \delta(t - kT), \quad (2.2)$$

in terms of impulses.

A continuous-time signal can be constructed from a discrete-time signal as represented symbolically in Figure 2-1. A discrete-time input to a continuous-time system implies first the generation of the continuous-time impulse train in (2.2), and then its application to a continuous-time filter $F(j\omega)$, yielding

$$y(t) = \sum_{k=-\infty}^{\infty} x_k f(t - kT). \quad (2.3)$$

2.1.1. Complex-Valued Signals

In digital communication systems, complex-valued signals are often a convenient mathematical representation for a pair of real-valued signals. A complex-valued signal consists of a *real* signal and an *imaginary* signal, which may be visualized as two voltages induced across two resistors or two sequences of numbers.

Example 2-1.

A complex-valued signal we encounter frequently is the complex exponential,

$$\begin{aligned} x_k &= e^{-j\omega kT} = \cos(\omega kT) - j \sin(\omega kT), \\ x(t) &= e^{-j\omega t} = \cos(\omega t) - j \sin(\omega t). \end{aligned} \quad (2.4)$$

We consistently use j to represent $\sqrt{-1}$. \square

Complex-valued signals are processed just as real-valued signals are, except that the rules of complex arithmetic are followed.

Exercise 2-1.

Draw diagrams specifying the addition and multiplication of two complex-valued continuous-time signals in terms of real-valued additions and multiplications. \square

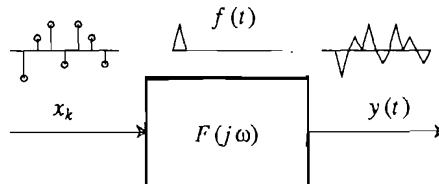


Figure 2-1. Construction of a continuous-time signal from a discrete-time signal. When we show a discrete-time input to a continuous-time system, we imply first the generation of the impulse train in (2.2). An example is shown above the system.

The real part of the signal $x(t)$ is written $\text{Re}\{x(t)\}$ and the imaginary part $\text{Im}\{x(t)\}$. In addition, we write the complex conjugate of a signal $x(t)$ as $x^*(t)$, and the squared modulus as $|x(t)|^2$. We don't use any special notation to distinguish real-valued from complex-valued signals because it will generally be clear from context. Complex signals will often be represented in block diagrams using double lines, as shown in Figure 2-2b.

2.1.2. Energy and Average Power

The energy of a signal $x(t)$ or $\{x_k\}$ is defined to be

$$\int_{-\infty}^{\infty} |x(t)|^2 dt , \quad \sum_{k=-\infty}^{\infty} |x_k|^2 . \quad (2.5)$$

The average power is

$$\lim_{\tau \rightarrow \infty} \frac{1}{2\tau} \int_{-\tau}^{+\tau} |x(t)|^2 dt , \quad \lim_{K \rightarrow \infty} \frac{1}{(2K+1)T} \sum_{k=-K}^{+K} |x_k|^2 . \quad (2.6)$$

2.2. LTI SYSTEMS AND FOURIER TRANSFORMS

The Fourier transform is valuable in the analysis of modulation systems and linear time-invariant systems. For the convenience of the reader, the properties of both discrete and continuous-time Fourier transforms are summarized in appendix 2-A. In this section we establish notation and review a few basic facts.

2.2.1. Linear Time Invariant (LTI) Systems

If a system *linear* and *time invariant* (LTI), then it is characterized by its pulse response h_k (for a discrete-time system) or $h(t)$ (for a continuous-time system). The output of the LTI system can be expressed in terms of the input and impulse response as a convolution; for the discrete-time case,

$$y_k = x_k * h_k = \sum_{m=-\infty}^{\infty} x_m h_{k-m} , \quad (2.7)$$

and the continuous-time case,

$$y(t) = x(t) * h(t) = \int_{-\infty}^{\infty} x(\tau) h(t - \tau) d\tau . \quad (2.8)$$

An LTI system is *real* if its impulse response is real-valued, and *complex* if its impulse response is complex-valued. A complex system can be represented, using the rules of complex arithmetic, as a set of four real systems, as shown in Figure 2-2.

Exercise 2-2.

Show that if a complex system has a real-valued input it can be implemented using two real

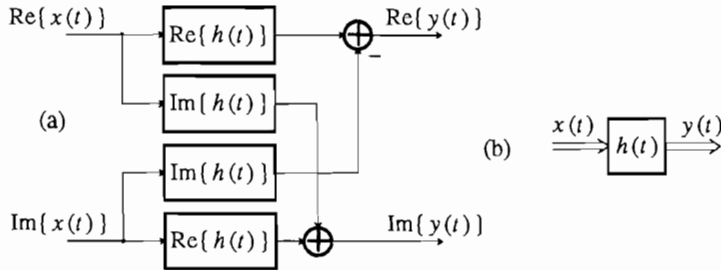


Figure 2-2. A complex-valued LTI system with a complex-valued input and output.

systems and sketch the configuration. Show that the same is true if a real system has a complex-valued input, and again sketch the configuration. \square

Exercise 2-3.

The notion of linearity extends to complex LTI systems. Demonstrate that if the four real systems required to implement a complex system are linear, then the resulting complex system is linear. It follows immediately that real-valued LTI systems are linear with respect to complex-valued inputs. \square

2.2.2. The Fourier Transform

The Fourier transform pair for a continuous-time signal $x(t)$ is

$$X(j\omega) = \int_{-\infty}^{\infty} x(t) e^{-j\omega t} dt, \quad x(t) = \frac{1}{2\pi} \int_{-\infty}^{\infty} X(j\omega) e^{+j\omega t} d\omega \quad (2.9)$$

while the discrete-time Fourier transform (DTFT) pair for x_k is

$$X(e^{j\omega T}) = \sum_{k=-\infty}^{\infty} x_k e^{-j\omega kT}, \quad x_k = \frac{T}{2\pi} \int_{-\pi/T}^{\pi/T} X(e^{j\omega T}) e^{j\omega kT} d\omega. \quad (2.10)$$

The notation $X(e^{j\omega T})$ deserves some explanation. $X(e^{j\omega T})$ is the Z-transform $X(z)$, defined as

$$X(z) = \sum_{k=-\infty}^{\infty} x_k z^{-k}, \quad (2.11)$$

evaluated at $z = e^{j\omega T}$. Furthermore, the argument of the function, $e^{j\omega T}$, is periodic in ω , emphasizing that the DTFT itself is periodic in ω with period equal to the sampling rate $2\pi/T$. The j in $X(j\omega)$ comes from the observation that $X(j\omega)$ is the Laplace transform $X(s)$ evaluated at $s = j\omega$.

If $h(t)$ is the impulse response of a continuous-time system, then the Laplace transform $H(s)$ is called the *transfer function*, and the Fourier transform $H(j\omega)$ is called the *frequency response*. Correspondingly, for a discrete-time impulse response h_k , the transfer function is $H(z)$ and the frequency response is $H(e^{j\omega T})$. Discrete-

time and continuous-time systems will often be distinguished only by the form of the argument of their transfer function or frequency response.

Exercise 2-4.

Starting with the convolution, show that the Fourier transform of the output of an LTI system is

$$Y(j\omega) = H(j\omega)X(j\omega), \quad Y(e^{j\omega T}) = H(e^{j\omega T})X(e^{j\omega T}) \quad (2.12)$$

for the continuous-time and discrete-time cases, where $X(j\omega)$ and $X(e^{j\omega T})$ are the Fourier transforms of the input signals. \square

The magnitude of the frequency response $|H(j\omega)|$ or $|H(e^{j\omega T})|$ is called the *magnitude response*. The argument of the frequency response $\arg(H(j\omega))$ or $\arg(H(e^{j\omega T}))$ is called the *phase response*. The reason for these terms is explored in Problem 2-2.

A fundamental result allows us to analyze any system with a combination of continuous-time and discrete-time signals.

Exercise 2-5.

Given the definition (2.2) of a continuous-time PAM signal $\hat{x}(t)$ derived from a discrete-time signal x_k , show that for all ω

$$\hat{X}(j\omega) = X(e^{j\omega T}). \quad (2.13)$$

In words, the Fourier transform of a PAM representation of a discrete-time signal is equal to the DTFT of the discrete time signal for all ω . \square

2.3. THE NYQUIST SAMPLING THEOREM

Suppose that we sample a continuous-time signal $x(t)$ to get

$$x_k = x(kT). \quad (2.14)$$

From (2.2) we obtain

$$\hat{x}(t) = x(t) \sum_{m=-\infty}^{\infty} \delta(t - mT). \quad (2.15)$$

Multiplication in the time-domain corresponds to convolution in the frequency domain, so

$$\begin{aligned}
 \hat{X}(j\omega) &= \frac{1}{2\pi} \left[X(j\omega) \right] * \left[\frac{2\pi}{T} \sum_{m=-\infty}^{\infty} \delta(\omega - \frac{2\pi}{T}m) \right] \\
 &= \frac{1}{T} \int_{-\infty}^{\infty} X(j\Omega) \sum_{m=-\infty}^{\infty} \delta(\omega - \Omega - \frac{2\pi m}{T}) d\Omega \\
 &= \frac{1}{T} \sum_{m=-\infty}^{\infty} X[j(\omega - \frac{2\pi m}{T})].
 \end{aligned} \tag{2.16}$$

Combining this with (2.13) we get the very important relation

$$X(e^{j\omega T}) = \frac{1}{T} \sum_{m=-\infty}^{\infty} X[j(\omega - \frac{2\pi m}{T})]. \tag{2.17}$$

This fundamental *sampling theorem* relates the signals $x(t)$ and x_k in the frequency domain. Systems with both discrete and continuous-time signals can now be handled easily.

Exercise 2-6.

Use (2.17) to show that the frequency response of a completely discrete-time system equivalent to that in Figure 2-3 is

$$F(e^{j\omega T}) = \frac{1}{T} \sum_m F[j(\omega + m\frac{2\pi}{T})]. \tag{2.18}$$

□

Notice that in (2.17) a component of $X(j\omega)$ at any $\omega = \omega_0$ is indistinguishable in the sampled version from a component at $\omega = \omega_0 + 2\pi m/T$ for any integer m . This phenomenon is called *aliasing*.

Example 2-2.

Given a signal $x(t)$ with Fourier transform $X(j\omega)$ shown in Figure 2-4a, the Fourier transform of the sampled signal $\hat{X}(j\omega) = X(e^{j\omega T})$ is shown in Figure 2-4b. The overlap evident in Figure 2-4b, called *aliasing distortion*, makes it very difficult to recover $x(t)$ from its samples. □

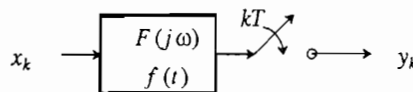


Figure 2-3. A discrete-time system using a continuous-time filter.

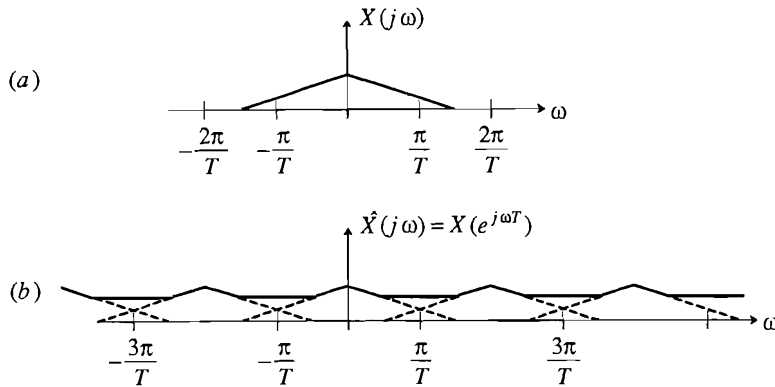


Figure 2-4. The Fourier transform of a continuous-time signal (a) and its sampled version (b), where the sample rate is $2\pi/T$.

Exercise 2-7.

(Nyquist sampling theorem.) Show that, from (2.17), a continuous-time signal can be reconstructed from its samples if it is sampled at a rate at least twice its highest frequency component. More precisely, if a signal $x(t)$ with Fourier transform $X(j\omega)$ is sampled at frequency $2\pi/T$ (radians per second), then $x(t)$ can be reconstructed from the samples if $X(j\omega) = 0$ for all $|\omega| > \pi/T$. \square

The sampling theorem gives a sufficient but not necessary condition for reconstructing a signal from its samples. In the absence of aliasing distortion, a lowpass signal can be reconstructed from its samples using an ideal low pass filter with cutoff frequency π/T ,

$$x(t) = \hat{x}(t) * \left[\frac{\sin(\pi t/T)}{\pi t/T} \right] = \sum_{m=-\infty}^{\infty} x_m \frac{\sin[\pi(t-mT)/T]}{\pi(t-mT)/T}. \quad (2.19)$$

2.4. PASSBAND SIGNALS and MODULATION

Passband signals are fundamentally important for digital communication over channels, such as radio, where the signal spectrum must be confined to a narrow band of frequencies. In this section we will first define a useful building block called a phase splitter, then develop a complex baseband representation for any passband signal, and finally describe several useful modulation techniques for translating the frequency spectrum of a signal.

2.4.1. Phase Splitter and Analytic Signal

A *phase splitter* is a filter with impulse response $\phi(t)$ and transfer function $\Phi(j\omega)$, where

$$\Phi(j\omega) = \begin{cases} 1, & \omega \geq 0 \\ 0, & \omega < 0 \end{cases} . \quad (2.20)$$

The filter passes only positive frequencies, and rejects negative frequencies. Clearly, since $\Phi(j\omega)$ does not display complex-conjugate symmetry, $\phi(t)$ is a complex-valued impulse response. Regardless of the input to a phase splitter, the output must have only positive frequency components. A signal with only positive frequency components is called an *analytic signal*. Obviously, any analytic signal is complex-valued in the time domain.

Closely related to the phase splitter is the *Hilbert transform*, a filter with transfer function

$$H(j\omega) = -j \operatorname{sgn}(\omega) . \quad (2.21)$$

It has a real-valued impulse response, since its transfer function has complex-conjugate symmetry. A Hilbert transform does not modify the amplitude spectrum of the input, but does give a $-\pi$ phase shift at all frequencies. If the input to $H(j\omega)$ is $x(t)$, then the output, the Hilbert transform of $x(t)$, is denoted by $\hat{x}(t)$.

Exercise 2-8.

If the real-valued input to a phase splitter is $x(t)$, then show that the output is $\frac{1}{2}\{x(t) + j\hat{x}(t)\}$. Thus, the real part of the output is half the input, and the imaginary part is half the Hilbert transform of the input. \square

The phase splitter and Hilbert transform filter both have a discontinuity in either amplitude or phase at d.c. They are therefore very difficult to implement at baseband frequencies. However, in many applications, we will apply a phase splitter to a passband signal, which makes the implementation much easier because the transfer function in the region of d.c. actually does not matter!

2.4.2. Complex Baseband Representation of Passband Signals

Suppose $y(t)$ is a real-valued passband signal that happens to have a spectrum centered at $\omega = \omega_c$. We can develop a representation of $y(t)$ in terms of a complex-valued baseband signal $u(t)$; that is, a signal with its spectrum concentrated at d.c. Consider the system shown in Figure 2-5a. Since $y(t)$ is real-valued, it has a spectrum concentrated at $-\omega_c$ as well as ω_c . If we pass $y(t)$ first through a phase splitter, then the output analytic signal is missing the negative frequency terms. The remaining positive frequency terms can be shifted to d.c. by multiplying by a complex exponential $e^{-j\omega_c t}$, yielding the complex baseband representation $u(t)$. We add the strange-looking factor of $\sqrt{2}$ for a good reason. Mathematically, the complex baseband signal can be represented as

$$u(t) = \frac{1}{\sqrt{2}}(y(t) + j\hat{y}(t))e^{-j\omega_c t} . \quad (2.22)$$

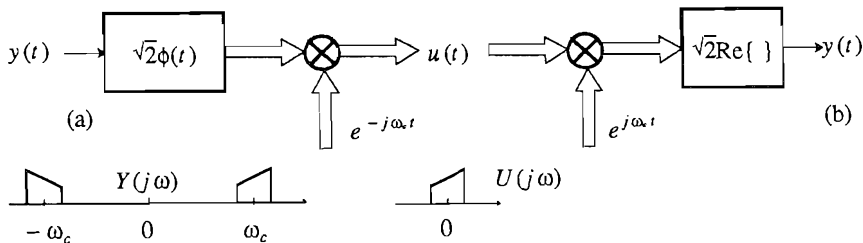


Figure 2-5. Derivation of the complex baseband representation $u(t)$ from a passband signal $y(t)$. (a) Obtaining $u(t)$ from $y(t)$. (b) Recovering $y(t)$ from $u(t)$. Also shown are typical spectra of the two signals, where $U(j\omega)$ is a replica of the positive-frequency components of $Y(j\omega)$ shifted to d.c.

Exercise 2-9.

Show that $u(t)$ has the same energy as $y(t)$, because of the factor of $\sqrt{2}$. This equal-energy property is important when we deal with noise and signal-to-noise ratios (Chapter 6). \square

As shown in Figure 2-5b, the original passband signal can be recovered from the complex baseband representation through the equation

$$y(t) = \sqrt{2} \cdot \text{Re}\{ u(t) e^{j\omega_c t} \}. \quad (2.23)$$

This can also be easily verified by substituting (2.22) into (2.23). (2.23) is called the *canonical representation* of a passband signal in terms of a complex baseband signal. Any real-valued passband signal can be represented in this canonical form, where $u(t)$ can be determined from (2.22) or Figure 2-5a.

2.4.3. Modulation

It is often useful to shift the spectrum of a signal, a process known as *modulation*.

Example 2-3.

A telephone channel passes only frequencies in the range from about 300Hz to about 3300Hz. Any signal transmitted over such a channel must be bandlimited in the same range, or it will not get through intact. Similarly, commercial broadcast AM radio occupies electromagnetic frequencies from 550kHz to 1.6MHz. An audio signal is limited to below 20kHz. Modulation is necessary to translate an audio signal into a frequency band suitable for AM transmission. \square

Actually, modulation is the opposite of the canonical representation; rather than deriving an equivalent baseband representation of a passband signal, modulation generates an equivalent passband representation of a baseband signal. The canonical representation teaches us that a real-valued passband signal (necessary to transmit over a physical medium, Chapter 5) corresponds in general to a complex-valued baseband signal. Thus, assume that the baseband signal $u(t)$ is complex-valued, and generate modulated signal (2.23). The resulting modulator and demodulator are shown in Figure 2-6, which is actually the same as Figure 2-5 reversed. Again, the factor $\sqrt{2}$ ensures

that the modulated signal $y(t)$ has the same energy as the baseband signal $u(t)$.

This representation of modulation is very general. All of the commonly used modulation techniques can be represented in this form. These techniques are distinguished by how they map an information-bearing signal into the complex baseband signal $u(t)$. We will illustrate this with three important modulation techniques: AM-DSB, AM-SSB, and QAM.

In *amplitude modulation double sideband (AM-DSB)*, a real-valued information-bearing signal $a(t)$ is mapped into a passband signal by letting $u(t) = a(t)$. The baseband signal $u(t)$ is therefore real-valued, and has a spectrum that is symmetric about the carrier frequency. The passband signal is represented mathematically as

$$y(t) = \sqrt{2} \cdot \text{Re}\{ a(t) e^{j\omega_c t} \} = \sqrt{2} \cdot a(t) \cdot \cos(\omega_c t). \quad (2.24)$$

The passband signal is complex-conjugate symmetric about the carrier frequency ω_c , because the baseband signal is real-valued.

In *amplitude modulation single sideband (AM-SSB)* we again have a real-valued information-bearing signal $a(t)$, but we let the complex baseband signal be an analytic signal obtained by passing $a(t)$ through a phase splitter, $u(t) = \frac{1}{2}(a(t) + j\dot{a}(t))$. Since the complex baseband signal is analytic, the passband signal has only upper-sideband frequency components above the carrier frequency. The advantage of AM-SSB over AM-DSB is that for the same $a(t)$, the bandwidth of the AM-SSB passband signal is half that of the AM-DSB signal, basically because the upper and lower sidebands of AM-DSB are complex-conjugate duplicates of one another. A disadvantage of AM-SSB is the baseband phase splitter, which can be difficult to realize because of the phase discontinuity at d.c. unless the baseband signal should happen to be missing frequencies near d.c. (as is true of telephone speech).

The third modulation technique is *quadrature amplitude modulation (QAM)*. In this case, we have two real-valued information-bearing signals $a(t)$ and $b(t)$, and simultaneously modulate them by letting $u(t) = a(t) + jb(t)$. The complex baseband signal is neither analytic, nor has complex-conjugate symmetry about d.c.; the passband signal has in general both upper and lower sidebands and no particular

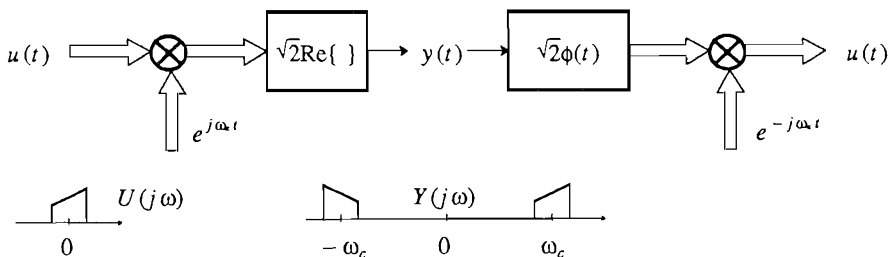


Figure 2-6. A modulator turns a complex baseband signal $u(t)$ into a real-valued passband signal $y(t)$, by simply reversing Figure 2-5.

symmetry about the carrier frequency. The term "QAM" arises from the representation

$$y(t) = \sqrt{2} \cdot \operatorname{Re}\{ (a(t) + jb(t))e^{j\omega_c t} \} = \sqrt{2} \cdot a(t) \cdot \cos(\omega_c t) - \sqrt{2} \cdot b(t) \cdot \sin(\omega_c t). \quad (2.25)$$

In other words, a QAM signal consists of two independently modulated carrier signals with a $\pi/2$ relative phase shift. For the same baseband signal bandwidth, QAM requires the same passband bandwidth as AM-DSB, which is double that required for AM-SSB; however, it transmits two real-valued information-bearing signals rather than one. Thus, it offers the same spectral efficiency as AM-SSB, but without the requirement for the difficult-to-implement baseband phase splitter. QAM and similar modulation techniques have therefore become the most widely used for digital communication (Chapter 6).

2.5. Z TRANSFORMS AND RATIONAL TRANSFER FUNCTIONS

The Z transform, which is closely related to the DTFT, is particularly useful in the study of rational transfer functions. The Z transform is defined as

$$H(z) = \sum_{k=-\infty}^{\infty} h_k z^{-k}, \quad (2.26)$$

where z is a complex variable. As pointed out before, the DTFT is the Z transform evaluated at $z = e^{j\omega T}$, or on the unit circle in the z plane, as shown in Figure 2-7. This justifies the notation $H(e^{j\omega T})$ for a DTFT. When $\{h_k\}$ is the impulse response of a discrete-time LTI system, then $H(z)$ is called the transfer function of the system. The transfer function on the unit circle is called the frequency response.

2.5.1. One Sided Sequences

A *causal* sequence $\{h_k\}$ has $h_k = 0$ for $k < 0$. An *anti-causal* sequence has $h_k = 0$ zero for $k > 0$. A *right-sided* sequence is one for which, for some K , $h_k = 0$ for $k < K$. A *left-sided* sequence correspondingly has $h_k = 0$ for $k > K$ for some K . When h_k is the impulse response of an LTI system, that system is obviously causal

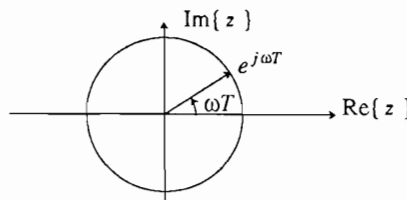


Figure 2-7. The Fourier transform of a discrete-time signal is the Z transform evaluated on the unit circle.

(anti-causal) if the impulse response is right-sided (left-sided) for $K = 0$. While physically realizable real-time LTI systems are causal, we will frequently find it useful to model systems as non-causal.

Example 2-4.

Assume a communication channel has the impulse response shown in Figure 2-8a. We can think of this channel as having a *flat propagation delay* of M samples plus the non-causal response $\{h_k\}$ as shown in Figure 2-8b. Often the flat delay will not be an essential feature of the channel, in which case we ignore it. \square

Example 2-5.

Suppose we come up with a non-causal filter $H(z)$ in a theoretical development. This need not concern us too much, since such a filter can be approximated by a causal filter $G(z)$ together with an additional flat delay z^{-M} . This extra flat delay which did not arise in the theoretical development will often not harm the system. \square

A particularly important class of causal or anti-causal sequences have a unity-valued sample at time zero ($h_0 = 1$). These sequences are said to be *monic*. A similar terminology is used for polynomials, which are monic if the constant term is unity. It is easy to see from (2.26) that $H(z)$ is the Z transform of a causal and monic sequence if and only if $H(\infty) = 1$. Similarly, it is anti-causal and monic if and only if $H(0) = 1$. When a sequence $\{h_k\}$ is monic, then $H(z)$, as a polynomial in z , is also monic.

The *region of convergence* (ROC) of the Z transform is the region of the z plane where the series in (2.26) is absolutely summable,

$$\sum_{k=-\infty}^{\infty} |h_k z^{-k}| < \infty . \quad (2.27)$$

Note that for any $z \in \text{ROC}$, $|H(z)| < \infty$, because

$$|H(z)| \leq \sum_{k=-\infty}^{\infty} |h_k z^{-k}| < \infty . \quad (2.28)$$

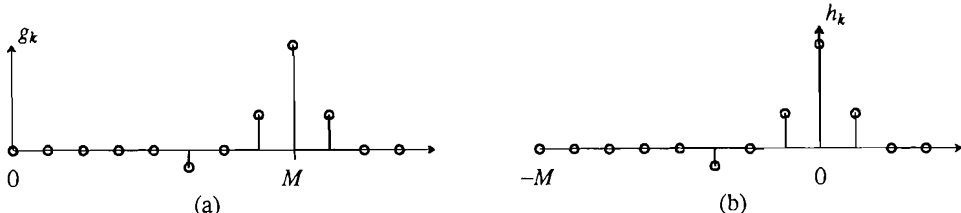


Figure 2-8. Illustration of the usefulness of a non-causal channel model. (a) Actual channel impulse response. (b) A non-causal version of the impulse response where the flat propagation delay is ignored.

Since the Fourier transform is the Z transform evaluated on the unit circle, for signals with a Fourier transform the ROC includes the unit circle.

A *bounded-input bounded-output (BIBO) stable* system has the property that any bounded input sequence with $|x_k| < L$ produces a bounded output sequence with $|y_k| < K$. We will often use the term "stable" to denote "BIBO stable".

Exercise 2-10.

Show that a system with impulse response $\{h_k\}$ is BIBO stable if and only if

$$S = \sum_{k=-\infty}^{\infty} |h_k| < \infty. \quad (2.29)$$

□

A consequence of this is that a system is BIBO stable if and only if the ROC includes the unit circle. To see this, note that (2.27) can be rewritten

$$\sum_{k=-\infty}^{\infty} |h_k| |z|^{-k} < \infty. \quad (2.30)$$

On the unit circle, $|z| = 1$, so this sum equals S in (2.29). By analogy with BIBO stable systems, a sequence $\{h_k\}$ (not necessarily an impulse response) is said to be stable if it is absolutely summable, as in (2.29).

It is evident from (2.30) that the ROC depends only on $|z|$; that is, it is of the form of an *annulus* or doughnut-shaped region. For a causal sequence, the ROC will be of the form $|z| > R$ for some constant R . In words, the ROC will be the region outside a circle of radius R . If the sequence is also stable, then $R < 1$, as shown in Figure 2-9a. To see this, note that for a causal sequence, the summation in (2.30) becomes

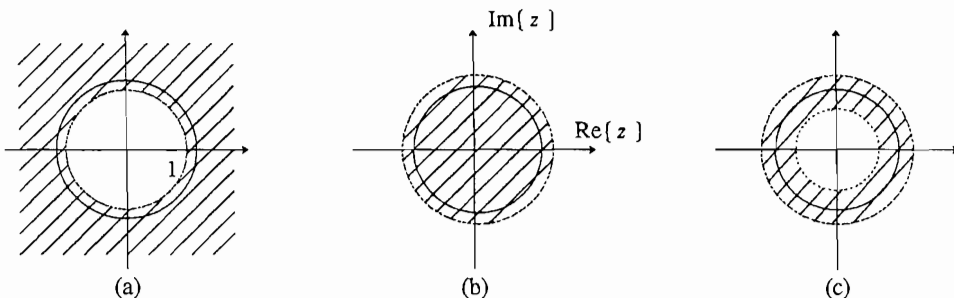


Figure 2-9. The ROC of the Z transform of a stable sequence must include the unit circle. Three cases of stable sequences are illustrated: (a) A right-sided, (b) left-sided, and (c) two-sided sequence. The ROC includes $|z| = \infty$ in (a) if the sequence is causal. It includes $z = 0$ in (b) if the sequence is anti-causal.

$$\sum_{k=0}^{\infty} |h_k| |z|^{-k} < \infty . \quad (2.31)$$

All the terms in the summation are positive powers of $|z|^{-1}$, and hence get smaller as $|z|$ gets larger. Thus, if absolute convergence occurs for some $|z_1| > R$, it will occur for all z such that $|z| \geq |z_1|$.

If the sequence is right-sided but not causal, (2.30) becomes

$$\sum_{k=-K}^{\infty} |h_k| |z|^{-k} < \infty . \quad (2.32)$$

for some $K < 0$. The positive powers of $|z|$ do not converge at $z = \infty$, but do converge at all other z . Thus, the ROC cannot include $|z| = \infty$, and should be written $R < |z| < \infty$. Similar results apply to left-sided sequences.

Exercise 2-11.

- (a) Show that the ROC of a left-sided stable sequence is of the form $0 < |z| < R$ for $R > 1$.
- (b) Show that a left-sided sequence is anti-causal if and only if its ROC includes the origin, $0 \leq |z| < R$, as shown in Figure 2-9b. \square

To summarize, a right-sided sequence has an ROC consisting of the region outside a circle. That region includes $|z| = \infty$ if and only if the sequence is causal. A left-sided sequence has an ROC consisting of the inside of a circle. That region includes $z = 0$ if and only if the sequence is anti-causal. In all cases, the ROC includes the unit circle if and only if the sequence is stable.

2.5.2. Rational Transfer Functions

A rational transfer function can be written in any of the forms

$$H(z) = z^r \cdot \frac{\sum_{k=0}^M b_k z^{-k}}{\sum_{k=0}^N a_k z^{-k}} = A \cdot z^r \cdot \frac{\prod_{k=1}^M (1 - c_k z^{-1})}{\prod_{k=1}^N (1 - d_k z^{-1})} = A \cdot z^m \cdot \frac{\prod_{k=1}^M (z - c_k)}{\prod_{k=1}^N (z - d_k)} , \quad (2.33)$$

where $A = b_0 / a_0$ and $m = N - M + r$. Notice that in the middle form, the numerator and denominator polynomials are both monic. The ratio of two such monic polynomials is also monic (carry out the long division to verify this).

The system has M zeros (roots of the numerator) at c_k , $1 \leq k \leq M$, and N poles (roots of the denominator) at d_k , $1 \leq k \leq N$. The factor z^m represents merely an advance or delay in the impulse response. If $m > 0$ this factor introduces m zeros at the origin and m poles at $|z| = \infty$ (conversely for $m < 0$). If h_k is real valued, then $H(z)$ in (2.33) has real-valued coefficients, and the zeros and poles are always either real valued or come in complex-conjugate pairs (Problem 2-20).

Including poles and zeros at $z = 0$ and $|z| = \infty$, every rational transfer function has the same number of poles and zeros. This will be illustrated by two examples.

Example 2-6.

The causal FIR transfer function $H(z) = 1 - 0.5 z^{-1}$ has one zero at $z = \frac{1}{2}$ and one pole at $z = 0$. The only possible ROC is $|z| > 0$, which is a degenerate case of Figure 2-9a. \square

Example 2-7.

The anti-causal FIR transfer function $H(z) = 1 - 0.5 z$ has one zero at $z = 2$ and one pole at $|z| = \infty$. The only possible ROC is $|z| < \infty$, which is a degenerate case of Figure 2-9b. \square

The ROC cannot include any of the poles, since $H(z)$ is unbounded there. Moreover, for rational transfer functions, the ROC is bordered by poles. Referring to Figure 2-9, for a causal and stable $H(z)$, all poles must be inside the unit circle. For an anti-causal and stable $H(z)$, all poles must be outside the unit circle. No stable $H(z)$ can have poles on the unit circle, although it can certainly have zeros on the unit circle.

Exercise 2-12.

LTI systems that can actually be implemented with computational hardware can be represented by linear constant-coefficient difference equations with zero initial conditions. Show that the system represented by

$$y_k = \frac{1}{a_0} \left(\sum_{l=0}^M b_l x_{k-l} - \sum_{l=1}^N a_l y_{k-l} \right) \quad (2.34)$$

has transfer function given by (2.33) with $r = 0$. \square

When the denominator in (2.33) is unity ($N = 0$), the system has a *finite impulse response (FIR)*, otherwise it has an *infinite impulse response (IIR)*. FIR systems are always stable, and are often a good approximation to physical systems. They can have poles only at $z = 0$ and $|z| = \infty$, and the ROC therefore includes the entire z plane with the possible exception of $z = 0$ and $|z| = \infty$. If an FIR system is causal, it has no poles at $|z| = \infty$. If it is anti-causal, it has no poles at $z = 0$.

Example 2-8.

Physical channels, such as a coaxial cable (Chapter 5), usually do not have, strictly speaking, a rational transfer function. However, they can be adequately approximated by a rational transfer function. Often the simplest approximation is FIR, obtained by simply truncating the actual impulse response for sufficiently large M . Alternatively, it may be possible to approximate the response with fewer parameters using an IIR transfer function. \square

2.5.3. Allpass Transfer Functions

An *allpass* transfer function is any transfer function where the magnitude frequency response is unity for all ω ,

$$|H_{\text{allpass}}(e^{j\omega T})| = 1 . \quad (2.35)$$

This can be written as

$$H_{\text{allpass}}(e^{j\omega T})H_{\text{allpass}}^*(e^{j\omega T}) = 1 . \quad (2.36)$$

Applying the inverse DTFT, we get

$$h_k * h_{-k}^* = \delta_k , \quad (2.37)$$

where h_k is the impulse response of $H_{\text{allpass}}(e^{j\omega T})$. Taking Z transforms we see that

$$H_{\text{allpass}}(z)H_{\text{allpass}}^*(1/z^*) = 1 . \quad (2.38)$$

For rational Z transforms, (2.38) implies that every pole of $H_{\text{allpass}}(z)$ is cancelled by a zero of $H_{\text{allpass}}^*(1/z^*)$. Therefore, if $H_{\text{allpass}}(z)$ has a pole at $z = c$, then $H_{\text{allpass}}^*(1/z^*)$ has a zero at $z = c$. The latter implies that $H_{\text{allpass}}(z)$ has a zero at $z = 1/c^*$. Therefore, any zero or pole must be accompanied by a matching pole or zero at the *conjugate-reciprocal* location.

Example 2-9.

A first-order allpass transfer function is given by

$$H_{\text{allpass}}(z) = \frac{z^{-1} - c^*}{1 - cz^{-1}} . \quad (2.39)$$

The pole-zero plot is shown in Figure 2-10. Note that the pole and zero form a conjugate-reciprocal pair. For the value of c shown in the figure, the impulse response will be complex valued. \square

Observe that c and $1/c^*$ have the same angle in the Z plane, but their magnitudes are the reciprocal of one another, as shown in Figure 2-10.

Consider a transfer function of the form

$$H_{\text{allpass}}(z) = z^M \frac{z^{-N} + a_1 z^{-N+1} + \cdots + a_N}{1 + a_1^* z^{-1} + \cdots + a_N^* z^{-N}} . \quad (2.40)$$

This can be rewritten as

$$H_{\text{allpass}}(z) = \frac{A(z)}{z^{N-M} A^*(1/z^*)} , \quad A(z) = 1 + a_1 z + \cdots + a_N z^N . \quad (2.41)$$

Such a transfer function is allpass,

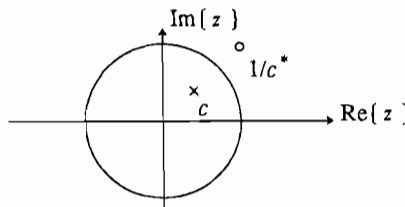


Figure 2-10. The pole-zero plot for a first-order allpass filter.

$$|H_{\text{allpass}}(e^{j\omega T})| = \left| \frac{A(e^{j\omega T})}{e^{j\omega TN} A^*(e^{j\omega T})} \right| = 1 . \quad (2.42)$$

Note that if $N \geq M$, the term z^{N-M} in the denominator contributes $N - M$ poles at $z = 0$ and $N - M$ zeros at $|z| = \infty$, the conjugate-reciprocal of 0. If $N < M$, then this term puts zeros $z = 0$ and poles at $|z| = \infty$. Thus, poles and zeros at zero and infinity also come in conjugate-reciprocal pairs. Since poles and zeros must come in conjugate-reciprocal pairs, any rational allpass transfer function can be written in the form of (2.41).

2.5.4. Minimum and Maximum-Phase Transfer Functions

A stable and causal transfer function is said to be *strictly minimum-phase* when all its poles and zeros are inside the unit circle. See Problem 2-22 for the intuition that explains the term "minimum phase". A stable and causal transfer function is *strictly maximum-phase* when all poles and zeros are outside the unit circle. Neither strictly minimum-phase nor strictly maximum-phase transfer functions are allowed to have zeros on the unit circle itself. If they have zeros on the unit circle, then we call them *loosely minimum-phase* or *loosely maximum-phase*. The strictly minimum-phase transfer function has the important property that it has a BIBO stable and causal inverse. This is because zeros of the transfer function become poles of the inverse, and for a strictly minimum-phase transfer function, all such poles will end up inside the unit circle. A loosely minimum-phase transfer function does not necessarily have a BIBO stable inverse, but it is still useful because it may display a mild form of instability.

Any causal and stable rational transfer function can be factored as

$$H(z) = H_{\text{allpass}}(z)H_{\text{min}}(z)H_{\text{zero}}(z), \quad (2.43)$$

where $H_{\text{allpass}}(z)$ is causal, stable, and allpass, $H_{\text{min}}(z)$ is strictly minimum phase, and $H_{\text{zero}}(z)$ is FIR with only zeros on the unit circle and corresponding poles at $z = 0$. The construction of this factorization, illustrated in Figure 2-11, is straightforward. All zeros of $H(z)$ on the unit circle are assigned to $H_{\text{zero}}(z)$. To ensure that $H_{\text{zero}}(z)$ is causal, it is given a pole at $z = 0$ for each zero on the unit circle. Such poles may be

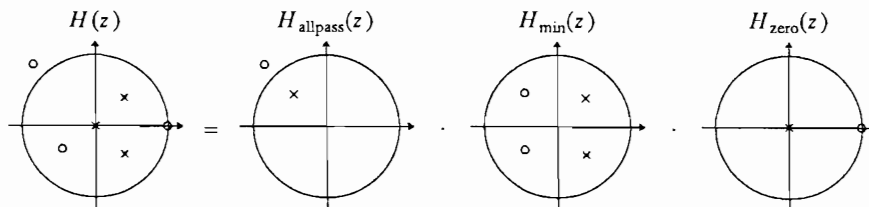


Figure 2-11. Factorization of a causal and stable rational transfer function into an allpass transfer function, a strictly minimum-phase transfer function, and a causal transfer function with only zeros on the unit circle. Notice that the number of poles at $z = 0$ is chosen so that there are no poles at $z = \infty$, ensuring that each transfer function is causal.

canceled by zeros at $z = 0$ in $H_{\min}(z)$, if necessary. All remaining poles in $H(z)$, which must lie inside the unit circle, are assigned to $H_{\min}(z)$. All zeros that lie inside the unit circle are also assigned to $H_{\min}(z)$. Each zero outside the unit circle is assigned to $H_{\text{allpass}}(z)$. To make sure $H_{\text{allpass}}(z)$ is allpass, it is assigned a pole at the conjugate-reciprocal location of each such zero. That pole will be inside the unit circle, ensuring that $H_{\text{allpass}}(z)$ is causal and stable. To cancel the effect of that pole, a zero at the same location is assigned to $H_{\min}(z)$. When all is done, $H_{\min}(z)$ should have an equal number of poles and zeros, all inside the unit circle.

We can develop another useful factorization of a stable (not necessarily causal) rational transfer function by dividing poles and zeros into four classes: those inside, on, and outside the unit circle, plus some zeros at the origin. The factorization is

$$H(z) = B \cdot z^L \cdot H_{\min}(z) \cdot H_{\max}(z) \cdot H_{\text{zero}}(z) \quad (2.44)$$

where $H_{\min}(z)$ is a strictly minimum-phase transfer function containing all the poles and zeros inside the unit circle, except possibly for some zeros at the origin, while $H_{\max}(z)$ is a strictly maximum-phase transfer function containing all the poles and zeros outside the unit circle. $H_{\text{zero}}(z)$ is an FIR transfer function containing all the zeros on the unit circle (stability rules out poles on the unit circle) with corresponding poles at the origin. In addition, we choose constants B and L so that $H_{\min}(z)$ and $H_{\text{zero}}(z)$ are causal and monic ($H_{\min}(\infty) = H_{\text{zero}}(\infty) = 1$), and $H_{\max}(z)$ is anti-causal and monic ($H_{\max}(0) = 1$).

With these constraints, the factorization is unique. In particular, the terms can always be written in the form

$$H_{\min}(z) = \frac{\prod_{k=1}^M (1 - c_k z^{-1})}{\prod_{k=1}^N (1 - d_k z^{-1})}, \quad |c_k| < 1, \quad |d_k| < 1, \quad (2.45)$$

$$H_{\text{zero}}(z) = \prod_{k=1}^K (1 - e_k z^{-1}), \quad |e_k| = 1, \quad (2.46)$$

$$H_{\max}(z) = \frac{\prod_{k=1}^I (1 - f_k z)}{\prod_{k=1}^J (1 - g_k z)}, \quad |f_k| < 1, \quad |g_k| < 1. \quad (2.47)$$

An example will serve to illustrate how we turn a general rational transfer function into this canonical form.

Example 2-10.

Given the rational transfer function

$$H(z) = \frac{(1 - 0.5z^{-1})(1 - z^{-1})}{(1 - 1.25z^{-1})}, \quad (2.48)$$

we can write

$$H(z) = -1.25 z (1 - 0.5z^{-1}) \frac{1}{(1 - 0.8z)} (1 - z^{-1}). \quad (2.49)$$

We can identify $B = -1.25$, $L = 1$, and

$$H_{\min}(z) = (1 - 0.5z^{-1}), \quad H_{\max}(z) = 1/(1 - 0.8z), \quad H_{\text{zero}}(z) = (1 - z^{-1}). \quad (2.50)$$

□

Given a transfer function in the second or third form of (2.33), the factorization in (2.44) is simple to obtain.

Given a transfer function $H(z)$, we define the *reflected* transfer function to be $H^*(1/z^*)$. It has impulse response h_{-k}^* (as is easy to verify). For a rational transfer function in the second form of (2.33), the reflected transfer function can be written

$$H^*(1/z^*) = A \cdot z^{-r} \cdot \frac{\prod_{k=0}^M (1 - c_k^* z)}{\prod_{k=0}^N (1 - d_k^* z)}. \quad (2.51)$$

The zeros c_k of $H(z)$ become zeros at the conjugate-reciprocal locations $1/c_k^*$ in $H^*(1/z^*)$. The poles are similarly reflected through the unit circle. If $H(z)$ is minimum-phase and monic, then $H^*(1/z^*)$ is maximum-phase and monic, and *vice versa*. If $H(z)$ is stable and causal (all poles are inside the unit circle) then $H^*(1/z^*)$ is stable and anti-causal (all poles are outside the unit circle). Zeros of $H(z)$ on the unit circle have corresponding zeros of $H^*(1/z^*)$ at identical locations on the unit circle.

To see the relationship between the frequency response of $H(z)$ and $H^*(1/z^*)$, just evaluate them at $z = e^{j\omega T}$, getting $H(e^{j\omega T})$ and $H^*(e^{j\omega T})$. Hence the frequency response of a reflected transfer function is simply the complex-conjugate of the original frequency response. That is, any transfer function and its reflected transfer function have the same magnitude frequency response, and their phase responses are the negative of one another.

Example 2-11.

Since $H(z)$ and $H^*(1/z^*)$ have the same magnitude response on the unit circle, the system $H_{\text{allpass}}(z) = H(z)/H^*(1/z^*)$ is an allpass system. □

Using the factorization in (2.44) and Example 2-11 is an alternative route to the factorization of (2.43) (see Problem 2-24).

2.5.5. Non-Negative Real Transfer Functions

In the study of random processes (Chapter 3), Z transforms that are real valued and non-negative on the unit circle arise frequently. In this subsection, we study the properties of such Z transforms.

Suppose $H(z)$ is a rational transfer function, and $S(z)$ is

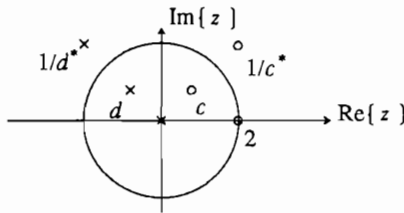


Figure 2-12. An example of a pole zero plot for an $S(z)$ that is real valued on the unit circle.

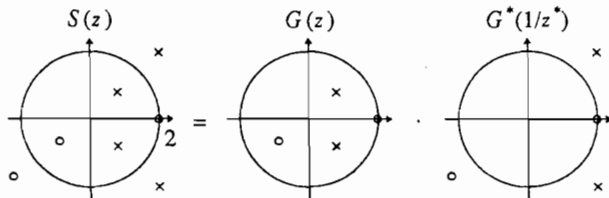


Figure 2-13. Spectral factorization of a transfer function $S(z)$, which is non-negative real on the unit circle. The zero at $z = 1$ has multiplicity two (in general its multiplicity could be any even integer). These two zeros on the unit circle are split between $G(z)$ and $G^*(1/z^*)$.

$$S(z) = H(z)H^*(1/z^*) . \quad (2.52)$$

Then $S(z)$ is always non-negative and real valued on the unit circle,

$$S(z) = H(z)H^*(1/z^*) \Big|_{z = e^{j\omega T}} = |H(e^{j\omega T})|^2 . \quad (2.53)$$

For $S(z)$ in (2.52), for every zero at z_0 , there is a zero at $1/z_0^*$. This follows trivially from the observation that

$$S(z) = S^*(1/z^*) . \quad (2.54)$$

Similarly, the poles must come in conjugate-reciprocal pairs.

Example 2-12.

An example pole-zero plot for a transfer function of form (2.52) is shown in Figure 2-12. The zero at $z = c$ has a matching zero at $z = 1/c^*$. The pole at $z = d$ also has a matching pole. The double zero at $z = 1$ illustrates another implication of (2.52); any zero on the unit circle must be double. The pole at $z = 0$ has a matching pole at $|z| = \infty$. Although the latter pole is not explicitly shown, it is implied because only three poles are shown, compared to four zeros. Note that the impulse response s_k is not real for this example, but nonetheless the frequency response $S(e^{j\omega T})$ is. \square

The conjugate-reciprocal symmetry of (2.52) is not the same as that found for allpass filters. It has conjugate-symmetric pole pairs and zero pairs, rather than pole-zero pairs as in the allpass filter. While allpass filters can be causal, only a trivial non-negative real transfer function in the form of (2.52) can be causal.

It is shown in Appendix 2-B that all stable rational transfer functions $S(z)$ that are non-negative real valued on the unit circle can be written in the form of (2.52); more strongly, $S(z)$ can be written as

$$S(z) = A^2 G(z) G^*(1/z^*) \quad (2.55)$$

where A is some real-valued constant, and $G(z)$ is a loosely minimum-phase rational transfer function,

$$G(z) = \frac{\prod_{k=1}^M (1 - c_k z^{-1})}{\prod_{k=1}^N (1 - d_k z^{-1})}, \quad |c_k| \leq 1, \quad |d_k| < 1. \quad (2.56)$$

$S(z)$ can thus be written as the product of a loosely minimum-phase monic transfer function and its reflected transfer function. The constant A is chosen so that $G(z)$ is monic, and turns out to be quite important.

Equation (2.55) is the *monic minimum-phase spectral factorization* of $S(z)$. It is obtained from $S(z)$ by accumulating within $G(z)$ all the poles and zeros of $S(z)$ within the unit circle, plus one of each double-zero pair of $S(z)$ on the unit circle. This factorization is illustrated in Figure 2-13, where we have, from left to right, the original $S(z)$, the loosely minimum-phase term (poles and zeros inside or on the unit circle), and its reflected transfer function.

A remarkable fact (derived in Appendix 2-B) is that A^2 is equal to the *geometric mean* of $S(e^{j\omega T})$,

$$A^2 = \exp \left\{ \frac{T}{2\pi} \int_{-\frac{\pi}{T}}^{\frac{\pi}{T}} \ln [S(e^{j\omega T})] d\omega \right\}, \quad (2.57)$$

where $\ln(\cdot)$ is the natural logarithm, equal to $\log_e(\cdot)$.

2.6. SIGNAL SPACE REPRESENTATIONS

It is possible to abstractly represent the signals in a digital communication system as vectors in a *linear space* or *vector space*, much like the familiar three-dimensional vectors in our physical world. This representation does not allow us to solve any problems that we cannot solve by other methods, but it gives valuable intuition. The linear space used in our context is often called *signal space*, since vectors in the space represent signals.

2.6.1. Definition of Signal Space

Formally, a *linear space* or *vector space* is a set of vectors together with two operators, addition of vectors and multiplication by a scalar.

Example 2-13.

Ordinary *Euclidean space* is the most familiar example of a linear space. In Euclidean space, a vector is specified by its coordinates, n coordinates in an n -dimensional space,

$$\mathbf{X} \leftrightarrow (x_1, x_2, \dots, x_n), \quad (2.58)$$

where \mathbf{X} is the vector and x_1, \dots, x_n are the n components of that vector. The notation " \leftrightarrow " means that \mathbf{X} is the vector which corresponds to components x_1, \dots, x_n . There are rules for adding two vectors (sum the individual components) and multiplying a vector by a scalar (multiply each of the components by that scalar). \square

Example 2-14.

A space of some importance in this book is the *Euclidean space of complex-valued vectors*. Vectors in this space are identical to (2.58) except that the components x_k of the vector are complex-valued. Ordinary Euclidean space is of course a special case of this, where the imaginary parts of the vectors are zero. \square

The addition rule produces a new vector $\mathbf{X} + \mathbf{Y}$ that must be in the linear space. Addition must obey familiar rules of arithmetic, such as the commutative and associative laws,

$$\mathbf{X} + \mathbf{Y} = \mathbf{Y} + \mathbf{X}, \quad \mathbf{X} + (\mathbf{Y} + \mathbf{Z}) = (\mathbf{X} + \mathbf{Y}) + \mathbf{Z}. \quad (2.59)$$

The direct sum of two vectors has the interpretation illustrated in Figure 2-14a for the two-dimensional Euclidean space. A linear space must include a zero vector $\mathbf{0}$, and every vector must have an *additive inverse*, denoted $-\mathbf{X}$, such that

$$\mathbf{0} + \mathbf{X} = \mathbf{X}, \quad \mathbf{X} + (-\mathbf{X}) = \mathbf{0}. \quad (2.60)$$

Multiplication by a scalar α produces a new vector $\alpha \cdot \mathbf{X}$ that must be in the vector space. Multiplications must obey the associative law,

$$\alpha \cdot (\beta \cdot \mathbf{X}) = (\alpha\beta) \cdot \mathbf{X} \quad (2.61)$$

and also follow the rules

$$1 \cdot \mathbf{X} = \mathbf{X}, \quad 0 \cdot \mathbf{X} = \mathbf{0}. \quad (2.62)$$

The geometric interpretation of multiplying a vector by a scalar is shown in Figure 2-14b. Finally, addition and multiplication must obey the distributive laws,

$$\alpha \cdot (\mathbf{X} + \mathbf{Y}) = \alpha \cdot \mathbf{X} + \alpha \cdot \mathbf{Y}, \quad (\alpha + \beta) \cdot \mathbf{X} = \alpha \cdot \mathbf{X} + \beta \cdot \mathbf{X}. \quad (2.63)$$

Real linear spaces have real-valued scalars as components of vectors, while *complex* linear spaces have complex-valued components. We will encounter both types.

Euclidean space as defined earlier meets all of these requirements, and is therefore a linear space. There are two other examples of linear spaces of particular importance in communication theory: the space of discrete-time signals (which is a generalization of Euclidean space to infinite dimensions), and the space of continuous-time signals. Since these linear spaces model the two basic types of signals we encounter in digital communication systems, we call them *signal spaces*.

Example 2-15.

Given a complex-valued discrete-time signal $\{y_k\}$, define a vector

$$\mathbf{Y} \leftrightarrow (\dots, y_{-1}, y_0, y_1, \dots). \quad (2.64)$$

The set of all such vectors is similar to Euclidean space as defined in (2.58), the difference being that the number of components is infinite rather than finite. An additional assumption often made is that

$$\sum_k |y_k|^2 < \infty, \quad (2.65)$$

or, in words, that the total energy in the discrete-time signal is finite. This assumption is necessary for mathematical reasons that will become evident shortly. Scalar multiplication and vector addition are the same as for Euclidean spaces. \square

Example 2-16.

Define a vector \mathbf{Y} to correspond to a continuous-time signal $y(t)$,

$$\mathbf{Y} \leftrightarrow y(t), -\infty < t < \infty, \quad (2.66)$$

where as in (2.65), there is an assumption of finite energy,

$$\int_{-\infty}^{\infty} |y(t)|^2 dt < \infty. \quad (2.67)$$

We can think of this space as a strange Euclidean space with a continuum of coordinates. The definition of multiplication of a signal vector by a scalar and the summation of two signal vectors are the obvious,

$$\alpha \cdot \mathbf{Y} \leftrightarrow \alpha y(t), \quad \mathbf{X} + \mathbf{Y} \leftrightarrow x(t) + y(t), \quad (2.68)$$

and the definition of a zero vector is the zero-valued signal. \square

Exercise 2-13.

Verify that the linear spaces given by Example 2-15 and Example 2-16 satisfy the properties of (2.59) through (2.63). \square

The following example relates these somewhat abstract concepts to a simple digital communication system.

Example 2-17.

In a digital communication system, suppose that we want to transmit and receive a single data symbol A , where A assumes a small number of values, for example two values in a binary system. For maximum generality consider A to be complex-valued, although the physical meaning of this will not become evident until Chapter 6. In a form of modulation called *pulse amplitude modulation (PAM)* (covered in more detail in Chapter 6), the amplitude of a transmitted pulse $h(t)$ is multiplied by the transmitted data symbol A . The transmitted signal is therefore of the form

$$x(t) = A h(t). \quad (2.69)$$

In accordance with our linear space notation, we can associate the transmitted pulse $h(t)$ with a vector in signal space

$$\mathbf{H} \leftrightarrow h(t) \quad (2.70)$$

in which case the transmitted signal corresponds to the vector

$$\mathbf{X} = \mathbf{A} \cdot \mathbf{H}. \quad (2.71)$$

□

2.6.2. Geometric Structure of Signal Space

The definition of a linear space does not capture the most important properties of Euclidean space; namely, its *geometric* structure. This structure includes such concepts as the length of a vector in the space, and the angle between two vectors. All these properties of Euclidean space can be deduced from the definition of *inner product* of two vectors. The inner product is defined to be

$$\langle \mathbf{X}, \mathbf{Y} \rangle = \sum_{i=1}^n x_i y_i^* \quad (2.72)$$

for an n -dimensional Euclidean space, where y_i^* is the complex conjugate of y_i . It has the interpretation illustrated in Figure 2-15; namely, the inner product of two vectors is equal to the product of the length of the first vector, the length of the second vector, and the cosine of the angle between the vectors.

In Figure 2-15, $\|\mathbf{X}\|$ denotes the length of a vector, which has not been defined. However, once the definition of inner product (2.72) has been given, we can *deduce* a reasonable definition for the length of a vector, since the inner product of a vector with itself, $\langle \mathbf{X}, \mathbf{X} \rangle$, is the square of the length of the vector (the angle θ is zero). A

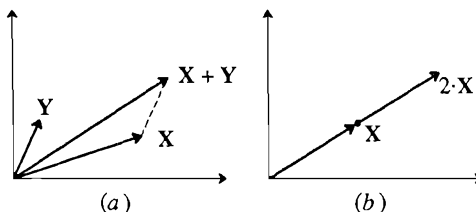


Figure 2-14. Elementary operations in a two-dimensional linear space. a. Sum of two vectors. b. Multiplication of a vector by a scalar.

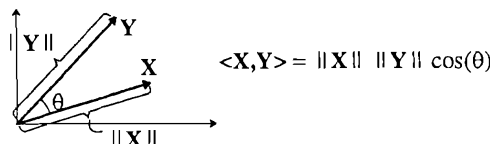


Figure 2-15. Geometrical interpretation of inner product.

special notation is used for $\langle \mathbf{X}, \mathbf{X} \rangle$,

$$\langle \mathbf{X}, \mathbf{X} \rangle = \|\mathbf{X}\|^2 = \sum_{i=1}^n |x_i|^2 \quad (2.73)$$

where $\|\mathbf{X}\|$ is called the *norm* of the vector \mathbf{X} and geometrically is the length of the vector. This notation is used in Figure 2-15.

Note that $\|\mathbf{Y}\| \cos(\theta)$ is the length of the component of \mathbf{Y} in the direction of \mathbf{X} . Hence we get a particularly useful interpretation of the inner product: $\langle \mathbf{X}, \mathbf{Y} \rangle / \|\mathbf{X}\|$ is the length of the component of \mathbf{Y} in the direction of \mathbf{X} , and $\langle \mathbf{X}, \mathbf{Y} \rangle / \|\mathbf{Y}\|$ is the length of the component of \mathbf{X} in the direction of \mathbf{Y} .

Two vectors \mathbf{X}, \mathbf{Y} are said to be *orthogonal* if

$$\langle \mathbf{X}, \mathbf{Y} \rangle = 0. \quad (2.74)$$

This means that \mathbf{X} has no component in the direction of \mathbf{Y} and vice versa; they are at right angles! This concept is crucial to the understanding of optimum receiver design in digital communication systems.

The inner product as applied to Euclidean space can be generalized to the other linear spaces of interest. The important consequence is that the geometric concepts familiar in Euclidean space can be applied to these spaces as well. Let \mathbf{X} and \mathbf{Y} be vectors of a linear space on which an inner product $\langle \mathbf{X}, \mathbf{Y} \rangle$ is defined. The inner product is a scalar (complex-valued number), and must obey the rules

$$\langle \mathbf{X} + \mathbf{Y}, \mathbf{Z} \rangle = \langle \mathbf{X}, \mathbf{Z} \rangle + \langle \mathbf{Y}, \mathbf{Z} \rangle \quad (2.75)$$

$$\langle \alpha \cdot \mathbf{X}, \mathbf{Y} \rangle = \alpha \langle \mathbf{X}, \mathbf{Y} \rangle, \quad \langle \mathbf{X}, \mathbf{Y} \rangle = \langle \mathbf{Y}, \mathbf{X} \rangle^* \quad (2.76)$$

$$\langle \mathbf{X}, \mathbf{X} \rangle > 0, \text{ for } \mathbf{X} \neq 0. \quad (2.77)$$

These rules are all obeyed by the familiar Euclidean space inner product of (2.72), as can be easily verified. For the other linear spaces of interest, analogous definitions of the inner product satisfying the rules can be made. In particular, define the inner product and norm (deduced from (2.73)) of two discrete-time signals as

$$\langle \mathbf{X}, \mathbf{Y} \rangle = \sum_{k=-\infty}^{\infty} x_k y_k^*, \quad \|\mathbf{X}\|^2 = \sum_{k=-\infty}^{\infty} |x_k|^2 \quad (2.78)$$

and of two continuous-time signals as

$$\langle \mathbf{X}, \mathbf{Y} \rangle = \int_{-\infty}^{\infty} x(t) y^*(t) dt, \quad \|\mathbf{X}\|^2 = \int_{-\infty}^{\infty} |x(t)|^2 dt. \quad (2.79)$$

These inner products can be given the same interpretation as in Euclidean space; namely, as the product of the length of two vectors times the cosine of the angle between them. Thus, the inner product serves to define the "angle" between two vectors.

Exercise 2-14.

Verify that the definitions of inner product of (2.78) and (2.79) satisfy the properties of

(2.75) through

(2.77). \square

Note that conditions (2.65) and (2.67) that were imposed correspond to the assumption that a vector has finite norm or length. This explains the need for these initial assumptions in the definition of the linear spaces.

Example 2-18.

Consider again the simple digital communication system of Example 2-17 in which a single transmitted pulse $h(t)$ is multiplied by a data symbol A . Suppose that this transmitted waveform is corrupted by noise before arriving at the receiver, and we decide to implement in the receiver a filter which rejects as much of this noise as possible. In particular, as shown in Figure 2-16, we implement a filter with impulse response $h^*(-t)$, the conjugate mirror image of the transmitted pulse, with corresponding frequency response $H^*(j\omega)$. As we will see in Chapters 6-8, this is not as arbitrary as it may seem, since this particular filter is an optimum filter to reject noise in a special sense, and is given the special name *matched filter*. The output of this filter is sampled at time $t = 0$, resulting in the value

$$y(0) = \int_{-\infty}^{\infty} x(t)h^*(t) dt = \langle \mathbf{X}, \mathbf{H} \rangle. \quad (2.80)$$

The inner product operation is interpreted geometrically as the component of the received signal \mathbf{X} in the direction of the transmitted signal vector \mathbf{H} (multiplied by the unimportant constant $\|\mathbf{H}\|$). Intuitively this seems to be a reasonable approach, since components in directions other than that of the transmitted signal may be irrelevant. Thus the optimality of the matched filter is not surprising from a geometric point of view. \square

The geometric properties are so important that the special name *inner product space* is given to a linear space on which an inner product is defined. Thus, both Example 2-15 and Example 2-16 defined earlier are inner product spaces. If the inner product space has the additional property of *completeness*, then it is defined to be a *Hilbert space*. Intuitively the notion of completeness means that there are no "missing" vectors that are arbitrarily close to vectors in the space but are not themselves in the space. Since the spaces used in this book are all complete and hence formally Hilbert spaces, we will not dwell on this property further. In the sequel, all linear spaces considered will be Hilbert spaces.

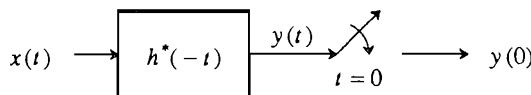


Figure 2-16. A matched filter.

2.6.3. Subspaces of Signal Space

A *subspace* of a linear space is a subset of the linear space that is itself a linear space. Roughly speaking this means that the sum of any two vectors in the subspace must also be in the subspace, and the product of any vector in the subspace by any scalar must also be in the subspace.

Example 2-19.

An example of a subspace in three-dimensional Euclidean space is either a line or a plane in the space, where in either case the vector $\mathbf{0}$ must be in the subspace. \square

Example 2-20.

A more general subspace is the set of vectors obtained by forming all possible weighted linear combinations of n vectors $\mathbf{X}_1, \dots, \mathbf{X}_n$. The subspace so formed is said to be *spanned* by the set of n vectors. This is illustrated in Figure 2-17 for three-dimensional Euclidean space. In Figure 2-17a, the subspace spanned by \mathbf{X} is the dashed line, which is infinite in length and co-linear with the vector \mathbf{X} . Any vector on this line can be obtained by multiplying \mathbf{X} by the appropriate scalar. In Figure 2-17b, the subspace spanned by \mathbf{X} and \mathbf{Y} is the plane of infinite extent (depicted by the dashed lines) that is determined by the two vectors. Any vector in this plane can be formed as a linear combination of the two vectors multiplied by appropriate scalars. \square

The *projection theorem* is an important result that can often be used to derive optimum filters and estimators. What follows is a statement of the projection theorem, which is proven in [1]:

(Projection Theorem) Given a subspace M of a Hilbert space H and a vector \mathbf{X} in H there is a unique vector $\mathbf{P}_M(\mathbf{X})$ in M called the *projection of \mathbf{X} on M* which has the property that

$$\langle \mathbf{X} - \mathbf{P}_M(\mathbf{X}), \mathbf{Y} \rangle = 0 \quad (2.81)$$

for every vector \mathbf{Y} in M . The notation \mathbf{P}_M denotes a *projection operator* that maps one vector \mathbf{X} into another vector $\mathbf{P}_M(\mathbf{X})$.

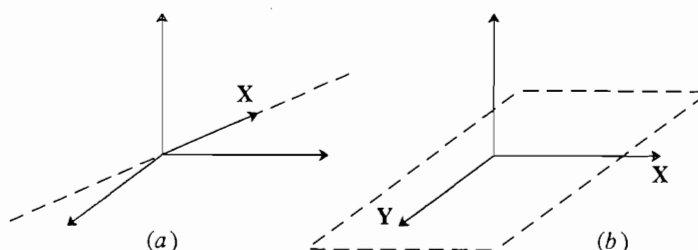


Figure 2-17. Subspaces in three-dimensional Euclidean space.

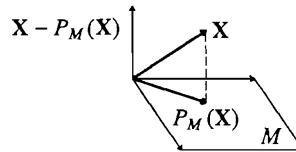


Figure 2-18. Illustration of projection for three-dimensional Euclidean space.

Example 2-21.

A projection is illustrated in Figure 2-18 for three-dimensional Euclidean space, where the subspace M is the plane formed by the x -axis and y -axis and \mathbf{X} is an arbitrary vector. The projection is the result of dropping a perpendicular line from \mathbf{X} down to the plane (this is the dashed line in Figure 2-18). The resulting vector $(\mathbf{X} - \mathbf{P}_M(\mathbf{X}))$ is the vector shown parallel to the dashed line. It is orthogonal to the plane M , and hence to every vector in M . \square

A consequence of the projection theorem is that the projection $\mathbf{P}_M(\mathbf{X})$ is the unique vector in M that is closest to \mathbf{X} .

Exercise 2-15.

Show that

$$\|\mathbf{X} - \mathbf{P}_M(\mathbf{X})\| < \|\mathbf{X} - \mathbf{Y}\| \quad (2.82)$$

for every $\mathbf{Y} \neq \mathbf{P}_M(\mathbf{X})$ in M . \square

This is illustrated geometrically in Figure 2-18, where the subspace M is a plane. The vector closest to \mathbf{X} is evidently the projection as shown, and any other vector in M is farther from \mathbf{X} .

2.6.4. Schwarz Inequality

A fundamental inequality that often gives bounds on the performance of a digital communication system is the *Schwarz inequality*.

Exercise 2-16.

Show that for two vectors \mathbf{X} and \mathbf{Y} in an inner product space,

$$|\langle \mathbf{X}, \mathbf{Y} \rangle| \leq \|\mathbf{X}\| \cdot \|\mathbf{Y}\| \quad (2.83)$$

with equality if and only if $\mathbf{X} = K \cdot \mathbf{Y}$ for some scalar K . \square

2.7. FURTHER READING

Many textbooks cover the topics of this chapter in a more introductory and complete fashion than we do here. McGillem and Cooper [2], Oppenheim and Willsky [3], and Ziemer, Tranter, and Fannin [4] are useful for techniques applicable to both continuous and discrete-time systems. For discrete-time techniques only, the texts by Oppenheim and Schafer [5] and Jackson [6] are recommended. For continuous-time systems, with some discussion of discrete-time systems, we recommend Schwarz and Friedland [7]. To explore the Fourier transform in more mathematical depth, we recommend Papoulis [8] and Bracewell [9].

APPENDIX 2-A SUMMARY OF FOURIER TRANSFORM PROPERTIES

The properties of both discrete and continuous-time Fourier transforms are summarized in this appendix. We define the even part $f_e(x)$ of a function $f(x)$ to be

$$f_e(x) = [f(x) + f^*(-x)]/2, \quad (2.84)$$

and the odd part $f_o(x)$ to be

$$f_o(x) = [f(x) - f^*(-x)]/2, \quad (2.85)$$

so for example,

$$X_e(e^{j\omega T}) = [X(e^{j\omega T}) + X^*(e^{-j\omega T})]/2. \quad (2.86)$$

We define the rectangular function as follows,

$$\text{rect}(x, X) = \begin{cases} 1; & |x| \leq X \\ 0; & |x| > X \end{cases}, \quad (2.87)$$

and the unit step function as

$$u(x) = \begin{cases} 1; & |x| \geq 0 \\ 0; & |x| < 0 \end{cases}. \quad (2.88)$$

FOURIER TRANSFORM SYMMETRIES

Continuous time	Discrete time
$x(t) \leftrightarrow X(j\omega)$	$x_k \leftrightarrow X(e^{j\omega T})$
$x(-t) \leftrightarrow X(-j\omega)$	$x_{-k} \leftrightarrow X(e^{-j\omega T})$
$x^*(t) \leftrightarrow X^*(-j\omega)$	$x_k^* \leftrightarrow X^*(e^{-j\omega T})$
$x^*(-t) \leftrightarrow X^*(j\omega)$	$x_{-k}^* \leftrightarrow X^*(e^{j\omega T})$
$\text{Re}\{x(t)\} \leftrightarrow X_c(j\omega)$	$\text{Re}\{x_k\} \leftrightarrow X_c(e^{j\omega T})$
$j\text{Im}\{x(t)\} \leftrightarrow X_o(j\omega)$	$j\text{Im}\{x_k\} \leftrightarrow X_o(e^{j\omega T})$
$x_e(t) \leftrightarrow \text{Re}\{X(j\omega)\}$	$x_{e,k} \leftrightarrow \text{Re}\{X(e^{j\omega T})\}$
$x_o(t) \leftrightarrow j\text{Im}\{X(j\omega)\}$	$x_{o,k} \leftrightarrow j\text{Im}\{X(e^{j\omega T})\}$

FOURIER TRANSFORMS PROPERTIES

Continuous time	Discrete time
$ax(t) + by(t) \leftrightarrow aX(j\omega) + bY(j\omega)$	$ax_k + by_k \leftrightarrow aX(e^{j\omega T}) + bY(e^{j\omega T})$
$x(t) * y(t) \leftrightarrow X(j\omega)Y(j\omega)$	$x_k * y_k \leftrightarrow X(e^{j\omega T})Y(e^{j\omega T})$
$x(t)y(t) \leftrightarrow \frac{1}{2\pi}X(j\omega) * Y(j\omega)$	$x_k y_k \leftrightarrow \frac{T}{2\pi} \int_{-\pi T}^{\pi T} X(e^{j\Omega T})Y(e^{j(\omega - \Omega)T})d\Omega$
$x(at) \leftrightarrow \frac{1}{ a }X(j\frac{\omega}{a})$	$x_{k-K} \leftrightarrow X(e^{j\omega T})e^{-j\omega KT}$
$x(t - \tau) \leftrightarrow X(j\omega)e^{-j\omega\tau}$	$e^{j\omega kT}x_k \leftrightarrow X(e^{j(\omega - \omega_0)T})$
$e^{j\omega_0 t}x(t) \leftrightarrow X(j\omega - j\omega_0)$	$\cos(\omega_0 kT)x_k \leftrightarrow \frac{1}{2}(X(e^{j(\omega - \omega_0)T}) + X(e^{j(\omega + \omega_0)T}))$
$\cos(\omega_0 t)x(t) \leftrightarrow \frac{1}{2}(X(j\omega - j\omega_0) + X(j\omega + j\omega_0))$	
$\frac{d^m x(t)}{dt^m} \leftrightarrow (j\omega)^m X(j\omega)$	
$(-jt)^m x(t) \leftrightarrow \frac{d^m X(j\omega)}{d\omega^m}$	
$\int_{-\infty}^t x(\tau)d\tau \leftrightarrow \frac{1}{j\omega}X(j\omega) + \pi\delta(\omega) \int_{-\infty}^{\infty} x(\tau)d\tau$	
$X(jt) \leftrightarrow 2\pi x(-\omega)$	

FOURIER TRANSFORM PAIRS¹

$e^{j\omega t}$	\leftrightarrow	$2\pi\delta(\omega - \omega_0)$	$e^{j\omega kT}$	\leftrightarrow	$\frac{2\pi}{T}\delta(\omega - \omega_0)$
$\delta(t - T)$	\leftrightarrow	$e^{-j\omega T}$	δ_{k-K}	\leftrightarrow	$e^{-j\omega KT}$
$\cos(\omega_0 t)$	\leftrightarrow	$\pi [\delta(\omega - \omega_0) + \delta(\omega + \omega_0)]$	$\cos(\omega_0 kT)$	\leftrightarrow	$\frac{\pi}{T}(\delta(\omega - \omega_0) + \delta(\omega + \omega_0))$
$\sin(\omega_0 t)$	\leftrightarrow	$\frac{1}{j}\pi [\delta(\omega - \omega_0) - \delta(\omega + \omega_0)]$	$\sin(\omega_0 kT)$	\leftrightarrow	$\frac{\pi}{jT}(\delta(\omega - \omega_0) - \delta(\omega + \omega_0))$
$\frac{\sin(Wt)}{Wt}$	\leftrightarrow	$\frac{\pi}{W}\text{rect}(\omega, W)$	$\frac{\sin(WkT)}{WkT}$	\leftrightarrow	$\frac{\pi}{WT}\text{rect}(\omega, W)$
$e^{-\alpha t}u(t)$	\leftrightarrow	$\frac{1}{j\omega + \alpha}; \text{Re}\{\alpha\} > 0$	$r^{-k}u_k$	\leftrightarrow	$\frac{1}{1 - r^{-1}e^{-j\omega T}}$
$u(t)$	\leftrightarrow	$\pi\delta(\omega) + \frac{1}{j\omega}$	$\sum_{k=-\infty}^{\infty} \delta(t - kT)$	\leftrightarrow	$\frac{2\pi}{T} \sum_{m=-\infty}^{\infty} \delta(\omega - \frac{2\pi}{T}m)$
$\sum_{k=-\infty}^{\infty} \delta(t - kT)$	\leftrightarrow	$\frac{2\pi}{T} \sum_{m=-\infty}^{\infty} \delta(\omega - \frac{2\pi}{T}m)$	$\text{rect}(t, T)$	\leftrightarrow	$2T \frac{\sin(\omega T)}{\omega T}$
$\frac{1}{jt}$	\leftrightarrow	$-\pi \text{sgn}(\omega)$	$\sum_{m=-\infty}^{\infty} \delta_{k-mN}$	\leftrightarrow	$\frac{2\pi}{NT} \sum_{m=-\infty}^{\infty} \delta(\omega - \frac{2\pi}{NT}m)$

APPENDIX 2-B
SPECTRAL FACTORIZATION

In this appendix we will derive the spectral factorization (2.55) of a rational transfer function that is non-negative real on the unit circle, and also derive the geometric mean representation of A^2 .

Exercise 2-17.

The purpose of this exercise is to show that any transfer function $S(z)$ that is real valued (not necessarily non-negative) on the unit circle, must have conjugate-reciprocal pole pairs and zero pairs.

- (a) Show that if $S(e^{j\omega T})$ is real valued for all ω , then the inverse Fourier transform s_k is conjugate symmetric, $s_k = s_{-k}^*$.
- (b) Show that the symmetry relationship in (a) implies (2.54). Hence, (2.54) is valid for any $S(z)$ that is real valued on the unit circle. \square

We can now study how the general factorization of (2.44) is modified for the non-negative real transfer function. Equation (2.44) tells us that for any stable $S(z)$ there exist monic strictly minimum-phase and strictly maximum-phase transfer functions

¹ The discrete-time Fourier transform expressions are valid in the range $-\pi/T \leq \omega \leq \pi/T$. To extend this range, the given expression should be repeated periodically.

such that

$$S(z) = B \cdot z^L H_{\min}(z) H_{\max}(z) H_{\text{zero}}(z), \quad (2.89)$$

where $H_{\min}(z)$ includes all zeros and poles inside the unit circle, $H_{\max}(z)$ includes all zeros and poles outside the unit circle, and $H_{\text{zero}}(z)$ includes all zeros on the unit circle. Exercise 2-17 implies that $H_{\min}(z) = H_{\max}^*(1/z^*)$, since poles and zeros come in conjugate-reciprocal pairs. Thus, the minimum-phase and maximum-phase parts are each reflected transfer functions of the other. Since they are reflected, we know that they are the complex conjugate of one another on the unit circle, and hence the contribution of $H_{\min}(z) H_{\max}(z)$ is real and non-negative on the unit circle.

Unfortunately, Exercise 2-17 does not tell us anything new about $H_{\text{zero}}(z)$, since for $|z| = 1$, it is automatically true that $z = 1/z^*$. We thus have to investigate further the nature of $B \cdot z^L H_{\text{zero}}(z)$. In particular, we are interested in whatever restrictions there are on its zeros in order for it to be real valued, or non-negative real valued.

Exercise 2-18.

Establish the following necessary and sufficient conditions on $B \cdot z^L H_{\text{zero}}(z)$ to be real valued on the unit circle: if its zeros are at $z_i = e^{j\theta_i}$, $1 \leq i \leq K$, then we must have that $K = 2L$ (the number of zeros on the unit circle must be even), and the constant coefficient B must be of the form

$$B = C \exp\left\{-j \sum_{i=1}^{2L} \theta_i/2\right\} \quad (2.90)$$

for any real-valued constant C . \square

The role of the z^L term is to force $z^L H_{\text{zero}}(z)$ to have the same number of terms in positive and negative powers of z (recall that $H_{\text{zero}}(z)$ is by assumption causal and monic, and hence only has non-positive powers of z). Exercise 2-18 says that any transfer function with zeros on the unit circle is real valued, as long as the number of zeros is even, the constant coefficient has the proper phase, and it is multiplied by the proper power of z . Exercise 2-18 still doesn't answer the question of when $B \cdot z^L H_{\text{zero}}(z)$ is non-negative real valued.

Exercise 2-19.

Show that when the conditions of Exercise 2-18 are satisfied, the resulting transfer function is non-negative real valued on the unit circle if and only if it has L double zeros and the constant C is of the form $C = (-1)^L A^2$ where A is real valued. \square

We can now assert that if $S(z)$ is non-negative real,

$$\begin{aligned} B \cdot z^L H_{\text{zero}}(z) &= (-1)^L A^2 \prod_{i=1}^L e^{-j\theta_i} z^L \prod_{i=1}^L (1 - e^{j\theta_i} z^{-1})^2 \\ &= A^2 \prod_{i=1}^L (1 - e^{-j\theta_i} z)(1 - e^{j\theta_i} z^{-1}), \end{aligned} \quad (2.91)$$

which is of the form of the product of a transfer function times its reflected transfer

function. Hence, combining (2.91) with (2.89), we obtain the spectral factorization (2.55).

To study the multiplicative constant A^2 , replace z by $(e^{j\omega T})$ in (2.56) to get

$$S(e^{j\omega T}) = A^2 \frac{\prod_{k=1}^M |1 - c_k e^{-j\omega T}|^2}{\prod_{k=1}^N |1 - d_k e^{-j\omega T}|^2}, \quad |c_k| \leq 1, \quad |d_k| < 1. \quad (2.92)$$

Taking the logarithm of both sides (the base does not matter), and then integrating over the full Nyquist bandwidth,

$$\begin{aligned} \frac{T}{2\pi} \int_{-\pi/T}^{\pi/T} \log S(e^{j\omega T}) d\omega &= \log A^2 + \sum_{k=1}^M \frac{T}{2\pi} \int_{-\pi/T}^{\pi/T} \log |1 - c_k e^{-j\omega T}|^2 d\omega \\ &\quad - \sum_{k=1}^N \frac{T}{2\pi} \int_{-\pi/T}^{\pi/T} \log |1 - d_k e^{-j\omega T}|^2 d\omega. \end{aligned} \quad (2.93)$$

Fortunately, the last two terms are zero. To see this, write c_k or d_k in polar form as $a^{j\theta}$, where $0 < |a| \leq 1$. Then we wish to evaluate the integral

$$\frac{T}{2\pi} \int_{-\pi/T}^{\pi/T} \log |1 - ae^{j\theta} e^{-j\omega T}|^2 d\omega. \quad (2.94)$$

After some manipulation (see Problem 2-30), this becomes

$$\frac{1}{\pi} \int_0^\pi \log (1 + a^2 - 2a \cdot \cos \omega) d\omega = 0. \quad (2.95)$$

Note that the angle θ of the pole or zero does not affect the integral. Integral (2.95) can be found in standard integral tables, which show that it evaluates to zero. Thus, we have established (2.57). While (2.57) was derived only for rational spectra, both the spectral factorization (2.55) and the geometric mean formula (2.57) apply to general (non-rational) spectra as well.

PROBLEMS

- 2-1.** A system with a complex-valued input and output can be described in terms of systems with real-valued inputs and outputs, as shown in Figure 2-2. Show that if the impulse response of the system is real-valued, then there is no crosstalk (or cross-coupling) between the real and imaginary parts, whereas if the impulse response is complex-valued then there is crosstalk.
- 2-2.**
- (a) Show that $e^{j\omega t}$ is an *eigenfunction* of a continuous-time LTI system with impulse response $h(t)$, meaning that the response to this input is the same complex exponential multiplied by a complex constant called the *eigenvalue*.
 - (b) Repeat for a discrete-time LTI system with impulse response h_k .

- (c) Show that for a fixed ω the eigenvalue in (b) is the Fourier transform $H(e^{j\omega T})$ of the discrete-time impulse response h_k . Specifically, show that when the input is $e^{j\omega kT}$, the output can be written

$$y_k = H(e^{j\omega T})e^{j\omega kT}. \quad (2.96)$$

Hence that magnitude response $|H(e^{j\omega T})|$ gives the gain of the system at each frequency, and the phase response $\arg(H(e^{j\omega T}))$ gives the phase change.

- 2-3. Consider the mixed discrete and continuous-time system in Figure 2-19.

- (a) Find the Fourier transform of $y(t)$.
- (b) Is the system linear? Justify.
- (c) Find conditions on $G(j\omega)$, $H(e^{j\omega T})$, and/or $F(j\omega)$ such that the system is time invariant.

- 2-4. Derive the following *Parseval's relationships* for the energy of a signal:

$$\int_{-\infty}^{\infty} |x(t)|^2 dt = \frac{1}{2\pi} \int_{-\infty}^{\infty} |X(j\omega)|^2 d\omega, \quad \sum_{m=-\infty}^{\infty} |x_m|^2 = \frac{T}{2\pi} \int_{-\pi/T}^{\pi/T} |X(e^{j\omega T})|^2 d\omega. \quad (2.97)$$

- 2-5. Given that a discrete-time signal x_k is obtained from a continuous-time signal $x(t)$ by sampling, can you relate the energy of the discrete-time signal to the energy of the continuous-time signal? What if the continuous-time signal is known to be properly bandlimited?
- 2-6. Given a discrete-time system with impulse response $h_k = \delta_k + \delta_{k-1}$, what is its transfer function and frequency response? If the input is $x_k = \cos(\omega_0 kT)$ what is the output? Show that the system has a phase response that is piecewise linear in frequency ω_0 .
- 2-7. Show that the phase response $\theta(\omega) = \arg(H(j\omega))$ of a real system is anti-symmetric.
- 2-8. What is the impulse response of a real system that produces a constant phase shift of θ and unity gain at all frequencies? Such a system is called a *phase shifter*.
- 2-9. Find the Fourier transform of
- $$x(t) = \sum_{m=-\infty}^{\infty} \frac{1}{j(t-mT) + \alpha}.$$
- 2-10. Show that the output of an LTI system cannot contain frequencies not present in the input.
- 2-11. Sketch both a QAM modulator and demodulator for two information-bearing signals $a(t)$ and $b(t)$, where your sketch includes real-valued signals only.
- 2-12.
- (a) Find an way to implement a general demodulator without using a phase splitter. Hint: You will need a lowpass filter.

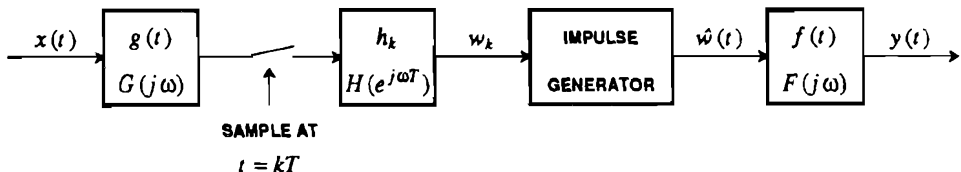


Figure 2-19. A mixed continuous and discrete-time system.

- (b) Repeat Problem 2-11 for this demodulator representation.

2-13.

- (a) Using (2.7), show that for any complex number z , the sequence z^k is an eigenfunction of a discrete-time LTI system. That is, the response to this signal is

$$y_k = H(z)z^k. \quad (2.98)$$

- (b) How is this related to the frequency response result discussed in Problem 2-2, part c?

2-14. Repeat Problem 2-13 using only the definition of a discrete-time LTI system and not using the convolution sum. (Hint: Note that $z^{k+m} = z^k z^m$.)

2-15. Calculate the Z transform of

$$x_k = a^k u_k, \quad u_k = \begin{cases} 1; & k \geq 0 \\ 0; & k < 0 \end{cases} \quad (2.99)$$

where u_k is the *unit step* function.

2-16. Show that for any complex number z , z^t is an eigenfunction of any continuous-time LTI system. Also show that for any z there exists an s such that $e^{st} = z^t$. Relate the eigenvalue of the system for a fixed z to the *Laplace transform*

$$H(s) = \int_{-\infty}^{\infty} e^{-st} h(t) dt. \quad (2.100)$$

The Fourier transform is the Laplace transform evaluated at $s = j\omega$, which explains the notation $H(j\omega)$ used in this book.

2-17.

- (a) Show that the signals

$$x_k = \begin{cases} a^k, & k \geq 0 \\ 0, & k < 0 \end{cases} \quad y_k = \begin{cases} -a^k, & k < 0 \\ 0, & k \geq 0 \end{cases} \quad (2.101)$$

have the same Z transform.

- (b) What are the ROC for the two cases?
(c) Under what conditions are the two signals stable? Relate this to the ROC.

2-18. Let

$$X(z) = \frac{z}{z - a} \quad (2.102)$$

and find the time domain signals for both possible ROC. Do this directly without using the results of Problem 2-17.

2-19. Given

$$X(z) = \frac{z^2}{z^2 - (a + b)z + ab} \quad (2.103)$$

where $|a| < 1 < |b|$, find the corresponding time-domain signal for the following two cases:

- (a) The time domain signal is known to be causal.
(b) The time domain signal is known to be neither causal nor anti-causal.
(c) Comment on whether the signal is stable in each case, and state your reasons.

2-20. Show that when the transfer function $H(z)$ given in (2.33) has real-valued coefficients, the zeros and poles are always either real valued or come in complex-conjugate pairs.

- 2-21. Given a transfer function in the middle form of (2.33) with $r = 0$, $A = 1$, zeros at $1.5 \cdot e^{\pm j\pi/4}$ and $\pm j$, and poles at $0.5 \cdot e^{\pm j\pi/8}$. Find all the terms in the factorization (2.44). Write them in terms of polynomials with *real-valued* coefficients.

2-22.

- (a) Let h_k be a causal strictly minimum-phase sequence with a rational Z transform, and let g_k be another causal sequence obtained by taking a zero of $H(z)$ at c and replacing it with a zero at $1/c^*$. Show that $|H(e^{j\omega T})| = |G(e^{j\omega T})|$. Hint: Find a transfer function $A(z)$ that when multiplied by $H(z)$ yields $G(z)$.
- (b) Show that

$$\sum_{k=0}^N |h_k|^2 \geq \sum_{k=0}^N |g_k|^2 \quad (2.104)$$

for all $N \geq 0$. Hint: Define $F(z) = H(z)/(1 - cz^{-1})$ and write g_k and h_k in terms of f_k .

- (c) Show that for any two rational transfer functions $H(z)$ and $G(z)$ such that $H(z)$ is minimum phase and $|H(e^{j\omega T})| = |G(e^{j\omega T})|$, (2.104) is true for all $N \geq 0$.

Thus, among all sequences with the same magnitude response, minimum-phase sequences are maximally concentrated near $k = 0$ in the mean-square sense. From Parseval's formula plus the unit magnitude of an allpass filter, clearly both sides of (2.104) approach one another as $N \rightarrow \infty$.

- 2-23. Pass a causal input signal x_k through a first-order stable causal allpass filter such as that in Example 2-9 to yield a causal output signal y_k . Show that for any $N \geq 0$

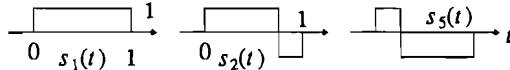
$$\sum_{k=0}^N |x_k|^2 \geq \sum_{k=0}^N |y_k|^2 \quad (2.105)$$

and hence the allpass filter is dispersive in the sense that it reduces the signal energy in the first N samples while keeping the total signal energy the same (since it has unit magnitude frequency response). Hint: Consider a solution method similar to Problem 2-22.

- 2-24. Use (2.44) and Example 2-11 to derive the factorization in (2.43).

- 2-25. What is the frequency response of the matched filter in Figure 2-16?

- 2-26. Given three signals S_1 , S_2 , and S_5 :



- (a) Find the norm of S_1 and S_2 and the inner product of these two signals in signal space. What is the angle between the two signals?
- (b) Find the norm of the signal $S_1 + S_2$.
- (c) Find a signal S_3 that is orthogonal to both S_1 and S_2 .
- (d) Find a signal S_4 that is in the subspace spanned by S_1 and S_2 and is orthogonal to S_1 .
- (e) Find the signal in the subspace spanned by S_1 and S_2 that is closest to S_5 .

- 2-27. Consider the space of all finite-energy continuous-time signals that are bandlimited to W radians/sec.

- (a) Show that this set of signals B is a subspace of signal space.
- (b) Characterize the subspace consisting of all signals orthogonal to every signal in B .
- (c) Find the projection of the signal S_1 in Problem 2-26 on B for $W = 1$.

- 2-28. Given two subspaces M_1 and M_2 of a Hilbert space, they are orthogonal if every vector in M_1 is orthogonal to every vector in M_2 . The sum of the two subspaces $M_1 \oplus M_2$ is the subspace consisting of vectors that are the sum of a vector in M_1 and a vector in M_2 . Given two orthogonal subspaces M_1 and M_2 of a Hilbert space H and an arbitrary vector X in H , show that the

projection of \mathbf{X} on $M_1 \oplus M_2$ can be expressed uniquely as

$$\mathbf{P}_{M_1 \oplus M_2}(\mathbf{X}) = \mathbf{P}_{M_1}(\mathbf{X}) + \mathbf{P}_{M_2}(\mathbf{X}), \quad (2.106)$$

or in words the sum of the projection on M_1 and the projection on M_2 .

- 2-29. Given a transmitted pulse $h(t)$ it is useful to define an *autocorrelation function*

$$\rho_h(k) = \int_{-\infty}^{\infty} h(t)h^*(t-kT) dt. \quad (2.107)$$

Show that

$$|\rho_h(k)| \leq \rho_h(0), \quad (2.108)$$

or in words, the autocorrelation function of a pulse can never be larger than the energy of the pulse.

- 2-30. Show that (2.95) is equivalent to (2.94).

REFERENCES

1. A. W. Naylor and G. R. Sell, *Linear Operator Theory in Engineering and Science*, Holt, Rinehart and Winston, Inc., New York (1971).
2. C. D. McGillem and G. R. Cooper, *Continuous and Discrete Signal and System Analysis*, Holt, Rinehart, and Winston (1984).
3. A. V. Oppenheim, A. S. Willsky, and Ian T. Young, *Signals and Systems*, Prentice Hall (1983).
4. R. E. Ziemer, W. H. Tranter, and D. R. Fannin, *Signals and Systems: Continuous and Discrete*, Macmillan Publishing Co., NY (1983).
5. A. V. Oppenheim and R. W. Schafer, *Discrete-Time Signal Processing*, Prentice-Hall, Inc. (1989).
6. L. Jackson, *Digital Filters and Signal Processing*, Kluwer Academic Publishers, Boston, MA (1985).
7. R. J. Schwarz and B. Friedland, *Linear Systems*, McGraw-Hill Book Co. (1965).
8. A. Papoulis, *The Fourier Integral and its Applications*, McGraw-Hill Book Co., New York (1962).
9. R. N. Bracewell, *The Fourier Transform and its Applications*, McGraw-Hill Book Co., New York (1965).

3

STOCHASTIC SIGNAL PROCESSING

Although modulation and demodulation are deterministic, the information to be transmitted over a communication system, as well as the noise encountered in the physical transmission medium, is random or stochastic. These phenomena cannot be predicted in advance, but they have certain predictable characteristics which can be summarized in a random process model. The design of a digital communication system heavily exploits these characteristics.

In this chapter we review the notation that will be used for random variables and processes, and cover several topics in detail that may be new to some readers and are particularly important in the sequel. These include Chernoff bounding techniques, Bayes' rule, and mixtures of discrete-time and continuous-time random processes. Markov chains are discussed in Section 3.3, and will be used in a diverse set of applications in Chapters 9, 10, 12-14, and 19. Section 3.4, on Poisson processes, uses the Markov chain results to describe Poisson processes and shot noise, which will be important to the understanding of optical fiber systems in Chapters 5 and 8.

3.1. RANDOM VARIABLES

Before reviewing the theory of the stochastic process, we review some theory and notation associated with random variables. In digital communication it is common to encounter combinations of discrete and continuous-valued random variables,

so this will be emphasized.

We denote a *random variable* by a capital letter, such as X , and an *outcome* of the random variable by a lower-case letter, such as x . The random variable is a real or complex-valued function defined on the *sample space* Ω of all possible outcomes. An *event* E is a set of possible outcomes and is assigned a probability, written $\Pr[E]$, where $0 \leq \Pr[E] \leq 1$. Since an event is a set, we can define the union of two events, $E_1 \cup E_2$ or the intersection of events $E_1 \cap E_2$. The basic formula

$$\Pr[E_1 \cup E_2] = \Pr[E_1] + \Pr[E_2] - \Pr[E_1 \cap E_2] \quad (3.1)$$

leads to the very useful *union bound*,

$$\Pr[E_1 \cup E_2] \leq \Pr[E_1] + \Pr[E_2]. \quad (3.2)$$

The *cumulative distribution function* (*c.d.f.*) of a real valued random variable X is the probability of the event $X \leq x$,

$$F_X(x) = \Pr[X \leq x]. \quad (3.3)$$

Where there can be no confusion, we often omit the subscript, writing the c.d.f. as $F(x)$. For a complex-valued random variable Y ,

$$F_Y(y) = \Pr[\operatorname{Re}\{Y\} \leq \operatorname{Re}\{y\}, \operatorname{Im}\{Y\} \leq \operatorname{Im}\{y\}]. \quad (3.4)$$

For a continuous real-valued random variable, the *probability density function* (*p.d.f.*) $f_X(x)$ is defined such that for any interval $I \subset \mathbb{R}$

$$\Pr[X \in I] = \int_I f_X(x) dx. \quad (3.5)$$

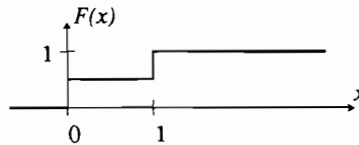
For a complex-valued random variable, I is a region in the complex plane. For a real-valued random variable X ,

$$f_X(x) = \frac{d}{dx} F_X(x), \quad (3.6)$$

where the derivative exists. We will often use the generalized derivative, so that when the c.d.f. includes a step function the corresponding p.d.f. has a Dirac delta function.

Example 3-1.

For the c.d.f. shown below,



the p.d.f. consists exclusively of Dirac delta functions,

$$f(x) = 0.5 \cdot \delta(x) + 0.5 \cdot \delta(x-1). \quad (3.7)$$

Such a density is characteristic of a discrete random variable. \square

For a discrete-valued random variable X , we will denote the probability of an outcome $x \in \Omega$ as

$$p_X(x) = \Pr[X = x], \quad (3.8)$$

where we will again omit the subscript where there can be no confusion. The p.d.f. can be written as

$$f_X(x) = \sum_{y \in \Omega_X} p_X(y) \delta(x - y). \quad (3.9)$$

The *expected value* or *mean* of X is defined as

$$\mathbb{E}[X] = \int_{-\infty}^{\infty} x f_X(x) dx \quad \text{or} \quad \mathbb{E}[X] = \sum_{x \in \Omega} x \cdot p_X(x), \quad (3.10)$$

for continuous-valued and discrete-valued random variables, respectively. For a complex-valued random variable Y , we integrate over the complex plane,

$$\mathbb{E}[Y] = \int_{-\infty}^{\infty} \int_{-\infty}^{\infty} (x + iz) f_Y(x + iz) dx dz. \quad (3.11)$$

The *fundamental theorem of expectation* states that if $g(\cdot)$ is any function defined on the sample space of X , then

$$\mathbb{E}[g(X)] = \int_{-\infty}^{\infty} g(x) f_X(x) dx. \quad (3.12)$$

Especially important expectations are the mean and variance, defined as

$$\mu = \mathbb{E}[X], \quad \sigma_X^2 = \mathbb{E}[(X - \mathbb{E}[X])^2] = \mathbb{E}[X^2] - \mathbb{E}[X]^2. \quad (3.13)$$

For complex-valued random variables, the variance is defined similarly as

$$\sigma_X^2 = \mathbb{E}[|X|^2] - |\mathbb{E}[X]|^2 = \mathbb{E}[XX^*] - \mathbb{E}[X]\{\mathbb{E}[X]\}^*. \quad (3.14)$$

The *joint c.d.f.* of two real-valued random variables X and Y is

$$F_{X,Y}(x, y) = \Pr(X \leq x, Y \leq y) = \int_{-\infty}^x \int_{-\infty}^y f_{X,Y}(\alpha, \beta) d\alpha d\beta, \quad (3.15)$$

where $f_{X,Y}(x, y)$ is the *joint p.d.f.*. The joint p.d.f. can be written in terms of the joint c.d.f. as

$$f(x, y) = \frac{\partial^2}{\partial x \partial y} F(x, y), \quad (3.16)$$

where we have omitted the subscripts as before. The *marginal density* $f_X(x)$ of a random variable X can be found from the joint p.d.f. from

$$f_X(x) = \int_{-\infty}^{\infty} f_{X,Y}(x, y) dy. \quad (3.17)$$

The random variables X and Y are *independent* or *statistically independent* if for all intervals I and J ,

$$\Pr[X \in I \cap Y \in J] = \Pr[X \in I] \Pr[Y \in J] , \quad (3.18)$$

which is equivalent to

$$f_{X,Y}(x,y) = f_X(x)f_Y(y) \quad \text{or} \quad F_{X,Y}(x,y) = F_X(x)F_Y(y) . \quad (3.19)$$

Independence implies that the *cross-correlation* is

$$E[XY] = E[X]E[Y] . \quad (3.20)$$

When (3.20) is satisfied, the random variables are said to be *uncorrelated*. Two random variables can be uncorrelated and yet not be independent.

3.1.1. Moment Generating Function and Chernoff Bound

The *characteristic function* of X is defined as

$$\Phi_X(s) = E[e^{sx}] = \int_{-\infty}^{\infty} e^{sx} f_X(x) dx \quad (3.21)$$

for a complex variable s . This is the Laplace transform of $f_X(x)$ evaluated at $x = -s$. When s is real-valued, which will suffice for applications in this book, (3.21) is called the *moment generating function*.

Exercise 3-1.

Define $Z = X + Y$ where X and Y are independent, and show that

$$\Phi_Z(s) = \Phi_X(s)\Phi_Y(s) . \quad (3.22)$$

□

Exercise 3-2.

Show that

$$E[X] = \frac{\partial}{\partial s} \Phi_X(s) \Big|_{s=0}, \quad E[X^2] = \frac{\partial^2}{\partial s^2} \Phi_X(s) \Big|_{s=0} . \quad (3.23)$$

□

The *Chernoff bound*, based on the moment generating function, is very useful for bounding the tail probability for a random variable where an exact evaluation is intractable.

Exercise 3-3.

- (a) Show that the probability of event $X > x$ is bounded by

$$1 - F_X(x) = \Pr[X > x] \leq e^{-sx} \Phi_X(s) \quad (3.24)$$

for any real-valued $s \geq 0$. This establishes that the tail of the p.d.f. decreases at least exponentially for any distribution for which the moment generating function exists. (Hint: Write the probability as the integral against a step function, and bound the step function by an exponential.)

(b) Find the similar bound

$$F_X(x) \leq e^{sx} \Phi_X(-s) \quad (3.25)$$

for $s \geq 0$.

(c) Show that the s that minimizes the bound (makes it tightest) in (a) and (b) must satisfy

$$x \Phi_X(s) = \frac{\partial \Phi_X(s)}{\partial s}, \quad -x \Phi_X(-s) = \frac{\partial \Phi_X(-s)}{\partial s}, \quad (3.26)$$

respectively. \square

3.1.2. Conditional Probabilities and Bayes' Rule

The *conditional probability* that a continuous-valued random variable X is in the interval I given that Y is in the interval J is defined for all J such that $\Pr[Y \in J] \neq 0$ to be

$$\Pr[X \in I | Y \in J] = \frac{\Pr[X \in I \cap Y \in J]}{\Pr[Y \in J]}, \quad (3.27)$$

where $\Pr[Y \in J]$ is called a *marginal probability* because it does not consider the possible effects of X on Y . For complex or vector-valued random variables, I and J are regions or volumes, rather than intervals. If X and Y are independent, then $\Pr[X \in I | Y \in J] = \Pr[X \in I]$. The joint probability can be written in terms of the conditional probabilities,

$$\Pr[X \in I \cap Y \in J] = \Pr[X \in I | Y \in J] \Pr[Y \in J]. \quad (3.28)$$

Equivalently,

$$f_{X|Y}(x|y) = \frac{f_{X,Y}(x,y)}{f_Y(y)}, \quad (3.29)$$

where $f_Y(y)$ is called a *marginal density*.

The *conditional density* $f_{X|Y}(x|y)$ is well defined only for y such that $f_Y(y) \neq 0$. Since $f_{X,Y}(x,y) = f_{Y,X}(y,x)$, (3.29) implies that

$$f_{X|Y}(x|y)f_Y(y) = f_{Y|X}(y|x)f_X(x), \quad (3.30)$$

which is a form of *Bayes' rule*.

It is common in digital communication systems to encounter both discrete-valued and continuous-valued random variables in the same system. In this case, (3.30) has Dirac delta functions.

Exercise 3-4.

Suppose that Y is discrete-valued and X is continuous-valued. Show that by integrating (3.30) over small intervals about y , we get the mixed form of Bayes' rule,

$$f_{X|Y}(x|y)p_Y(y) = p_{Y|X}(y|x)f_X(x). \quad (3.31)$$

This involves both probabilities and probability density functions. It has no delta functions as long as X is continuous-valued. If X is also discrete-valued, show that then

$$p_{X|Y}(x|y)p_Y(y) = p_{Y|X}(y|x)p_X(x), \quad (3.32)$$

which has only discrete probabilities. \square

For discrete-valued distributions, the marginal probability can be written in terms of the conditional probabilities as

$$p_Y(y) = \sum_{x \in \Omega} p_{Y|X}(y|x)p_X(x) = \sum_{x \in \Omega} p_{Y,X}(y,x), \quad (3.33)$$

where Ω is the countable sample space for X . This relation shows us how to obtain the marginal probabilities of a random variable given only joint probabilities, or given only conditional probabilities and the marginal probabilities of the other random variable. Using this relation, we can write the conditional probability of X given Y in terms of the conditional probability of Y given X and the marginal probability of X

$$p_{X|Y}(x|y) = \frac{p_{Y|X}(y|x)p_X(x)}{\sum_{x \in \Omega_X} p_{Y|X}(y|x)p_X(x)}. \quad (3.34)$$

This relation is known as *Bayes' theorem*. The analogous Bayes' theorem for continuous-valued random variables is

$$f_{X|Y}(x|y) = \frac{f_{Y|X}(y|x)f_X(x)}{\int\limits_{x \in \Omega_X} f_{Y|X}(y|x)f_X(x) dx}. \quad (3.35)$$

3.1.3. Gaussian Random Variables and the Central Limit Theorem

A *Gaussian* or *normal* random variable has the p.d.f.

$$f_X(x) = \frac{1}{\sigma\sqrt{2\pi}} e^{-(x-\mu)^2/2\sigma^2}, \quad (3.36)$$

where σ^2 is the variance and μ is the mean. The c.d.f. can be expressed only as an integral,

$$F_X(x) = \frac{1}{\sigma\sqrt{2\pi}} \int_{-\infty}^x e^{-(\alpha-\mu)^2/2\sigma^2} d\alpha \quad (3.37)$$

for which there is no closed-form expression. The *standard Gaussian* random variable is a zero-mean Gaussian random variable X with variance $\sigma^2 = 1$. The *complementary distribution function* of this standard Gaussian is denoted by the special notation $Q(x)$,

$$Q(x) = \Pr[X > x] = 1 - F_X(x) = \frac{1}{\sqrt{2\pi}} \int_x^\infty e^{-\alpha^2/2} d\alpha. \quad (3.38)$$

$Q(x)$, therefore, is the integral of the tail of the Gaussian density. It is plotted in Figure 3-1 using a log scale for probability. The function is related to the well-tabulated *error function* ($\text{erf}(x)$) and the *complementary error function* ($\text{erfc}(x)$) by

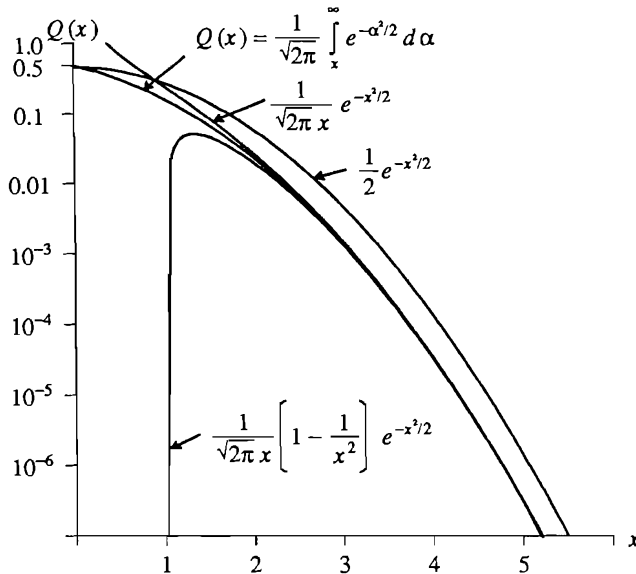


Figure 3-1. The probability $Q(x)$ that a zero-mean, unit-variance Gaussian random variable X (the standard Gaussian) exceeds x , plotted on a log scale.

$$Q(x) = \frac{1}{2} \operatorname{erfc}\left[\frac{x}{\sqrt{2}}\right] = \frac{1}{2} \left[1 - \operatorname{erf}\left[\frac{x}{\sqrt{2}}\right]\right]. \quad (3.39)$$

Exercise 3-5.

Show that for a Gaussian random variable X with mean μ and variance σ^2 ,

$$\Pr[X > x] = Q\left(\frac{x - \mu}{\sigma}\right). \quad (3.40)$$

□

Although $Q(\cdot)$ can only be tabulated or numerically determined, a useful bound follows from the Chernoff bound of Exercise 3-3.

Exercise 3-6.

- (a) Show that the moment generating function of a Gaussian random variable with mean μ and variance σ^2 is

$$\log_e \Phi_X(s) = \mu s + \sigma^2 s^2 / 2. \quad (3.41)$$

- (b) Show from the Chernoff bound (Exercise 3-3) that

$$1 - F_X(x) \leq e^{-(x - \mu)^2 / 2\sigma^2} \quad (3.42)$$

and thus that

$$Q(x) \leq e^{-x^2/2}. \quad (3.43)$$

□

Tighter bounds are derived in Problem 3-3 and plotted in Figure 3-1.

Use of the Gaussian distribution for modeling noise phenomena can be justified on physical grounds by the *central limit theorem*. It states, roughly, that the Gaussian distribution is a good model for the cumulative effect of a large number of independent random variables, regardless of the nature of their individual distributions. More precisely, let $\{Y_i\}$ for $1 \leq i \leq N$ denote a set of N statistically independent zero-mean random variables, each with the same p.d.f. $f_{Y_i}(y) = f(y)$ and finite variance σ^2 . That is, the random variables are *independent and identically distributed* (i.i.d.). Define a random variable Z that is a normalized sum of the Y_i ,

$$Z = \frac{1}{\sqrt{N}} \sum_{i=1}^N Y_i. \quad (3.44)$$

Then the distribution function of Z approaches Gaussian, $(1 - Q(z/\sigma))$, as $N \rightarrow \infty$. If each random variable Y_i represents some individual physical phenomenon, and Z is the cumulative effect of these phenomena, then as N gets large, the distribution of Z becomes Gaussian, regardless of the distribution of each Y_i .

In view of this theorem, it is hardly surprising that the sum of independent Gaussian random variables is Gaussian.

Exercise 3-7.

For an arbitrary linear combination of N zero mean independent Gaussian random variables X_i , each with variance σ^2 ,

$$Z = a_1 X_1 + \cdots + a_N X_N, \quad (3.45)$$

use the moment generating function to show that Z is itself zero-mean Gaussian with variance

$$\sigma_Z^2 = (a_1^2 + \cdots + a_N^2)\sigma^2. \quad (3.46)$$

□

Two zero-mean Gaussian random variables with variance σ^2 are *jointly Gaussian* if their joint p.d.f. is

$$f_{X,Y}(x, y) = \frac{1}{2\pi\sigma^2\sqrt{1-\rho^2}} \exp\left[-\frac{x^2 - 2\rho xy + y^2}{2\sigma^2(1-\rho^2)}\right], \quad (3.47)$$

where ρ is called the *correlation coefficient*,

$$\rho = \frac{\text{E}[XY]}{\sigma^2}. \quad (3.48)$$

Note that $-1 \leq \rho \leq 1$, and if X and Y are uncorrelated then $\rho = 0$.

Exercise 3-8.

Show that two jointly Gaussian random variables are statistically independent if and only if they are uncorrelated. \square

This definition can be extended to $N > 2$ jointly Gaussian random variables. If a random vector \mathbf{X} has components that are jointly zero-mean independent Gaussian random variables with the same variance σ^2 , then the joint p.d.f. is

$$f_{\mathbf{X}}(\mathbf{x}) = \frac{1}{(2\pi)^{M/2}\sigma^M} \exp\left(-\frac{1}{2\sigma^2} \|\mathbf{x}\|^2\right), \quad (3.49)$$

where M is the number of components in the vector and $\|\mathbf{x}\|$ is the Euclidean norm (2.73) of the vector. When \mathbf{X} is complex-valued with independent real and imaginary parts, (3.49) still holds. Any linear combination of jointly Gaussian random variables is Gaussian (as we saw in Exercise 3-7 for independent zero-mean Gaussian random variables).

This can be further generalized. A vector \mathbf{X} with M jointly Gaussian real-valued random variables has p.d.f.

$$f_{\mathbf{X}}(\mathbf{x}) = \frac{1}{(2\pi)^{M/2} |\mathbf{C}_{\mathbf{X}}|^{1/2}} \exp\left(-\frac{1}{2} (\mathbf{x} - \mathbf{m}_{\mathbf{X}})^T \mathbf{C}_{\mathbf{X}}^{-1} (\mathbf{x} - \mathbf{m}_{\mathbf{X}})\right), \quad (3.50)$$

where

$$\mathbf{C}_{\mathbf{X}} = \mathbb{E}[(\mathbf{x} - \mathbf{m}_{\mathbf{X}})(\mathbf{x} - \mathbf{m}_{\mathbf{X}})^T] \quad (3.51)$$

is the *covariance matrix*, $|\mathbf{C}_{\mathbf{X}}|$ is its determinant, and $\mathbf{m}_{\mathbf{X}} = \mathbb{E}[\mathbf{X}]$ is the vector mean. In the special case that the vector mean is zero and elements of the random vector are independent with equal variances, $\mathbf{C}_{\mathbf{X}}$ becomes diagonal and (3.50) reduces to (3.49). An important observation from (3.50) is that the p.d.f. of a Gaussian random vector is completely specified by the vector mean and the pairwise covariances contained in the covariance matrix. Consequently, these two sets of parameters completely specify all the statistical properties of a Gaussian random vector.

3.1.4. Geometric Interpretation

Random variables can be interpreted geometrically using the approach of Section 2.6. In particular, consider the set of all complex-valued random variables X with bounded second moments, $E[|X|^2] < \infty$, and associate a vector \mathbf{X} with each random variable,

$$\mathbf{X} \leftrightarrow X . \quad (3.52)$$

Exercise 3-9.

Make reasonable definitions for the operations of addition of vectors, multiplication by a scalar, the vector 0, and the additive inverse. Show that the set of such vectors form a linear space (Section 2.6.1). \square

An inner product on this space can be defined as

$$\langle \mathbf{X}, \mathbf{Y} \rangle = E[\mathbf{XY}^*]. \quad (3.53)$$

Exercise 3-10.

Show that (3.53) is a legitimate inner product (Section 2.6.2). \square

This geometric interpretation pays dividends in understanding the results of linear prediction theory (Section 3.2.3).

3.2. RANDOM PROCESSES

A discrete-time random process $\{X_k\}$ is a sequence of random variables indexed by integers k , while a continuous-time random process $X(t)$ is indexed by a real variable t . We write an *outcome* of $\{X_k\}$ or $\{X(t)\}$ as the lower case deterministic signal $\{x_k\}$ or $\{x(t)\}$. When there can be no confusion between a *signal* and a *sample of the signal*, we omit the braces $\{\cdot\}$. Each random sample X_k or $X(t)$ may be complex, vector-valued, or real-valued.

Example 3-2.

A real-valued random process $X(t)$ is a *Gaussian random process* if its samples $\{X(t_1), \dots, X(t_N)\}$ are jointly Gaussian random variables for any N and for any $\{t_1, \dots, t_N\}$. \square

The first and second moments of the random process are the *mean*

$$m_k = E[X_k], \quad m(t) = E[X(t)] \quad (3.54)$$

and the *autocorrelation*

$$R_{XX}(k, i) = E[X_k X_i^*], \quad R_{XX}(t_1, t_2) = E[X(t_1) X^*(t_2)], \quad (3.55)$$

where X^* is the complex conjugate of X .

Example 3-3.

Consider a real-valued, zero-mean Gaussian random process. A random vector \mathbf{X} can be constructed from some arbitrary set of samples. For such a vector, the covariance matrix of (3.51) can be obtained from the autocorrelation function (3.55). Consequently, the joint p.d.f. (3.50) of any set of samples can be obtained from the autocorrelation function. Thus, the statistical properties of a zero-mean real-valued Gaussian random process are completely specified by its autocorrelation function. \square

A random process is *strict-sense stationary* if the p.d.f. for any sample is independent of the time index of the sample, and the joint p.d.f. of any set of samples depends only on the time differences between samples, and not on the absolute time of any sample. It is *wide-sense stationary (WSS)* if its mean is independent of the time

index, and its autocorrelation depends only on the time difference between samples, and not on the absolute time. In other words, m_k or $m(t)$ must be constant and $R_{XX}(k, i)$ or $R_{XX}(t_1, t_2)$ must be a function only of the difference $k - i$ or $t_1 - t_2$. Strict sense stationarity implies wide-sense stationarity, but not the reverse, unless the process is Gaussian.

Example 3-4.

A real-valued WSS Gaussian random process is also strict-sense stationary. The autocorrelation function and mean of such a process can be used to construct the covariance matrix (3.51) for any set of samples. Since the process is WSS, the entries in the matrix will be independent of the absolute time index of the samples, and will depend instead only on the time differences between samples. Consequently, the joint p.d.f. (3.50) of any set of samples will depend only on these time differences. Hence the process is strict-sense stationary. \square

For a WSS random process the autocorrelation function can be written in terms of the time difference between samples, $m = k - i$ or $\tau = t_1 - t_2$, yielding the simpler notation

$$R_X(m) = E[X_{k+m} X_k^*], \quad R_X(\tau) = E[X(t + \tau) X^*(t)]. \quad (3.56)$$

$R_X(0)$ is the second moment of the samples

$$R_X(0) = E[|X_k|^2], \quad R_X(0) = E[|X(t)|^2], \quad (3.57)$$

and can be interpreted as the *power* of a random process. For a WSS random process, the *power spectral density* or *power spectrum* is the Fourier transform of the autocorrelation function,

$$S_X(e^{j\omega T}) = \sum_{m=-\infty}^{\infty} R_X(m) e^{-j\omega mT}, \quad S_X(j\omega) = \int_{-\infty}^{\infty} R_X(\tau) e^{-j\omega \tau} d\tau, \quad (3.58)$$

where T is the sample interval of the discrete-time random process. The power therefore is the integral of the power spectrum,

$$R_X(0) = \frac{T}{2\pi} \int_{-\pi/T}^{+\pi/T} S_X(e^{j\omega T}) d\omega, \quad R_X(0) = \frac{1}{2\pi} \int_{-\infty}^{\infty} S_X(j\omega) d\omega. \quad (3.59)$$

The power spectrum is real-valued since the autocorrelation function is conjugate symmetric, $R_X(m) = R_X^*(-m)$ or $R_X(\tau) = R_X^*(-\tau)$. It is also non-negative (see Problem 3-9). Furthermore, if X_k or $X(t)$ is real-valued, then the power spectrum is symmetric about $\omega = 0$. We can also write the power spectrum as a Z transform or a Laplace transform,

$$S_X(z) = \sum_{m=-\infty}^{\infty} R_X(m) z^{-m}, \quad S_X(s) = \int_{-\infty}^{\infty} R_X(\tau) e^{-s\tau} d\tau. \quad (3.60)$$

Evaluating $S_X(z)$ on the unit circle or $S_X(s)$ on the $j\omega$ axis yields (3.58).

Example 3-5.

Consider a zero-mean random process $\{X_k\}$ where the samples X_k are all independent and identically distributed (i.i.d.) zero-mean random variables with variance σ_x^2 . In this case $R_X(k) = \sigma_x^2 \delta_k$ and the power spectrum is a constant, $S_X(e^{j\omega T}) = \sigma_x^2$, independent of the frequency, with power $R_X(0) = \sigma_x^2$. \square

Any zero-mean process with a constant power spectrum is said to be a *white random process*. This may or may not imply that the samples of the random process are independent, although for the important Gaussian case they are.

Example 3-6.

As in Example 3-5, consider a continuous-time random process $\{X(t)\}$ with the autocorrelation function

$$R_X(\tau) = N_0 \delta(\tau). \quad (3.61)$$

The power spectrum of this process is a constant, $S_X(j\omega) = N_0$, so $\{X(t)\}$ is white. The power $R_X(0)$ of this continuous-time white process is infinite. So we immediately run into mathematical difficulties for the continuous-time case that we did not encounter in the discrete-time case. \square

Although the continuous-time white random process of Example 3-6 leads to the non-physical condition that the power is infinite (or undefined), it is an extremely important model. It would appear from the fact that $R_X(\tau) = 0$ for all $\tau \neq 0$ that any two distinct samples of a continuous-time white random process are uncorrelated, but, unfortunately, this makes no mathematical or physical sense. Sampling a continuous-time white random process is an ill-defined concept. Roughly speaking, a continuous-time white random process varies so quickly that it is not possible to determine its characteristics at any instant in time.

In spite of these mathematical difficulties, the continuous-time white random processes is useful as a model for noise which has an approximately constant power spectrum over a bandwidth larger than the bandwidth of the system we are considering. In such a system we will always bandlimit the noise to eliminate any out-of-band component. In this event, it makes no difference if we start with a white noise or a more accurate model; the result will be very nearly the same. But using the white noise model results in significantly simpler algebraic manipulation. In this book we will often use the white noise model, and take care to always bandlimit this noise process prior to other operations such as sampling. After bandlimiting, we obtain a well-behaved process with finite power.

Example 3-7.

Thermal or *Johnson* noise in electrical resistors has a power spectrum that is flat to more than 10^{12} Hz, a bandwidth much greater than most systems of interest (see [1]). Thus, we can safely use white noise as a model for this thermal noise without compromising accuracy. The noise in the model at frequencies greater than 10^{12} Hz will always be filtered out at the input to our system anyway. By contrast, in optical systems (Section 5.3), thermal noise is generally insignificant at optical frequencies. Thermal noise is modeled as a Gaussian random process, from the central limit theorem, since it is comprised of the superposition of many independent events (thermal fluctuations of individual electrons). \square

3.2.1. Cross-Correlation and Complex Processes

Given two random processes $X(t)$ and $Y(t)$, we can define a *cross-correlation* function,

$$R_{XY}(t_1, t_2) = E[X(t_1)Y^*(t_2)]. \quad (3.62)$$

If $X(t)$ and $Y(t)$ are each wide-sense stationary, then they are *jointly wide-sense stationary* if $R_{XY}(t_1, t_2)$ is a function only of $(t_1 - t_2)$.

A complex-valued random process $X(t)$ is defined as

$$X(t) = \operatorname{Re}\{X(t)\} + j \cdot \operatorname{Im}\{X(t)\}, \quad (3.63)$$

where $\operatorname{Re}\{X(t)\}$ and $\operatorname{Im}\{X(t)\}$ are real-valued random processes. The second order statistics of such a process consist of the two autocorrelation functions of the real and imaginary parts, as well as their cross-correlation functions. Complex Gaussian random processes are very important in digital communication systems; they have some special properties that are considered in detail in Chapter 8.

3.2.2. Filtered Random Processes

A particular outcome x_k or $x(t)$ of a random process is a signal, and therefore may be filtered or otherwise processed. We can also talk about filtering the random process X_k or $X(t)$ itself, rather than an outcome. Then we get a new random process with a sample space that is obtained by applying every element of the sample space of the original random process to the input of the filter.

Example 3-8.

A filtered Gaussian random process is a Gaussian random process. Intuitively, this is true because filtering is linear, and any linear combination of jointly Gaussian random variables is a Gaussian random variable. \square

Consider the two continuous-time LTI systems shown in Figure 3-2 with WSS continuous-time random process inputs.

Exercise 3-11.

Show that the output of the filter $h(t)$ is WSS, and that its autocorrelation function and power spectrum are given by

$$R_W(\tau) = h(\tau) * h^*(-\tau) * R_X(\tau), \quad S_W(j\omega) = S_X(j\omega) |H(j\omega)|^2, \quad (3.64)$$

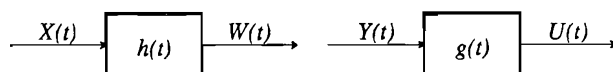


Figure 3-2. Two linear systems with WSS random process inputs.

$$S_W(s) = S_X(s)H(s)H^*(-s^*) . \quad (3.65)$$

□

Exercise 3-12.

Show that if a WSS discrete-time random process X_k is filtered by a filter that has impulse response h_k , and the result is W_k , then W_k is WSS and

$$R_W(m) = h_m * h_{-m}^* * R_X(m) , \quad S_W(e^{j\omega T}) = S_X(e^{j\omega T})|H(e^{j\omega T})|^2 , \quad (3.66)$$

$$S_W(z) = S_X(z)H(z)H^*(1/z^*) . \quad (3.67)$$

□

Example 3-9.

A white random process $X(t)$ has power spectrum $S_X(j\omega) = N_0$, a constant. If it is filtered by an ideal LPF with transfer function

$$H(j\omega) = \text{rect}(\omega, 2\pi \times 10^{12}) = \begin{cases} 1; & |\omega| < 2\pi \times 10^{12} \\ 0; & \text{otherwise} \end{cases} \quad (3.68)$$

then the power spectrum of the output is

$$S_W(j\omega) = N_0 \text{rect}(\omega, 2\pi \times 10^{12}) = \begin{cases} N_0; & |\omega| < 2\pi \times 10^{12} \\ 0; & \text{otherwise} \end{cases} \quad (3.69)$$

which is a reasonable approximation to thermal noise in a resistor. Furthermore, since thermal noise is the cumulative effect of random motion of a huge number of individual particles, we can apply the central limit theorem to argue that a sample of such thermal noise should be a Gaussian random variable. Thus we conclude that thermal noise is reasonably modeled as white Gaussian noise. □

The *cross-spectral density* of two jointly WSS random processes at the filter inputs in Figure 3-2 is defined as the Fourier transform of the cross-correlation function,

$$S_{XY}(j\omega) = \int_{-\infty}^{\infty} R_{XY}(\tau) e^{-j\omega\tau} d\tau , \quad R_{XY}(\tau) = E[X(t + \tau)Y^*(t)] . \quad (3.70)$$

Exercise 3-13.

Show that the cross-power spectrum of the outputs in Figure 3-2 is

$$S_{WU}(j\omega) = H(j\omega)G^*(j\omega)S_{XY}(j\omega) . \quad (3.71)$$

□

3.2.3. The Innovations Process

Given a wide-sense stationary random process $\{X_k\}$ with power spectrum $S_X(e^{j\omega T})$, a natural *innovations representation* of that random process follows from the monic minimum-phase spectral factorization of $S_X(z)$ (see (2.55) in Section

2.5.5). In particular, since $S_X(z)$ is real-valued and non-negative on the unit circle, it can be decomposed as

$$S_X(z) = A_x^2 G_x(z) G_x^*(1/z^*) \quad (3.72)$$

where $G_x(z)$ is a monic loosely minimum-phase causal filter, and A_x^2 is a constant to be interpreted shortly. If $S_X(z)$ has no zeros on the unit circle ($S_X(e^{j\omega T}) > 0$ for all ω), then $G_x(z)$ is strictly minimum phase. In this case, its inverse filter $G_x^{-1}(z)$ is stable, and is also a monic minimum-phase causal filter. If we filter the process X_k with the filter $G_x^{-1}(z)$, as shown in Figure 3-3, then from (3.67), the output I_k is a white random process with power spectrum $S_I(z) = A_x^2$. The random process $\{I_k\}$ is called the *innovations process*. Its power is A_x^2 .

The innovations process and the filter $G_x(z)$ can be used to generate the random process X_k , as shown in Figure 3-3. This helps to explain the terminology. Since I_k is white, each new sample is uncorrelated with previous samples. Thus each new sample brings new information (an "innovation") about the random process X_k . Viewed another way, the *whitening filter* $G^{-1}(z)$ removes redundant information from X_k by removing correlated components in the samples. What is left has only uncorrelated samples. Thus we can think of X_k as having two components; the innovation is the new or "random" part, while the remainder is a linear combination of past innovations.

3.2.4. Linear Prediction

A *linear predictor* forms an estimate of the current sample of a discrete-time random process from a linear combination of the past samples. It uses the correlation between samples to construct an informed estimate of the current sample based on the past.

If the transfer function of the predictor is $F(z)$, it must be strictly causal,

$$F(z) = \sum_{k=1}^{\infty} f_k z^{-k}. \quad (3.73)$$

This ensures that only past samples are used in constructing the prediction. The *prediction error*, formed by taking the difference between the current sample and the prediction, is generated by applying a filter with transfer function

$$E(z) = 1 - F(z) \quad (3.74)$$

to the random process. $E(z)$ must be stable, causal, and monic to be a legitimate

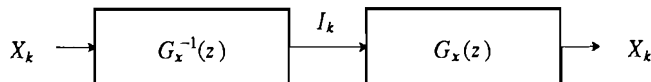


Figure 3-3. Generation of the innovations I_k from X_k , and the recovery of X_k from its innovations.

prediction error filter. The prediction error filter $E(z)$ (or equivalently $F(z)$) should be designed to minimize the power of the prediction error sequence E_k . We will now show that $E(z) = G_x^{-1}(z)$ is optimal, where $G(z)$ results from the spectral factorization in (3.72).

In Figure 3-4a we show the innovations representation of X_k , where it is generated by filtering the innovations process I_k with the filter $G_x(z)$. Two prototype prediction error filters are shown, a general filter $E(z)$, which is constrained to be causal and monic, and a specific filter $G_x^{-1}(z)$, which is causal and monic. We will now demonstrate that the lower output E_k cannot have less power than the upper output I_k , so the upper filter $G_x^{-1}(z)$ is an optimal prediction error filter. The prediction error for the optimal predictor is therefore precisely the innovation I_k , and the prediction error power is A_x^2 .

To show this, consider Figure 3-4b, where $E(z)$ is split into two filters $G_x^{-1}(z)$ and $G_x(z)E(z)$. Such a split might be absurd in implementation, but mathematically it is perfectly reasonable. The output of the first filter is the innovations process I_k . We will now show that the output of the second filter cannot have lower power than that of I_k . Since both $G_x(z)$ and $E(z)$ are causal and monic filters ($G_x(\infty) = E(\infty) = 1$) it follows that $G_x(z)E(z)$ must also be causal and monic ($G_x(\infty)E(\infty) = 1$). Let this filter have impulse response f_k , $0 \leq k < \infty$, where $f_0 = 1$. Since the input innovations process is white with variance A_x^2 , the output variance is

$$A_x^2 \sum_{k=0}^{\infty} |f_k|^2 \geq A_x^2, \quad (3.75)$$

with equality if and only if $f_k = 0$, $k \geq 1$, or in other words $E(z) = G_x^{-1}(z)$.

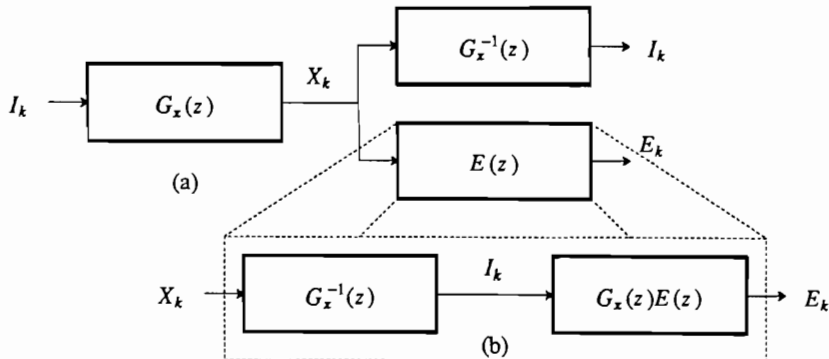


Figure 3-4. Steps in the derivation of the optimal linear prediction error filter. (a) Comparison of two prediction error filters. (b) Decomposition of the general filter $E(z)$.

Intuitively, since the predictor is exploiting the correlation of input samples, we would expect the prediction error to be white, since otherwise there would still be correlation to further exploit. Thus, the second filter in Figure 3-4b is counterproductive, since it introduces correlation. However, this intuitive explanation is incomplete, because $G_x(z)E(z)$ could have a flat frequency response, in which case E_k would still be white even though it is not the innovations process for X_k ! This case is addressed by the following exercise.

Exercise 3-14.

Show that if $H(z)$ is rational, causal, and monic, and has a flat frequency response $|H(e^{j\omega T})| = K$, then $K > 1$. Thus, a monic filter with a flat frequency response must have gain larger than unity, and thus its white output has a larger variance than its input. \square

This exercise is instructive, because it shows that any causal and monic filter with a flat frequency response will amplify its inputs. The optimal prediction error filter $G_x^{-1}(z)$ thus has two key properties: it is a *whitening filter*, resulting in a white prediction error, and it is *minimum-phase*. The whitening filter property of the prediction error filter (if not the minimum-phase property) can also be demonstrated by orthogonality arguments (see Problem 3-5), and has a simple geometric interpretation (see Problem 3-6).

3.2.5. Sampling a Random Process

A finite power continuous-time random process $X(t)$ can be sampled, yielding a discrete-time random process $Y_k = X(kT)$. Since we will be performing this sampling operation often in digital communication systems, it is important to relate the statistics of the continuous-time random processes with those of the discrete-time random process obtained by sampling it. Assuming $X(t)$ is WSS,

$$R_{YY}(k,i) = E[X(kT)X^*(iT)] = R_X(mT), \quad (3.76)$$

where $m = k - i$, so the sampled process is WSS with autocorrelation equal to a sampled version of the autocorrelation $R_X(\tau)$ of the original continuous-time signal. From (2.17), the power spectrum of the continuous-time random process and its sampled discrete-time process are related by

$$S_Y(e^{j\omega T}) = \frac{1}{T} \sum_{m=-\infty}^{\infty} S_X(j(\omega - m\frac{2\pi}{T})). \quad (3.77)$$

As in the deterministic case, aliasing distortion results when the bandwidth is greater than half the sampling rate, where bandwidth in this case is defined in terms of the power spectrum.

Example 3-10.

Consider the approximation to thermal noise in Example 3-9. We wish to determine whether samples of such noise are uncorrelated; if they are, then sampled thermal noise is a discrete-time white Gaussian process. From (3.69), the autocorrelation function of the bandlimited noise $W(t)$ is

$$R_W(\tau) = N_0 \frac{B}{\pi} \frac{\sin(Bt)}{Bt} \quad (3.78)$$

where $B = 2\pi \times 10^{12}$, or 1,000 GHz. $R_W(\tau)$ has zero crossings at multiples of π/B , implying that samples of the random process taken at multiples of π/B will be uncorrelated. That is,

$$R_W(m \frac{\pi}{B}) = E[W(m \pi/B)W(0)] = N_0 \frac{B}{\pi} \delta_m. \quad (3.79)$$

For these particular sampling rates, therefore, samples of the approximation to thermal noise are a discrete-time Gaussian white noise process. In practice, we are unlikely to sample any signal anywhere near the rate B/π , or 2,000 GHz. Since $|R_W(\tau)|$ decays as τ increases, samples at any reasonable sampling rate are *nearly* uncorrelated. \square

Using the techniques discussed so far, we should have no difficulty considering systems that mix discrete and continuous-time random processes as well as deterministic signals. However, there are some subtleties. Consider a discrete-time random process X_k filtered by a continuous-time filter with impulse response $h(t)$ in the sense defined in Section 2.1. The output can be written

$$Y(t) = \sum_{m=-\infty}^{\infty} X_m h(t-mT). \quad (3.80)$$

This is *pulse amplitude modulation* (PAM), described in detail in Chapter 6.

Example 3-11.

The transmission of a discrete-time sequence of data symbols X_m over a continuous-time channel often takes the form of the random process in (3.80). Suppose that $h(t)$ is as shown in Figure 3-5a and that X_k is a random sequence with i.i.d. samples taking values ± 1 with equal probability. A possible outcome is shown in Figure 3-5b. The first important observation is that the process $Y(t)$ is not wide-sense stationary because $E[Y(t+\tau)Y(t)]$ is not independent of t . For example,

$$E[Y(T/4)Y(0)] = E[X_0^2] = 1 \neq E[Y(T)Y(3T/4)] = 0.$$

This process is actually *cyclostationary*, a weaker form of stationarity. Since this process is not wide-sense stationary, its power spectrum is not defined. \square

The fact that $Y(t)$ in (3.80) is not wide-sense stationary is a major inconvenience. A common gimmick changes our random process into a wide-sense stationary process. Define the random variable Θ , called a *random phase epoch*, that is uniformly

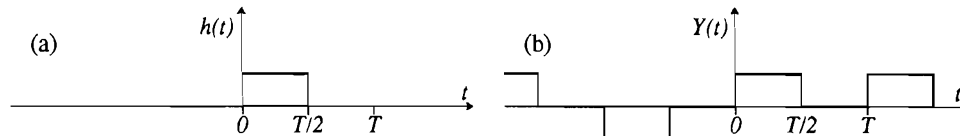


Figure 3-5. a. An example of a pulse shape for transmitting bits. b. An example of a waveform using this pulse shape.

distributed on $[0, T]$ and independent of $\{X_k\}$. Then define the new random process

$$Z(t) = Y(t + \Theta) = \sum_{m=-\infty}^{\infty} X_m h(t + \Theta - mT). \quad (3.81)$$

This process has a *random phase* which is constant over time but chosen randomly at the beginning of time. Physically, this new process reflects our uncertainty about the phase of the signal; the origin in the time axis is of course arbitrary. This redefined process is wide-sense stationary, as shown in Appendix 3-A, with power spectrum

$$S_Z(j\omega) = \frac{1}{T} |H(j\omega)|^2 S_X(e^{j\omega T}). \quad (3.82)$$

Note the dependence on the power spectrum of the discrete-time process and the magnitude-squared spectrum of the pulse $h(t)$.

Example 3-12.

Consider transmission of a random sequence of uncorrelated random variables X_k with equally probable values ± 1 using a pulse shape $h(t)$. The sequence X_k is white and the variance is unity, so the power spectrum of the data sequence is

$$S_X(e^{j\omega T}) = 1, \quad (3.83)$$

and the power spectrum of the random phase transmitted signal is

$$S_Z(j\omega) = \frac{1}{T} |H(j\omega)|^2. \quad (3.84)$$

With a white data sequence, the power spectrum has the shape of the magnitude squared of the Fourier transform of the pulse. \square

3.2.6. Reconstruction of Sampled Signal

It might appear that (3.77) establishes the conditions under which a random process can be recovered from its samples, just as (2.17) does for deterministic signals. However, this appearance is deceiving because two random processes can have the same power spectrum and not be "equal" in any sense. The power spectrum is merely a second-order statistic, not a full characterization of the process. By a derivation similar to that in Appendix 3-A, we can investigate the recovery of the original continuous-time random process from its samples. A method of sampling and recovering a random process analogous to the deterministic case is shown in Figure 3-6. We first filter the random process using an anti-aliasing filter $F(j\omega)$, then sample, and

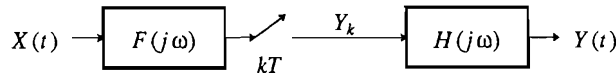


Figure 3-6. Sampling and recovery of a random process using anti-aliasing filter $F(j\omega)$ and recovery filter $H(j\omega)$.

finally recover using recovery filter $H(j\omega)$ to yield the random process $Y(t)$. To make $Y(t)$ WSS we must again introduce a random phase. The way to tell whether the system recovers the input random process is not to calculate the output power spectrum, but rather to investigate the error signal between input and output. In particular, define

$$E(t) = X(t + \Theta) - Y(t + \Theta), \quad (3.85)$$

where Θ is uniformly distributed over $[0, T]$. We would conclude that the recovery is exact (in a mean-square sense) if

$$E[|E(t)|^2] = 0. \quad (3.86)$$

This is not the same as showing that $E(t) = 0$, which cannot be shown using second order statistics only. However, (3.86) is just as good for engineering purposes. The conditions under which (3.86) is valid can be inferred from the following exercise, which can be solved using similar techniques to those used in Appendix 3-A.

Exercise 3-15.

Show that the power spectrum of $E(t)$ is

$$\begin{aligned} S_E(j\omega) &= \frac{1}{T^2} |H(j\omega)|^2 \sum_{m \neq 0} S_X(j(\omega + m\frac{2\pi}{T})) |F(j(\omega + m\frac{2\pi}{T}))|^2 \\ &\quad + |1 - \frac{1}{T} H(j\omega) F(j\omega)|^2 S_X(j\omega). \end{aligned} \quad (3.87)$$

□

Examining (3.87), the first term is aliasing distortion resulting from a signal at the output of the anti-aliasing filter, if it is not sufficiently bandlimited. In particular, if $H(j\omega) = 0$ and $F(j\omega) = 0$ for $|\omega| \geq \pi/T$ then this term is identically zero. The second term is in-band distortion due to an improper reconstruction filter $H(j\omega)$ and also distortion due to bandlimiting of the input prior to sampling. For an ideal reconstruction filter,

$$H(j\omega)F(j\omega) = T, \quad |\omega| < \pi/T, \quad (3.88)$$

in which case the error signal has power spectrum

$$S_E(j\omega) = \begin{cases} 0; & |\omega| < \pi/T \\ S_X(j\omega); & |\omega| \geq \pi/T \end{cases} \quad (3.89)$$

and the total error power is

$$E[E^2(t)] = 2 \cdot \frac{1}{2\pi} \int_{\pi T}^{\infty} S_X(j\omega) d\omega. \quad (3.90)$$

The fact that the reconstruction error is just the error in initially bandlimiting $X(t)$ is not surprising, and corresponds to the deterministic signal case.

The results of this subsection are important not only for their implications to the recovery of sampled random processes, but also in the techniques used. We will find

the need for similar techniques in the optimization problems of Chapter 9.

3.3. MARKOV CHAINS

A *discrete-time Markov process* $\{\Psi_k\}$ is a random process that satisfies

$$p(\Psi_{k+1} | \Psi_k, \Psi_{k-1}, \dots) = p(\Psi_{k+1} | \Psi_k). \quad (3.91)$$

In words, the future sample Ψ_{k+1} is independent of past samples $\Psi_{k-1}, \Psi_{k-2}, \dots$ if the present sample $\Psi_k = \psi_k$ is known. The particular case of a Markov process where the samples take on values from a discrete and countable set Ω_Ψ is called a *Markov chain*. In this section, we will often take Ω_Ψ to be a set of integers. Markov chains are a useful model of a finite state machine with a random input, where the samples of the random input are statistically independent of one another. Since any digital circuit with internal memory (flip flops, registers, or RAMs) is a finite state machine, most digital communication systems contain finite state machines. Markov chains are useful signal generation models for digital communication systems with intersymbol interference or convolutional coding (Chapters 9, 13, and 14). Markov chain theory is also useful in the analysis of error propagation in decision-feedback equalizers (Chapter 10) and in the calculation of the power spectrum of line codes (Chapter 12). The following treatment uses Z-transform techniques familiar to the readers of this book. Sections 3.3.2 through 3.3.4, as well as Appendix 3-B, can be skipped on a first reading, since the techniques are not used until Chapter 10.

3.3.1. State Transition Diagrams

Consider a random process Ψ_k (real, complex, or vector valued) whose sample outcomes are members of a finite or countably infinite set Ω_Ψ of values. The random process Ψ_k is a Markov chain if (3.91) is satisfied. The next sample Ψ_{k+1} of a Markov chain is independent of the past samples $\Psi_{k-1}, \Psi_{k-2}, \dots$ given the present sample Ψ_k . Furthermore, *all* future samples of the Markov chain are independent of the past given knowledge of the present, as shown in the following exercise.

Exercise 3-16.

Let Ψ_k be a Markov chain and show that for any $n > 0$,

$$p(\Psi_{k+n} | \Psi_k, \Psi_{k-1}, \dots) = p(\Psi_{k+n} | \Psi_k). \quad (3.92)$$

□

Since knowledge of the current sample Ψ_k makes the past samples irrelevant, Ψ_k is all we need to predict the future behavior of the Markov chain. For this reason, Ψ_k is said to be the *state* of the Markov chain at time k , and Ω_Ψ is the set of all possible states.

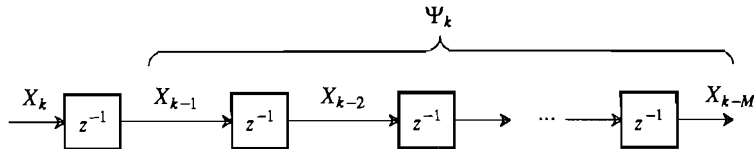


Figure 3-7. A shift register process with independent inputs X_k is a Markov chain with state Ψ_k .

Example 3-13.

A *shift register process* is shown in Figure 3-7. If X_k is independent of X_{k-M-1} , X_{k-M-2} , ... and we define the vector

$$\Psi_k = [X_{k-1}, \dots, X_{k-M}] \quad (3.93)$$

(M is the memory of the system) then the Markov property (3.91) is satisfied. This follows since Ψ_{k+1} is a function of X_{k+1} and Ψ_k only. Hence $\{\Psi_k\}$ is a vector-valued discrete-time Markov process. If the inputs X_k are discrete-valued, then it is also a Markov chain. \square

A Markov chain can be described graphically by a *state transition diagram*. This graph displays each state of the Markov chain as a node, and also displays the input and output or some other relevant properties for the transitions between states.

Example 3-14.

The *parity* of a bit stream X_k is defined to be the accumulated modulo-two summation of the bits, and is computed by the circuit in Figure 3-8a. It is sufficient for the input bits to be independent for the random process $\Psi_k = Y_{k-1}$ to be Markov. It is easily seen from the diagram that Ψ_{k+1} depends only on the current state Ψ_k and the current input X_k . Ψ_k has a finite sample space $\Omega_\Psi = \{0,1\}$, so the parity checker can be represented by the state transition diagram Figure 3-8b, where the arcs are labeled with the input that stimulates the state transition and the output resulting from the transition. The arcs of such a state diagram can alternatively be labeled with the transition probabilities, if the transition probabilities are independent of time. \square

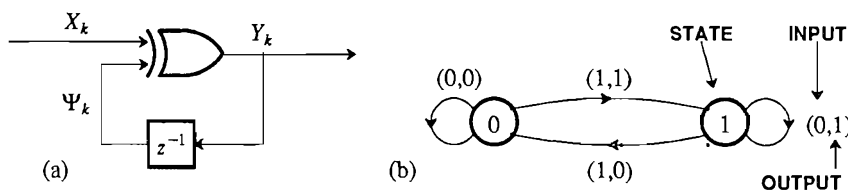


Figure 3-8. a. A circuit that computes the parity of the bit stream X_n . b. The state transition diagram of the corresponding Markov chain.

A Markov chain Ψ_k is called *homogeneous* if the conditional probability $p(\psi_k | \psi_{k-1})$ is not a function of k . Homogeneity is therefore a kind of stationarity or time invariance. A homogeneous Markov chain can be characterized by its *state transition probabilities*, which we write with the shorthand

$$p(j|i) = p_{\Psi_{k+1}|\Psi_k}(j|i) \quad (3.94)$$

for $i \in \Omega_\Psi$ and $j \in \Omega_\Psi$.

Example 3-15.

If in the previous example the incoming bits are not only independent but also identically distributed, then the Markov chain is homogeneous. If furthermore the incoming bits are equally likely to be one and zero, then the state transition probabilities are all 0.5. \square

It is often convenient to define a random process that is some real-valued function of the state trajectory of a Markov chain,

$$X_k = f(\Psi_k). \quad (3.95)$$

This is encountered in the modeling of line coding (Chapter 12). The transmitted power spectrum is an important property of the line code, and thus we need to calculate the power spectrum of (3.95). This problem is considered in Appendix 3-B.

3.3.2. Transient Response of a Markov Chain

For a homogeneous Markov chain, we can find a relation for the evolution of the state probabilities with time. Using (3.33) we write

$$p_{k+1}(j) = \sum_{i \in \Omega_\Psi} p(j|i)p_k(i) \quad (3.96)$$

for all $j \in \Omega_\Psi$, where we have defined a notation for the probability of being in state i at time k ,

$$p_k(i) = \Pr\{\Psi_k = i\}. \quad (3.97)$$

The new notation emphasizes that $p_k(i)$ is a discrete-time sequence. In applications we often want to determine the probability of being in a certain state j at a certain time k given a set of probabilities for being in those states at initial time $k=0$. We can accomplish this by analyzing (3.96), a system of *time-invariant* difference equations, using Z-transform techniques. If we define $p_k(j)=0$ for $k < 0$, then the Z-transform of the state probability for state j is

$$P_j(z) = \sum_{k=0}^{\infty} p_k(j)z^{-k}. \quad (3.98)$$

Exercise 3-17.

Take the Z-transform of both sides of (3.96) to show that

$$P_j(z) = p_0(j) + \sum_{i \in \Omega_\Psi} p(j|i)z^{-1}P_i(z). \quad (3.99)$$

\square

If there are N states, (3.99) gives us N equations with N unknowns $P_j(z)$. These equations can be solved and the inverse Z-transform calculated to determine the state probability $p_k(i)$.

Example 3-16.

Continuing Example 3-14, the parity check circuit, suppose that the initial state is equally likely to be either zero or one, so

$$p_0(0) = p_0(1) = 0.5. \quad (3.100)$$

Suppose further that the incoming bits X_k are equally likely to be zero or one, so the transition probabilities $p(j|i)$ are all $\frac{1}{2}$. Then (3.99) becomes

$$\begin{aligned} P_0(z) &= 0.5 + 0.5z^{-1}P_0(z) + 0.5z^{-1}P_1(z) \\ P_1(z) &= 0.5 + 0.5z^{-1}P_1(z) + 0.5z^{-1}P_0(z). \end{aligned} \quad (3.101)$$

Solving this set of two simultaneous equations, the Z-transforms of the state probabilities are equal,

$$P_0(z) = P_1(z) = \frac{0.5}{1 - z^{-1}}. \quad (3.102)$$

Using the Z-transform pair in Problem 2-15 we can invert the Z-transform to get

$$p_k(0) = p_k(1) = 0.5 \cdot u_k \quad (3.103)$$

where u_k is the unit step function. The chain is therefore equally likely to be in either state at any point in time beginning at $k = 0$. A Markov chain in which the state probabilities are independent of time is called *stationary*. \square

3.3.3. Signal Flow Graph Analysis

Translation of a state diagram into a set of equations to be solved is often made easier using signal flow graphs. A signal flow graph is a graphical representation of a linear equation, and in particular can represent the system of equations given by (3.99). Its value lies in the fact that the state diagram can be directly translated into a topologically equivalent signal flow graph representing the equations. In fact, the experienced can write down the signal flow graph directly without ever generating a state diagram. The idea of a graph representing linear equations is illustrated by the following simple example.

Example 3-17.

The equation $w = au + x$ can be represented by the signal flow graph shown in Figure 3-9a. The nodes of the graph represent the variables u , w , and x , while the two arcs represent the multiplication of the variables by constants, and also the addition. The signal flow graph in Figure 3-9b represents the recursive equation $x = au + bw + cx$. \square

In general, a node in a signal flow graph represents a variable that is equal to the sum of the incoming arcs. A weight on an arc is a multiplicative factor. Our interest is in signal flow graphs in which the variables are all Z-transforms.

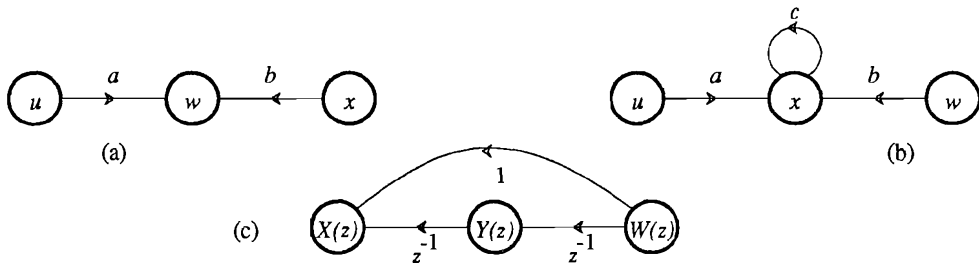


Figure 3-9. Several signal flow graphs representing linear equations.

Example 3-18.

The signal flow graph in Figure 3-9c represents a dynamical system described by the equations $X(z) = z^{-1}Y(z) + W(z)$ and $Y(z) = z^{-1}W(z)$. \square

From the last example, it is clear that the equations (3.99) can be represented using a signal flow graph for any given Markov chain, as shown in Figure 3-10. Shown are just two of the states, i and j . Each of the states is represented by two nodes of the graph, one for the Z-transform of the state probability sequence, $P_i(z)$, and the other for the initial probability of that state $p_0(i)$ (the latter is not a variable in the equations, but a constant). In many cases the initial probability is zero so the corresponding node can be omitted.

Example 3-19.

Returning to the parity check example of Example 3-14, the equations (3.101) are represented by the signal flow graph in Figure 3-11. Note that this one figure takes the place of the state diagram of Figure 3-8 and the set of equations of (3.101). \square

In retrospect, the signal flow graph is intuitive. Each state transition has a delay

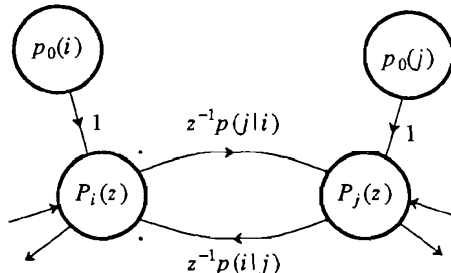


Figure 3-10. A signal flow graph representation of the Markov chain dynamical equations (3.99).

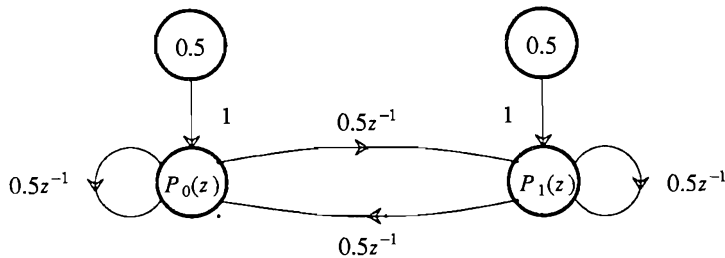


Figure 3-11. A signal flow graph representation of the system of state probabilities for the parity examples.

operator z^{-1} corresponding to the time it takes for that transition to occur, as well as the probability of that transition. The arcs from the initial state probabilities have no such delay since the initialization is instantaneous, and we can think of that transition as occurring only once at $k = 0$. For Markov chains that start in a particular state, there will only be one such node corresponding to the starting state.

Once we have a signal flow graph, we can easily write down the set of equations and then solve them for the Z-transform of the state probabilities. For some problems, a shortcut known as *Mason's gain formula* allows us to solve these equations directly by inspection of the signal flow graph [2,3,4,5].

3.3.4. First Passage Problem

When we use Markov chains to model the behavior of framing recovery circuits (Chapter 19) and error propagation (Chapter 10), we would like to calculate the *average first passage time* for an *absorption state* of the chain. An absorption state is defined as a state with an entry but no exit, so that the steady-state probability of that state is unity. This is illustrated in Figure 3-12 for the case where the absorption state is N . An absorption state must have a self-loop with gain z^{-1} indicating that the chain stays in that state forever. The figure also assumes that there is only one way to get to the absorption state, from state $N-1$, although that is not necessary for the following analysis.

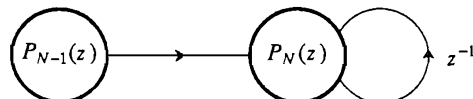


Figure 3-12. A part of a signal flow graph for a Markov chain in which state N is an absorption state, with only one entry from the outside, namely from state $N-1$.

What we are often interested in is the *first passage time to state N*, which is defined as the time-index of the first time we enter that state. Define the probability of entering state N at time k as $q_k(N)$. Then we have that

$$p_k(N) = p_{k-1}(N) + q_k(N), \quad (3.104)$$

or in words, the probability of being in state N at time k is equal to the probability of being in that state at time $k-1$ plus the probability of first entry into that state at time k . This relation follows from the fact that there are only two mutually exclusive ways to be in state N at time k — either we were there before or else we entered the state at time k . From (3.104) we can relate the first passage probability to the state probability that has already been calculated. Assuming that $p_0(N) = 0$, taking the Z transform of (3.104) we get

$$Q_N(z) = (1 - z^{-1})P_N(z). \quad (3.105)$$

Since $P_N(z)$ is an absorption state, it turns out that it will always have a factor of $(1 - z^{-1})$ in the denominator which will be canceled, resulting in a $Q_N(z)$ which is simpler than the $P_N(z)$ that we started with.

If we define the average or expected time for first entry into state N as f_N , then it turns out that we can find this time without the need to take the inverse Z-transform of $Q_N(z)$.

Exercise 3-18.

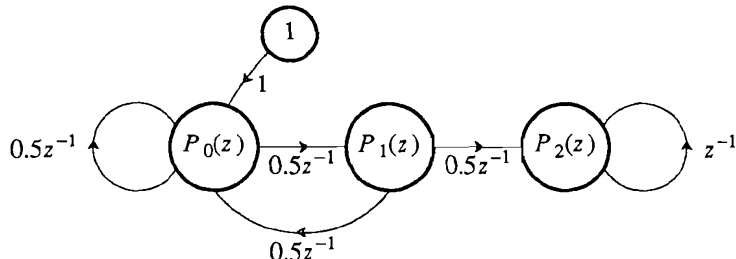
Show that the mean first passage time is

$$f_N = - \frac{\partial}{\partial z} Q_N(z) \Big|_{z=1}. \quad (3.106)$$

□

Example 3-20.

If we toss a fair coin, what is the average number of tosses until we have seen two heads in a row? The signal flow graph for this example is shown below:



The numbering of states is the number of heads in a row. We assume that we start with zero heads in a row. At each toss the number of heads in a row increases by one with probability $\frac{1}{2}$, or goes back to zero with probability $\frac{1}{2}$ (that is, we get a tail). We define state two (two heads in a row) as an absorption state so that we can calculate the first passage time. Solving the linear equations, we get

$$P_2(z) = \frac{z}{4z^3 - 6z^2 + z + 1} = \frac{z}{(z-1)(4z^2 - 2z - 1)} . \quad (3.107)$$

Finally,

$$f_N = -\frac{\partial}{\partial z} \frac{1}{4z^4 - 2z - 1} \Big|_{z=1} = 6 . \quad (3.108)$$

□

3.4. THE POISSON PROCESS AND QUEUEING

There was a time when no random processes could challenge the Gaussian process for the attention of communication theorists. However, the *Poisson process*, and its generalization, the *birth and death process* can reasonably claim to hold that distinction. The question often arises in communications as to the distribution for the times of discrete events, such as the arrivals of messages at a digital communication multiplex, or the arrivals of photons in a light beam at an optical detector in an optical communication system. The Poisson process models the most random such distribution, and is an excellent model for many of these situations.

To proceed, we need to define the notion of *random points in time*, where a point in time might denote the arrival of a message from a random source or a photon at a photodetector. Defining some notation, let the time of the k -th arrival be denoted by t_k , where of course $t_k \geq t_j$ for $k > j$. Further, define a continuous-time random process $N(t)$ that equals the number of arrivals from some starting time t_0 to the current time t . We call $N(t)$ a *counting process* since it counts the accumulated number of random points in time. Thus, $N(t)$ assumes only non-negative integer values, has initial condition $N(t_0) = 0$, and at each random point in time t_k , $N(t)$ increases by one. Such a counting process is pictured in Figure 3-13a, where the arrival times and the value of the counting process are pictured for one typical outcome.

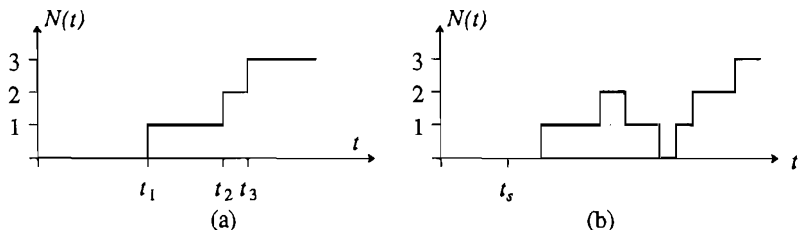


Figure 3-13. Typical outcomes from a counting process $N(t)$. a. A counting process which is monotone increasing. b. A counting process, which has both arrivals and departures and hence can increase or decrease.

In some situations there are only arrivals, so that a counting process of the type pictured in Figure 3-13a is the appropriate model. In other situations, there are departures as well as arrivals. A typical situation is the *queue* pictured in Figure 3-14. We can define a counting process $N(t)$ to be the difference between the accumulated number of arrivals and the accumulated number of departures.

Example 3-21.

Consider a computer communication system that stores arriving messages in a buffer before retransmitting them to some other location. $N(t)$ gives a current count of the number of messages in the system at time t . A typical outcome of such a process is pictured in Figure 3-13b, where it should be noted that the process can never go below zero (since nothing can depart if there is nothing in the buffer). \square

In many instances of practical importance, the count $N(t)$ at time t is all we need to know to predict the future evolution of the system after time t . The manner in which system reached $N(t)$ is irrelevant in terms of predicting the future. For this case, the counting process denotes the *state of the system* in the same sense as Markov chains in the last section. In particular, we say that the system is in state j at time t if $N(t) = j$. This is similar to a Markov chain with one important distinction — a Markov chain can only change states at discrete points in time, whereas we now allow the state to change at any continuous point in time. Like Markov chains, a sample of the counting process $N(t_0)$ is a discrete-valued random variable. Just as for Markov chains (3.97), we define a probability of being in state j at time t as

$$q_j(t) = \Pr[N(t) = j] = P_{N(t)}(j). \quad (3.109)$$

This notation emphasizes that this probability is a continuous-time function. The only real distinction between (3.97) and (3.109) is that the later is defined for continuous-time and the former for discrete-time.

In the following subsections, we analyze a counting process under the specific conditions appropriate for optical communication (Section 3.4.3) and statistical multiplexing (Section 3.4.2).

3.4.1. Birth and Death Process

The cases of interest to us are subsumed by a general process called a *birth and death process*, which is a mathematician's macabre terminology for a counting process with both arrivals and departures. This analysis is given in this section.

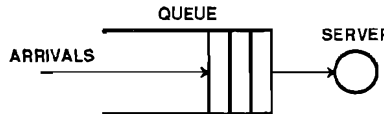


Figure 3-14. A queueing system, which models among other things the status of a buffer in a communication system.

We have to somehow model the evolution of the system from one state to another. The approach for the Markov chain in (3.94) is inappropriate, since the probability of transition between any two states at any point in time t is most likely zero! While we cannot characterize the *probability* of transition, what we can characterize is the *rate* of transition between two states. Suppose for two particular states, the rate of transitions between one state and the other is a constant R . What we mean by this is that in a time δt we can expect an average $R \delta t$ transitions. If δt is very small, then $R \delta t$ is a number much smaller than unity, and the probability of more than one transition in time δt is vanishingly small. Under these conditions, we can think of $R \delta t$ as the probability of one transition in time δt , and $(1 - R \delta t)$ as the probability of no transition.

This logic leads us to a transition diagram and associated set of differential equations. The transition diagram in Figure 3-15 associates a node with each state, and within that node we put the probability of being in that state at time t , which we denote $q_j(t)$. Each transition in the diagram is labeled with the rate at which that transition occurs, where the rates in the general case are allowed to be time-varying (non-homogeneous). Each rate is labeled with a subscript indicating the state in which it originates, where $\lambda_j(t)$ is the rate for transitions corresponding to births or arrivals and $\mu_j(t)$ corresponds to deaths or departures. Reiterating, the interpretation of these rates is as follows: for a very small time interval δt , the probability of a particular transition is equal to the rate times the time interval.

The set of differential equations which describe the evolution of the birth and death process are

$$\frac{dq_j(t)}{dt} = \lambda_{j-1}(t)q_{j-1}(t) + \mu_{j+1}(t)q_{j+1}(t) - (\lambda_j(t) + \mu_j(t))q_j(t), \quad j \geq 0 \quad (3.110)$$

$$q_{-1}(t) = 0.$$

These equations can be derived rigorously from fundamental principles [6], but for our purposes they are evident from intuitive considerations. The equations say that the rate of increase of a probability with time for state j is equal to the rate at which transitions into that state from states $j-1$ and $j+1$ are occurring (times the current probability of those states) minus the rate at which transitions out of state j are occurring (times the current probability of state j).

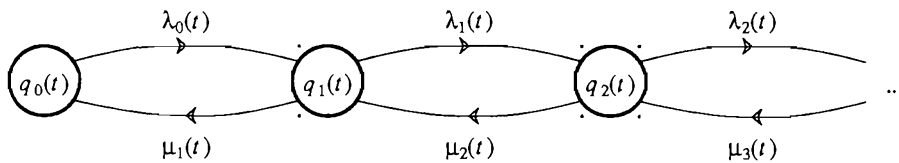


Figure 3-15. State transition diagram for a birth and death process.

We must also specify an initial condition, which for our purposes specifies that the process starts in state zero (no arrivals) at time t_0 ,

$$q_j(t_0) = \begin{cases} 1, & j = 0 \\ 0, & j > 0 \end{cases} \quad (3.111)$$

The first order differential equations can be solved for many special cases.

Example 3-22.

Consider the important case of a *pure birth process* in which $\mu_j(t) = 0$. Also assume the birth rates are all the same and a constant with time, $\lambda_j(t) = \lambda$. The transition diagram for this model is shown in Figure 3-16. This corresponds to the important case where the arrival rate does not depend on the state of the system, the usual case in the problems that we will encounter. Then (3.110) becomes

$$\frac{dq_j(t)}{dt} + \lambda q_j(t) = \lambda q_{j-1}(t) \quad (3.112)$$

which is a simple first order differential equation with constant coefficients. Assume that the initial condition is

$$q_0(0) = 1 \quad (3.113)$$

implying that the initial count at $t = 0$ is 0. We can solve this using very similar techniques to our solution of the Markov chain, but use the Laplace transform in place of the Z-transform. In analogy to (3.98), defining the Laplace transform of the state probability,

$$Q_j(s) = \int_0^\infty q_j(t) e^{-st} dt \quad (3.114)$$

Taking the Laplace transform of both sides of (3.112),

$$sQ_j(s) - q_j(0) + \lambda Q_j(s) = \lambda Q_{j-1}(s) \quad (3.115)$$

Using (3.111), with $t_0 = 0$, this becomes

$$Q_0(s) = \frac{1}{s + \lambda}, \quad Q_j(s) = \frac{\lambda}{s + \lambda} Q_{j-1}(s), \quad j > 0 \quad (3.116)$$

This set of iterative equations for the state probability Laplace transform is easily solved by iteration,

$$Q_j(s) = \frac{\lambda^j}{(s + \lambda)^{j+1}} \quad (3.117)$$

and taking the inverse Laplace transform, we find that for $t \geq 0$ and $j \geq 0$,

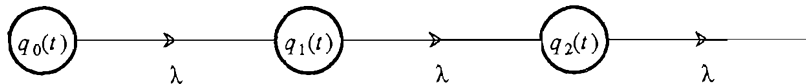


Figure 3-16. State transition diagram for a constant-rate pure birth process.

$$\Pr[N(t) = j] = q_j(t) = \frac{(\lambda t)^j}{j!} e^{-\lambda t}. \quad (3.118)$$

This is the well-known *Poisson distribution* with parameter λt . For this reason, the pure birth process $N(t)$ we have just analyzed is called a *Poisson process* with constant rate. We will generalize this to a variable rate in the next subsection. \square

The Poisson distribution is an important one in the theory of birth and death processes, so we summarize its properties in the following exercise.

Exercise 3-19.

Consider a Poisson distribution with parameter a ,

$$p_N(k) = e^{-a} \frac{a^k}{k!}. \quad (3.119)$$

- (a) Show that the mean and variance of this distribution are

$$E[N] = a, \quad \text{Var}[N] = a. \quad (3.120)$$

(Hint: Form a power series for e^a and differentiate it twice.)

- (b) Show that the moment generating function is given by

$$\log_e \Phi_N(s) = a(e^s - 1). \quad (3.121)$$

\square

The last example can be generalized with respect to the initial condition.

Exercise 3-20.

Show that if $N(t_0) = k$ (there have been k counts up to time t_0), then

$$q_j(t) = \frac{(\lambda(t-t_0))^{j-k}}{(j-k)!} e^{-\lambda(t-t_0)}, \quad j \geq k, t \geq t_0. \quad (3.122)$$

\square

This result implies that the number of counts starting at $t = t_0$ is a Poisson distribution with parameter $\lambda(t - t_0)$, which is the expected number of arrivals since the start time. Furthermore, index $j - k$ of the Poisson distribution is the number of counts since the start time. The important conclusion is that the number of arrivals in the interval starting at $t = t_0$ has a distribution which does not depend in any way on what happened prior to t_0 . This is roughly the definition of a *Markov process*, and a Poisson counting process is in fact a Markov process. For such a process, the number of arrivals in the interval $[t_0, t]$ is statistically independent of the number of arrivals in any other non-overlapping interval of time. It is in this sense that the Poisson process is the most random among all monotone non-decreasing counting processes.

Exercise 3-21.

(*Pure death process.*) For $\lambda_j(t) = 0$, consider the case where departures from the system are proportional to the state index, $\mu_j(t) = j\mu$. This is an appropriate model for a system in which the departure or death rate is proportional to the size of the population, as in a

human population. Further, assume that the initial state at $t = 0$ is n . Draw the state transition diagram and show that the state probabilities obey a binomial distribution,

$$\Pr[N(t) = j] = q_j(t) = \begin{bmatrix} n \\ j \end{bmatrix} p^j(t)(1 - p(t))^{n-j}, \quad p(t) = e^{-\mu}. \quad (3.123)$$

□

Now we give an example of a problem in which both births and deaths occur. This is an example of a *queueing problem*, and it is appropriate at this point to define some terminology used in queueing, particularly as it relates to digital communication. A queue is a *buffer* or *memory* which stores messages. There is some mechanism which clears messages from the queue, which is usually the transmission of the message to another location. This mechanism is called the *server* to the queue. Assume a server can process only one message at a time, so that if more than one message is being processed (there are multiple communication channels for transmission of messages), then there are an equivalent number of servers. Typically the buffer contains space for a maximum number of messages to wait for service, and the number of messages that can be waiting at any time is called the *number of waiting positions*. The *state of the system*, which naturally tracks a counting process, is the number of messages waiting for service plus the number of messages currently being served. Messages arrive at the queue (births) at random times, and they depart from the queue (deaths) due to the completion of service.

Exercise 3-22.

(*Queue with one server and no waiting positions.*) Assume that a queue has constant arrival rate λ , a single server which clears a message being served at rate μ , and no waiting positions. If a message arrives while the server is busy then since there are no waiting positions that arrival is lost and leaves the system permanently. Draw the state transition diagram for the system and show that the probability that the server is not busy is

$$q_0(t) = \frac{\mu}{\lambda + \mu} + \left[q_0(0) - \frac{\mu}{\mu + \lambda} \right] e^{-(\mu + \lambda)t}. \quad (3.124)$$

□

The differential equation approach we have described is capable of describing the transient response of a system starting with any initial condition. Often, however, it is sufficient to know what the state probabilities are in the steady state. There is no such steady state distribution for a Poisson process, since the state grows without bound. However, for queueing systems where the service rate is always guaranteed to be higher than the arrival rate, and where all the rates are independent of time, there will be a steady state distribution. This distribution can be obtained by letting $t \rightarrow \infty$ in the transient solution we have obtained, or can be obtained much more simply by setting the time derivatives in the differential equations to zero and solving for the resulting probabilities.

Example 3-23.

Continuing Exercise 3-22, letting $t \rightarrow \infty$ in (3.124), the steady state probability is

$$q_0(\infty) = \frac{\mu}{\lambda + \mu}. \quad (3.125)$$

We can get this same result without solving the differential equation by setting the derivative in (3.110) to zero. \square

In the following two sections we will specialize the general birth and death process to two situations of particular interest to us.

3.4.2. M/M/1 Queue

Consider the following queueing model which characterizes a single server queue with the most mathematically tractable assumptions. This model is actually a combination of the pure birth process of Example 3-22 and a pure death process (Exercise 3-21). Assume arrivals occur at a constant rate λ independent of the number of waiting positions occupied, there are an infinite number of waiting positions so that no arrival ever encounters a full buffer, arrivals wait indefinitely for service, and there is a single server with service rate μ . The departure rate is independent of the number of messages waiting in the queue, as long as there is at least one. The state transition diagram for this queueing model is shown in Figure 3-17.

As in most queueing problems, we are content to know the steady state distribution of states. This distribution will only exist if the service rate μ is greater than the arrival rate λ , because otherwise the buffer size will grow to infinity. Making that assumption, the differential equations governing the queue are

$$\begin{aligned} \frac{dq_j(t)}{dt} &= \lambda q_{j-1}(t) + \mu q_{j+1}(t) - (\lambda + \mu)q_j(t), \quad j > 0 \\ \frac{dq_0(t)}{dt} &= \mu q_1(t) - \lambda q_0(t) \end{aligned} \quad (3.126)$$

with initial condition (assuming there are no positions occupied at time $t = 0$),

$$q_j(0) = \begin{cases} 1, & j = 0 \\ 0, & j > 0 \end{cases} \quad (3.127)$$

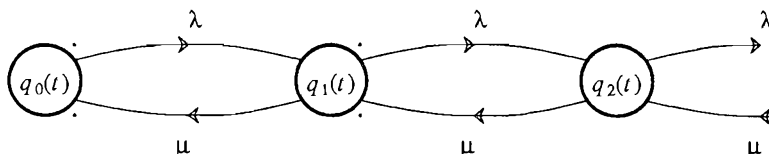


Figure 3-17. The state transition diagram for the single server queue with an infinite number of waiting positions.

We could attempt to solve this system of differential equations, but since we are content with the steady state solution, set the derivatives to zero,

$$\begin{aligned} 0 &= \lambda q_{j-1} + \mu q_{j+1} - (\lambda + \mu)q_j; \quad j > 0 \\ 0 &= \mu q_1 - \lambda q_0 \end{aligned} \quad (3.128)$$

where we have also taken the liberty of suppressing the time dependence since we are looking only at the steady state. These equations are easily solved.

Exercise 3-23.

Show that the solution to (3.128) is

$$q_j = \rho^j (1 - \rho) \quad (3.129)$$

where ρ is called the *offered load*,

$$\rho = \lambda/\mu \quad (3.130)$$

and is less than unity by assumption. Note from (3.129) that the probability that the single server is busy is $1 - q_0 = \rho$, which is obvious since the server has more "capacity" than the arrivals require by a factor of μ/λ . Thus, ρ is also called the *server utilization*. \square

In many queueing problems the most critical parameter is the delay that a new arrival experiences before being served. This is also called the *queueing delay*, and represents a significant impairment in communication systems that utilize a buffer delay discipline to increase the capacity of a communication link (Chapter 18). A related parameter is the *waiting time*, which is defined to be the queueing delay plus the service time. The calculation of the delay is a little more complicated than what we have done heretofore, so we will simply state the results [6]. The mean delay is given by

$$D = \frac{\rho}{\mu(1 - \rho)}. \quad (3.131)$$

Note that as the offered load or server utilization approaches unity, the mean delay grows without bound; conversely, as the utilization approaches zero, the lightly loaded queue, the delay approaches zero. The mean queueing delay is equal to the average service time $1/\mu$ for a utilization of $\rho = 1/2$.

3.4.3. Poisson Process With Time-Varying Rate

In optical communication systems, the counting process which gives the accumulated number of arrival times for photons is a Poisson process (Section 5.3). The Poisson process is a pure birth process where the arrival rate is independent of the state of the system, and we have already been exposed to it in Example 3-22 for a constant arrival rate. In optical communication, the arrival rate is actually signal dependent, so in this section we discuss that case.

The Poisson process with time-varying rate is the pure birth process in which the incoming rate $\lambda(t)$ is independent of the state of the system. Thus, the system is governed by a first-order differential equation with time-varying coefficients,

$$\frac{dq_j(t)}{dt} + \lambda(t)q_j(t) = \lambda(t)q_{j-1}(t), \quad q_{-1}(t) = 0, \quad (3.132)$$

and we assume the system starts at time t_0 in state $j = 0$. Because of the time-varying coefficients, the Laplace transform is of no help, and we must resort to solving the differential equation directly. This is straightforward (since it is a first order equation), but tedious, so the solution is relegated to Appendix 3-C. Define

$$\Lambda(t) = \int_{t_0}^t \lambda(u) du, \quad (3.133)$$

which has the interpretation as the average total number of arrivals in the interval $[t_0, t]$. Then the probability of n arrivals in the interval $[t_0, t]$ is governed by a Poisson distribution with parameter $\Lambda(t)$,

$$q_n(t) = \frac{\Lambda^n(t)}{n!} e^{-\Lambda(t)}. \quad (3.134)$$

This reduces to the solution given in Example 3-22 for the constant rate case.

As a reminder, (3.134) specifies the number $N(t)$ of arrivals during the time interval $[t_0, t]$. This random number of arrivals is Poisson distributed with parameter $\Lambda(t)$, and hence has mean and variance

$$E[N(t)] = \Lambda(t), \quad \sigma_{N(t)}^2 = \Lambda(t). \quad (3.135)$$

As in the constant rate case, it can be shown that the number of arrivals in any two non-overlapping intervals are statistically independent.

3.4.4. Shot Noise

In optical communication, a waveform is generated in the photodetector by generating impulses at times corresponding to random arrival times of photons and then filtering these impulses. This is known as a *filtered Poisson process*, or a *shot noise process*.

If a Poisson process is characterized by a set of arrival times t_k for the k -th arrival, and given a filter with impulse response $h(t)$, then a shot noise process is a continuous-time random process $X(t)$ with outcome

$$x(t) = \sum_k h(t - t_k). \quad (3.136)$$

An outcome of this random process is illustrated in Figure 3-18 for a particular impulse response. In this figure, it is assumed that qualitatively the duration of the impulse response is short relative to the average time between arrivals. If the impulse response were long, this would have an averaging effect resulting in a much smoother outcome.

It is shown in Appendix 3-D that the moment generating function of the shot noise process at time t is

$$\log_e \Phi_{X(t)}(s) = \lambda(t) * (e^{sh(t)} - 1). \quad (3.137)$$

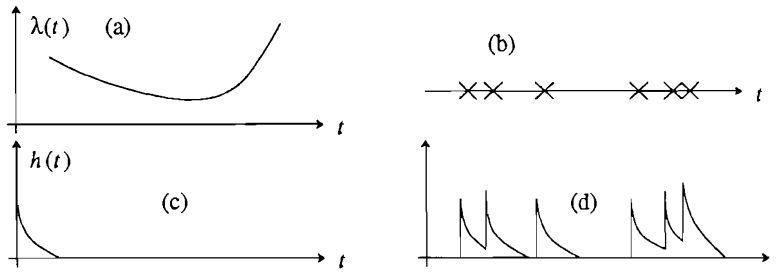


Figure 3-18. Illustration of an outcome of a shot noise process. a. The average arrival rate vs. time. b. The random actual times of arrival, where arrivals occur at the average rate given in a. c. The impulse response of the filter. d. The corresponding outcome.

The mean and variance of shot noise are easily derived from (3.137).

Exercise 3-24.

Show that the mean value of shot noise is the convolution of the filter impulse response with the arrival rate,

$$m_X(t) = E[X(t)] = \lambda(t) * h(t) \quad (3.138)$$

and that the variance is the convolution of the square of the filter impulse response with the arrival rate,

$$\sigma_X^2(t) = E[X^2(t)] - m_X^2(t) = \lambda(t) * h^2(t) . \quad (3.139)$$

These relations are known as *Campbell's theorem*. \square

3.4.5. High-Intensity Shot Noise

When the intensity of shot noise is high, the statistics become that of a Gaussian random process. The intuition behind this is that $X(t)$ is the sum of a large number of independent events, and hence approaches a Gaussian by the central limit theorem. To demonstrate this more rigorously, we will show that the moment generating function of shot noise approaches a Gaussian moment generating function in the limit of high intensity.

In order to avoid an infinitely large power of shot noise, as the intensity grows we need to scale the size of the impulse response $h(t)$ also. Therefore, let us use a scaling constant β , which we will allow to grow to infinity, and let

$$\lambda(t) = \beta \lambda_0(t) , \quad h(t) = \frac{1}{\sqrt{\beta}} h_0(t) . \quad (3.140)$$

With this scaling, we get from Campbell's theorem that

$$m_X(t) = \sqrt{\beta} \lambda_0(t) * h_0(t) , \quad \sigma_X^2(t) = \lambda_0(t) * h_0^2(t) . \quad (3.141)$$

Hence, as the scaling factor β grows, the variance of the process stays constant and the mean value grows without bound. We cannot help this, because as the intensity grows

the variance becomes a smaller fraction of the mean. In this sense high-intensity shot noise approaches a deterministic signal $m_X(t)$ as the intensity grows.

Only two terms in the moment generating function are important as the scaling constant β grows.

Exercise 3-25.

Show that for large β the only significant terms in the moment generating function of (3.137) are

$$\log_e \Phi_{X(t)}(s) \approx s\sqrt{\beta}\lambda_0(t) * h_0(t) + 0.5s^2\lambda_0(t) * h_0^2(t) \quad (3.142)$$

Comparing this with the Gaussian moment generating function of (3.41), we see that high intensity shot noise is approximately Gaussian with mean and variance given by (3.141). \square

3.4.6. Random-Multiplier Shot Noise

In optical communication systems, it is sometimes appropriate to introduce a random multiplier into the shot noise process, *viz.*

$$X(t) = \sum_k G_k h(t-t_k) \quad (3.143)$$

where G_k is a sequence of mutually statistically independent identically distributed random variables which are also statistically independent of the arrival times t_j for all j .

Exercise 3-26.

Use Campbell's theorem and the assumptions to show that the mean-value of (3.143) is

$$m_X(t) = E[G] \lambda(t) * h(t) \quad (3.144)$$

and the variance is

$$\sigma_X^2(t) = E[G^2] \lambda(t) * h^2(t) \quad (3.145)$$

where $E[G]$ and $E[G^2]$ are the mean-value and second moment of the random multiplier G_k for all k . \square

3.5. FURTHER READING

For a general introduction to random variables and processes, Papoulis [7], Stark and Woods [8], and Ross [9] are recommended. Papoulis has more of an engineering perspective. Both books have comprehensive treatments of Markov chains and Poisson and shot noise processes. An excellent introduction to Poisson processes can be found in Ross [10]. There are a number of books that give comprehensive treatment to the application of Poisson and birth and death processes to queueing models, such as Cooper [6], Hayes [11], and Kleinrock [12].

APPENDIX 3-A POWER SPECTRUM OF A CYCLOSTATIONARY PROCESS

In this appendix we determine the power spectrum of the PAM random process with a random phase epoch (3.81). Calculating the autocorrelation function of (3.81),

$$\begin{aligned} E[Z(t+\tau)Z^*(t)] &= E[Y(t+\Theta+\tau)Y^*(t+\Theta)] \\ &= E\left[\sum_{n=-\infty}^{\infty} \sum_{m=-\infty}^{\infty} X_m X_n^* h(t+\Theta-mT+\tau) h^*(t+\Theta-nT)\right]. \end{aligned} \quad (3.146)$$

Assuming we can interchange expectation and summation, we use the fact that Θ is independent of X_k to get

$$E[Z(t+\tau)Z^*(t)] = \sum_{n=-\infty}^{\infty} \sum_{m=-\infty}^{\infty} E[X_m X_n^*] E[h(t+\Theta-mT+\tau) h^*(t+\Theta-nT)]. \quad (3.147)$$

The first expected value is simply the autocorrelation function $R_X(m-n)$. The second expected value can be computed using the definition of expectation and the p.d.f. of the uniform random variable Θ

$$E[h(t+\Theta-mT+\tau) h^*(t+\Theta-nT)] = \int_0^T \frac{1}{T} h(t+\theta-mT+\tau) h^*(t+\theta-nT) d\theta. \quad (3.148)$$

Changing variables, letting $i = m-n$, using (3.148), and exchanging summations, we get

$$E[Z(t+\tau)Z^*(t)] = \frac{1}{T} \sum_{i=-\infty}^{\infty} R_X(i) \sum_{n=-\infty}^{\infty} \int_0^T h(t+\theta-(i+n)T+\tau) h^*(t+\theta-nT) d\theta. \quad (3.149)$$

Changing variables again and defining $\alpha = t+\theta-nT$, we get

$$E[Z(t+\tau)Z^*(t)] = \frac{1}{T} \sum_{i=-\infty}^{\infty} R_X(i) \sum_{n=-\infty}^{\infty} \int_{t-nT}^{t-nT+T} h(\alpha-iT+\tau) h^*(\alpha) d\alpha. \quad (3.150)$$

The second summation is the sum of integrals with adjoining limits, so it can be replaced with a single infinite integral

$$E[Z(t+\tau)Z^*(t)] = \frac{1}{T} \sum_{i=-\infty}^{\infty} R_X(i) \int_{-\infty}^{\infty} h(\alpha-iT+\tau) h^*(\alpha) d\alpha, \quad (3.151)$$

which is independent of t , so the process $Z(t)$ is wide sense stationary. To get the power spectrum, we take the Fourier transform with τ as the time index

$$S_Z(j\omega) = \frac{1}{T} \sum_{i=-\infty}^{\infty} R_X(i) \int_{-\infty}^{\infty} h^*(\alpha) \left[\int_{-\infty}^{\infty} h(\alpha-iT+\tau) e^{-j\omega\tau} d\tau \right] d\alpha. \quad (3.152)$$

The expression in brackets is the Fourier transform of $h(t)$ with a time shift of $\alpha-iT$,

so it equals $e^{j\omega(\alpha-iT)}H(j\omega)$. Therefore,

$$S_Z(j\omega) = \frac{1}{T}H(j\omega) \sum_{i=-\infty}^{\infty} R_X(i) \left[\int_{-\infty}^{\infty} h^*(\alpha)e^{j\omega(\alpha-iT)} d\alpha \right].$$

The expression in brackets is $e^{-j\omega T}H^*(j\omega)$, getting

$$S_Z(j\omega) = \frac{1}{T}H(j\omega)H^*(j\omega) \sum_{i=-\infty}^{\infty} R_X(i)e^{-j\omega iT}. \quad (3.153)$$

The summation is simply the discrete-time Fourier transform $S_X(e^{j\omega T})$ of the auto-correlation function. The final result is

$$S_Z(j\omega) = \frac{1}{T}|H(j\omega)|^2 S_X(e^{j\omega T}). \quad (3.154)$$

APPENDIX 3-B POWER SPECTRUM OF A MARKOV CHAIN

In this appendix we solve the problem of finding the power spectrum of the random process (3.95). The power spectrum only exists if the random process is wide sense stationary. Strictly speaking, this requires that the Markov chain be running over all time, although we can interpret the results as indicative of the power spectrum for a chain that was initialized but has been running long enough to be in the steady-state. We approach this by assuming that the initial probability of each state is the same as its steady-state probability, so that the state probability is in fact constant with time (a *stationary* Markov chain).

We first determine the autocorrelation function of (3.95),

$$R_X(n) = E[f(\Psi_k)f(\Psi_{k+n})], \quad (3.155)$$

assuming $f(\cdot)$ is a real-valued function. Assuming wide-sense stationarity, we can take $k = 0$ and this can be written

$$R_X(n) = \sum_{i \in \Omega_\Psi} \sum_{j \in \Omega_\Psi} f(i)f(j) p_{0,n}(i,j). \quad (3.156)$$

where by Bayes' rule

$$p_{0,n}(i,j) = p_{n|0}(j|i)p_0(i) \quad (3.157)$$

is the joint probability of being in state i at time 0 and state j at time n . Assuming we have already calculated the steady-state state probabilities $p(i)$ for the chain, by the stationarity assumption we can write

$$p(i) = p_0(i). \quad (3.158)$$

One way to think of this is as forcing the initial state probability to equal the steady-state probability, thus suppressing any transient solution. Finally, we must carefully

note the d.c. component of the random process, since it contributes a delta-function to the power spectrum that can easily be lost if we are not careful. Specifically, the d.c. component is

$$\mu_X = \sum_{i \in \Omega_\Psi} f(i)p(i). \quad (3.159)$$

The power spectrum is simply the Z transform of the autocorrelation function evaluated at $z = e^{j\omega T}$ (see (3.58)). Rather than calculate the Z transform $S_X(z)$ directly, let us first concentrate on the quantity

$$S_X^+(z) = \sum_{n=0}^{\infty} R_X(n)z^{-n} \quad (3.160)$$

that includes only the positive index terms in the summation making up the Z transform. From (3.156), (3.157), and (3.158), this can be written as

$$S_X^+(z) = \sum_{i \in \Omega_\Psi} \sum_{j \in \Omega_\Psi} f(i)f(j)p(i)P_{j|i}(z) \quad (3.161)$$

where

$$P_{j|i}(z) = \sum_{n=0}^{\infty} p_{n|0}(j|i)z^{-n}. \quad (3.162)$$

This latter quantity can be interpreted as the Z-transform of $p_{n|0}(j|i)$, which is in turn the probability of being in state j at time n given that we started (with probability one) in state i at time 0. This quantity is easy to calculate using the techniques we have previously displayed, since it is simply the Z-transform of a transient solution starting with probability one in a particular state. The signal flow graph for this solution is shown in Figure 3-19, where only the states i and j are shown. This signal flow graph must be solved for $P_{j|i}(z)$ for all (i,j) for which $f(i)f(j)$ is non-zero in (3.161).

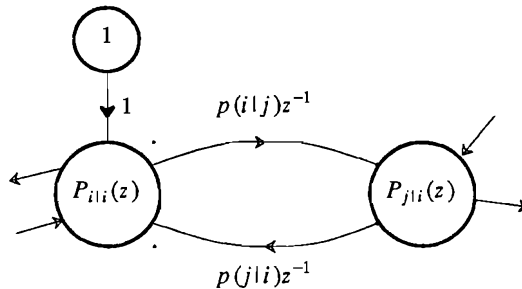


Figure 3-19. Signal flow graph representation of equations that must be solved to find $P_{j|i}(z)$.

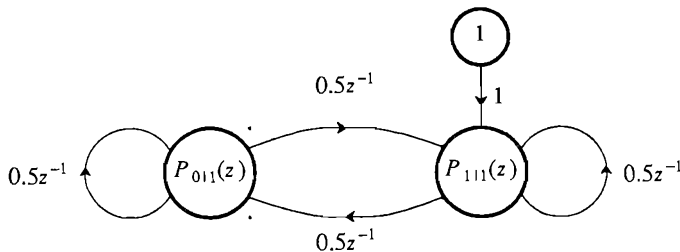


Figure 3-20. Signal flow graph for the parity check circuit.

Example 3-24.

Again returning to the parity check circuit of Example 3-14, let us compute $S_X^+(z)$. In this case $f(i) = i$, so that the random process $X_k = f(\Psi_k) = \Psi_k$ assumes the values 0 and 1. For that case, we only need evaluate one term in (3.156), corresponding to $i = j = 1$, and all the others are zero. This term is shown by the signal flow graph in Example 3-24. Solving this flow graph, we get

$$P_{111}(z) = \frac{1 - 0.5z^{-1}}{1 - z^{-1}} \quad (3.163)$$

and

$$S_X^+(z) = 0.5 \frac{1 - 0.5z^{-1}}{1 - z^{-1}} \quad (3.164)$$

since there is only one term in the sum and $p(0) = p(1) = \frac{1}{2}$. Inverting the Z transform, we find that

$$R_X(n) = \begin{cases} \frac{1}{2}; & \text{for } n = 0 \\ \frac{1}{4}; & \text{for } n > 0 \end{cases} \quad (3.165)$$

This result says that the power of the process is $\frac{1}{2}$, which is obvious, and that the process has a d.c. component of $\frac{1}{2}$ since the autocorrelation function approaches $\frac{1}{4}$ for large n , which is also obvious. \square

We have determined the one-sided terms in the power spectrum, and we must generate the two-sided spectrum $S_X(z)$. However, before doing this, we must first remove any d.c. component, since that d.c. component can be represented by the one-sided transform but is problematic in the two-sided transform. This is simple, since we only need to replace $S_X^+(z)$ by

$$S_X^+(z) - \frac{\mu_X^2}{1 - z^{-1}} \quad (3.166)$$

to remove this d.c. component. Alternatively we could have defined a new random process with the d.c. component removed, although that method is often harder.

Example 3-25.

For the parity check circuit of Example 3-14, the d.c. component is $\mu_X = \frac{1}{2}$, and subtracting the appropriate term from (3.164),

$$S_X^+(z) - \frac{\mu_X^2}{1-z^{-1}} = 0.25 . \quad (3.167)$$

Note that for this process this result would have been much more difficult to obtain if we had defined a d.c. free random process, since then we would have to evaluate all four terms in (3.161) rather than just one. \square

We must now turn the one-sided version of the power spectrum into a two-sided version. The Z transform of the autocorrelation function can be written

$$S_X(z) = \sum_{m=-\infty}^{\infty} R_X(m)z^{-m} = \sum_{m=0}^{\infty} R_X(m)z^{-m} + \sum_{m=0}^{\infty} R_X(m)z^m - R_X(0) , \quad (3.168)$$

where we have used the symmetry of the autocorrelation function. Noting that $R_X(0) = S_X^+(\infty)$, we get finally

$$S_X(z) = S_X^+(z) + S_X^+(z^{-1}) - S_X^+(\infty) . \quad (3.169)$$

Example 3-26.

To finish with the parity check example of Example 3-14,

$$S_X(z) = 0.25 + 0.25 - 0.25 = 0.25 \quad (3.170)$$

and the process is white with power $\frac{1}{4}$. However, recall that this power spectrum does not include the d.c. term, so that in fact

$$S_X(e^{j\omega T}) = \frac{1}{4} + \frac{\pi}{2} \delta(\omega) . \quad (3.171)$$

The area of the delta function has been chosen so that this area divided by 2π is $\frac{1}{4}$, the power of the d.c. component. \square

APPENDIX 3-C DERIVATION OF POISSON PROCESS

In this appendix we show that the Poisson distribution for the accumulated number of arrivals as given by (3.134) is valid. To begin with, we need the solution to a first-order differential equation, which is given in the following exercise[13].

Exercise 3-27.

Consider the following first order differential equation,

$$\dot{x}(t) + a(t)x(t) = b(t) . \quad (3.172)$$

- (a) Let $A(t) = a(t)$ and show that

$$\frac{d}{dt}(e^{\Lambda(t)}x(t)) = b(t)e^{\Lambda(t)}. \quad (3.173)$$

(b) Integrate both sides of (3.173) to obtain the solution for $x(t)$

$$x(t) = x(t_0)e^{\Lambda(t)} + e^{-\Lambda(t)} \int_{t_0}^t b(u)e^{\Lambda(u)}du, \quad \Lambda(t) = \int_{t_0}^t a(v)dv. \quad (3.174)$$

□

Returning to the Poisson process, identify

$$a(t) = \lambda(t), \quad b(t) = \lambda(t)q_{j-1}(t). \quad (3.175)$$

Therefore, given the definition of (3.133) for $\Lambda(t)$,

$$q_j(t) = q_j(t_0)e^{-\Lambda(t)} + e^{-\Lambda(t)} \int_{t_0}^t \lambda(u)q_{j-1}(u)e^{\Lambda(u)}du. \quad (3.176)$$

The solution follows immediately for $j = 0$ using the initial condition of (3.132),

$$q_0(t) = e^{-\Lambda(t)} \quad (3.177)$$

and the rest is easy!

Exercise 3-28.

Verify the validity of (3.134) by induction on (3.176). □

APPENDIX 3-D MOMENT GENERATING FUNCTION OF SHOT NOISE

In this appendix we derive the moment generating function of a shot noise process $X(t)$ corresponding to impulse response $h(t)$. A sample function of such a process is given by (3.136).

To find the moment generating function, divide the time axis into small intervals of length δt , where the k -th interval is $[(k - \frac{1}{2})\cdot\delta t, (k + \frac{1}{2})\cdot\delta t]$. Group all the arrivals in the k -th interval together into a single impulse of height N_k located at time $k\cdot\delta t$, where N_k is the number of arrivals in the k -th interval. Thus, the shot noise of (3.136) becomes approximately

$$X(t) = \sum_{k=-\infty}^{\infty} N_k h(t - k\cdot\delta t) \quad (3.178)$$

where this equation becomes increasingly accurate as $\delta t \rightarrow 0$.

Since the intervals are non-overlapping, the N_k are independent Poisson random variables with parameter $\lambda(k\cdot\delta t)\cdot\delta t$, the average number of arrivals in the interval. The moment generating function of N_k is therefore

$$\log_e \Phi_{N_k}(s) = \lambda(k \cdot \delta t) \cdot \delta t (e^s - 1) \quad (3.179)$$

and the moment generating function of (3.178) is

$$\begin{aligned} \Phi_{X(t)}(s) &= E[\exp\{s \sum_{k=-\infty}^{\infty} N_k h(t - k \cdot \delta t)\}] = \prod_{k=-\infty}^{\infty} E[\exp\{s N_k h(t - k \cdot \delta t)\}] \\ &= \prod_{k=-\infty}^{\infty} \Phi_{N_k}(s h(t - k \cdot \delta t)) . \end{aligned} \quad (3.180)$$

Taking the logarithm of the moment generating function, and substituting from (3.179),

$$\log_e \Phi_{X(t)} = \sum_{k=-\infty}^{\infty} \lambda(k \cdot \delta t) (\exp\{s h(t - k \cdot \delta t)\} - 1) \cdot \delta t \quad (3.181)$$

and as $\delta t \rightarrow 0$ this approaches the integral

$$\log_e \Phi_{X(t)} = \int_{-\infty}^{\infty} \lambda(\tau) (\exp\{s h(t - \tau)\} - 1) d\tau \quad (3.182)$$

which we recognize as the convolution of (3.137).

PROBLEMS

- 3-1. Use the moment generating function of (3.41) to show that the mean of the Gaussian distribution is μ and the variance σ^2 .
- 3-2. Show that the marginal p.d.f.s of X and Y in (3.47) are those of a zero-mean Gaussian random variable with variance σ^2 .
- 3-3. Show that for $y > 0$

$$\frac{1}{y\sqrt{2\pi}} e^{-y^2/2} \left[1 - \frac{1}{y^2} \right] < Q(y) < \frac{1}{y\sqrt{2\pi}} e^{-y^2/2} . \quad (3.183)$$

These bounds are plotted in Figure 3-1. Hint: Write the definition of $Q(\cdot)$ from (3.38) and integrate by parts.

- 3-4. Let X and Y be two complex-valued random variables.
 - (a) Form an estimate of X as $\hat{X} = a \cdot Y$ for some complex number a . Find the a that minimizes the mean-square error $E[|\hat{X} - X|^2]$.
 - (b) Reformulate the problem of (a) in terms of linear space and inner products.
 - (c) Re-solve the problem of (a) using the projection theorem of Section 2.6.3.
- 3-5. In Figure 3-4a let E_k be a prediction error generated by filter $E(z)$ such that

$$E[E_{k+m} X_k^*] = R_{EX}(m) = 0 , \quad m > 0 , \quad (3.184)$$

and let E_k' be the output generated by any other causal and monic filter.

- (a) Show that

$$E|E_k'|^2 = E|E_k' - E_k|^2 + E|E_k|^2 , \quad (3.185)$$

thus establishing that the output MSE is minimized when $E_k' = E_k$.

- (b) Show that it follows from the orthogonality property of (3.184) that $R_E(m) = 0$ for all $m \neq 0$, and hence the optimal prediction error must be white.

3-6.

- (a) Restate the results of Problem 3-5 in geometric terms, using the interpretation of Section 3.1.4.
 (b) Re-derive the results of Problem 3-5 using the projection theorem of Section 2.6.3.

- 3-7.** Given a WSS random process $X(t)$ with power $R_X(0)$, show that the sampled random process $Y_k = X(kT)$ has the same power,

$$\mathbb{E}[|Y_k|^2] = R_Y(0) = R_X(0). \quad (3.186)$$

- 3-8.** Given a sequence of i.i.d. random variables A_k which take on values ± 1 with equal probability, find an expression for $\mathbb{E}[A_p A_q A_r A_s]$.

- 3-9.** Consider a random process $X(t)$ filtered by an ideal bandpass filter with frequency response

$$H(j\omega) = \begin{cases} 1; & \omega_a < \omega < \omega_b \\ 0; & \text{otherwise} \end{cases}.$$

Let $Y(t)$ be the output of the filter. Show that

$$R_Y(0) = \frac{1}{2\pi} \int_{\omega_a}^{\omega_b} S_X(j\omega) d\omega.$$

Use this to show that $S_X(j\omega) \geq 0$ for all ω .

- 3-10.** Extending Exercise 2-6 to random signals, assume the input to the possibly complex-valued LTI system shown in Figure 2-3 is a wide sense stationary complex-valued discrete-time random process with power spectral density $S_X(e^{j\omega T}) = N_0$. Show that the autocorrelation of the output is

$$R_Y(k) = N_0 f(kT) * f^*(-kT) = N_0 \sum_m f(mT)f^*((m-k)T) \quad (3.187)$$

- 3-11.** Show that the cross-correlation function has symmetry

$$R_{XY}(\tau) = R_{YX}^*(-\tau). \quad (3.188)$$

Is the cross-spectral density of two random processes necessarily real-valued?

- 3-12.** Where a Markov chain has unique steady-state probabilities $p_k(i) = p(i)$, they can be found from the condition that the state probabilities will not change with one time increment. Assume $\Omega_\Psi = \{0, \dots, M\}$, define the matrix of state transition probabilities \mathbf{P} to contain $p(j|i)$ in its $(i,j)^{\text{th}}$ entry, and define the vector $\boldsymbol{\pi} = [p(0), \dots, p(M)]$ to contain the steady-state probabilities, if they exist. Show that the steady-state probabilities can be obtained by solving the system of equations $\boldsymbol{\pi} = \boldsymbol{\pi}\mathbf{P}$ with the constraint

$$\sum_{i=0}^M p(i) = 1. \quad (3.189)$$

- 3-13.** Assume you toss a coin that is not fair, where p is the probability of a tail and $q = 1 - p$ is the probability of a head.

- (a) Draw a signal flow graph representation for a Markov chain representing the number of heads tossed in a row. Define N as an absorption state, since in part (c) we will be interested in the first passage time to state N .
 (b) Show that

$$P_N(z) = \frac{q^N z(z-q)}{(z-1)(z^{N+1} - z^N + pq^N)}. \quad (3.190)$$

- (c) Show that the first passage time to N heads in a row is

$$f_N = \frac{1 - q^N}{pq^N}. \quad (3.191)$$

- (d) Interpret this equation for $p \approx 1$ and N large.

- 3-14.** Show that for a Markov chain Ψ_k ,

$$p(\psi_0, \psi_1, \dots, \psi_n) = p(\psi_0 | \psi_{n-1})p(\psi_{n-1} | \psi_{n-2}) \cdots p(\psi_1 | \psi_0)p(\psi_0).$$

In words, show that the joint probability of the states at times zero through n is the product of the initial state probability $p(\psi_0)$ and the transition probabilities $p(\psi_k | \psi_{k-1})$.

- 3-15.** Show that for a Markov chain Ψ_k

$$p(\psi_n | \psi_{n+1}, \psi_{n+2}, \dots, \psi_{n+m}) = p(\psi_n | \psi_{n+1}). \quad (3.192)$$

In words, show that a Markov chain is also Markov when time is reversed.

- 3-16.** Show that for the Markov chain Ψ_k , the future is independent of the past if the present is known. In other words, for any $n > r > s$,

$$p(\psi_n, \psi_s | \psi_r) = p(\psi_n | \psi_r)p(\psi_s | \psi_r).$$

- 3-17.** Consider the parity checker example in Figure 3-8. Suppose that the initial state is zero, $p_0(0) = 1$. Sketch the signal flow graph describing the state probabilities. Compute $p_k(0)$ and $p_k(1)$ as a function of k . Sketch these functions. Is the Markov chain stationary?

- 3-18.** Consider tossing a fair coin. We are interested in the probability that at the k^{th} toss we have seen at least two heads in a row. Define the random process Ψ_k to have value two if there have been two heads in a row, to have value one if not and the last toss was heads, and to have value zero otherwise.

- (a) Show that the random process Ψ_k is Markov and sketch the state diagram of the Markov chain.
- (b) Sketch the signal flow graph describing the state probabilities. Assume that the coin is fair.
- (c) Solve for the probability that at the k^{th} toss we have seen at least two heads in a row. You may leave the solution in the Z domain.

- 3-19.** Using the results of Exercise 3-3, show that the Chernoff bounds on the distribution function for a Poisson random variable N with parameter a are

$$1 - F_N(n) \leq \left(\frac{a}{n}\right)^n e^{n-a}, \quad a < n, \quad F_N(n) \leq \left(\frac{a}{n}\right)^n e^{n-a}, \quad a > n. \quad (3.193)$$

- 3-20.** Find the mean and variance at time t_1 of a Poisson process $N(t)$ with constant rate λ .

- 3-21.** Show that if $t_1 < t_2$ then

$$P_{N(t_1), N(t_2)}(k, k+n) = \frac{\lambda^{k+n}(t_2 - t_1)^n t_1^k}{n! k!} e^{-\lambda t_2}.$$

- 3-22.** Consider a pure birth process in which the birth rate is proportional to the state ($\lambda_j(t) = j\lambda$), as might model the growth of a biological population. Assume the initial condition is $q_1(0) = 1$, that is we start with a population of one. Find $Q_j(s)$ for all j .

- 3-23.** Shot noise can be generated from a Poisson process by linear filters as shown in Figure 3-21. Assume without further justification that expectation and differentiation can be interchanged; that is, the mean value of $\frac{dN(t)}{dt}$ is $\frac{d}{dt}E[N(t)]$.

- (a) For $N(t)$ a Poisson process, show that the mean value of $\frac{dN(t)}{dt}$ is $\lambda(t)$.

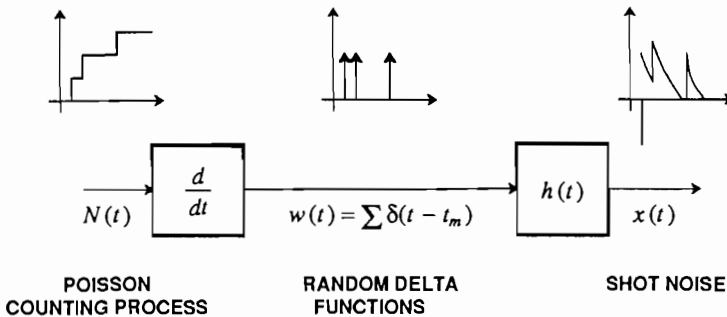


Figure 3-21. The generation of the shot noise from a Poisson counting process.

- (b) Similarly show that the mean value of $X(t)$ is given by (3.138).
- (c) For a random process $N(t)$, show that the derivative of this process $\dot{N}(t)$ has autocorrelation

$$R_{\dot{N}\dot{N}}(t_1, t_2) = \frac{\partial^2 R_{NN}(t_1, t_2)}{\partial t_1 \partial t_2}. \quad (3.194)$$

- (d) Consider a linear time-invariant system with input $W(t)$ and output $X(t)$, where $W(t)$ has autocorrelation function $R_{WW}(t_1, t_2)$. Show that

$$R_{WX}(t_1, t_2) = R_{WW}(t_1, t_2) * h(t_2), \quad R_{XX}(t_1, t_2) = R_{WW}(t_1, t_2) * h(t_1). \quad (3.195)$$

- 3-24.** For the Poisson process $N(t)$ in Figure 3-21, consider two times $0 < t_1 < t_2$, and note the statistical independence of $(N(t_1) - N(0))$ and $(N(t_2) - N(t_1))$. Using this fact, and assuming $N(0) = 0$, show that

$$R_{NN}(t_1, t_2) = \Lambda(t_1)[1 + \Lambda(t_2)], \quad t_1 \leq t_2 \quad (3.196)$$

where $\Lambda(t)$ is defined in (3.133). Exchange the role of t_1 and t_2 to show that

$$R_{NN}(t_1, t_2) = \Lambda(t_2)[1 + \Lambda(t_1)], \quad t_1 \geq t_2. \quad (3.197)$$

- 3-25.** Using the results of Problem 3-23 and Problem 3-24, show that the autocorrelation of shot noise is

$$R_X(t_1, t_2) = [\lambda(t_1) * h(t_1)][\lambda(t_2) * h(t_2)] + [\lambda(t_2)h(t_1 - t_2)] * h(t_2), \quad (3.198)$$

and evaluating at $t_1 = t_2 = t$,

$$R_X(t, t) = [\lambda(t) * h(t)]^2 + \lambda(t) * h^2(t) \quad (3.199)$$

thereby establishing Campbell's theorem (3.139) by a different method.

- 3-26.** For the constant rate case ($\lambda(t) = \lambda$), the shot noise process is wide-sense stationary. Find the autocorrelation and power spectrum.

- 3-27.** Let a Poisson process have rate

$$\lambda(t) = \begin{cases} 0, & t < 0 \\ \lambda_0, & t \geq 0 \end{cases}$$

Show that a shot noise with this rate has mean value proportional to the step function of the system.

- 3-28. Consider a shot noise with rate function

$$\lambda(t) = \lambda_0 + \lambda_1 \cos(\omega_1 t).$$

Find the mean value of this shot noise.

- 3-29. Show that the power spectrum of the output of the parity checker of Figure 3-8 when the input bits are not equally probable is

$$S_X(z) = \frac{p(1-p)}{(1 - (1-2p)z^{-1})(1 - (1-2p)z)} \quad (3.200)$$

where p is the probability of a one-bit.

REFERENCES

1. R. E. Ziemer and W. H. Tranter, *Principles of Communications: Systems Modulation and Noise*, Houghton Mifflin Co., Boston (1985).
2. S. J. Mason, "Feedback Theory - Some Properties of Signal Flow Graphs," *Proc. IEEE* **41**(Sep. 1953).
3. S. J. Mason, "Feedback Theory — Further Properties of Signal Flow Graphs," *Proc. IRE* **44**(7) p. 920 (July 1956).
4. B. C. Kuo, *Automatic Control Systems*, Prentice-Hall, Englewood Cliffs, N.J. (1962).
5. C. L. Phillips and R. D. Harbor, *Feedback Control Systems*, Prentice-Hall, Englewood Cliffs, N.J. (1988).
6. R. B. Cooper, *Introduction to Queueing Theory*, MacMillan, New York (1972).
7. A. Papoulis, *Probability, Random Variables, and Stochastic Processes*, McGraw-Hill, New York (1991).
8. H. Stark and J. W. Woods, *Probability, Random Processes, and Estimation Theory for Engineers*, Prentice-Hall, Englewood Cliffs, NJ (1986).
9. S. M. Ross, *Stochastic Processes*, John Wiley & Sons, New York (1983).
10. Sheldon M. Ross, *Introduction to Probability Models*, 2nd Ed., Academic Press, New York (1980).
11. J. F. Hayes, *Modeling and Analysis of Computer Communication Networks*, Plenum Press, New York (1984).
12. L. Kleinrock, *Queueing Systems. Volume I: Theory*, John Wiley & Sons, New York (1975).
13. E. A. Coddington, *An Introduction to Ordinary Differential Equations*, Prentice Hall, Englewood Cliffs, N.J. (1961).

4

LIMITS OF COMMUNICATION

In the late 1940's, Claude Shannon of Bell Laboratories developed a mathematical theory of information that profoundly altered our basic thinking about communication, and stimulated considerable intellectual activity, both practical and theoretical. This theory, among other things, gives us some fundamental boundaries within which communication can take place. Often we can gain considerable insight by comparing the performance of a digital communication system design with these limits.

Information theory provides profound insights into the situation pictured in

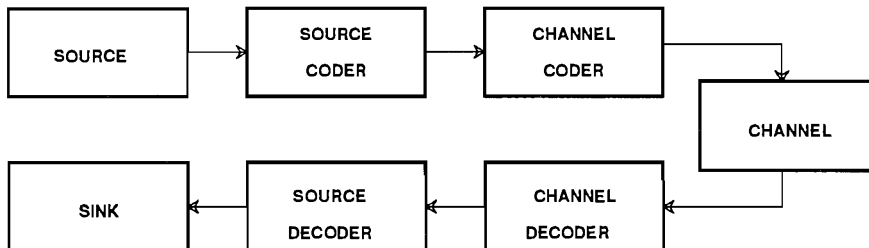


Figure 4-1. A general picture of a source communicating over a channel using source and channel coding.

Figure 4-1, in which a *source* is communicating over a *channel* to a *sink*. The source and channel are both modeled statistically. The objective is to provide the source information to the sink with the greatest fidelity. To that end, Shannon introduced the general idea of *coding*. The objective of *source coding* is to minimize the bit rate required for representation of the source at the output of a source coder, subject to a constraint on fidelity. Shannon showed that the interface between the source coder and channel coder can be, without loss of generality, a bit stream, regardless of the nature of the source and channel. The objective of *channel coding* is to maximize the information rate that the channel can convey sufficiently reliably (where reliability is normally measured as a bit error probability). Our primary focus in this book will be on the channel and the associated channel coder, although understanding source coding will also be helpful.

Given the statistics of a source, modeled as a discrete-time random process, the minimum number of bits per unit time required to represent it at the output of the source coder with some specified distortion can be determined. The *source coding theorem* is the key result of this *rate distortion theory* (see for example [1]). This theory offers considerable insight into the bit rates required for digital communication of an analog signal via PCM (Chapter 1).

Example 4-1.

We limit our attention here to the simple special case of a *discrete-time discrete-valued* random process $\{X_k\}$ with independent and identically distributed (i.i.d.) samples. Because the process is discrete-valued, it is possible to encode the signal as a bit stream with *perfect fidelity*. In fact, the minimum average number of bits required to represent each sample without distortion is equal to the *entropy* of X , defined to be

$$H(X) = E[-\log_2 p_X(x)] = - \sum_{x \in \Omega_X} p_X(x) \log_2 p_X(x), \quad (4.1)$$

where Ω_X is the alphabet (sample space) of X . This result is developed in Section 4.1. \square

Since the entropy determines the number of bits required to represent a sample at the output of the source coder, it is said to determine the amount of *information* in the sample, measured in bits. This concept is explained in Section 4.1.

A second concept due to Shannon is the *capacity* of a noisy communication channel, defined as the maximum bit rate that can be transmitted over that channel with a vanishingly small error rate. The various forms of the *channel coding theorem* specify the capacity. The fact that an error rate approaching zero can be achieved was very surprising at the time, and it motivated the practical forms of channel coding to be discussed in Chapters 13 and 14.

Example 4-2.

Consider transmitting a random process $\{X_k\}$, with similar characteristics to Example 4-1, over a noisy discrete-time memoryless channel, defined as one for which the current output Y_k is dependent on only the current input X_k . Because the channel is memoryless, the samples Y_k are also independent and identically distributed. The capacity of this channel can be obtained from the *mutual information* between the input random variable X and the output random variable Y .

$$I(X,Y) = H(X) - H(X|Y), \quad (4.2)$$

where $H(X|Y)$ is the *conditional entropy*. The channel capacity equals the mutual information maximized over all possible probability distributions for the input X . This result is developed in Section 4.2. \square

The result of Example 4-2 can also be used to determine the channel capacity of a bandlimited continuous-time channel using the Nyquist sampling theorem, as will be discussed in Section 4.3.

4.1. JUST ENOUGH INFORMATION ABOUT ENTROPY

Intuitively, *observing the outcome* of a random variable gives us *information*. Rare events carry more information than common events.

Example 4-3.

You learn very little if I tell you that the sun rose this morning, but you learn considerably more if I tell you that San Francisco was destroyed by an earthquake this morning. The reason the latter observation carries more information is that it has a lower prior probability. \square

In 1928 Hartley proposed a logarithmic measure of information that reflects this intuition. Consider a random variable X with sample space $\Omega_X = \{a_1, a_2, \dots, a_K\}$. The *self-information* in an outcome a_m is defined to be

$$h(a_m) = -\log_2 p_X(a_m). \quad (4.3)$$

The self-information of a rare event is greater than the self-information of a common event, conforming with intuition. Furthermore, the self-information is non-negative. But why the logarithm? One intuitive justification arises from considering two independent random variables X and Y , where $\Omega_Y = \{b_1, b_2, \dots, b_N\}$. The information in the joint events a_m and b_n intuitively should be the sum of the information in each. The self information defined in (4.3) has this property,

$$\begin{aligned} h(a_m, b_n) &= -\log_2 p_{X,Y}(a_m, b_n) = -\log_2 p_X(a_m) - \log_2 p_Y(b_n) \\ &= h(a_m) + h(b_n). \end{aligned} \quad (4.4)$$

The *average information* $H(X)$ in X , defined in (4.1), is also called the *entropy* of X because of its formal similarity to thermodynamic entropy. Equivalent interpretations of $H(X)$ are

- the average information obtained by observing an outcome,
- the average uncertainty about X before it is observed, and
- the average uncertainty removed by observing X .

Because of the base-two logarithm in (4.1), information is measured in *bits*.

Example 4-4.

Consider a binary random variable X with alphabet $\Omega_X = \{0,1\}$. Suppose that $q = p_X(1)$, so

$$H(X) = -q \log_2 q - (1-q) \log_2 (1-q). \quad (4.5)$$

This is plotted as a function of q in Figure 4-2. Notice that the entropy peaks at 1 bit when $q = \frac{1}{2}$ and goes to zero when $q = 0$ or $q = 1$. This agrees with our intuition that there is no information in certain events. \square

Although the intuitive justification given so far may seem adequate, the key to the interpretation of entropy as an information measure lies in the *asymptotic equipartition theorem*, which is further justified in Appendix 4-A. Define the random vector $\mathbf{X} = (X_1, \dots, X_n)$ where X_i are independent trials of a discrete random variable X with entropy $H(X)$. Define the vector \mathbf{x} to be an outcome of the random vector \mathbf{X} . The theorem says that asymptotically as $n \rightarrow \infty$, there is a set of "typical" outcomes S for which

$$p_{\mathbf{X}}(\mathbf{x}) \approx 2^{-nH(X)}, \quad \mathbf{x} \in S, \quad (4.6)$$

and the total probability that the outcome is in S is very close to unity. Since the "typical" outcomes all have approximately the same probability, there must be approximately $2^{nH(X)}$ outcomes in S . This approximation becomes more accurate as n gets large.

We can now conceptually design a source coder as follows. This source coder will assign to each outcome \mathbf{x} a binary word, called the *code*. If n is large, we can assign binary words only to the "typical" outcomes, and ignore the "nontypical" ones. If we use $nH(X)$ -bit code words, we can encode each of the $2^{nH(X)}$ typical outcomes with a unique binary word, for an average of $H(X)$ bits per component of the vector \mathbf{x} . Since each outcome of the component random variable X requires on average $H(X)$ bits, $H(X)$ is the average information obtained from the observation. It is important to note, however, that this argument applies only if we encode a large number of components collectively, and not each component separately. The statement that $H(X)$ is the average number of bits required to encode a component X applies only to an average of n components, not to an individual component.

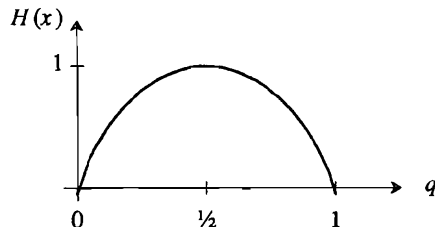


Figure 4-2. The entropy of a binary random variable as a function of the probability $q = p_X(1)$.

We will now state (but not prove) the *source coding theorem* for discrete-amplitude discrete-time sources. If a source can be modeled as repeated independent trials of a random variable X at r trials per second, we define the *rate* of the source to be $R = rH(X)$. The source can be encoded by a source coder into a bit stream with bit rate less than $R + \epsilon$ for any $\epsilon > 0$.

Constructing practical codes that come close to R is difficult, but constructing good sub-optimal codes is often easy.

Example 4-5.

For the source of Example 4-4, if $q = 1/2$ then $H(X) = 1$. This implies that to encode repeated outcomes of X we need one bit per outcome, on average. In this case, this is also adequate for each sample, not just on average, since the source is binary. A source coder that achieves rate R just transmits outcomes of X unaltered. \square

Example 4-6.

When $q = 0.1$ in Example 4-4,

$$H(X) = -0.1 \cdot \log_2(0.1) - 0.9 \cdot \log_2(0.9) \approx 0.47, \quad (4.7)$$

implying that less than half a bit per outcome is required, on average. This is not so intuitive; however, there are coding schemes in which the average number of bits per outcome will be lower than unity but greater than 0.47. One simple coding scheme takes a pair of outcomes and assigns them bits according to the following table.

outcomes	bits
0,0	0
0,1	10
1,0	110
1,1	111

A bit stream formed by repeated trials can be easily decoded. The average number of bits produced by this coder is 0.645 bits per trial. But note that the pair of trials 1,1 requires three bits, or 1.5 bits per trial. This emphasizes that the entropy is an average quantity. \square

Example 4-7.

Consider a particularly unfair coin that *always* comes up heads. Then

$$H(X) = 0, \quad (4.8)$$

using the identity $0 \log_2 0 = 0$. This says that no bits are required to specify the outcome, which is valid. \square

Exercise 4-1.

It is clear from the definition of entropy that $H(X) \geq 0$. Use the inequality $\log x \leq x - 1$ to show that

$$H(X) \leq \log_2 K, \quad (4.9)$$

where K is the size of the alphabet of X , with equality if and only if the outcomes of X are equally likely. \square

The conclusion of Exercise 4-1 is that $\log_2 K$ bits *always* suffices to specify the outcomes, as is obvious since $2^{\log_2 K} = K$ possible outcomes can be encoded by a straightforward assignment, at least when K is a power of two. The less obvious conclusion is that the maximum number of bits, $\log_2 K$, is *required* only when the outcomes are equally likely.

4.2. CAPACITY OF DISCRETE-TIME CHANNELS

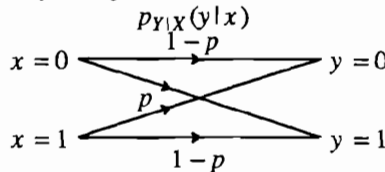
The concept of entropy and information can be extended to channels, yielding considerable information about their fundamental limits. This section considers discrete-time channels, deferring continuous-time channels to Section 4.3. We consider three different types of discrete-time channels: discrete-valued inputs and outputs, discrete-valued inputs and continuous-valued outputs, and continuous-valued inputs and outputs.

4.2.1. Discrete-Valued Inputs and Outputs

Consider a *discrete-time* channel with input random process $\{X_k\}$ and output $\{Y_k\}$. We consider here only *memoryless channels* for which the current output Y_k is independent of all inputs except X_k . Such a channel is fully characterized by the conditional probabilities $p_{Y|X}(y|x)$ for all $x \in \Omega_X$ and $y \in \Omega_Y$.

Example 4-8.

Consider a channel with input and output alphabet $\Omega_X = \Omega_Y = \{0,1\}$ such that $p_{Y|X}(0|1) = p_{Y|X}(1|0) = p$. This *binary symmetric channel (BSC)* offers a useful model of a channel that introduces independent random errors with probability p . The transition probabilities may be illustrated by a diagram:



□

If the input samples are independent, the information per sample at the input is $H(X)$ and the information per n samples is $nH(X)$. The question is how much of this information gets through the channel. We can answer this question by finding the uncertainty in X after observing the output of the channel Y . Suppose that y is an outcome of Y . Then the uncertainty in X given the event $Y = y$ is

$$H(X|y) = E \left[-\log_2 p_{X|Y}(X|y) \right] = - \sum_{x \in \Omega_X} p_{X|Y}(x|y) \log_2 p_{X|Y}(x|y). \quad (4.10)$$

To find the average uncertainty in X after observing Y , we must average this over the distribution of Y , yielding a quantity called the *conditional entropy*,

$$H(X|Y) = \sum_{y \in \Omega_Y} H(X|y)p_Y(y) = - \sum_{y \in \Omega_Y} \sum_{x \in \Omega_X} p_{X,Y}(x,y) \log_2 p_{X|Y}(x|y). \quad (4.11)$$

This conditional entropy, on a channel such as the BSC, is a measure of the average uncertainty about the input of the channel after observing the output.

The uncertainty about X must be larger before observing Y than after; the difference is a measure of the information passed through the channel on average. Thus we define

$$I(X,Y) = H(X) - H(X|Y) \quad (4.12)$$

as the *average mutual information* (as in (4.2)). In other words, $I(X,Y)$ is interpreted as the uncertainty about X that is removed by observing Y , or the information about X in Y .

Exercise 4-2.

- (a) Show that $I(X,Y)$ can be written directly in terms of the transition probabilities (channel) and the input distribution (input) as

$$I(X,Y) = \sum_{x \in \Omega_X} p_X(x) \sum_{y \in \Omega_Y} p_{Y|X}(y|x) \log_2 \left[\frac{p_{Y|X}(y|x)}{\sum_{x \in \Omega_X} p_X(x)p_{Y|X}(y|x)} \right]. \quad (4.13)$$

- (b) Show that (4.12) can be written alternatively as

$$I(X,Y) = H(Y) - H(Y|X) = I(Y,X). \quad (4.14)$$

Thus, the information about X in Y is the same as the information about Y in X . \square

The transition probabilities are fixed by the channel. The input probabilities are under our control through the design of the channel coder. The mutual information (information conveyed through the channel) is a function of both transition and input probabilities. It makes intuitive sense that we would want to choose the input probabilities so as to maximize this mutual information. The *channel capacity per symbol* is defined as the maximum information conveyed over all possible input probability distributions,

$$C_s = \max_{p_X(x)} I(X,Y). \quad (4.15)$$

This capacity is in bits/symbol, where a symbol is one sample of X . If the channel is used s times per second, then the channel capacity in bits per second is

$$C = sC_s. \quad (4.16)$$

Exercise 4-3.

For the BSC of Example 4-8, let the probability of the two inputs be q and $1-q$.

- (a) Show that the mutual information is

$$I(X,Y) = H(Y) + p \log_2 p + (1-p) \log_2 (1-p). \quad (4.17)$$

- (b) By maximizing over q , show that the channel capacity per symbol is

$$C_s = 1 + p \log_2 p + (1-p) \log_2 (1-p). \quad (4.18)$$

The capacity is zero if $p = 1/2$, since then the channel inputs and outputs are independent, and is unity when $p = 0$ or $p = 1$, since then the channel is binary and noiseless. \square

Using the channel capacity theorem and the source coding theorem, we will now state (but not prove) a general *channel capacity theorem*. Given a source with rate $R = rH(X)$ bits/second, and a channel with capacity $C = sC_s$ bits/sec, then if $R < C$ there exists a combination of source and channel coders such that the source can be communicated over the channel with fidelity arbitrarily close to perfect. If the source is a bit stream, the channel coder can achieve *arbitrarily low probability of error* if the bit rate is below the channel capacity. In practice, achieving vanishingly small error probability requires arbitrarily large computational complexity and processing delay. Nevertheless, the channel capacity result is very useful as an ideal against which to compare practical modulation and coding systems.

4.2.2. Discrete Inputs and Continuous Outputs

Another useful channel model is a discrete-time channel with a discrete-valued input and a continuous-valued output.

Example 4-9.

In an *additive noise channel*, the output is

$$Y = X + N \quad (4.19)$$

where X is a discrete random input to the channel and N is a continuous noise variable. This model arises often in this book in the situation where a discrete *data symbol* taking on a finite number of possible values is transmitted over a channel with additive Gaussian noise (i.e. N is Gaussian). \square

This model is useful because most communications media (Chapter 5) have continuous-valued outputs, due to thermal noise, whereas digital signals are discrete-valued.

The previous definitions of entropy carry over to continuous-valued random variables, if we are careful about replacing summations with integrals. For example, the entropy of a continuous-valued random variable Y is defined as

$$H(Y) = E[-\log_2 f_Y(y)] = - \int_{\Omega_Y} f_Y(y) \log_2 f_Y(y) dy. \quad (4.20)$$

Just as with discrete-valued random variables, it is possible to bound the entropy of a continuous-valued random variable.

Exercise 4-4.

Show that if Y has zero mean and variance σ^2 , then

$$0 \leq H(Y) \leq \log_2(\sigma\sqrt{2\pi e}) \quad (4.21)$$

with equality if and only if Y is Gaussian. **Hint:** Show that

$$H(Y) \leq - \int_{-\infty}^{\infty} f_Y(y) \log_2 g(y) dy \quad (4.22)$$

for any probability density function $g(y)$, using the inequality $\log x \leq x - 1$. Then substitute a Gaussian p.d.f. for $g(y)$. \square

It is important to note that we have constrained the variance of the random variable in this exercise. A different constraint would lead to a different bound; or, no constraint could lead to *unbounded* entropy.

The conditional entropy is a little trickier because it involves both discrete and continuous-valued random variables. Following the second expression in (4.11), we can define

$$H(Y|X) = \sum_{x \in \Omega_X} p_X(x) \int_{\Omega_Y} f_{Y|X}(y|x) \log_2 f_{Y|X}(y|x) dy. \quad (4.23)$$

Exercise 4-5.

Consider the additive Gaussian noise of Example 4-9. Show that $H(Y|X) = H(N)$. This result is intuitive, since after observing the outcome of X , the uncertainty in Y is precisely the entropy of the noise. \square

The mutual information and capacity are defined as before, in (4.12) and (4.15).

Exercise 4-6.

Following (4.13), the mutual information can be written in terms of the channel transition probability $f_{Y|X}(y|x)$ and the probability distribution of the input $p_X(x)$,

$$I(X, Y) = \sum_{x \in \Omega_X} p_X(x) \int_{\Omega_Y} f_{Y|X}(y|x) \log_2 \frac{f_{Y|X}(y|x)}{\sum_{x' \in \Omega_X} p_X(x') f_{Y|X}(y|x')} dy. \quad (4.24)$$

Derive this from (4.20) and (4.11). \square

The channel capacity for the continuous-output channel depends on the values in the discrete input Ω_X . For example, on an additive noise channel, we would expect the capacity of a channel with inputs ± 100 to be larger than the capacity with inputs ± 1 when the noise is the same. The set Ω_X of channel inputs is called the input *alphabet*.

Example 4-10.

Some common channel alphabets that we will encounter in Chapter 6 are shown in Figure 4-3. The K -AM alphabets are real-valued, containing K equally spaced points centered at the origin. The remaining alphabets are complex-valued, as appropriate for complex-valued discrete-time channels. The noise in this case is assumed to be complex white Gaussian noise, where the real and imaginary parts have the same power but are independent of one another and of the channel input. \square

One approach to calculating channel capacity would be not to constrain the alphabet at all; this is done in Section 4.2.3. Another approach is to choose an input alphabet,

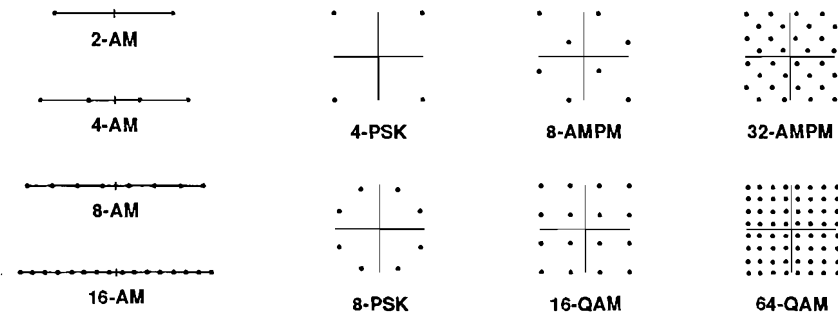


Figure 4-3. Some real-valued and complex-valued channel alphabets for a discrete-valued channel input. The acronyms refer to signaling methods that will be discussed in Chapter 6.

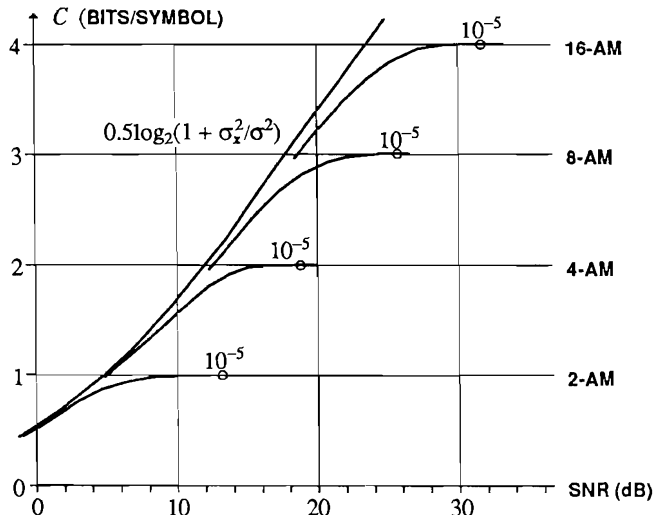


Figure 4-4. Bounds on the information conveyed by a real-valued discrete-time channel with additive white Gaussian noise as a function of SNR for four input alphabets defined in Figure 4-3. It is assumed that the symbols in the alphabet are equally likely. Also shown is the channel capacity for continuous-valued input signals, derived in Section 4.2.3. The points labeled 10^{-5} indicate the SNR at which a probability of error of 10^{-5} is achieved with direct techniques (no coding). The significance of these points will be discussed further in Chapter 14. The variance of the transmitted symbols is σ_x^2 , so the SNR is defined as σ_x^2/σ^2 , and is expressed in dB. (After Ungerboeck [2].)

getting the discrete-input channel model of this subsection, and then determine the capacity by maximizing the mutual information over the probabilities of the inputs using (4.24). Going one step further, we can assume a particular distribution for the input alphabet, and then find the information $I(X,Y)$ conveyed by the channel. In a classic paper that is credited with establishing the practical importance of *trellis*

coding (Chapter 14), Ungerboeck makes this calculation assuming that the input symbols in the alphabet are equally likely and that the channel adds independent Gaussian noise [2]. He computes the information conveyed by the channel as a function of the *signal-to-noise ratio* (SNR) for the input alphabets in Figure 4-3. The results are shown in Figure 4-4 (real alphabets) and Figure 4-5 (complex alphabets).

Example 4-11.

Consider the curve corresponding to 4-AM. As the signal to noise ratio increases, the information conveyed approaches two bits per symbol. This is intuitive because if the noise is small, nearly two bits per symbol can be sent with an alphabet of four symbols with low probability of error. For each input alphabet Ω_X with size $|\Omega_X|$, the information conveyed asymptotically approaches $\log_2 |\Omega_X|$ as the signal to noise ratio increases. While a capacity of two bits per symbol is not achievable with 4-AM, it is achievable with 8-AM for an SNR as low as 13 dB. Furthermore, using 16-AM to transmit two bits per symbol does not gain much noise immunity. This suggests that there is very little lost if we use 8-AM to transmit two bits per symbol. This observation is exploited in Chapter 14, where we discuss trellis coding. \square

4.2.3. Continuous-Valued Inputs and Outputs

The question arises as to what is lost by choosing a specific discrete alphabet at the channel input. We can answer this question by determining the capacity with a continuous-valued input, which is an infinite alphabet. For the additive Gaussian channel considered in Example 4-9, for any given SNR, we lose very little in capacity

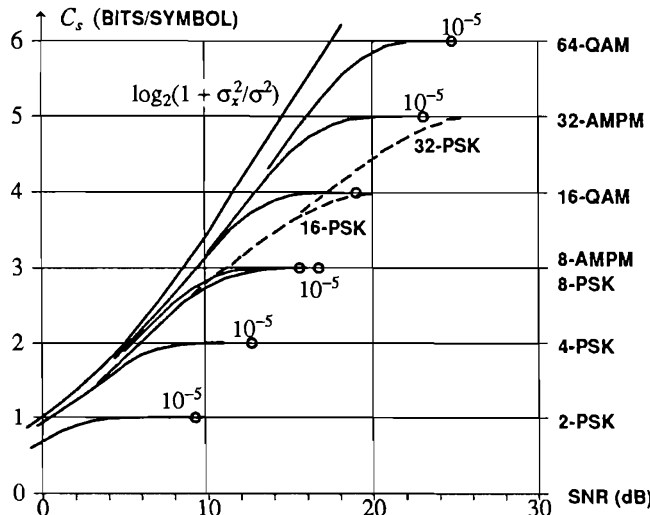


Figure 4-5. An analog to Figure 4-4 for a discrete-time complex-valued alphabet (defined in Figure 4-3) and channel. (After Ungerboeck [2].)

by choosing a discrete input alphabet, as long as the alphabet is sufficiently large (the higher the SNR, the larger the required alphabet). This result is important in that it justifies many of the digital communication techniques used in practice (Chapter 6).

Let X be a continuous-valued random variable. The entropy of Y is still given by (4.20), but the summation over x in the conditional entropy (4.23) must be replaced by an integral,

$$H(Y|X) = \int_{\Omega_X} f_X(x) \int_{\Omega_Y} f_{Y|X}(y|x) \log_2 f_{Y|X}(y|x) dy. \quad (4.25)$$

We obtain the channel capacity by maximizing $I(X, Y)$ over $f_X(x)$.

Scalar Additive Gaussian Noise Channel

Assume an additive Gaussian noise channel, $Y = X + N$ where N is an independent zero-mean Gaussian random variable with variance σ^2 . What is the capacity under the constraint that the variance of X is σ_x^2 ? The result of Exercise 4-5 is trivially extended to get $H(Y|X) = H(N)$, which is not a function of the input distribution, so the channel capacity is obtained by maximizing $H(Y)$. The variance of Y is constrained to be $\sigma_x^2 + \sigma^2$, so from (4.21),

$$H(Y) \leq \frac{1}{2} \log_2 [2\pi e (\sigma_x^2 + \sigma^2)], \quad (4.26)$$

with equality if and only if Y is Gaussian. Fortunately, Y is Gaussian if X is Gaussian, so the bound can in fact be achieved. Therefore channel capacity is achieved with a Gaussian input, and from (4.14),

$$C_s = \frac{1}{2} \log_2 [2\pi e (\sigma_x^2 + \sigma^2)] - \frac{1}{2} \log_2 (2\pi e \sigma^2) = \frac{1}{2} \log_2 (1 + \frac{\sigma_x^2}{\sigma^2}) \quad (4.27)$$

in bits per symbol. This channel capacity is plotted in both Figure 4-4 and Figure 4-5, where the SNR is σ_x^2/σ^2 . Note that this capacity is very similar to the capacity for any particular discrete alphabet at low SNR, and diverges significantly at large SNR. The capacity in Figure 4-5 is twice that of Figure 4-4 because each of the real and imaginary parts has the capacity given by (4.27).

The conclusion is that for the Gaussian channel and any particular SNR, there is a sufficiently large discrete input alphabet that has a capacity very close to the continuous-input capacity. This result gives a solid theoretical underpinning to the practical use of discrete input alphabets, which are also very convenient for implementation (Chapter 6).

Capacity of Vector Additive Gaussian Noise Channel

These results for the additive Gaussian channel are easily extended to a vector channel model. This extension will prove to be critically important in Chapters 8 and 10, where we consider continuous-time bandlimited Gaussian channels. We will show there that, for a given finite time interval, such a channel can be reduced to a vector Gaussian channel. Consider a channel modeled by

$$\mathbf{Y} = \mathbf{X} + \mathbf{N} \quad (4.28)$$

where \mathbf{X} , \mathbf{Y} , and \mathbf{N} are N -dimensional vectors, \mathbf{X} and \mathbf{N} are independent, and the components of \mathbf{N} are independent Gaussian random variables each with variance σ^2 . It is easily shown, as a generalization of Exercise 4-5, that

$$I(\mathbf{X}, \mathbf{Y}) = H(\mathbf{Y}) - H(\mathbf{Y} | \mathbf{X}) = H(\mathbf{Y}) - H(\mathbf{N}) \quad (4.29)$$

and that

$$H(\mathbf{N}) = \frac{N}{2} \cdot \log_2(2\pi e \sigma^2). \quad (4.30)$$

The entropy of a random vector is the same as that of a scalar random variable, (4.1) or (4.20), except that the sample space has vector-valued members. The noise entropy is proportional to the dimension N because each component of the noise contributes the same entropy as in the scalar case. All that remains, then, is to find the maximum of $H(\mathbf{Y})$ over all input distributions $f_{\mathbf{X}}(\mathbf{x})$.

Exercise 4-7.

- (a) Generalize (4.21) to show that

$$H(\mathbf{Y}) \leq - \int_{\Omega_Y} f_{\mathbf{Y}}(\mathbf{y}) \log_2 g(\mathbf{y}) d\mathbf{y} \quad (4.31)$$

for any probability density function $g(\mathbf{y})$.

- (b) Substitute a vector Gaussian density with independent components with mean zero and variance $(\sigma^2 + \sigma_{x,n}^2)$ for the n -th component to obtain

$$H(\mathbf{Y}) \leq \frac{1}{2} \sum_{n=1}^N \log_2 [2\pi e (\sigma^2 + \sigma_{x,n}^2)], \quad (4.32)$$

and thus show that

$$I(\mathbf{X}, \mathbf{Y}) \leq \frac{1}{2} \sum_{n=1}^N \log_2 \left(1 + \frac{\sigma_{x,n}^2}{\sigma^2} \right), \quad (4.33)$$

with equality if \mathbf{Y} is Gaussian with independent zero-mean components. Fortunately, this upper bound can be achieved if the input vector \mathbf{X} is chosen to have independent Gaussian components, each with mean zero and with variance $\sigma_{x,n}^2$ for the n th component.

- (c) Using the inequality $\log x \leq (x-1)$, show that if the variance of \mathbf{X} is constrained to some σ_x^2 ,

$$\sigma_x^2 = \sum_{n=1}^N \sigma_{x,n}^2, \quad (4.34)$$

then

$$I(\mathbf{X}, \mathbf{Y}) \leq \frac{N}{2} \log_2 \left(1 + \frac{\sigma_x^2}{N \sigma^2} \right), \quad (4.35)$$

with equality if and only if all the components of \mathbf{X} have equal variance. \square

The conclusion is that the capacity of the vector Gaussian channel with input variance constrained to $E[|\mathbf{X}|^2] = \sigma_x^2$ is given by

$$C = \frac{N}{2} \log_2 \left(1 + \frac{\sigma_x^2}{N\sigma^2} \right), \quad (4.36)$$

and the input distribution that achieves capacity is a zero-mean Gaussian vector with independent components, each with variance σ_x^2/N . The interpretation of this result is that the capacity is N , the number of degrees of freedom, times $0.5 \cdot \log_2(1 + SNR)$, where the signal to noise ratio $SNR = \sigma_x^2/N\sigma^2$ is the total input signal power divided by the total noise power.

4.3. FURTHER READING

Abramson [3] gives a short elementary introduction to information theory, particularly the channel coding theorem. Gallager [4] has long been a standard advanced text and includes an extensive discussion of continuous-time channels. McEliece [5] provides a readable introduction with qualitative sections devoted to describing the more advanced work in the field. An excellent recent text is by Cover and Thomas [6]. Also recommended is the text by Blahut [7]. A collection of key historical papers, edited by Slepian [8] provides an easy way to access the most important historical papers, including twelve by Shannon. "A Mathematical Theory of Communication" and "Communication in the Presence of Noise", two of Shannon's best known papers, are highly recommended reading, for their lucidity, relevance, and historical value. Especially interesting, and mandatory reading for anyone with an interest in the subject, Shannon gives an axiomatic justification of entropy as a measure of information. He simply assumes three properties that a reasonable measure of information should have, and derives entropy as the only measure that has these properties [9,10]. Viterbi and Omura [11] provide an encyclopedic coverage of information theory, with an emphasis throughout on convolutional codes. Finally, Wolfowitz [12] gives a variety of generalizations of the channel coding theorem.

APPENDIX 4-A ASYMPTOTIC EQUIPARTITION THEOREM

In this appendix we give a non-rigorous derivation of the asymptotic equipartition theorem that gives a great deal of insight. Define a random process Y_k in which each sample is an independent trial of the random variable Y with alphabet $\Omega_Y = \{b_1, \dots, b_K\}$. Let there be n trials, and define n_i to be the number of outcomes equal to b_i . The relative-frequency interpretation of probabilities tells us that if n is large, then with high probability,

$$\frac{n_i}{n} \approx p_Y(b_i) . \quad (4.37)$$

(A rigorous development depends mainly on defining precisely what we mean by "high probability". One approach is to show that given any $\epsilon > 0$, the probability that $[p_Y(b_i) - \epsilon] < n_i/n < [p_Y(b_i) + \epsilon]$ approaches unity as n gets large.) Suppose that we are interested in the product of the n observations. We can write the product as

$$\begin{aligned} y_1 \cdots y_n &= (b_1)^{n_1} \cdots (b_K)^{n_K} = \left[(b_1)^{n_1/n} \cdots (b_K)^{n_K/n} \right]^n \\ &= \left[2^{\frac{n_1}{n} \log_2 b_1} \cdots 2^{\frac{n_K}{n} \log_2 b_K} \right]^n = \left[2^{\sum_{i=1}^K \frac{n_i}{n} \log_2 b_i} \right]^n . \end{aligned} \quad (4.38)$$

Then using (4.37),

$$y_1 \cdots y_n \approx \left[2^{\sum_{i=1}^K p_Y(b_i) \log_2 b_i} \right]^n = \left[2^{E[\log_2 Y]} \right]^n , \quad (4.39)$$

with high probability. A rigorous proof is left to Problem 4-16. Since (4.39) is true for any discrete-valued random variable Y , it is certainly true for a random variable

$$Y = f(X) , \quad (4.40)$$

where f is any function defined on the alphabet of X . Define $f(x) = p_X(x) = \Pr[X = x]$ for all $x \in \Omega_X$, certainly a legitimate function defined on the alphabet of X . Then (4.39) implies that for large n

$$\begin{aligned} y_1 \cdots y_n &= f(x_1) \cdots f(x_n) = \prod_{i=1}^n f(x_i) = \prod_{i=1}^n p_X(x_i) \\ &\approx \left[2^{E[\log_2 p_X(X)]} \right]^n = 2^{-nH(X)} \end{aligned} \quad (4.41)$$

with high probability. Since the X_i are independent,

$$p_X(\mathbf{x}) = \prod_{i=1}^n p_X(x_i) \quad (4.42)$$

so with high probability (4.6) holds.

PROBLEMS

- 4-1.** Consider an unfair coin that produces heads with probability 1/4. What is the entropy of the coin flip outcome? Suppose the coin is flipped once per second. What is the rate in this source? Devise a coder to encode successive coin flips outcomes so that the average number of bits per flip is less than one. How does your coder compare with the rate of the source?
- 4-2.** Consider a random variable X with alphabet $\Omega_X = \{a_1, a_2, a_3, a_4\}$ and probabilities

$$p_X(a_1) = 1/2 \quad p_X(a_2) = 1/4 \quad p_X(a_3) = 1/8 \quad p_X(a_4) = 1/8 . \quad (4.43)$$

Find the entropy of the random variable. Suppose independent trials of the random variable

occur at rate $r = 100$ trials/second. What is the rate of the source? Devise a coder that exactly achieves the rate of the source.

- 4-3.** The well known *Jensen's inequality* from probability theory implies that

$$E[\log_2 X] \leq \log_2 E[X].$$

Use this to prove the *p-q inequality*: Given p_i and q_i , both strictly positive and defined for $i \in \{1, 2, \dots, M\}$ such that

$$\sum_{i=1}^M p_i = 1$$

(so p_i could be a probability distribution) and

$$\sum_{i=1}^M q_i = \alpha > 0$$

then

$$-\sum_{i=1}^M p_i \log_2 p_i \leq -\sum_{i=1}^M p_i \log_2 q_i + \log_2 \alpha$$

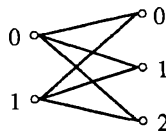
with equality if and only if $q_i = \alpha p_i$ for all i .

- 4-4.** For a discrete-valued random variable X , use the p-q inequality of Problem 4-3 to give another derivation of the results in Exercise 4-1.
- 4-5.** Let \mathbf{X} denote a vector of n i.i.d. random variables each taking the value zero or one. Show that

$$H(\mathbf{X}) \leq n \quad (4.44)$$

with equality if and only if the two outcomes have equal probability.

- 4-6.** Consider the following discrete memoryless channel, where all transition probabilities are $1/3$:



- (a) Find the two conditional entropies and the mutual information in terms of the input and output entropies.
- (b) Find the channel capacity.
- 4-7.** Repeat Problem 4-6 for the following channel:
- $$\begin{array}{ccc} 0 & \xrightarrow{1} & 0 \\ 1 & \xrightarrow{1} & 1 \end{array}$$
- 4-8.** Repeat Problem 4-6 for the following channel, called a binary erasure channel:
- $$\begin{array}{ccc} 0 & \xrightarrow{1-p} & 0 \\ 0 & \xrightarrow{p} & 1 \\ 1 & \xrightarrow{p} & 1 \\ 1 & \xrightarrow{1-p} & 2 \end{array}$$
- (Answer to b: $C_s = 1 - p$.)
- 4-9.**
- (a) Show that when p_i and q_i are probability distributions,

$$-\sum_i p_i \log_2 p_i \leq -\sum_i p_i \log_2 q_i . \quad (4.45)$$

- (b) Use (4.45) to establish the result of Exercise 4-1.
- 4-10.** Consider a cascade of L BSC's each with the same transition probability, where the output of each BSC is connected to the input of the next.
- (a) Show that the resulting overall channel is a BSC.
 - (b) Find the error probability of the overall channel as a function of L .
 - (c) What happens as $L \rightarrow \infty$?
- 4-11.** Consider a distribution $\{p_i, 1 \leq i \leq K\}$, where $p_1 > p_2$. Further define a second distribution $\{q_i, 1 \leq i \leq K\}$, where $q_1 = p_1 - \delta$ and $q_2 = p_2 + \delta$ and $q_i = p_i, i > 2$, where $\delta > 0$. Show that the second distribution has larger entropy. **Hint:** Use the results of Problem 4-9.
- 4-12.** Consider a continuous-valued random variable X uniformly distributed on the interval $[-a, a]$:
- (a) What is its entropy?
 - (b) How does its entropy compare to that of a Gaussian distribution with the same variance?
- 4-13.** Use the p-q inequality of Problem 4-3 to show the following.
- (a) For any two discrete-valued random variables X and Y , $I(X, Y) \geq 0$.
 - (b) $H(X) \geq H(X|Y)$
 - (c) $H(X) + H(Y) \geq H(X, Y)$
 - (d) When are these inequalities equalities?
- 4-14.** Show that by replacing the summations in (4.24) with integrals, the mutual information of two continuous-valued random variables can be written
- $$I(X, Y) = \int_{\Omega_x} \int_{\Omega_y} f_{X,Y}(x, y) \log_2 \frac{f_{X,Y}(x, y)}{f_X(x)f_Y(y)} dy dx. \quad (4.46)$$
- 4-15.** Investigate the capacity of the vector Gaussian channel of (4.36) as the number of degrees of freedom N increases. Interpret the result.
- 4-16.** Consider a random process $\{X_k\}$, where the components are independent observations of a random variable X . The law of large numbers for sums of random variables states that for any $\varepsilon > 0$,
- $$\Pr \left[E[X] - \varepsilon < \frac{1}{n} (X_1 + \dots + X_n) < E[X] + \varepsilon \right] \rightarrow 1 \text{ as } n \rightarrow \infty. \quad (4.47)$$
- Use this to prove (4.39).
- 4-17.** Consider the following betting game. You bet \$100 and toss a die. If a six comes up, you win \$500, otherwise you win \$20. Next you bet your \$500 or \$20 and the game is repeated with the same rate of return. In other words, on the n^{th} iteration, you bet M_n dollars (your previous winnings) and win $5M_n$ if a six comes up and $M_n/5$ otherwise. What is the expected value of the money you have after n flips? Show that with high probability, M_n goes to zero for large n . Would you play this game?
- 4-18.** Consider an analog continuous-time communication circuit with cascaded amplifiers. Suppose that the amplifiers have random gain, each independently taken from the same distribution. If the number of amplifiers is large, which is a better estimate of the gain of the system, (a) the expected value of the product of the gains of the amplifiers, or (b) the expected value of the sum of the gains expressed in dB?

REFERENCES

1. T. Berger, *Rate Distortion Theory*, Prentice-Hall, Englewood Cliffs, NJ (1971).
2. G. Ungerboeck, "Channel Coding with Multilevel/Phase Signals," *IEEE Trans. on Information Theory* **IT-28**, No. 1(Jan. 1982).
3. N. Abramson, *Information Theory and Coding*, McGraw-Hill Book Co., New York (1963).
4. R. Gallager, *Information Theory and Reliable Communication*, John Wiley and Sons, Inc., New York (1968).
5. R. J. McEliece, *The Theory of Information and Coding*, Addison Wesley Pub. Co. (1977).
6. T. M. Cover and J. A. Thomas, "Elements of Information Theory," *Wiley*, (1991).
7. R. E. Blahut, "Principles and Practice of Information Theory," *Addison-Wesley*, (1987).
8. D. Slepian (editor), *Key Papers in the Development of Information Theory*, IEEE Press, New York (1974).
9. C. E. Shannon, "A Mathematical Theory of Communication," *BSTJ*, (Oct. 1948).
10. C. E. Shannon and W. Weaver, *The Mathematical Theory of Communication*, University of Illinois Press, Urbana, Illinois (1963).
11. A. J. Viterbi and J. K. Omura, *Principles of Digital Communication and Coding*, McGraw-Hill (1979).
12. J. Wolfowitz, *The Coding Theorems of Information Theory*, 3d ed., Springer-Verlag, Berlin (1978).

5

PHYSICAL MEDIA AND CHANNELS

Ultimately the design of a digital communication system depends on the properties of the channel. The channel is typically a part of the digital communication system that we cannot change. Some channels are simply a physical medium, such as a wire pair or optical fiber. On the other hand, the radio channel is part of the electromagnetic spectrum, which is divided by government regulatory bodies into bandlimited radio channels that occupy disjoint frequency bands. In this book we do not consider the design of the *transducers*, such as antennas, lasers, and photodetectors, and hence we consider them part of the channel. Some channels, notably the telephone channel, are actually composites of multiple transmission subsystems. Such *composite channels* derive their characteristics from the properties of the underlying subsystems.

Section 5.1 discusses composite channels. Sections 5.2 through 5.4 review the characteristics of the most common channels used for digital communication, including the transmission line (wire pair or coaxial cable), optical fiber, and microwave radio (satellite, point-to-point and mobile terrestrial radio). Section 5.5 discusses the composite voiceband telephone channel, which is often used for voiceband data transmission. Finally, Section 5.6 discusses magnetic recording of digital data, as used in tape and disk drives, which has characteristics similar in many ways to the other channels discussed.

The most prevalent media for new installations in the future will be optical fiber and microwave radio, and possibly lossless transmission lines based on

superconducting materials. However, there is a continuing strong interest in lossy transmission lines and voiceband channels because of their prevalence in existing installations. Thus all the media discussed in this chapter are important in new applications of digital communication.

5.1. COMPOSITE CHANNELS

It is common for many users to share a common communication medium, for example by *time-division* and *frequency-division multiplexing* (Chapter 16).

Example 5-1.

Voice signals are roughly bandlimited to frequencies lower than 4 kHz. A suitable baseband channel therefore needs to pass only frequencies up to 4 kHz. Such a channel is often derived from a much higher bandwidth physical medium that is shared with other users. A *voice frequency (VF) channel* derived from a coaxial cable (Section 5.2) using *single-sideband modulation* is shown in Figure 5-1. The SSB modulator translates the VF channel to the neighborhood of a frequency ω_c for transmission on the coaxial cable. A VF channel can be used for digital communication, as long as the modulation technique conforms to the limitations of the channel. \square

The channel in Example 5-1 is an example of a *composite channel*, because it consists of multiple subsystems. If the VF channel was designed for voice transmission, it has certain characteristics which are beyond the control of the designer of the digital communication system. The VF channel characteristics in this case depend not only on the properties of the physical medium, but also on the design of the SSB modulation system.

Composite channels usually arise in the context of *multiple access*, which is defined as access to a physical medium by two or more independent users. This is again illustrated by example.

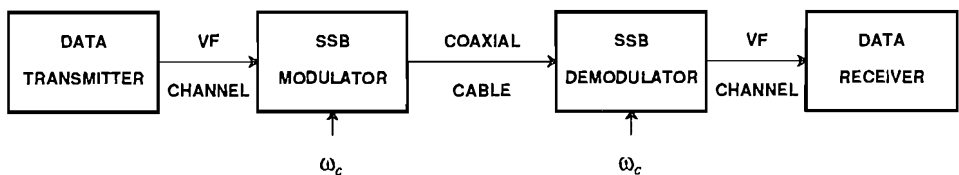


Figure 5-1. Composite data channel derived from an SSB modulation system, where ω_c is the carrier frequency.

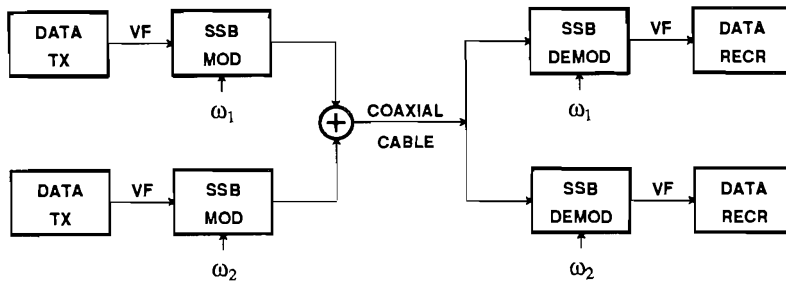


Figure 5-2. Two data channels derived from a single coaxial cable by FDM, where ω_1 and ω_2 are distinct carrier frequencies. "TX" is the transmitter and "RECR" is the receiver.

Example 5-2.

Figure 5-2 shows a *frequency-division multiplexing (FDM)* approach using SSB modulation. In this case two VF channels are derived from a single physical medium such as coaxial cable or microwave radio (thousands rather than just two as in the example!).

In fact FDM is a very common technique in the telephone network for deriving many VF channels from a single physical medium such as coaxial cable or microwave radio (thousands rather than just two as in the example!).

Another common composite channel is illustrated in the following example.

Example 5-3.

A VF channel derived from a digital transmission system using *pulse-code modulation (PCM)* is illustrated in Example 5-3. The PCM system samples the VF channel at 8 kHz, corresponding to a maximum bandwidth of 4 kHz, and then quantizes each sample to eight bits. The total bit rate for the PCM encoded VF channel is 64 kb/s. This derived VF channel may be used for data transmission; again, any digital modulation technique can be used subject to basic constraints imposed by the PCM system. The total bit rate that can be transmitted through this derived VF channel is less than 64 kb/s, in fact more of the order of 20-30 kb/s. The direct transmission of the bit stream over the digital transmission system would obviously be more efficient, but the situation in Figure 5-3 is still very common due



Figure 5-3. Data transmission over a PCM-derived VF channel.

to the presence of much existing PCM equipment for voice transmission and the desire to transmit data over a channel designed primarily for voice. □

Physical media as well as the composite channels derived from them impose constraints on the design of a digital communication system. Many of these constraints will be mentioned in this chapter for particular media. The nature of these constraints usually fall within some broad categories:

- A *bandwidth constraint*. Sometimes this is in the form of a channel attenuation which increases gradually at high frequencies, and sometimes (particularly in the case of composite channels) it is in the form of a very hard bandwidth limit.
- A *transmitted power constraint*. This is often imposed to limit interference of one digital communication system with another, or imposed by the inability of a composite channel to transmit a power level greater than some threshold, or by a limitation imposed by the power supply voltage of the digital communication system itself. This power constraint can be in the form of a *peak-power constraint*, which is essentially a limit on the transmitted voltage, or can be an *average power constraint*.

Example 5-4.

An FDM system such as that in Figure 5-2, where there are perhaps thousands of channels multiplexed together, is designed under assumptions on the average power of the channels. From this average power, the total power of the multiplexed signal can be deduced; this power is adjusted relative to the point at which amplifiers in the system start to become nonlinear. If a significant number of VF channels violate the average power constraint, then the multiplexed signal will overload the amplifiers, and the resulting nonlinearity will cause *intermodulation distortion* and interference between VF channels. □

Example 5-5.

The PCM system of Figure 5-3 imposes a bandwidth constraint on the data signal, which must be less than half the sampling rate. A peak power constraint is also imposed by the fact that the quantizer in the PCM system has an overload point beyond which it clips the input signal. □

Example 5-6.

The regenerative repeaters in Figure 1-3 are usually powered by placing a high voltage on the end of the system and then stringing the repeaters in series (like Christmas tree lights!); a fraction of the total voltage appears across each repeater. The power consumption of the repeaters is limited by the applied voltage, the ohmic loss of the cable, and the number of repeaters. This places an average power constraint on the transmitted signal at each repeater. In practice there is also a peak power constraint due to the desire not to have to generate a signal voltage higher than the supply voltage drop across the repeater. An additional factor limiting the transmitted power for wire-pair systems is crosstalk into other communication systems in the same multi-pair cable, as discussed in Section 5.2.4. □

Example 5-7.

The optical fiber medium (Section 5.3) becomes significantly nonlinear when the input power exceeds about one milliwatt. Thus, in many applications there is a practical limit on the average transmitted power. \square

In addition to placing constraints on the transmitted signal, the medium or composite channel introduces *impairments* which limit the rate at which we can communicate. We will see many examples of this in this Chapter.

5.2. TRANSMISSION LINES

One of the most common media for data transmission in the past has been the transmission line composed of a pair of wires or a coaxial cable. Coaxial cable is commonly used for digital communication within a building, as in a local-area network, and for high-capacity long-distance facilities in the telephone network. Wire pairs are much more extensively used, primarily for relatively short distance trunking in the telephone network between switching machines in metropolitan areas. The spacing between regenerative repeaters is typically about 1.5 km, with bit rates in the range of 1.5-6 Mb/s on wire pair to 270-400 Mb/s on coaxial cable. In addition, wire pairs are used for connection of the telephone instrument to the central office, and while this connection is primarily for analog voiceband transmission, there is work proceeding to use this same medium for digital communication at 144 kb/s or higher in the Integrated Services Digital Network (ISDN). This is called the *digital subscriber loop*, and requires a distance for transmission of about 4-5 kilometers without repeaters.

5.2.1. Review of Transmission Line Theory

A *uniform transmission line* is a two-conductor cable with a uniform cross-section. It may consist of a pair of wires twisted together (*twisted wire cable*) or a cable with a cylindrical outer conductor surrounding a wire (*coaxial cable*). While the details of the cable characteristics depend on the cross-section geometry, the basic theory does not.

A uniform transmission line can be represented by a pair of conductors as shown

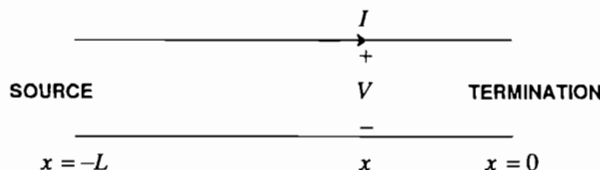


Figure 5-4. A uniform transmission line, where x is the distance along the line.

in Figure 5-4. We denote the termination of the line on the right as $x = 0$, and the source on the left as $x = -L$, where x is the distance along the line and L is the length of the line. Assume that the line is excited with a complex exponential with radian frequency ω . The voltage and current along the line will be a function of both the frequency ω and the distance x . Writing the voltage and current at a point x , the dependence on time is given by the complex exponential,

$$V(x, \omega) = V(x)e^{j\omega t}, \quad I(x, \omega) = I(x)e^{j\omega t} \quad (5.1)$$

where $V(x)$ and $I(x)$ are complex numbers which summarize the amplitude and phase of the complex exponential at distance x .

The voltage and current as a function of distance along the line consists of two propagating waves, one from source to termination and the other from termination to source. The first we call the *source wave*, and the latter we call the *reflected wave*. The total voltages and currents are the sum of the two waves, given by

$$V(x) = V_+e^{-\gamma x} + V_-e^{\gamma x}, \quad I(x) = \frac{1}{Z_0}(V_+e^{-\gamma x} - V_-e^{\gamma x}) \quad (5.2)$$

In these equations the V_+ terms correspond to the source wave, and the V_- terms correspond to the reflected wave. The complex impedance Z_0 is called the *characteristic impedance* of the transmission line, since it equals the ratio of the voltage to current at any point of the line (independent of x) for either the source or reflected wave. The other complex quantity in this equation is γ , which is called the *propagation constant*. The real and imaginary parts of γ are of importance in their own right, so in

$$\gamma = \alpha + j\beta \quad (5.3)$$

the real part α and imaginary part β are called respectively the *attenuation constant* and *phase constant*. The attenuation constant has the units of *nepers per unit distance* and the phase constant has the units of *radians per unit distance*.

There are three things that distinguish the source wave and its reflection:

- The amplitude and phase as expressed by V_+ and V_- are different.
- The current is flowing in opposite directions.
- The sign of the exponent is different.

The third difference is illustrated in Figure 5-5. The dependence of both waves on time at any point along the line is shown in Figure 5-5a. This is of course just a sinusoid of constant amplitude and phase, where both amplitude and phase depend on the frequency of the wave. For a fixed time $t = t_0$, the source wave is shown in Figure 5-5b as a function of distance x , and is given by

$$V(x) = V_+e^{-\alpha x} e^{-j\beta x}. \quad (5.4)$$

The amplitude of this wave decreases with distance x . The *wavelength* of the wave, or distance between nulls, is $2\pi/\beta$.

The phase shift of the complex exponential with radian frequency ω for a transmission line of length L is βL radians, which corresponds to $\beta L/2\pi$ cycles. This

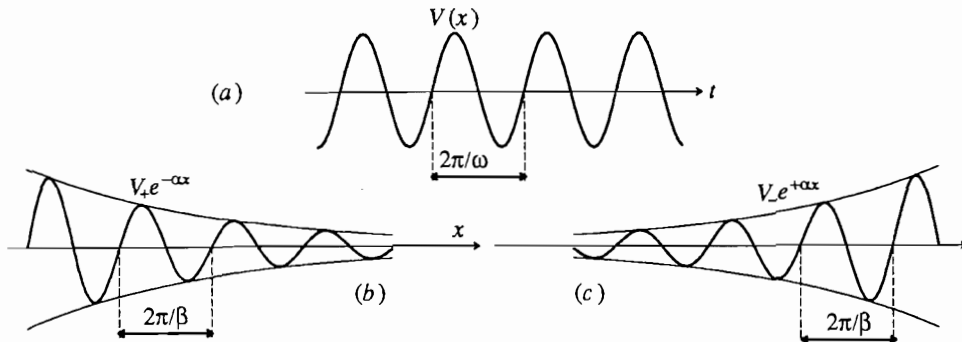


Figure 5-5. The voltage on a uniform transmission line. a. The voltage at one point in the line as a function of time. b. The magnitude of the voltage vs. distance for the source wave at a fixed time. c. (b) repeated for the reflected wave.

phase shift represents a propagation delay of the sinusoid, and we can readily figure out the size of the delay. Since each cycle corresponds to $2\pi/\omega$ seconds from Figure 5-5a, it follows that the total delay of the complex exponential is

$$\frac{\beta L}{2\pi} \text{ cycles} \cdot \frac{2\pi}{\omega} \frac{\text{sec}}{\text{cycles}} = \frac{\beta}{\omega} L \text{ sec.} \quad (5.5)$$

The propagation velocity of the wave on the transmission line is therefore related to the frequency and phase constant by

$$v = \frac{\omega}{\beta}. \quad (5.6)$$

Since α is always greater than zero, the magnitude of the wave is also decaying exponentially with distance in accordance with the term $e^{-\alpha x}$. This implies that at any frequency the loss of the line in dB is proportional to the length of the line. We get a power loss in dB

$$\gamma_0 L = 10 \log_{10} \left(\frac{P_T}{P_R} \right), \quad (5.7)$$

where $\gamma_0 = 20 \alpha \log_{10} e$ is the loss in dB per unit distance. Since α is frequency dependent, so to is γ_0 .

Similarly, shown in Figure 5-5c is the reflected wave amplitude as a function of distance along the line. This wave is also decaying exponentially with distance in the direction of propagation, which is from termination to source.

Based on these relationships, we can determine the voltage along the line for any source and termination impedances by simply matching up boundary conditions.

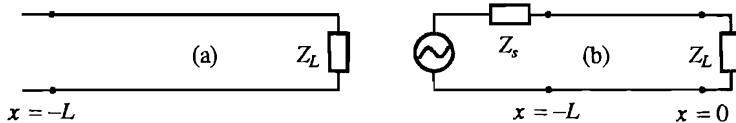


Figure 5-6. A terminated transmission line. a. Without a source termination. b. With a source termination.

Example 5-8.

A transmission line terminated in impedance Z_L is shown in Figure 5-6a. What is the relative size of the incident and reflected waves at the termination? This quantity is called the *voltage reflection coefficient* and is usually denoted by Γ . The boundary condition is that Z_L is the ratio of the voltage to current at $x = 0$, so from (5.2),

$$Z_L = Z_0 \frac{V_+ + V_-}{V_+ - V_-}, \quad \Gamma = \frac{V_-}{V_+} = \frac{Z_L - Z_0}{Z_L + Z_0}. \quad (5.8)$$

Several special cases are of interest. When the load impedance is equal to the characteristic impedance, $Z_L = Z_0$, then the reflection coefficient is zero, $\Gamma = 0$. When the line is open circuited, $Z_L = \infty$, then $\Gamma = 1$ indicating that the reflected voltage is the same as the incident wave at the point of the open circuit. Finally, when the line is closed circuited, $Z_L = 0$, then $\Gamma = -1$ indicating that the reflected voltage is the negative of the incident voltage. \square

Example 5-9.

For the terminated transmission line of Figure 5-6a, what is the impedance looking into the line as a function of its length? Taking the ratio of the voltage to current from (5.2) and (5.8),

$$\frac{V(x)}{I(x)} = Z_0 \frac{e^{-\gamma x} + \Gamma e^{\gamma x}}{e^{-\gamma x} - \Gamma e^{\gamma x}}, \quad Z_{in} = \frac{V(-L)}{I(-L)} = Z_0 \frac{1 + \Gamma e^{-2\gamma L}}{1 - \Gamma e^{-2\gamma L}}. \quad (5.9)$$

When the line is terminated in its characteristic impedance, $\Gamma = 0$ and the input impedance is equal to the characteristic impedance. \square

Example 5-10.

For the terminated line of Figure 5-6b with a source impedance of Z_s , what is the voltage transfer function from source V_{in} to the load? Writing the node voltage equation at the source,

$$V(-L) = V_{in} - I(-L)Z_s \quad (5.10)$$

and we have the two additional relations

$$V(-L) = V_+(e^{\gamma L} + \Gamma e^{-\gamma L}), \quad I(-L) = \frac{V_+}{Z_0}(e^{\gamma L} - \Gamma e^{-\gamma L}), \quad (5.11)$$

which enable us to solve for the three constants V_+ , $V(-L)$, and $I(-L)$. Finally, the output voltage is

$$V(0) = V_+(1 + \Gamma) \quad (5.12)$$

Putting this all together, the desired voltage transfer function is

$$\frac{V(0)}{V_{in}} = \frac{Z_0(1 + \Gamma)}{(Z_0 + Z_S)e^{\gamma L} + \Gamma(Z_0 - Z_S)e^{-\gamma L}} \quad (5.13)$$

When the source impedance is equal to the characteristic impedance, $Z_S = Z_0$ this simplifies to

$$\frac{V(0)}{V_{in}} = \frac{1 + \Gamma}{2} e^{-\gamma L}. \quad (5.14)$$

When further the line is terminated in its characteristic impedance, $\Gamma = 0$ and the transfer function consists of the attenuation and phase shift of the transmission line (times another factor of 0.5 corresponding to the attenuation due to the source and termination impedances). When the line is short-circuited, then the transfer function is zero as expected since $\Gamma = -1$. What happens when the line is open circuited? \square

Transmission lines are often analyzed, particularly where computer programs are written, using the concept of a *chain matrix* [1]. A *twoport network* is a network as illustrated in Figure 5-7, which has an input port and output port and for which the input and output currents are complementary as shown. The chain matrix relates the input voltage and current to the output voltage and current, *viz.*

$$\begin{bmatrix} V_1 \\ I_1 \end{bmatrix} = \begin{bmatrix} A & B \\ C & D \end{bmatrix} \begin{bmatrix} V_2 \\ I_2 \end{bmatrix} \quad (5.15)$$

where all quantities are complex functions of frequency. The chain matrix characterizes the twoport transfer function completely, and can be used to analyze connections of twoports (such as transmission lines, thereby serving to analyze nonuniform transmission lines). Its importance arises from the following fact.

Exercise 5-1.

Show that if two twoports are connected in series, then the chain matrix of the combination twoport is the product of the first chain matrix times the second chain matrix. \square

The chain matrix of a uniform transmission line is easily calculated, giving us a ready technique for systematically analyzing combinations of transmission lines with other



Figure 5-7. Illustration of a twoport network with definition of voltages and currents for the chain matrix.

circuit elements.

Exercise 5-2.

Show that the chain matrix of a uniform transmission line is

$$\begin{bmatrix} \cosh(\gamma L) & Z_0 \sinh(\gamma L) \\ \frac{\sinh(\gamma L)}{Z_0} & \cosh(\gamma L) \end{bmatrix}. \quad (5.16)$$

□

5.2.2. Cable Primary Constants

The characteristic impedance and propagation constant are called *secondary parameters* of the cable because they are not related directly to physical parameters. A simple model for a short section of the transmission line is shown in Figure 5-8. This model is in terms of four parameters: the conductance G in mhos per unit length, the capacitance C in farads per unit length, the inductance L in henries per unit length, and the resistance R in ohms per unit length. All of these parameters of the transmission line are functions of frequency in general, and they differ for different cross-sections (for example, twisted pair vs. coaxial cable). In general these parameters are determined experimentally for a given cable.

This lumped-parameter model becomes an exact model for the transmission line as the length of the line $dx \rightarrow 0$, and is useful since it displays directly physically meaningful quantities. These parameters are called the *primary constants* of the transmission line. The secondary parameters can be calculated directly in terms of the primary constants as

$$Z_0 = \sqrt{\frac{R + j\omega L}{G + j\omega C}}, \quad \gamma = \sqrt{(R + j\omega L)(G + j\omega C)}. \quad (5.17)$$

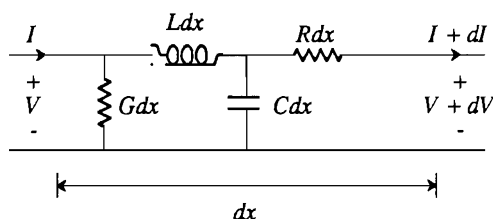


Figure 5-8. Lumped-parameter model for a short section of transmission line.

Example 5-11.

A *lossless transmission* line is missing the two dissipative elements, resistance and conductance. New superconducting materials show promise of actually being able to realize this ideal. The secondary parameters in this case are

$$Z_0 = \sqrt{\frac{L}{C}}, \quad \gamma = j\omega\sqrt{LC}. \quad (5.18)$$

The characteristic impedance of a lossless transmission line is real-valued and hence resistive. A pure resistive termination is often used as a reasonable approximation to the characteristic impedance of a *lossy* transmission line, although the actual characteristic impedance increases at low frequencies and includes a capacitive reactive component. The propagation constant is imaginary, and since $\alpha = 0$ the lossless transmission line has no attenuation as expected. The propagation velocity on a lossless transmission line is

$$v = \frac{\omega}{\beta} = \frac{1}{\sqrt{LC}}. \quad (5.19)$$

□

The primary constants of actual cables depend on many factors such as the geometry and the material used in the insulation. For twisted wire pairs [2] the capacitance is independent of frequency for the range of frequencies of interest (0.083 μ Farads per mile, or 0.0515 μ Farads per kilometer is typical), the conductance is negligibly small, the inductance is a slowly varying function of frequency decreasing from about one mili-Henries (mH) per mile or 0.62 mH per km, at low frequencies to about 70% of that value at high frequencies, and the resistance is proportional to the square root of frequencies at high frequencies due to the *skin effect* (the tendency of the current to flow near the surface of the conductor, increasing the resistance).

Example 5-12.

What is the velocity of propagation on a twisted wire cable? From (5.19), for a lossless line

$$v = \frac{1}{\sqrt{(0.083 \cdot 10^{-6})(10^{-3})}} = 1.1 \cdot 10^5 \text{ miles/sec} = 1.76 \cdot 10^5 \text{ km/sec}. \quad (5.20)$$

Since the speed of light is freespace is $3 \cdot 10^5$ km/sec, the velocity on the line is a little greater than half the speed of light. The delay is about 5.65 μ sec per km. This approximation is valid on practical twisted wire pairs for frequencies where $R \ll \omega L$. □

Coaxial cable is popular for higher frequency applications primarily because the outer conductor effectively shields against radiation to the outside world and conversely interference from outside sources. At lower frequencies near voiceband this shielding is ineffective and hence the coaxial cable does not have any advantage over the more economical twisted wire pair. In terms of primary constants, the main difference between coaxial cable and wire pair is that the coaxial inductance is essentially independent of frequency.

Example 5-13.

A more accurate model than Example 5-11 of a cable, wire pair or coaxial, would be to assume that G only is zero. Then the propagation constant of (5.17) becomes

$$\alpha = \omega \sqrt{\frac{LC}{2}} \left\{ \left(1 + \frac{R^2}{\omega^2 L^2} \right)^{\frac{1}{2}} - 1 \right\}^{\frac{1}{2}}, \quad \beta = \omega \sqrt{\frac{LC}{2}} \left\{ \left(1 + \frac{R^2}{\omega^2 L^2} \right)^{\frac{1}{2}} + 1 \right\}^{\frac{1}{2}}. \quad (5.21)$$

At frequencies where $R \ll \omega L$,

$$\alpha \approx \frac{R}{2} \sqrt{\frac{C}{L}} \text{ nepers per unit length} \quad (5.22)$$

$$\beta \approx \omega \sqrt{LC}. \quad (5.23)$$

Hence the velocity relation of (5.19) is still valid in this range of frequencies. Since at high frequencies R increases as the square root of frequency, the attenuation constant in nepers (or dB) has the same dependency. It follows that the loss of the line in dB at high frequencies is proportional to the square root of frequency. \square

Example 5-14.

If the loss of a cable is 40 dB at 1 Mhz, what is the approximate loss at 4 MHz? The answer is 40 dB times the square root of 4, or 80 dB. \square

The results of Example 5-13 suggest that the propagation constant is proportional to frequency. This *linear phase* model suggests that the line offers, in addition to attenuation, a constant delay at all frequencies. However, a more refined model of the propagation constant [3] shows that there is an additional term in the phase constant proportional to the square root of frequency. This implies that the cable will have some *group delay*, which is delay dependent on frequency. This implies that the different frequency components of a pulse launched into the line will arrive at the termination with slightly different delays. Both the frequency-dependent attenuation and the group delay cause *dispersion* on the transmission line, or spreading in time of a transmitted pulse. The attenuation causes dispersion because the bandlimiting effect broadens the pulse, and delay distortion causes dispersion because the different frequency components arrive with different delays.

5.2.3. Impedance Discontinuities

The theory presented thus far has considered a single uniform transmission line. In practice, it is common to encounter different *gauges* (diameters) of wire connected together. These gauge changes do not affect the transmission materially, except for introducing a slight discontinuity in impedance, which will result in small reflections. A more serious problem for digital transmission in the subscriber loop between central office and customer premises is the *bridged tap*, an additional open circuited wire pair bridged onto the main cable pair.

5.2.4. Crosstalk

An important consideration in the design of a digital communication system using a transmission line as a physical medium is the *range* or *distance* which can be achieved between regenerative repeaters. This range is generally limited by the high frequency gain which must be inserted into the receiver equalization to compensate for cable attenuation. This gain amplifies noise and interference signals which may be present, causing the signal to deteriorate as the range increases. The most important

noise and interference signals are thermal noise (due to random motion of electrons), impulse noise (caused by switching relays and similar mechanisms), and crosstalk between cable pairs. Crosstalk, and interference from external sources such as power lines, can be minimized by using *balanced transmission*, in which the signal is transmitted and received as a difference in voltage between the two wires; this helps because external interference couples approximately equally into the two wires and hence is approximately canceled when the difference in voltage is taken at the receiver. A common way to achieve balanced transmission is to use *transformer coupling* of the transmitter and receiver to the wire pair; in addition, this affords additional protection against damage to the electronics due to foreign potentials such as lightning strikes.

There are two basic crosstalk mechanisms, *near-end crosstalk (NEXT)* and *far-end crosstalk (FEXT)*, illustrated in Figure 5-9. NEXT [4] represents a crosstalk of a local transmitter into a local receiver, and experiences an attenuation which is accurately modeled by

$$|H_{\text{NEXT}}(j\omega)|^2 = K_{\text{NEXT}} |\omega|^{1.5} \quad (5.24)$$

where $H_{\text{NEXT}}(j\omega)$ is the transfer function experienced by the crosstalk. FEXT represents a crosstalk of a local transmitter into a remote receiver, with an attenuation given by

$$|H_{\text{FEXT}}(j\omega)|^2 = K_{\text{FEXT}} |C(j\omega)|^2 |\omega|^2 \quad (5.25)$$

where $C(f)$ is the loss of the cable. Where present, NEXT will dominate FEXT because FEXT experiences the loss of the full length of the cable (in addition to the crosstalk coupling loss) and NEXT does not. Both forms of crosstalk experience less attenuation as frequency increases, and hence it is advantageous to minimize the bandwidth required for transmission in a crosstalk limited environment.

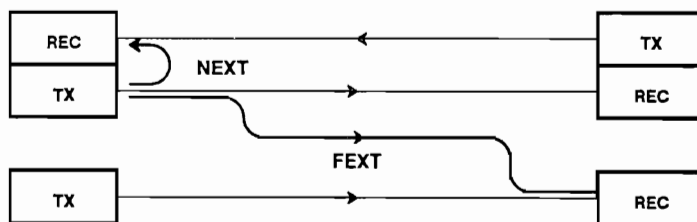


Figure 5-9. Illustration of two types of crosstalk -- far-end crosstalk (FEXT) and near-end crosstalk (NEXT).

5.3. OPTICAL FIBER

The optical fiber cable is capable of transmitting light for long distances with high bandwidth and low attenuation. Not only this, but it offers freedom from external interference, immunity from interception by external means, and inexpensive and abundant raw materials. It is difficult to imagine a more ideal medium for digital communication!

The use of an optical dielectric waveguide for high performance communication was first suggested by Kao and Hockham in 1966 [5]. By 1986 this medium was well developed and was rapidly replacing wire pairs and coax in many new cable installations. It allows such a great bandwidth at modest cost that it will also replace many of the present uses for satellite and radio transmission. Thus, it appears that digital communication over wire-pairs and coax will be mostly limited to applications constrained to use existing transmission facilities (such as in the digital subscriber loop).

Digital transmission by satellite and radio will be limited to special applications that can make use of their special properties. For example, radio communication is indispensable for situations where one or both terminals are mobile, for example in digital mobile telephony (Section 5.4) or deep space communication. Radio is also excellent for easily bridging geographical obstacles such as rivers and mountains, and satellite is excellent for spanning long distances where the total required bandwidth is modest and the installation of an optical fiber cable would not be justified. Furthermore, satellite has unique capabilities for certain types of multiple-access situations (Chapter 18) spread over a wide geographical area.

5.3.1. Fiber Optic Waveguide

The principle of an optical fiber waveguide [6] can be understood from the concept of *total internal reflection*, shown in Figure 5-10. A light wave, represented by a single ray, is incident on a boundary between two materials, where the angle of incidence is θ_1 and the angle of refraction is θ_2 . We define a *ray* as the path that the center of a slowly diverging beam of light takes as it passes through the system; such

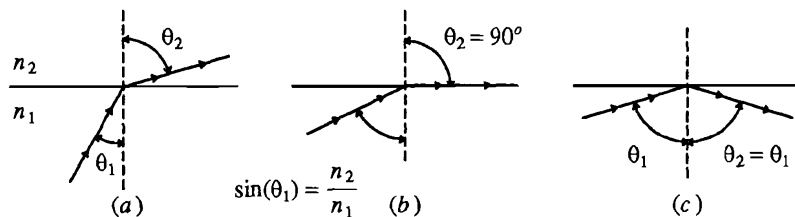


Figure 5-10. Illustration of Snell's Law and total internal reflection. a. Definition of angles of incidence θ_1 and refraction θ_2 . The angle of refraction is larger if $n_1 > n_2$. b. The critical angle of incidence at which the angle of refraction is ninety degrees. c. At angles larger than the critical angle, total internal reflection occurs.

a beam must have a diameter large with respect to the wavelength in order to be approximated as a plane wave [7]. Assuming that the index of refraction n_1 in the incident material is greater than the index of refraction of the refraction medium, n_2 , or $n_1 > n_2$. Then Snell's Law predicts that

$$\frac{\sin(\theta_1)}{\sin(\theta_2)} = \frac{n_2}{n_1} < 1. \quad (5.26)$$

The angle of refraction is larger than the angle of incidence. Shown in Figure 5-10b is the case of a critical incidence angle where the angle of refraction is ninety degrees, so that the light is refracted along the material interface. This corresponds to *critical* incident angle

$$\sin(\theta_1) = \frac{n_2}{n_1}. \quad (5.27)$$

For angles larger than (5.27), there is total internal reflection as illustrated in Figure 5-10c, where the angle of reflection is always equal to the angle of incidence.

This principle can be exploited in an *optical fiber waveguide* as illustrated in Figure 5-11. The *core* and *cladding* materials are glass, which transmits light with little attenuation, while the *sheath* is an opaque plastic material that serves no purpose other than to lend strength, absorb any light that might otherwise escape, and prevent any light from entering (which would represent interference or crosstalk). The core glass has a higher index of refraction than the cladding, with the result that incident rays with a small angle of incidence are captured by total internal reflection. This is illustrated in Figure 5-12, where a light ray incident on the end of the fiber is captured by total internal reflection as long as the angle of incidence θ_1 is below a critical angle (Problem 5-4). The ray model predicts that the light will bounce back and forth, confined to the waveguide until it emerges from the other end. Furthermore, it is obvious that the path length of a ray, and hence the transit time, is a function of the incident angle of the ray (Problem 5-5).

This variation in transit time for different rays manifests itself in *pulse broadening* — the broadening of a pulse launched into the fiber as it propagates — which in

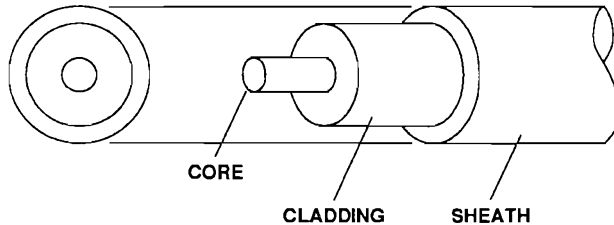


Figure 5-11. An optical fiber waveguide. The core and cladding serve to confine the light incident at narrow incident angles, while the opaque sheath serves to give mechanical stability and prevent crosstalk or interference.

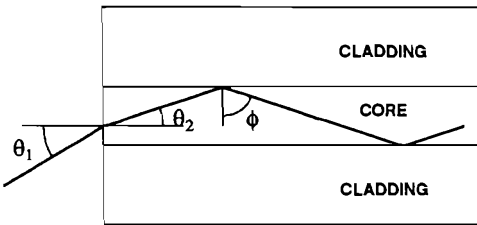


Figure 5-12. Ray model of propagation of light in an optical waveguide by total internal reflection. Shown is a cross-section of a fiber waveguide along its axis of symmetry, with an incident light ray at angle θ_1 which passes through the axis of the fiber (a meridional ray).

turn limits the pulse rate which can be used or the distance that can be transmitted or both. The pulse broadening can be reduced by modifying the design of the fiber, and specifically by using a *graded-index fiber* in which the index of refraction varies continuously with radial dimension from the axis.

The foregoing ray model gives some insight into the behavior of light in an optical fiber waveguide; for example, it correctly predicts that there is a greater pulse broadening when the index difference between core and cladding is greater. However, this model is inadequate to give an accurate description since in practice the radial dimensions of the fiber are on the order of the wavelength of the light. For example, the ray model of light predicts that there is a continuum of angles for which the light will bounce back and forth between core-cladding boundaries indefinitely. A more refined model uses Maxwell's equations to predict the behavior of light in the waveguide, and finds that in fact there are only a discrete and finite number of angles at which light propagates in zigzag fashion indefinitely. Each of these angles corresponds to a *mode* of propagation, similar to the modes in a metallic waveguide carrying microwave radiation. When the core radius is many times larger than the wavelength of the propagating light, there are many modes; this is called a *multimode* fiber. As the radius of the core is reduced, fewer and fewer modes are accommodated, until at a radius on the order of the wavelength only one mode of propagation is supported. This is called a *single mode* fiber. For a single mode fiber the ray model is seriously deficient since it depends on physical dimensions that are large relative to the wavelength for its accuracy. In fact, in the single mode fiber the light is not confined to the core, but in fact a significant fraction of the power propagates in the cladding. As the radius of the core gets smaller and smaller, more and more of the power travels in the cladding.

For various reasons, as we will see, the transmission capacity of the single mode fiber is greater. However, it is also more difficult to splice with low attenuation, and it also fails to capture light at the larger incident angles that would be captured by a multimode fiber, making it more difficult to launch a given optical power. In view of its much larger ultimate capacity, there is a trend toward exclusive use of single mode fiber in new installations, even though multimode fiber has been used extensively in the past [8]. In the following discussion, we emphasize the properties of single mode

fiber.

We will now discuss the factors which limit the bandwidth or bit rate which can be transmitted through a fiber of a given length. The important factors are:

- *Material attenuation*, the loss in signal power that inevitably results as light travels down an optical waveguide. There are four sources of this loss in a single mode fiber — scattering of the light by inherent inhomogeneities in the molecular structure of the glass crystal, absorption of the light by impurities in the crystal, losses in connectors, and losses introduced by bending of the fiber. Generally these losses are affected by the wavelength of the light, which affects the distribution of power between core and cladding as well as scattering and absorption mechanisms. The effect of these attenuation mechanisms is that the signal power loss in dB is proportional to the length of the fiber. Therefore, for a line of length L , if the loss in dB per kilometer is γ_0 , the total loss of the fiber is $\gamma_0 L$ and hence the ratio of transmitted power P_T to received power P_R obeys

$$\gamma_0 L = 10 \log_{10} \frac{P_T}{P_R}, \quad P_R = P_T \cdot 10^{-\frac{\gamma_0 L}{10}}. \quad (5.28)$$

This exponential dependence of loss vs. length is the same as for the transmission lines of Section 5.2.

- *Mode dispersion*, or the difference in group velocity between different modes, results in the broadening of a pulse which is launched into the fiber. This broadening of pulses results in interference between successive pulses which are transmitted, called *intersymbol interference* (Chapter 6). Since this pulse broadening increases with the length of the fiber, this dispersion will limit the distance between regenerative repeaters. One significant advantage of single mode fibers is that mode dispersion is absent since there is only one mode.
- *Chromatic or material dispersion* is caused by differences in the velocity of propagation at different wavelengths. For infrared and longer wavelengths, the shorter wavelengths arrive earlier than relatively longer wavelengths, but there is a crossover point at about $1.3 \mu\text{m}$ beyond which relatively longer wavelengths arrive earlier. Since practical optical sources have a non-zero bandwidth, called the *linewidth*, and signal modulation increases the optical bandwidth further, material dispersion will also cause intersymbol interference and limit the distance between regenerative repeaters. Material dispersion is qualitatively similar to the dispersion that occurs in transmission lines (Section 5.2) due to frequency-dependent attenuation. The total dispersion is usually expressed in units of picoseconds pulse spreading per GHz source bandwidth per kilometer distance, with typical values in the range of zero to 0.15 in the $1.3\text{-}1.6 \mu\text{m}$ minimum attenuation region [9,10]. It is very important that since the dispersion passes from positive to negative in the region of $1.3 \mu\text{m}$ wavelength, the dispersion is very nearly zero at this wavelength. A typical curve of the magnitude of the chromatic dispersion vs. wavelength is shown in Figure 5-13, where the zero is evident. The chromatic dispersion can be made negligibly small over a relatively wide range of wavelengths. Furthermore, the frequency of this zero in chromatic dispersion can be shifted through waveguide design to correspond

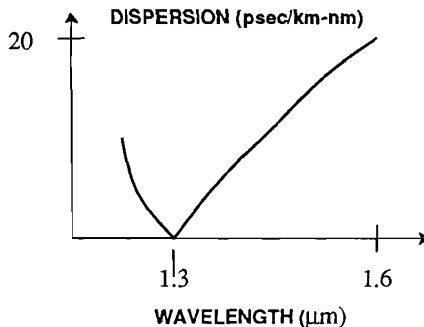


Figure 5-13. Typical chromatic dispersion in silica fiber [10]. Shown is the magnitude of the dispersion; the direction of the dispersion actually reverses at the zero-crossing.

to the wavelength of minimum attenuation.

With these impairments in mind, we can discuss the practical and fundamental limits on information capacity for a fiber. The fundamental limit on attenuation is due to the intrinsic material scattering of the glass in the fiber — this is known as *Rayleigh scattering*, and is similar to the scattering in the atmosphere of the earth that results in our blue sky. The scattering loss decreases rapidly with wavelength (as the fourth power), and hence it is generally advantageous to choose a longer wavelength. The attenuation due to intrinsic absorption is negligible, but at certain wavelengths large attenuation due to certain impurities is observed. Particularly important are hydroxyl (OH) radicals in the glass, which absorb at 2.73 μmeters wavelength and harmonics. At long wavelengths there is infrared absorption associated fundamentally with the glass, which rises sharply starting at 1.6 μmeters .

A loss curve for a state-of-the-art fiber is shown in Figure 5-14. Note the loss curves for two intrinsic effects which would be present in an ideal material, Rayleigh scattering and infrared absorption, and additional absorption peaks at 0.95, 1.25, and 1.39 μm due to OH impurities. The lowest losses are at approximately 1.3 and 1.5 μm , and these are the wavelengths at which the highest performance systems operate. The loss is as low as about 0.2 dB/km, implying potentially a much larger repeater spacing for optical fiber digital communication systems as compared to wire-pairs and coax. A curve of attenuation vs. frequency in Figure 5-15 for wire cable media and for optical fiber illustrates that the latter has a much lower loss.

The loss per unit distance of the fiber is a much more important determinant of the distance between repeaters than is the bit rate at which we are transmitting. This is illustrated for a single-mode fiber in Figure 5-16, where there is an attenuation-limited region where the curve of repeater spacing vs. bit rate is relatively flat. As we increase the bit rate, however, we eventually approach a region where the repeater spacing is limited by the dispersion (mode dispersion in a multimode fiber and chromatic dispersion in a single mode fiber). The magnitude of the latter can be quantified simply by considering the Fourier transform of a transmitted pulse, and in particular its bandwidth W . The spreading of the pulse will be proportional to the

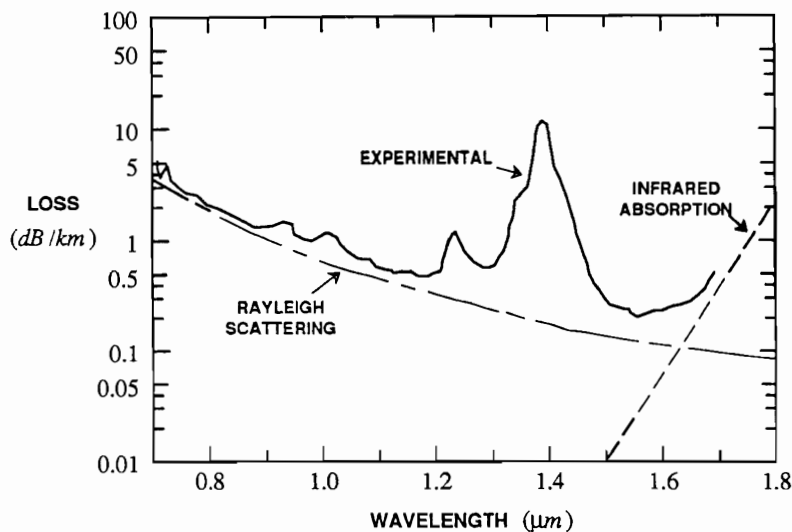


Figure 5-14. Observed loss spectrum of an ultra-low-loss germanosilicate single mode fiber together with the loss due to intrinsic material effects [11].

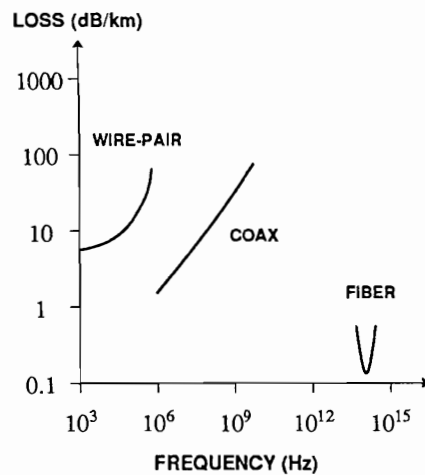


Figure 5-15. Attenuation vs. frequency for wire cable and fiber guiding media [10]. The band of frequencies over which the fiber loss is less than 1 dB/km is more than 10^{14} Hz.

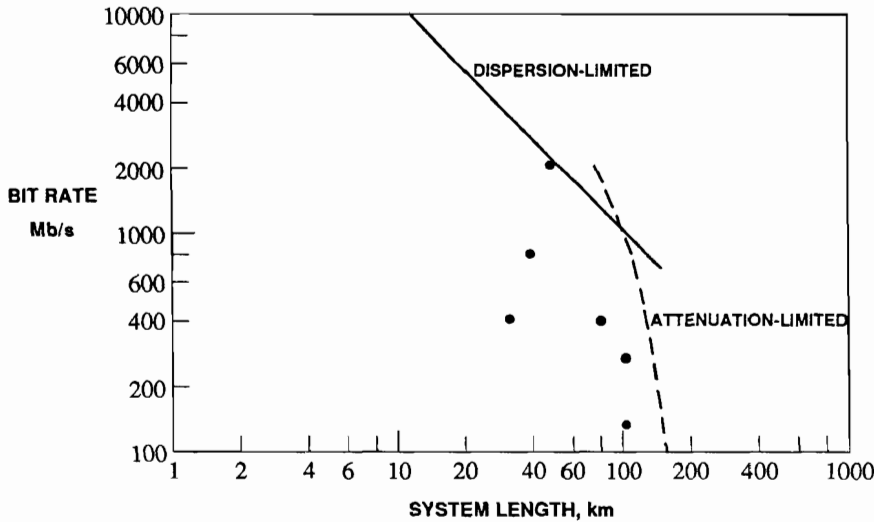


Figure 5-16. Tradeoff between distance and bit rate for a single mode fiber with a particular set of assumptions [8]. The dots represent performance of actual field trial systems.

repeater spacing L and the bandwidth W , with a constant of proportionality D . Thus, if we require that this dispersion be less than half a pulse-time at a pulse rate of R pulses per second,

$$D \cdot L \cdot W < \frac{1}{2R}. \quad (5.29)$$

The bandwidth W of the source depends on the *linewidth*, or intrinsic bandwidth in the absence of modulation, and also on the *modulation*. Since a non-zero linewidth will increase the bandwidth and hence the chromatic dispersion, we can understand fundamental limits by assuming zero linewidth. We will show in Chapter 6 that the bandwidth due to modulation is approximately equal to the pulse rate, or $W \approx R$, and hence (5.29) becomes

$$R^2 L < \frac{1}{2D}. \quad (5.30)$$

This equation implies that in the region where dispersion is limiting, the repeater spacing L must decrease rather rapidly as the bit rate is increased, as shown in Figure 5-16. More quantitative estimates of the limits shown in Figure 5-16 are derived in Problem 5-6 and Problem 5-11.

As a result of these considerations, first generation (about 1980) optical fiber transmission systems typically used multimode fiber at a wavelength of about 0.8 μ meter, and achieved bit rates up to about 150 Mb/s. The Rayleigh scattering is about 2 dB per km at this wavelength, and the distance between regenerative repeaters was in the 5 to 10 km range. Second generation systems (around 1985) moved to single mode fibers and wavelengths of about 1.3 μ meters, where Rayleigh scattering attenuation is about 0.2 dB/km (and practical attenuations are more on the order of 0.3

dB/km).

The finite length of manufactured fibers and system installation considerations dictate fiber connectors. These present difficult alignment problems, all the more difficult for single mode fibers because of the smaller core, but in practice connector losses of 0.1 to 0.2 dB can be obtained even for single mode fibers. Since it must be anticipated in any system installation that accidental breakage and subsequent splicing will be required at numerous points, in fact connector and splicing loss is the dominant loss in limiting repeater spacing.

Bending loss is due to the different propagation velocities required on the outer and inner radius of the bend. As the bending radius decreases, eventually the light on the outer radius must travel faster than the speed of light, which is of course impossible. What happens instead is that significant attenuation occurs due to a loss of confined power. Generally there is a tradeoff between bending loss and splicing loss in single mode fibers, since bending loss is minimized by confining most of the power to the core, but that makes splicing alignment more critical.

In Figure 5-16, the tradeoff between maximum distance and bit rate is quantified for a single mode fiber for a particular set of assumptions (the actual numerical values are dependent on these assumptions). At bit rates below about one Gb/s (10^9 bits per second) the distance is limited by attenuation and receiver sensitivity. In this range the distance decreases as bit rate increases since the receiver sensitivity decreases (see Section 5.3.3). At higher bit rates, pulse broadening limits the distance before attenuation becomes important. The total fiber system capacity is best measured by a figure of merit equal to the product of the bit rate and the distance between repeaters (Problem 5-10), measured in Gb-km/sec. Current commercial systems achieve capacities on the order of 100 to 1000 Gb-km/sec.

5.3.2. Sources

While optical fiber transmission uses light energy to carry the information bits, at the present state of the art the signals are generated and manipulated electrically. This implies an electrical-to-optical conversion at the input to the fiber medium and an optical-to-electrical conversion at the output. There are two available light sources for fiber digital communication systems: the *light-emitting diode (LED)* and the *semiconductor injection laser*. The semiconductor laser is the more important for high-capacity systems, so we emphasize it here. In contrast to the LED, the laser output is *coherent*, meaning that it is nearly confined to a single frequency. In fact the laser output does have non-zero linewidth, but by careful design the linewidth can be made small relative to signal bandwidths using a structure called *distributed feedback (DFB)*. Thus, coherent modulation and demodulation schemes are feasible (Chapter 8), although commercial systems use intensity modulation. The laser output can be coupled into a single mode fiber with very high efficiency (about 3 dB power loss), and can generate powers in the 0 to 10 mwatt range [9] with one mW (0 dBm) typical [10]. The laser is necessary for single mode fibers, except for short distances, because it emits a narrower beam than the LED. The light output of the laser is very temperature dependent, and hence it is generally necessary to monitor the light output and control the driving current using a feedback circuit.

There is not much room for increasing the launched power into the fiber because of nonlinear effects which arise in the fiber [9], unless, of course, we can find ways to circumvent or exploit these nonlinear phenomena.

5.3.3. Photodetectors

The optical energy at the output of the fiber is converted to an electrical signal by a *photodetector*. There are two types of photodetectors available — the *PIN photodiode*, popular at about 100 Mb/s and below, and the *avalanche photodiode (APD)* (popular above 1 Gb/s) [12,10]. The cross-section of a PIN photodiode is shown in Figure 5-17. This diode has an intrinsic (non-doped) region (not typical of diodes) between the n- and p-doped silicon. Photons of the received optical signal are absorbed and create hole-electron pairs. If the diode is reverse biased, there is an electric field across the depletion region of the diode (which includes the intrinsic portion), and this electric field separates the holes from electrons and sweeps them to the contacts, creating a current proportional to the incident optical power. The purpose of the intrinsic region is to enlarge the depletion region, thereby increasing the fraction of incident photons converted into current (carriers created outside the depletion region, or beyond diffusion distance of the depletion region, recombine with high probability before any current is generated).

The fraction of incident photons converted into carriers that reach the electrodes is called the *quantum efficiency* of the detector, denoted by η . Given the quantum efficiency, we can easily predict the current generated as a function of the total incident optical power. The energy of one photon is $h\nu$ where h is Planck's constant ($6.6 \cdot 10^{-34}$ Joule-sec) and ν is the optical frequency, related to the wavelength λ by

$$\nu\lambda = c \quad (5.31)$$

where c is the speed of light ($3 \cdot 10^8$ m/sec). If the incident optical power is P watts,

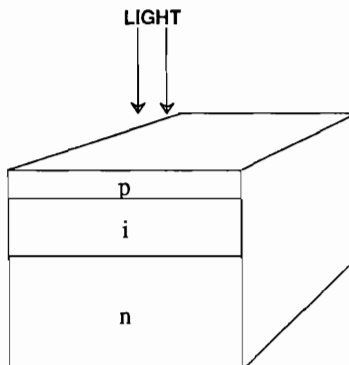


Figure 5-17. A PIN photodiode cross-section. Electrode connection to the n-and p-regions creates a diode, which is reverse-biased.

then the number of photons per second is $P/h\nu$, and if a fraction η of these photons generate an electron with charge q ($1.6 \cdot 10^{-19}$ Coulombs) then the total current is

$$i = \eta q \left(\frac{P}{h\nu} \right). \quad (5.32)$$

Example 5-15.

For a wavelength of $1.5 \mu\text{m}$ and quantum efficiency of unity, what is the *responsivity* (defined as the ratio of output current to input power) for a PIN photodiode? It is

$$\frac{i}{P} = \frac{q}{h\nu} = \frac{q \lambda}{h c} = \frac{1.6 \cdot 10^{-19} 1.5 \cdot 10^{-6}}{6.6 \cdot 10^{-34} 3.0 \cdot 10^8} = 1.21 \text{ amps/watt}. \quad (5.33)$$

If the incident optical power is a nanowatt, the maximum current from a PIN photodiode is 1.21 nanoamperes. \square

With PIN photodiodes (and more generally all photodetectors), there is a tradeoff between quantum efficiency and speed. Quantum efficiencies near unity are achievable with a PIN photodiode, but this requires a long absorption region. But a long intrinsic absorption region results in a correspondingly smaller electric field (with resulting slower carrier velocity) and a longer drift distance, and hence slower response to an optical input. Higher speed inevitably results in reduced sensitivity.

Since very small currents are difficult to process electronically without adding significant thermal noise, it is desirable to increase the output current of the diode before amplification. This is the purpose of the APD, which has internal gain, generating more than one electron-hole pair per incident photon. Like the PIN photodiode, the APD is also a reverse-biased diode, but the difference is that the reverse voltage is large enough that when carriers are freed by a photon and separated by the electric field they have enough energy to collide with the atoms in the semiconductor crystal lattice. The collisions ionize the lattice atoms, generating a second electron-hole pair. These secondary carriers in turn collide with the lattice, and additional carriers are generated. One price paid for this gain mechanism is an inherently lower bandwidth. A second price paid in the APD is the probabilistic nature of the number of secondary carriers generated. The larger the gain in the APD, the larger the statistical fluctuation in current for a given optical power. In addition, the bandwidth of the device decreases with increasing gain, since it takes some time for the avalanche process to build up.

Both PIN photodiodes and APD's exhibit a small current which flows in the absence of incident light due to thermal excitation of carriers. This current is called *dark current* for obvious reasons, and represents a background noise signal with respect to signal detection.

5.3.4. Model for Fiber Reception

Based on the previous background material and the mathematics of Poisson processes and shot noise (Section 3.4) we can develop a statistical model for the output of an optical fiber detector. This signal has quite different characteristics from that of other media of interest, since random quantum fluctuations in the signal are important. Since the signal itself has random fluctuations, we can consider it to have a

type of *multiplicative noise*.

In commercial systems, the *direct detection* mode of transmission is used, as pictured in Figure 5-18. In this mode, the intensity or power of the light is directly modulated by the electrical source (data signal), and a photodetector turns this power into another electrical signal. If the input current to the source is $x(t)$, then the output power of the source is proportional to $x(t)$.

Two bad things happen to this launched power as it propagates down the fiber. First, it is attenuated, reducing the signal power at the detector. Second, it suffers dispersion due to chromatic dispersion (and mode dispersion for a multimode fiber), which can be modeled as a linear filtering operation. Let $g(t)$ be the impulse response of the equivalent dispersion filter, including the attenuation, so that the received power at the detector is

$$P(t) = x(t) * g(t). \quad (5.34)$$

In the final conversion to electrical current in the photodetector, the situation is a bit more complicated since quantum effects are important. The incident light consists of discrete photons which are converted to photoelectron-hole pairs in the detector. Hence, the current generated consists of discrete packets of charge generated at discrete points in time. Intuitively we might expect that the arrival times of the charge packets for a Poisson process (Section 3.4) since there is no reason to expect the interarrival times between photons to depend on one other. In fact, this is predicted by quantum theory. Let $h(t)$ be the response of the photodetector circuit to a single photoelectron, and then an outcome for the detected current $y(t)$ is a filtered Poisson process

$$Y(t) = \sum_m h(t - t_m) \quad (5.35)$$

where the t_m are Poisson arrival times. The Poisson arrivals are characterized by the rate of arrivals, which is naturally proportional to the incident power,

$$\lambda(t) = \frac{\eta}{hv} \cdot P(t) + \lambda_0 \quad (5.36)$$

where η is the quantum efficiency and λ_0 is a dark current. Note from Campbell's theorem (Section 3.4.4) that the expected detected current is

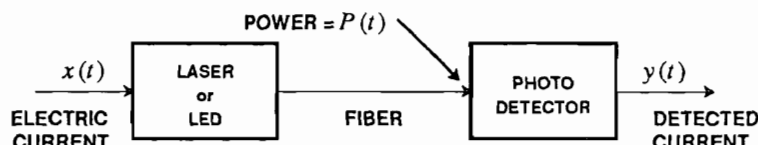


Figure 5-18. Elements of a direct detection optical fiber system.

$$E[Y(t)] = \lambda(t) * h(t) = \frac{\eta}{hv} \cdot x(t) * g(t) * h(t) + \lambda_0 H(0) . \quad (5.37)$$

The equivalent input-output relationship of the channel is therefore characterized, with respect to the mean-value of the detector output current, by the convolution of the two filters — the dispersion of the fiber and the response of the detector circuitry. Of course, there will be statistical fluctuations about this average that will be characterized in Chapter 8. This simple linear model for the channel that is quite accurate unless the launched optical power is high enough to excite nonlinear effects in the fiber and source-detector.

Avalanche Photodetector

In the case of an APD, we have to modify this model by adding to the filtered Poisson process of (5.35) the random multiplier resulting from the avalanche process,

$$y(t) = \sum_m g_m h(t - t_m) , \quad (5.38)$$

the statistics of which has already been considered in (3.143). Define the mean and second moment of the avalanche gain,

$$\bar{G} = E[G_m] , \quad \bar{G^2} = E[G_m^2] . \quad (5.39)$$

Then from Section 3.4.6, we know that the effect of the avalanche gain on the second order statistics of (5.35) is to multiply the mean value of the received random process by \bar{G} and the variance by \bar{G}^2 .

If the avalanche process were deterministic, that is precisely \bar{G} secondary electrons were generated for each primary photoelectron, then the second moment would be the square of the mean,

$$\bar{G^2} = \bar{G}^2 . \quad (5.40)$$

The effect of the randomness of the multiplication process is to make the second moment larger, by a factor F_G greater than unity,

$$\bar{G^2} = F_G \bar{G}^2 \quad (5.41)$$

where of course $F_G = \bar{G^2}/\bar{G}^2$. The factor F_G is called the *excess noise factor*. In fact, a detailed analysis of the physics of the APD [13] yields the result

$$F_G = k \cdot \bar{G} + (2 - \frac{1}{\bar{G}}) \cdot (1 - k) \quad (5.42)$$

where $0 \leq k \leq 1$ is a parameter under the control of the device designer called the *carrier ionization ratio*. Note that as $k \rightarrow 1$, $F_G \rightarrow \bar{G}$, or the excess noise factor is approximately equal to the avalanche gain. This says that the randomness gets larger as the avalanche gain gets larger. On the other hand, as $k \rightarrow 0$, $F_G \rightarrow 2$ for large \bar{G} , or the excess noise factor is approximately independent of the avalanche gain. Finally, when $\bar{G} = 1$ (there is no avalanche gain), $F_G = 1$ and there is no excess noise. This is the PIN photodiode detector.

Fiber and Preamplifier Thermal Noise

Any physical system at non-zero temperature will experience noise due to the thermal motion of electrons, and optical fiber is no exception. This noise is often called *thermal noise* or *Johnson noise* in honor of J.B. Johnson, who studied this noise experimentally at Bell Laboratories in 1928. Theoretical study of this noise based on the theory of quantum mechanics was carried out by H. Nyquist at about the same time. Thermal noise is usually approximated as white Gaussian noise. The Gaussian property is a result of the central limit theorem and the fact that thermal noise is composed of the superposition of many independent actions. The white property cannot of course extend to infinite frequencies since otherwise the total power would be infinite, but rather this noise can be considered as white up to frequencies of 300 GHz or so. Nyquist's result was that thermal noise has an available noise power per Hz of

$$N(v) = \frac{h v}{e^{hv/kT_n} - 1} \quad (5.43)$$

where h is Planck's constant, v is the frequency, k is Boltzmann's constant ($1.38 \cdot 10^{-23}$ Joules per degree Kelvin), and T_n is the temperature in degrees Kelvin. By *available noise power* we mean the power delivered into a load with a matched impedance. If we consider this as a two sided spectral density, we have to divide by two.

At frequencies up through the microwave, the exponent in (5.43) is very small, and if we approximate e^x by $1 + x$ we get that the spectrum is approximately white,

$$N(v) \approx kT_n . \quad (5.44)$$

This corresponds to a two-sided spectral density of size

$$N_0 = \frac{kT_n}{2} . \quad (5.45)$$

However, at high frequencies, this spectrum approaches zero exponentially, yielding a finite total power.

There are two possible sources of thermal noise — at the input to the detector, and in the receiver preamplifier. At the input to the detector only thermal noise at optical frequencies is relevant (the detector will not respond to lower frequencies), and at these frequencies the thermal noise will be negligible.

Example 5-16.

At room temperature kT_n is $4 \cdot 10^{-21}$ Joules. At 1 GHz, or microwave frequencies, $h v$ is about 10^{-24} Joules, and we are well in the regime where the spectrum is flat. However, at 1 μm wavelength, or $v = 3 \cdot 10^{14}$ Hz, $h v$ is about $2 \cdot 10^{-19}$ Joules, and $\frac{h v}{kT_n}$ is about 50. Thus, the thermal noise is much smaller than kT_n at these frequencies. Generally thermal noise at optical frequencies is negligible in optical fiber systems at wavelengths shorter than about 2 μm [14]. \square

Since the signal level is very low at the output of the detector in Figure 5-18, we must amplify the signal using a preamplifier as the first stage of a receiver. Thermal

noise introduced in the preamplifier is a significant source of noise, and in fact in many optical systems is the dominant noise source. Since the signal at this point is the baseband digital waveform, it occupies a bandwidth extending possibly up to microwave frequencies but not optical frequencies, hence the importance of thermal noise. We will see in Chapter 8 that this thermal noise is the primary reason for considering the use of an APD detector in preference to a PIN photodiode. A more detailed consideration of the design of the preamplifier circuitry is given in [14] and the problems in Chapter 8.

5.3.5. Advanced Techniques

Two exciting developments have been demonstrated in the laboratory: *soliton transmission* and *erbium-doped fiber amplifiers*. The soliton operates on the principle of the *optical Kerr effect*, a nonlinear effect in which the index of refraction of the fiber depends on the optical power. As previously mentioned, in chromatic dispersion, the index of refraction also depends on the wavelength. Solitons are optical pulses that have a precise shape and peak power chosen so that the Kerr effect produces a chirp (phase modulation) that is just appropriate to cancel the pulse broadening induced by group-velocity dispersion. The result is that all the wavelengths can be made to travel at the same speed, essentially eliminating material dispersion effects. In soliton transmission, material attenuation is the only effect that limits repeater spacing.

An optical amplifier can be constructed out of a fiber doped with the rare-earth element erbium, together with a semiconductor laser pumping source. If the pumping source wavelength is 0.98 or 1.48 μm , then the erbium atoms are excited into a higher state, and reinforce 1.55 μm incident light by stimulated emission. With about 10 mW of pumping power, gains of 30 to 40 dB at 1.55 μm can be obtained. A receiver designed using this optical amplifier is shown in Figure 5-19. The optical amplifier has gain G , which actually depends on the input signal power because large signals deplete the excited erbium atoms and thereby reduce the gain. The amplifier also generates a spurious noise due to spontaneous emission, and the purpose of the optical bandpass filter is to filter out spontaneous noise outside the signal bandwidth (which depends on source linewidth as well as signal modulation). There is a premium on narrow linewidth sources, because that enables the optical filter bandwidth to be minimized.

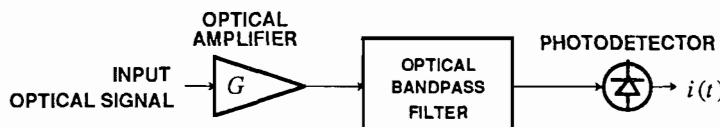


Figure 5-19. A direct-detection optical receiver using an optical amplifier.

The effect of the amplifier is similar to an avalanche detector, in that it increases the signal power (rendering electronic thermal noise insignificant) while adding additional spontaneous noise. The major distinction between the amplifier and avalanche detector, however, is that much of the spontaneous noise in the amplifier can be optically filtered out, whereas in the detector it cannot. It is also possible to place optical amplifiers at intermediate points in a fiber system, increasing the repeater spacing dramatically. The design of the receiver in Figure 5-19 will be considered further in Chapter 8.

5.4. MICROWAVE RADIO

The term "radio" is used to refer to all electromagnetic transmission through free space at microwave frequencies and below. There are many applications of digital transmission which use this medium, primarily at microwave frequencies, a representative set of which include *point-to-point terrestrial digital radio*, *digital mobile radio*, *digital satellite communication*, and *deep-space digital communication*.

Terrestrial digital radio systems use microwave horn antennas placed on towers to extend the horizon and increase the antenna spacing. This medium has been used in the past principally for analog transmission (using FM and more recently SSB modulation), but in recent years has gradually been converted to digital transmission due to increased demand for data services.

Example 5-17.

In North America there are frequency allocations for telephony digital radios centered at frequencies of 2, 4, 6, 8, and 11 GHz [15]. In the United States there were over 10,000 digital radio links in 1986, including a cross-country network at 4 GHz. □

A related application is digital mobile radio.

Example 5-18.

The frequency band from 806 to 947 MHz is allocated in the United States to land mobile radio services [16]. This band is used for *cellular mobile radio* [17], in which a geographical area is divided into a lattice of cells, each with its own fixed omni-directional base antenna for transmission and reception. As a vehicle passes through the cells, the associated base antenna is automatically switched to the closest one. An advantage of this concept is that additional mobile telephones can be accommodated by decreasing the size of the cells and adding additional base antennas. □

Satellites are used for long-distance communication between two terrestrial antennas, where the satellite usually acts as a non-regenerative repeater. That is, the satellite simply receives a signal from a terrestrial transmitting antenna, amplifies it, and transmits it back toward another terrestrial receiving antenna. Satellite channels offer an excellent alternative to fiber and cable media for transmission over long distances, and particularly over sparse routes where the total communication traffic is small. Satellites also have the powerful characteristic of providing a natural multiple access medium, which is invaluable for random-access communication among a

number of users. A limitation on satellites is limited power available for transmission, since the power is derived from solar energy or expendable resources. In addition, the configuration of the launch vehicles usually limit the size of the transmitting and receiving antennas (which are usually one and the same). Most communication satellites are put into synchronous orbits, so that they appear to be stationary over a point on the earth. This greatly simplifies the problems of antenna pointing and satellite availability.

In deep-space communication, the object is to transmit data to and receive data from a platform that is at a great distance from earth. This application includes the features of both satellite and mobile communication, in that the vehicle is usually in motion. As in the satellite case, the size of the antenna and the power resources at the space vehicle are limited.

With the exception of problems of multipath propagation in terrestrial links, the microwave transmission channel is relatively simple. There is an attenuation introduced in the medium due to the spreading of the energy, where this attenuation is frequency-independent, and thermal noise introduced at the antenna and in the amplifiers in the receiver. These aspects of the channel are covered in the following subsections followed by a discussion of multipath distortion.

5.4.1. Microwave Antennas and Transmission

Microwave propagation through free-space is very simple, as there is an attenuation due to the spreading of radiation. The attenuation varies so slowly with frequency that it can be considered virtually fixed within the signal bandwidth. Consider first an *isotropic antenna*; namely, one that radiates power equally in all directions. Assume the total radiated power is P_T watts, and assume that at distance d meters from this transmit antenna there is a receive antenna with area A_R meters². Then the maximum power that the receive antenna could capture is the transmit power times the ratio of A_R to the area of a sphere with radius d , which is $4\pi d^2$. There are two factors which modify this received power. First, the transmit antenna can be designed to focus or concentrate its radiated energy in the direction of the receiving antenna. This adds a factor G_T called the *transmit antenna gain* to the received power. The second factor is the *antenna efficiency* η_R of the receive antenna, a number less than (but hopefully close to) unity; the receive antenna does not actually capture all the electromagnetic radiation incident on it. Thus, the received power is

$$P_R = P_T \frac{A_R}{4\pi d^2} G_T \eta_R. \quad (5.46)$$

At microwave frequencies, aperture antennas (such as horn or parabolic) are typically used, and for these antennas the achievable antenna gain is

$$G = \frac{4\pi A}{\lambda^2} \eta, \quad (5.47)$$

where A is the area of the antenna, λ is the wavelength of transmission, and η is an efficiency factor. Expression (5.47) applies to either a receiving or transmitting antenna, where the appropriate area and efficiency are substituted. This expression is

intuitively pleasing, since it says that the antenna gain is proportional to the square of the ratio of antenna dimension to wavelength. Thus, the transmit antenna size in relation to the wavelength is all that counts in the directivity or gain of the antenna. This antenna gain increases with frequency for a given antenna area, and thus higher frequencies have the advantage that a smaller antenna is required for a given antenna gain. The efficiency of an antenna is typically in the range of 50 to 75 percent for a parabolical reflector antenna and as high as 90 percent for a horn antenna [18].

An alternative form of the received power equation can be derived by substituting for the area of the receive antenna in (5.46) in terms of its gain in (5.47),

$$\frac{P_R}{P_T} = G_T G_R \left[\frac{\lambda}{4\pi d} \right]^2 ; \quad (5.48)$$

this is known as the *Friis transmission equation*. The term in brackets is called the *path loss*, while the terms G_T and G_R summarize the effects of the two antennas. While this loss is a function of wavelength, the actual power over the signal bandwidth does not generally vary appreciably where the bandwidth is very small in relation to the center frequency of the modulated signal. The Friis equation does not take into account other possible sources of loss such as rain attenuation and antenna mispointing.

The application of these relations to a particular configuration can determine the received power and the factors contributing to the loss of signal power. This process is known as generating the *link power budget*, as illustrated by the following examples.

Example 5-19.

Determine the received power for the link from a synchronous satellite to a terrestrial antenna for the following parameters: Height 40,000 km, satellite transmitted power 2 watts, transmit antenna gain 17 dB, receiving antenna area 10 meters² with perfect efficiency, and frequency 11 GHz. The wavelength can be obtained from (5.31),

$$\lambda = \frac{c}{v} = \frac{3 \cdot 10^8}{11 \cdot 10^9} = 27.3 \text{ mm} . \quad (5.49)$$

The receive antenna gain is

$$10\log_{10}G_R = 10\log_{10}\frac{4\pi \cdot 10}{(27.3 \cdot 10^{-3})^2} = 52.2 . \quad (5.50)$$

Next, the path loss is

$$10\log_{10}\left[\frac{\lambda}{4\pi d}\right]^2 = 20\log_{10}\left[\frac{27.3 \cdot 10^{-3}}{4\pi \cdot 4 \cdot 10^7}\right] = -205.3 \text{ dB} . \quad (5.51)$$

Finally, we are in a position to calculate the received power, which we express in dBW (decibels relative to one watt) and recognizing that the transmit power is 3 dBW,

$$10\log_{10}P_R = 3 \text{ dBW} + 17 + 52.3 - 205.3 = -133 \text{ dBW} . \quad (5.52)$$

□

Example 5-20.

The Mariner-10 deep-space mission to Mercury in 1974 used a transmitter power of 16.8 watts and frequency 2.3 GHz. The transmit antenna diameter on the spacecraft was 1.35 meters with efficiency 0.54, which results in an antenna gain of 27.6 dB. The terrestrial receive antenna diameter was 64 meters with efficiency 0.575, for an antenna gain of 61.4 dB. The distance from the spacecraft to ground was $1.6 \cdot 10^{11}$ meters, for a path loss of 263.8 dB. Finally, the received power was

$$10\log_{10}P_R = 10\log_{10}16.8 + 27.6 + 61.4 - 263.8 = -162.6 \text{ dBW.} \quad (5.53)$$

□

The two dominant effects of microwave propagation are attenuation and delay. It is of interest to determine the effect on a passband signal, represented by the complex-baseband signal of Section 2.4. Assume the attenuation is A , the distance of propagation is d , and the speed of propagation is c . The delay the signal experiences is $\tau = d/c$, and given a passband signal of the form of Figure 2-6, the output of the channel is

$$\sqrt{2}A \cdot \operatorname{Re}\{ u(t - \tau)e^{j\omega_c(t - \tau)} \} = \sqrt{2} \operatorname{Re}\{ A u(t - \tau) e^{-jkd} e^{j\omega_c t} \} \quad (5.54)$$

where

$$k = \frac{\omega_c \tau}{d} = \frac{\omega_c}{c} = \frac{2\pi}{\lambda}, \quad (5.55)$$

is called the *propagation constant*. The equivalent complex-baseband channel, shown in Figure 5-20, characterizes the effect of propagation on the equivalent complex-baseband signal. Not surprisingly, the baseband signal is delayed by τ , the same as the passband signal. In addition, there is a phase shift by $kd = 2\pi d/\lambda$ radians, or 2π radians for each wavelength of propagation distance. The equivalent complex-valued impulse response of the propagation is an impulse with delay τ and area $A \cdot e^{-jkd}$, and the equivalent transfer function is $Ae^{-j\omega\tau}e^{-jkd}$. The only frequency dependence is

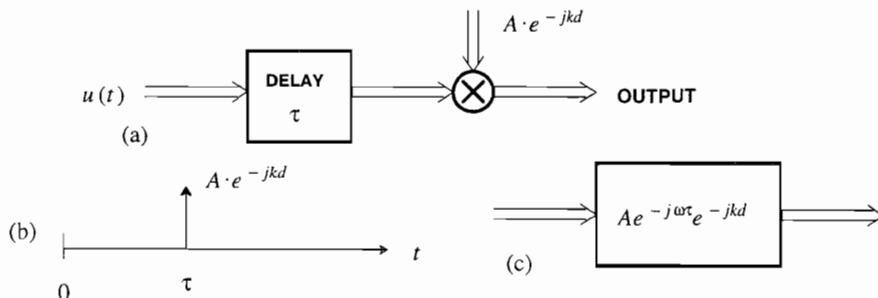


Figure 5-20. The equivalent complex baseband channel for a freespace propagation with attenuation A and distance d . a) Equivalent system, b) the equivalent impulse response, and c) the equivalent baseband transfer function.

linear in frequency, due to the delay. For mobile receivers, the effect of small changes in d on the baseband channel response is particularly significant. The effect is dramatically more pronounced for the phase shift than for the delay.

Example 5-21.

For a carrier frequency of 1 GHz (typical for mobile radio), the propagation constant is $k = \omega_c/c = 21$ radians/meter. Thus, a $\pi/2 = 1.57$ radian phase shift, which will be very significant to demodulators, occurs with every 7.4 centimeters change in propagation distance. In contrast, the propagation delay changes by 3.3 nanoseconds for each meter change in propagation distance. In relation to typical baseband bandwidths, this is totally insignificant. For example, at 1 MHz, the change in phase shift due to this delay change is only $\omega\tau = 2\pi \cdot 0.0033$, or roughly one degree. \square

5.4.2. Noise in Microwave Amplifiers

On a radio link noise enters the receiver both through the antenna and as internal noise sources in the receiver. We saw in (5.45) that both sources of noise are Gaussian and can be considered as white up through the microwave frequencies. White noise is completely specified by the spectral density N_0 , given by (5.45). However, in radio transmission it is common to express this spectral density in terms of an equivalent parameter, the *noise temperature* expressed in degrees Kelvin. This custom derives from the functional form of (5.45), where N_0 is strictly a function of the temperature. The custom of specifying noise temperature derives from the fact that T_n is reasonable in size, on the order of tens or hundreds of degrees, whereas N_0 is a very small number. Note however that the total thermal noise at some point in a system may be the superposition of many thermal noise sources at different temperatures. Hence, the noise temperature is merely a convenient specification of the noise power, and is not necessarily equal to the physical temperature of any part of the system! For example, if we amplify the noise we increase the noise temperature without affecting the physical temperature of the source that generated that noise.

There are two sources of noise — the noise incident on the antenna and the noise introduced internally in the receiver. The noise incident on the antenna depends on the effective noise temperature in the direction the antenna is pointed. For example, the sun has a much higher effective temperature than the atmosphere. The noise introduced internal to the receiver depends on the design and sophistication of the receiver. It is customary to refer all noise sources to the input to the receiver (the antenna), and define an equivalent noise temperature at that point. Since the stages of a receiver typically have large gains, the noise introduced internal to the receiver usually has a much smaller noise temperature when referred to the receiver input. These receiver noise temperatures range from about four degrees Kelvin for supercooled maser amplifiers to the range of 70 to 200 degrees Kelvin for receivers without physical cooling.

Example 5-22.

Continuing Example 5-20 for the Mariner-10 mission the effective noise temperature of the antenna plus receiver was 13.5 degrees Kelvin. A bit rate of 117.6 kb/s was used. What is the signal-to-noise ratio in the receiver assuming the bandwidth of the system is half the bit

rate, 58.8 kHz? (We will see in Chapter 6 that this is the minimum possible bandwidth for binary transmission.) The total noise power within the receiver bandwidth would be

$$P_n = kT_n B = 1.38 \cdot 10^{-23} \cdot 13.5 \cdot 58.8 \cdot 10^3 = -169.6 \text{ dBW} \quad (5.56)$$

The signal-to-noise ratio is therefore

$$SNR = -162.6 + 169.6 = 7.0 \text{ dB}. \quad (5.57)$$

In practice the noise bandwidth will be larger than this, and the SNR will be lower, perhaps by a couple of dB. This SNR will support data transmission, albeit at a rather poor error rate. Coding techniques (Chapters 13 and 14) can compensate for the poor SNR. \square

The SNR as calculated in this example is a useful quantity since it will not be changed by the large gain introduced in the receiver (both signal and noise will be affected the same way).

5.4.3. Emission Masks

A radio channel does not in itself provide any significant restriction on the bandwidth that we can use for digital communication. Moreover, the free-space channel introduces only a slowly varying dependence of attenuation on frequency (due to antenna gain). Thus, there is nothing inherent about the channel to introduce significant motivation to be spectrally efficient. Enter the regulatory agencies! Since the radio spectrum is a scarce commodity, it is carefully allocated to individual users. Unlike optical-fiber, where different users can install their own fiber, we must all share a single radio environment. To prevent significant interference between users, *spectral emission masks* are specified by regulation. An example of such a mask is shown in Figure 5-21. In this case, the regulatory agency has assigned a nominal 30 MHz bandwidth centered at f_c to a particular user, but for practical reasons has allowed that user to transmit a small amount of power (down more than 50 dB)

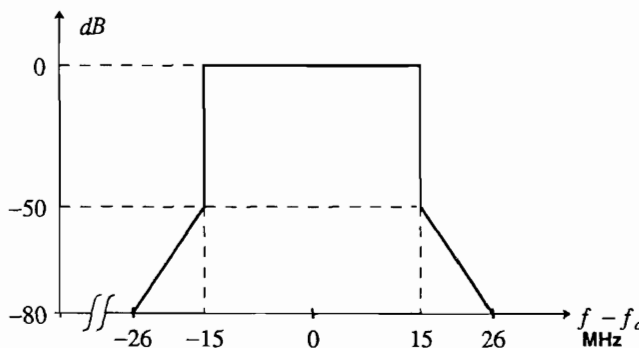


Figure 5-21. A spectral emission mask referenced to a nominal 30 MHz channel bandwidth. The vertical axis is transmitted power spectrum referenced to the power of an unmodulated carrier. The user signal must stay under the mask. (This mask applies to the United States.)

outside that band.

This mask is usually adhered to by placing a very sharp cutoff filter in the radio transmitter. Since this filter is imposed by external constraints, it is natural to think of this filter as being part of the channel (this logic is oversimplified of course since the filter requirements depend on the spectrum of the signal feeding the filter). From this perspective, the microwave radio channel has a very sharp cutoff at the band edges, in contrast to the media we have seen earlier which have at most a gradual increase of attenuation with frequency. This characteristic is shared by the voiceband data channel in the next section, and for this reason similar modulation techniques are often employed on the two media.

5.4.4. Multipath Fading

We have seen how the link budget can be determined for a radio link. The calculation we made assumed for the most part idealized circumstances, whereas in practice additional *system margin* must be included in the link budget to account for foreseen or unforeseen circumstances. For example, at higher frequencies there will be an additional *rain attenuation* during rainstorms at the earth receiving antenna. In terrestrial microwave systems, there is an additional important source of attenuation that must be accounted for — *multipath fading* [19]. Both rain attenuation and multipath fading result in an attenuation on the signal path that varies with frequency. A significant difference is that unlike rain attenuation, multipath fading can result in a large frequency-dependent attenuation within the narrow signal bandwidth. This phenomenon is known as *selective fading*.

The mechanism for multipath fading, shown in Figure 5-22, is very similar to mode distortion in multimode optical fibers and to the distortion introduced by bridged taps in wire-pairs, except that it is time varying. The atmosphere is inhomogeneous to electromagnetic radiation due to spatial variations in temperature, pressure, humidity, and turbulence. This inhomogeneity results in variations in the index of refraction, resulting in possibly two or more ray paths for electromagnetic waves to travel from transmitter to receiver. Another source of multipath is the reflection of radio waves off of obstacles, such as buildings. The effective path lengths may be different for the different rays, and in general will interfere with one another since the receiver will perceive only the sum of the signals.

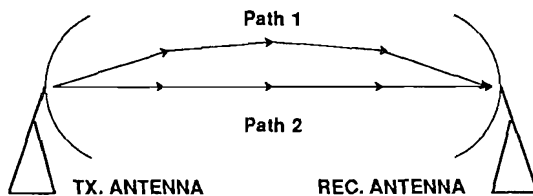


Figure 5-22. Illustration of two ray paths between a transmit and receive radio antenna. Fading attenuation results when the two paths have different propagation delays.

We can determine the effect of multipath fading on a passband signal using the equivalent complex-baseband response for a single path and applying superposition. If we assume two paths have attenuations A_1 and A_2 and propagation distances d_1 and d_2 , corresponding to propagation delays $\tau_1 = d_1/c$ and $\tau_2 = d_2/c$, we can define two parameters $\Delta d = d_1 - d_2$ and $\Delta\tau = \tau_1 - \tau_2$. Then by superposition the equivalent complex-baseband channel transfer function is

$$\begin{aligned} A_1 e^{-j\omega\tau_1} e^{-jkd_1} + A_2 e^{-j\omega\tau_2} e^{-jkd_2} \\ = A_1 e^{-j\omega\tau_1} e^{-jkd_1} \cdot \left(1 + \frac{A_2}{A_1} e^{j\omega\Delta\tau} e^{jk\Delta d}\right). \end{aligned} \quad (5.58)$$

The first terms have a constant and linear phase shift due to the delay τ_1 , identical to the first path. The term in parentheses is important, because it can display a complicated dependence on frequency due to constructive and destructive interference of the two signals at the receiver.

The critically important parameter is $\Delta\tau$, which is called the *delay spread*. Two distinct cases can be distinguished. The first occurs when, for baseband frequencies of interest, $|\omega\cdot\Delta\tau| \ll \pi$, so that the frequency-dependence of the second term is insignificant. This is called the *narrowband model*. For this case, the two path propagation is similar to a single path, in that it results in a delay (linear phase shift with frequency) plus a constant phase shift. The contrary case is called the *broadband model*, and results in a more complicated frequency dependence due to constructive and destructive interference.

Example 5-23.

Assume that we define the transition between the narrowband and broadband model as a delay spread such that $|\omega\cdot\Delta\tau| = 0.01\cdot\pi$ (1.8 degrees) at the highest baseband frequency of interest. Equivalently, we expect that $f = 1/200\Delta\tau$ for the highest frequency. Then if the delay spread is 1 nanosecond, baseband channels with a bandwidth less than 5 MHz are considered narrowband, and bandwidths greater than 5 MHz (especially those significantly greater) are considered broadband. If the delay spread increases to 100 nanoseconds, then the narrowband channel has bandwidth less than 50 kHz according to this criterion. Note that all that counts is the delay spread, and not the absolute delay nor the carrier frequency. Also note that the actual passband signal has a bandwidth double the equivalent complex baseband signal. \square

Example 5-24.

For the two-path case, the magnitude-squared of the frequency response for the frequency-dependent term of interest is

$$|1 + \rho e^{j\omega\Delta\tau}|^2 = 1 + |\rho|^2 + 2 \cdot \text{Re}\{\rho e^{j\omega\Delta\tau}\} \quad (5.59)$$

for some complex constant ρ . We will chose a delay spread of 10 nanoseconds (a typical worst-case number in an urban environment) and a fairly large $|\rho| = 0.99$. This is plotted in dB in Figure 5-23 over a ± 50 MHz frequency range, a broadband model, and a narrower frequency range, a narrowband model. Note the large notches due to destructive interference at some frequencies, accentuated by the fact that the two paths are nearly the same amplitude. Also note the close to 6 dB gain at some frequencies due to constructive interference. The narrowband model is plotted over a ± 500 kHz frequency range, which by

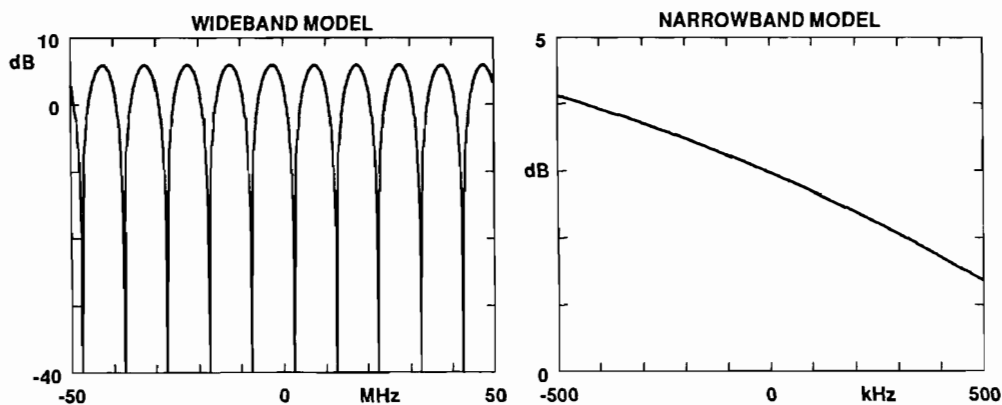


Figure 5-23. Complex baseband channel amplitude response over a wide frequency range and a narrow frequency range for a two-path model with $p = 0.99j$.

the criterion of Example 5-23 is a narrowband model. Note that the channel response varies only a couple of dB over this range. \square

The two-path model, which is usually adequate for fixed terrestrial microwave systems, suggests that fading may result in either a monotonic gain change (or slope) across the channel or as a dip (or notch) in the channel response within the bandwidth. A typical faded channel response is shown in Figure 5-24, and the typical parameters that characterize the fade are identified [15].

In Section 5.4.1, we showed that the power loss in freespace radio propagation obeys a square-law relationship; that is, the receive power decreases as d^{-2} , or the path loss in dB increases as $20 \cdot \log_{10}d$. For terrestrial microwave transmission, the path loss increases more rapidly than in freespace, typically more like d^{-4} or

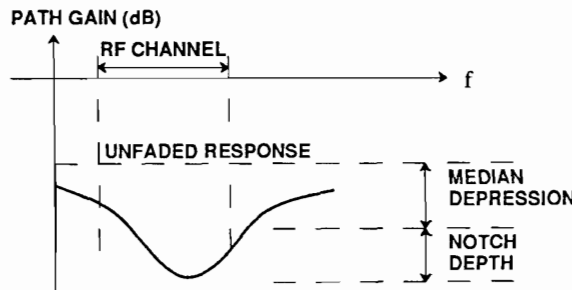


Figure 5-24. A typical frequency-selective notch due to fading with some terminology. Note that the impact on the channel depends strongly on the location of the notch relative to the channel bandwidth.

$40 \cdot \log_{10} d$ in dB. This can be explained using the simple model of Figure 5-25. Even for highly directional antennas, for a large d there will be a substantial reflection off the ground interfering at the receive antenna. Typically the ground is close to a short circuit for oblique angles of incidence at microwave frequencies, implying a reflection coefficient near -1 (so that the net incident and reflected electric fields sum to zero).

Exercise 5-3.

For the geometry of Figure 5-25, consider only the reflection resulting if the ground acts like a perfect mirror, and that both the direct and indirect paths suffer a freespace loss. Assuming the distance between antennas is much higher than the antenna heights, show that the resulting net power loss is approximately

$$\frac{P_R}{P_T} = \left[\frac{P_R}{P_T} \right]_{\text{freespace}} \cdot \left[\frac{4\pi h_t h_r}{\lambda d} \right]^2. \quad (5.60)$$

Hence, the effect of the reflection is a destructive interference that increases the path loss by another factor of d^{-2} over and above the freespace loss. \square

Note that, not unexpectedly, it is advantageous to have high antennas (the loss decreases as the square of the antenna heights).

Even when the transmitter and receiver are at fixed locations relative to one another, fading is a time-varying phenomenon for large distances (30 km or greater) due to atmospheric phenomena. Of considerable importance to designers of radio systems is not only the depth but also the duration of fades. Fortunately, it has been observed that the deeper the fade, the less frequently it occurs and the shorter its duration when it does occur. Also, the severity of fades increases as the distance between antennas increases or as the carrier frequency increases. Fading can also be mitigated

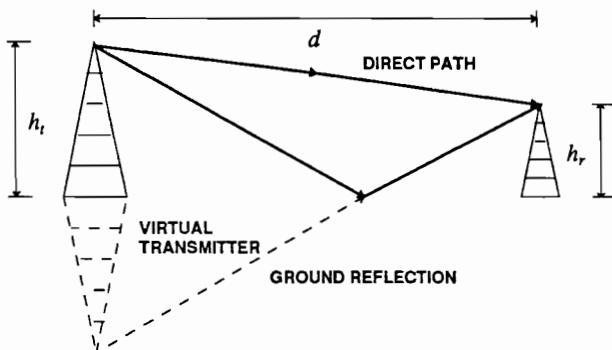


Figure 5-25. The attenuation of a terrestrial microwave system is increased by the ground reflection. There will be ground reflections from all points between the two antennas, but the single reflection resulting if the ground acts like a perfect mirror is shown. The transmit antenna height is h_t , the receive antenna height is h_r , and the distance between antennas is d .

by using *diversity techniques*, in which two or more independent channels are somehow combined [20]. The philosophy here is that only one of these channels at a time is likely to be affected by fading.

5.4.5. Mobile Radio

One of the most appealing uses for radio transmission is for communication with people or vehicles on the move. For this type of communication there is really no alternative to radio transmission, except for infrared, which does not work well outdoors. Mobile radio exhibits some characteristics that are different from point-to-point transmission. First, antennas must generally be omni-directional, and thus they exhibit much less antenna gain. Second, there can be obstacles to direct propagation, causing a *shadowing effect* that results in large variations in received signal power with location. Third, the most common application is in urban areas, where there are many opportunities for multiple reflections, and the two-path model is usually not accurate. Fourth, the user is often moving, resulting in extreme time-variations in transmission conditions over even short distances, as well as Doppler shift in the carrier frequency.

The two-path model is easily extended to an M -path model, again using superposition. In this case, the complex-baseband output of the channel is

$$\sum_{i=1}^M A_i u(t - \tau_i) e^{-jkd_i} \quad (5.61)$$

where the A_i are real-valued attenuation coefficients, d_i is the length of the i -th path, and τ_i is the propagation delay of the i -th path. There may be a dominant path whose attenuation coefficient obeys the fourth-power law with distance, but the other coefficients depend on the reflection coefficients of indirect paths and hence bear a complicated relationship to position. Furthermore, due to shadow effects, there may even be no dominant path. for example if the mobile receiver is located behind a building; the radio waves will suffer a diffraction loss. This shadowing loss typically varies markedly over a distance of tens to hundreds of meters. If we average the received power over an area on the order of 1 km^2 , we will see the fourth-power loss with distance, but if we average over an area on the order of 1 meter^2 we will see an additional fluctuation with position due to shadowing. Shadowing is often assumed to result in a log-normal distribution in local-average received power; that is, the power expressed in dB has a Gaussian distribution. The standard deviation of the power expressed in dB is roughly 4 dB for typical urban areas.

When we examine local received power, not averaged over an area, we begin to see wild fluctuations due to multipath fading. For a moving vehicle, fades of 40 dB and more below the local-average level are frequent, with successive minima occurring every half wavelength or so (a fraction of a meter at microwave frequencies). Thus, the motion of the vehicle introduces a whole new dimension to the fading experienced on a point-to-point system, where the fluctuations are much slower. This rapid fluctuation is known as *Rayleigh fading* because the distribution of the envelope of the received carrier often obeys a Rayleigh distribution [21].

To understand Rayleigh fading, we must examine the effect of vehicle motion, which results in a time variation in received carrier phase. As before, this can be understood by considering a single path, and then applying superposition to multiple paths. The geometry of a single path is shown in Figure 5-26, including a reflection between the transmitter and receiver. As shown, a virtual transmitter can be defined behind the reflector with a linear propagation to the receiver. Let \mathbf{d} be a vector from virtual transmitter to receiver at time $t = 0$, let \mathbf{v} be the velocity vector for the vehicle at time $t = 0$, and let θ be the angle between \mathbf{d} and \mathbf{v} , or the angle of incidence of the propagation path relative to the vehicle velocity. Let the scalar initial distance and velocity be $d = \|\mathbf{d}\|$ and $v = \|\mathbf{v}\|$. The vector from transmitter to receiver is $\mathbf{d} + \mathbf{v} \cdot t$, and the propagation distance as a function of time is

$$\|\mathbf{d} + \mathbf{v} \cdot t\| = \left[d^2 + v^2 t^2 + 2\langle \mathbf{d}, \mathbf{v} \rangle t \right]^{1/2} \quad (5.62)$$

where the inner product is $\langle \mathbf{d}, \mathbf{v} \rangle = dv \cdot \cos\theta$. This distance is not changing linearly with time, but can be approximated by a linear function of time.

Exercise 5-4.

Show that if $t \ll d/v$, then (5.62) can be approximated accurately by $d + vt \cdot \cos\theta$. For example, if $d = 1$ km and $v = 30$ m/sec (approximately 100 km/hr) then the approximation holds for $t \ll 66$ sec. \square

The time scale over which the linear approximation to distance is valid is quite large relative to the significant carrier phase fluctuations, and hence it is safe to assume that the distance to the receiver is changing as $v \cdot \cos\theta \cdot t$. This change in distance has slope $+v$ when the receiver is moving directly away from the transmitter, $-v$ when it is moving directly toward the transmitter, and zero when the receiver is moving orthogonally to the transmitter.

With this basic geometric result in hand, the received complex-baseband signal is

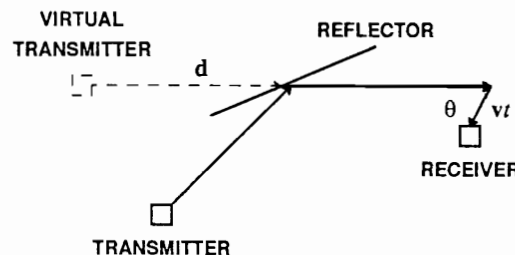


Figure 5-26. Trajectory of motion for a vehicle moving at constant velocity, relative to a propagation path including a reflection.

$$A \cdot \operatorname{Re} \left\{ u(t - \frac{d}{c} - \frac{v}{c} \cos \theta t) e^{-jkd} e^{-jkv \cos \theta t} e^{j\omega_c t} \right\}. \quad (5.63)$$

We see here several propagation effects. First, the baseband signal $u(t)$ is delayed by a time-varying amount, due to the changing propagation distance. This effect is generally insignificant at the baseband frequencies of interest. Second, there is a static phase shift e^{-jkd} due to the propagation distance at $t = 0$. Third, and most interesting, is a phase shift that is linear with time. In effect, this is a frequency offset, known as the *Doppler shift*. The carrier frequency is shifted from ω_c to $\omega_c - \omega_d$, where the Doppler frequency is

$$\omega_d = kv \cos \theta = \frac{2\pi v}{\lambda} \cos \theta. \quad (5.64)$$

When the receiver is moving away from the transmitter, the Doppler shift is negative; it is positive when the receiver is moving toward the transmitter.

Example 5-25.

If the vehicle velocity is $v = 30$ m/sec (100 km/hr), and the carrier frequency is 1 GHz ($\lambda = 0.3$ meters), then the maximum Doppler shift is $f_d = v/\lambda = 100\text{Hz}$. This illustrates that relative to the carrier frequency, the Doppler shift is typically quite small, but relative to baseband frequencies it can be relatively large. Also observe that for a constant vehicle velocity, the Doppler shift becomes larger as the carrier frequency increases. \square

In addition to affecting the propagation distance and angle of incidence, the reflection in Figure 5-26 will also affect the attenuation constant and add an unknown phase shift due to the reflection coefficient.

The Doppler shift by itself might not be a big issue, since it results in an offset in a carrier frequency that might not be too precisely known in the first place. The more substantive effect occurs when there are two or more paths, each with different Doppler shifts because their incident angles at the receiver are different. If the delay spread of the different paths is small, we can assume a narrowband model; that is, the different delays of the arriving replicas of the baseband signal $u(t)$ are insignificant for the baseband frequencies of interest. The resulting superposition of different Doppler shifts can result in a rapidly fluctuating phase and amplitude. For example, for a set of paths with amplitudes A_i , delays $\tau_i = \tau$ assumed to be the same on all paths (which is the narrowband model), phase shifts ϕ_i at time zero, maximum Doppler shift

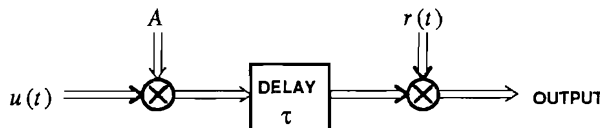


Figure 5-27. A model for the baseband channel with a receiver in motion at uniform velocity.

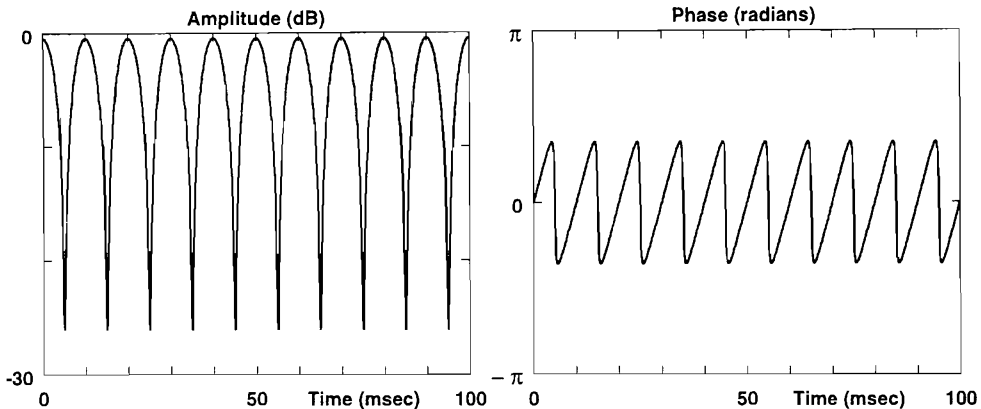


Figure 5-28. Amplitude and phase of $r(t)$ resulting from the superposition of two paths with Doppler shift of 0 and 100 Hz, with $A_1 = 1$ and $A_2 = 0.9$.

ω_d , and angles of incidence θ_i , the receive complex baseband signal is

$$\sqrt{2} \cdot \operatorname{Re} \left\{ \sum_i A_i u(t - \tau_i) e^{j(\phi_i - \omega_d \cos \theta_i t)} \right\} = \sqrt{2} \cdot \operatorname{Re} \{ u(t - \tau) r(t) \}, \quad (5.65)$$

where

$$r(t) = \sum_i A_i e^{j(\phi_i - \omega_d \cos \theta_i t)}. \quad (5.66)$$

The basic equivalent baseband channel model is shown in Figure 5-27. The effect is multiplication by a complex-valued waveform $r(t)$. It is instructive to plot this waveform for a couple of cases. For example, we show in Figure 5-28 the effect of adding two carriers with a relative 100 Hz Doppler shift. The result is fades at 10 msec intervals, the 10 msec being the reciprocal of the relative Doppler shift. There are periodic very rapid phase jumps, corresponding precisely to the times at which there are large amplitude fades. This effect is explained by Figure 5-29, which shows a polar plot. The waveform $r(t)$ follows the circular trajectory shown, where the angular velocity is constant. The amplitude fades occur when the trajectory comes near the origin, which coincides with time that the phase changes most rapidly.

These plots are repeated for 40 signals arriving from uniformly-spaced directions in Figure 5-30 and Figure 5-31. While the result is qualitatively similar, the trajectory is much more complicated and random-looking. Again there are occasional deep amplitude fades, which coincide with rapid phase variations. The timescale of these deep fades is again on the order of 10 msec, which is the reciprocal of the maximum Doppler frequency. This also corresponds to the time the receiver traverses a half of a wavelength at the carrier frequency.

The very chaotic change in amplitude and phase with time shown in Figure 5-30 can be characterized statistically employing the central limit theorem. Returning to the model of Figure 5-27, we can model the multiplicative signal $r(t)$ as a random process $R(t)$. Examining this process at some point in time t_0 , the phase of the i -th

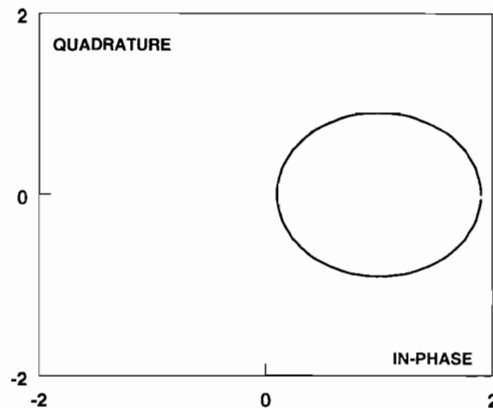


Figure 5-29. Polar plot of the trajectory of $r(t)$ for the same case as Figure 5-28.

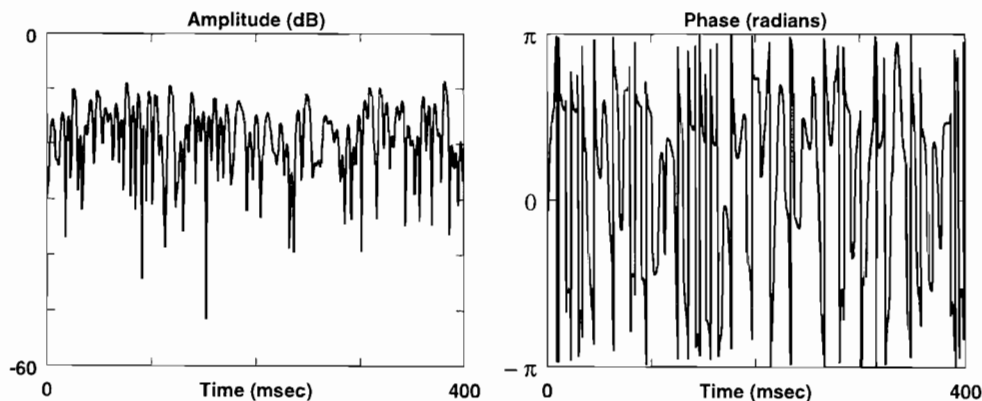


Figure 5-30. a) The amplitude and b) phase for the superposition of 40 signals arriving at uniform angles, each with the same amplitude and random phases.

incident path is given by $\xi_i = \phi_i - \omega_d \cos \theta_i t_0$. Since the phases ϕ_i are very sensitive functions of the initial position, it is reasonable to assume that the ξ_i are i.i.d. uniform random variables on the interval $[0, 2\pi]$. Writing the real and imaginary parts independently,

$$\operatorname{Re}\{R(t_0)\} = \sum_i A_i \cos \xi_i, \quad \operatorname{Im}\{R(t_0)\} = \sum_i A_i \sin \xi_i \quad (5.67)$$

where each term is the sum of independent random variables. By the central limit theorem, as the number of terms increases both $\operatorname{Re}\{R(t_0)\}$ and $\operatorname{Im}\{R(t_0)\}$ will be Gaussian distributed, and hence $R(t)$ will be a complex-valued Gaussian random variable.

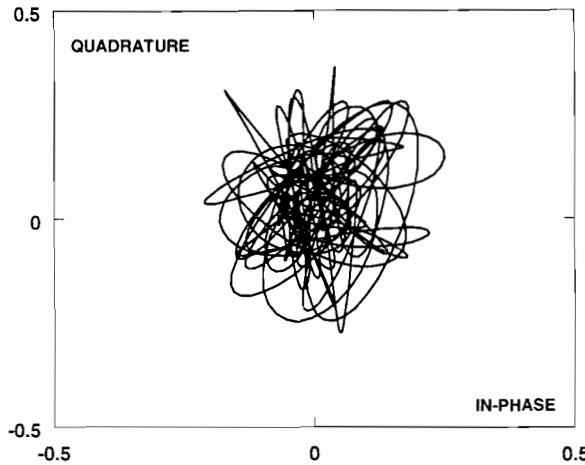


Figure 5-31. Polar plot for the same case as Figure 5-30.

Exercise 5-5.

Show that, with the assumption that the ξ_i are i.i.d. uniform random variables,

$$E[(\operatorname{Re}\{R(t_0)\})^2] = E[(\operatorname{Im}\{R(t_0)\})^2] = \sigma^2, \quad (5.68)$$

$$\sigma^2 = \frac{1}{2} \sum_i A_i^2, \quad (5.69)$$

$$E[\operatorname{Re}\{R(t_0)\}\operatorname{Im}\{R(t_0)\}] = 0. \quad (5.70)$$

□

When

$$R(t_0) = Re^{j\Theta} \quad (5.71)$$

is a complex-valued Gaussian random variable with identically-distributed and independent real and imaginary parts, then R is a Rayleigh-distributed random variable,

$$f_R(r) = \begin{cases} \frac{r}{\sigma} e^{-\frac{r^2}{2\sigma}}, & r \geq 0 \\ 0, & r < 0 \end{cases} \quad (5.72)$$

and the phase Θ will be uniformly distributed on $[0, 2\pi]$. The amplitude R is the envelope of the received carrier, and Θ is the phase, so we can say that the envelope has a Rayleigh distribution and the phase is uniform.

The conclusion is that when a CW carrier is transmitted, the received signal $R(t)$ is well approximated as a complex Gaussian process. The power spectrum of that

process can be calculated, if we make assumptions about the distribution of arriving power vs. angle. This is because the frequency of an arriving component depends directly on the cosine of the angle of arrival. Let $R(t)$ have power spectrum $S_R(j\omega)$. The contribution to $R(t)$ arriving at angle θ is at frequency $(\omega_c + kv) \cdot \cos\theta$. This implies that $S_R(j\omega)$ is confined to frequency band $[\omega_c - kv, \omega_c + kv]$. In particular, the total power arriving in band $[\omega_0, \omega_c + kv]$ corresponds to angle of arrivals in the range

$$kv \cdot \cos\theta + \omega_c \geq \omega_0, \quad \text{or } |\theta| \leq \theta_0 = \cos^{-1} \left[\frac{\omega_0 - \omega_c}{kv} \right]. \quad (5.73)$$

If we assume, for example, that a total received power P is arriving uniformly spread over all angles $|\theta| \leq \pi$, then the portion of the power arriving in band $[\omega_0, \omega_c + kv]$ must be $P \cdot \theta_0/\pi$. Thus,

$$\int_{\omega_0}^{\omega_c + kv} S_R(j\omega) \frac{d\omega}{2\pi} = \frac{P}{\pi} \cdot \cos^{-1} \left[\frac{\omega_0 - \omega_c}{kv} \right], \quad (5.74)$$

and differentiating both sides with respect to ω_0 , the power spectrum is

$$S_R(j\omega) = \frac{2P}{\sqrt{(kv)^2 - (\omega - \omega_c)^2}}, \quad |\omega - \omega_c| \leq kv, \quad (5.75)$$

and zero elsewhere (of course the spectrum is symmetric about $\omega = 0$). This power spectrum is plotted for positive frequencies in Figure 5-32, where we see that the power is concentrated in the region of frequencies $\omega_c \pm kv$. A sample function of a random process with this power spectrum will look like a random version of the deterministic signal $\cos(\omega_c t) \cos(kvt)$, since the latter has a Fourier transform that consists of delta functions at $\omega_c \pm kv$. This AM-DSB signal is the carrier multiplied by an envelope with periodic zero crossings (fades) spaced at $\pi/kv = \lambda/2v$ sec intervals.

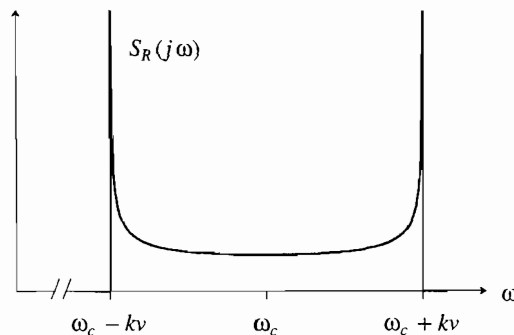


Figure 5-32. The Doppler power spectrum of the received carrier for a vehicle traveling at velocity v , assuming the received signal power is spread uniformly over all angles of arrival.

This is just the time it takes for the vehicle to travel a half wavelength. Thus, temporally, Rayleigh fading exhibits a strong tendency toward fades every half wavelength when the power is uniformly spread over all incoming angles.

Example 5-26.

If the vehicle velocity is 100 km/hr and the carrier frequency is 1 GHz, the maximum Doppler frequency is approximately 100 Hz. This means that the individual paths coming into the receiver can have Doppler shifts on the order of ± 100 Hz, or the bandwidth of the passband signal is increased by approximately 200 Hz due to the motion of the vehicle. The wavelength is about 0.3 meters, so that the time it takes the vehicle to travel a half wavelength is

$$t = \frac{0.15 \text{ meters}}{30 \text{ meters/sec}} = 5 \text{ msec} . \quad (5.76)$$

We can expect significant fades approximately every 5 msec, which happens to be the reciprocal of the 200 Hz range of Doppler shifts. \square

The model of Figure 5-27 and the Rayleigh fading derivation assumed a narrowband model; that is, the delay spread is small with respect to the reciprocal of the bandwidth, or equivalently that delays τ_i in (5.65) are identical over all paths. Thus, the model must be modified to accommodate a wideband model, when the signal bandwidth is too large. Usually this is handled as follows. First, any given reflection, like off a high-rise building, is actually a complicated superposition of multiple reflections, where the delay spread across these reflections is small enough to obey the narrowband model. Thus, this single reflection can actually be represented by a narrowband Rayleigh fading model with an associated delay τ_1 . Now if there is a second reflection with a significantly different delay, it can be represented by another narrowband Rayleigh fading model with delay $\tau_2 \neq \tau_1$. The broadband model follows from superposition of these narrowband models.

A two-path broadband model is illustrated in Figure 5-33. The complex-baseband signal $u(t)$ experiences the two path delays τ_1 and τ_2 , and the two delay outputs are multiplied by independent complex-Gaussian processes $r_1(t)$ and $r_2(t)$. Each path also has an associated attenuation A_i , and a static phase shift which can be

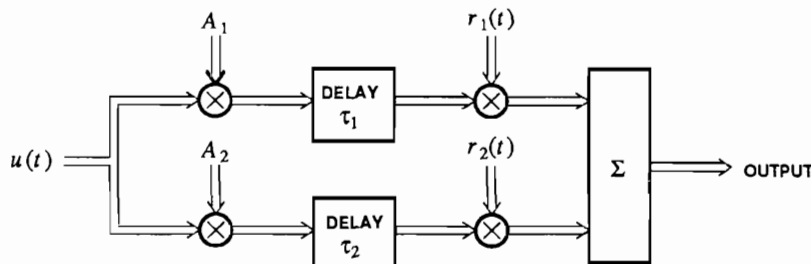


Figure 5-33. A broadband two-path model, where each path is assumed to be independently Rayleigh fading.

subsumed in $r_1(t)$ and $r_2(t)$. This broadband model is easily generalized to an arbitrary number of paths.

5.5. TELEPHONE CHANNELS

Most locations in the world can be reached over the public telephone network, so the voiceband channel is an almost universal vehicle for data communication. The design of digital modems for telephone channels is challenging, because the channel was designed primarily for voice, and impairments that are not serious for voice can be debilitating for data signals. The telephone channel is a prime example of a composite channel, consisting of many media such as wire pairs, satellite channels, coaxial cables, terrestrial microwave links, and optical fiber. Even more important than the media are the many modulation systems built on top of these media, such as pulse-code modulation and single-sideband modulation. The characteristics of the channel vary widely depending on the particular connection. It is useful to discuss these characteristics, not only because of the importance of this particular channel, but also because we encounter many impairments that occur in other situations as well.

5.5.1. Measured Performance of Telephone Channels

Because of the wide variety of possible connections, there is no simple analytical characterization of the telephone channel. Modem designers rely rather on statistical surveys of telephone circuits. In the U.S., a comprehensive survey was conducted in 1969-70 [22] and again in 1982-83 [23]. The data in this section comes primarily from interpretation of the second survey. A modem designer needs to determine the acceptable percentage of telephone connections over which the modem will perform, and then find the parameter thresholds that are met or exceeded by that percentage of channels. The resulting thresholds can be quite sensitive to the percentage.

Example 5-27.

According to the 1982-83 connection survey, 99% of end-to-end channels attenuate a 1004 Hz tone 27 dB or less. But 99.9% of channels attenuate the same tone 40 dB or less. To get the extra 0.9% coverage, an additional 13 dB of loss must be tolerated. \square

In Table 5-1 we give typical worst-case figures assumed for some of the impairments on the channel. The percentage of telephone channels that exceed this performance is roughly 99%. Linear distortion is a major impairment that is missing from the table because it is difficult to summarize concisely. It is discussed below, followed by discussions of the remaining impairments.

Linear Distortion

The frequency response of a telephone channel can be approximated by a linear transfer function $B(j\omega)$, roughly a bandpass filter from 300 to 3300 Hz. This bandwidth is chosen to give acceptable voice quality in the network, and is enforced by bandpass filters in analog and digital modulation systems used in the network. A typical transfer function of a telephone channel is illustrated in Figure 5-34, using

Impairment	level
Attenuation of a 1004 Hz tone	27 dB
Signal to C-notched noise ratio	20 dB
Signal to second harmonic distortion ratio	34 dB
Signal to third harmonic distortion ratio	33 dB
Frequency offset	3 Hz
Peak to peak phase jitter (2-300 Hz)	20 degrees
Peak to peak phase jitter (20-300 Hz)	13 degrees
Impulse noise (-4 dB threshold)	4 per minute
Phase hits (20 degree threshold)	1 per minute
Round trip delay (no satellites)	50 ms

Table 5-1. Typical worst-case impairments assumed for telephone channels. Roughly 99% of the telephone circuits measured in the 1982-83 connection survey [23] meet or exceed this performance.

traditional terminology that we now will explain. Amplitude distortion, the magnitude of the frequency response, is plotted as attenuation (or loss) vs. frequency. Amplitude distortion is often summarized as a set of *slope distortion* numbers, which attempt to capture images such as Figure 5-34a. A typical slope distortion measure is

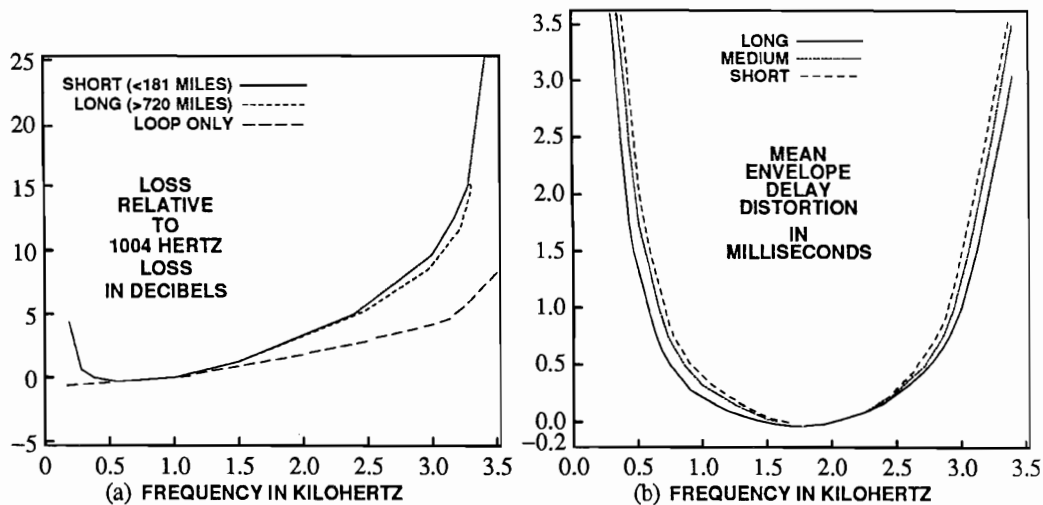


Figure 5-34. The attenuation (a) and envelope delay distortion (b) of a typical telephone channel as a function of frequency. The attenuation is given relative to the attenuation of a 1004 Hz tone, and the envelope delay distortion relative to 1704 Hz, where it is near its minimum value [23].

the worst of two differences, (1) the loss at 404 Hz minus the loss at 1004 Hz and (2) the loss at 2804 Hz minus the loss at 1004 Hz. For 99% of telephone connections, that number is less than 9 dB. Several other slope distortion characterizations are found in the literature, but they are difficult to use in practice. We refer interested readers to the connection survey [23].

Interestingly, the attenuation in Figure 5-34a is almost precisely the typical attenuation of the local loop from the 1980 survey [24] combined with the typical frequency response of the filters in the PCM modulators in Figure 5-3, suggesting that these are the dominant sources of frequency-dependent attenuation.

Phase distortion, the deviation from linear of the phase response of $B(j\omega)$, is traditionally described as *envelope delay distortion*. *Envelope delay* is defined as the negative of the derivative of the phase of the received signal with respect to frequency, and hence measures the deviation from a linear phase response. Envelope delay distortion is often summarized by a set of numbers, much as the magnitude response is summarized by slope distortion. For details see [24].

The overall attenuation of the channel is typically measured at 1004 Hz, where the attenuation is usually near its minimum. The attenuation is usually about 6 dB between one local switch and another, to which is added the loss of the local loops at each end.

Noise Sources

In addition to attenuation, there is noise present on the voiceband channel, primarily from four sources: *quantization noise*, *thermal noise*, *crosstalk*, and *impulse noise*. We discuss them in order of increasing importance.

Crosstalk of the type discussed in Section 5.2 is one impairment that is more severe for voice than for data, so it has largely been eliminated from the network. Induction of interfering tones at 60 Hz and its harmonics (50 Hz in Europe) from power lines is more significant. As on other communication channels, thermal noise is an important impairment. *Impulse noise* consists of sudden, large spikes of short duration and is measured by counting the number of times the noise exceeds a given threshold. Impulse noise is due to electromechanical switches in the network, such as in telephone switches and dial telephones. Impulse noise is not well characterized, and modem designs are not heavily influenced by its presence.

The dominant source of noise is *quantization error* introduced by PCM systems, as in Figure 5-3. Quantization error is a consequence of using a limited number of bits to represent each sample in the PCM system. While the quantization error is deterministically dependent on the signal, the randomness of the signal usually gives quantization error a "noise-like" characteristic. It has an approximately white power spectrum, and the level of noise is usually measured by the *signal-to-quantization-noise ratio (SQNR)*. The SQNR for a single quantizer as encountered in the U.S. telephone network is illustrated in Figure 5-35. Note that over an input range of about 30 dB (-40 to -10 dBm0) the SQNR varies by only about 6 dB (33 to 39 dB). This relatively constant SQNR implies that the quantization error power varies almost in direct proportion to the signal power; that is, it is not constant independent of the signal as for thermal noise. A thorough study of this noise is given in [25]. For the fastest

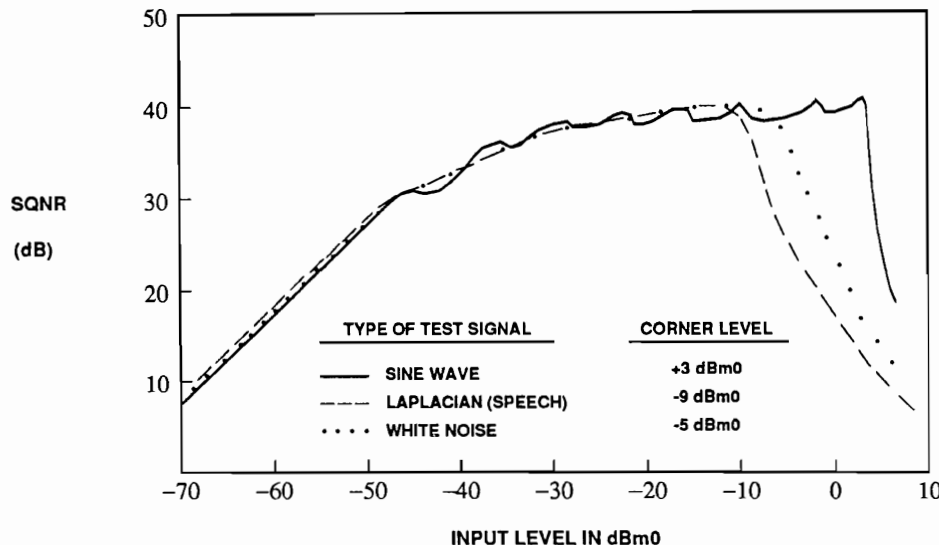


Figure 5-35. SQNR as a function of the absolute input signal power for three different types of inputs. The Gaussian and Laplacian inputs are random, with the latter approximating the p.d.f. of speech samples [23].

voiceband data modems, it can be the dominant impairment. For lower speed modems, it is adequately approximated by white Gaussian noise.

In Table 5-1, the noise is labeled *C-notched noise*, which refers to a particular filter applied to the noise prior to measurement of power. This filter is chosen on the basis of subjective effects for voice, and if the noise is white has no effect beyond a fixed offset in the measured power. Quantization error power is measured by applying a *holding tone*, usually at 1004 Hz, and filtering out this tone with a deep (-50 dB) notch filter prior to the measurement of the remaining quantization error with a C-message weighted filter.

Nonlinear Distortion

Nonlinear distortion is due to imperfections in amplifiers and also to tracking errors between A/D and D/A converters. Because of its relatively low level, nonlinear distortion is a significant impairment only for the most elaborate, highest data-rate modems.

Frequency Offset

Frequency offset is peculiar to telephone channels and channels with Doppler shift. If the input to the channel is $x(t)$, with Fourier transform $X(j\omega)$, and the channel has a frequency offset of ω_0 radians, and no other impairments, then the output of the channel has Fourier transform

$$Y(j\omega) = \begin{cases} X(j\omega - j\omega_0) & \text{for } \omega > 0 \\ X(j\omega + j\omega_0) & \text{for } \omega < 0. \end{cases} \quad (5.77)$$

This small shift in the spectrum of signal has important implications for carrier recovery (Chapter 16) and echo cancellation (Chapter 19).

Exercise 5-6.

We saw in Chapter 2 that passband data signals can be expressed in the form

$$x(t) = \operatorname{Re}\{s(t)e^{j\omega_c t}\}, \quad (5.78)$$

where $s(t)$ is a complex-valued baseband data signal and ω_c is the carrier frequency. Show that the effect of a frequency offset on the channel is a received signal

$$y(t) = \operatorname{Re}\{s(t)e^{j(\omega_c - \omega_0)t}\}. \quad (5.79)$$

In effect, the carrier frequency has been shifted by ω_0 . Assume that $\omega_0 > 0$ and $s(t)$ is bandlimited so that $S(j\omega) = 0$ for $|\omega| > \omega_c$. \square

Frequency offset is a consequence of using slightly different frequencies to modulate and demodulate single-sideband (SSB) signals in analog transmission facilities (Figure 5-1). It is allowed because it has no perceptible effect on speech quality, and can be compensated by proper design in voiceband data modems.

Phase Jitter

Phase jitter on telephone channels is primarily a consequence of the sensitivity of oscillators used for carrier generation in SSB systems (Figure 5-1) to fluctuations in power supply voltages. Since power supply fluctuations are often at 60 Hz or harmonics thereof, the largest components of phase jitter are often at these frequencies. Phase jitter is measured by observing the deviation of the zero crossings of a 1004 Hz tone from their nominal position in time.

Phase jitter can be viewed as a generalization of frequency offset. If the phase jitter on a channel is $\theta(t)$, the effect on the transmitted signal of (5.78) is a received signal of the form

$$y(t) = \operatorname{Re}\{s(t)e^{j(\omega_c t + \theta(t))}\}. \quad (5.80)$$

A phase jitter of $\theta(t) = \omega_0 t$, amounts to frequency offset. It is common for $\theta(t)$ to have oscillatory components at the power line frequency (50 or 60 Hz) and harmonics. If we simply demodulate this signal using the carrier $e^{j\omega_c t}$, we recover a distorted baseband signal $s(t)e^{j\theta(t)}$ rather than the desired $s(t)$. To mitigate this distortion, it is common in carrier recovery (Chapter 16) to include algorithms designed to track and remove this undesired phase jitter.

A phase hit is an abrupt change in the nominal phase of a received sinusoidal signal lasting at least 4 ms. There is little that can be done to defend a modem against this degradation, but it must be taken into account in the design of the carrier recovery (Chapter 16).

Delay and Echo

Delay and *echo* are the final impairments in telephone channels that we will consider. A simplified telephone channel is shown in Figure 5-36. The *local loop*, which is the twisted wire pair connecting the central office with customer premise, is used for transmission in both directions. Both signals share the same wire pair. At the central office, a circuit called a *hybrid* separates the two directions of transmission. Longer distance facilities are *four-wire*, meaning that the two directions of transmission are physically separated.

One possible implementation of the hybrid circuit is shown in Figure 5-37. The signal from the other end of the two-wire facility is fed through to the receive port. The transmit signal appears at the transformer as a voltage divider with impedances R and Z_B , where the latter is the input impedance of the two-wire facility. We cancel

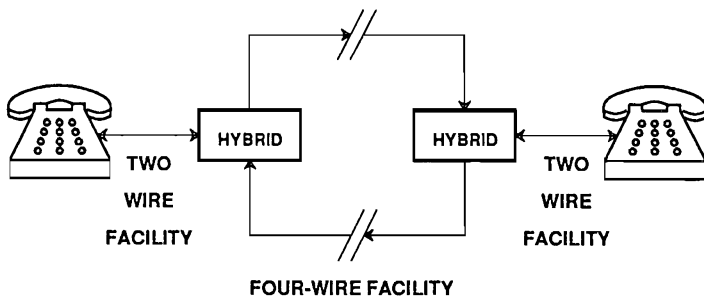


Figure 5-36. A simplified telephone channel, showing the two-wire local loop and the four-wire transmission facility.

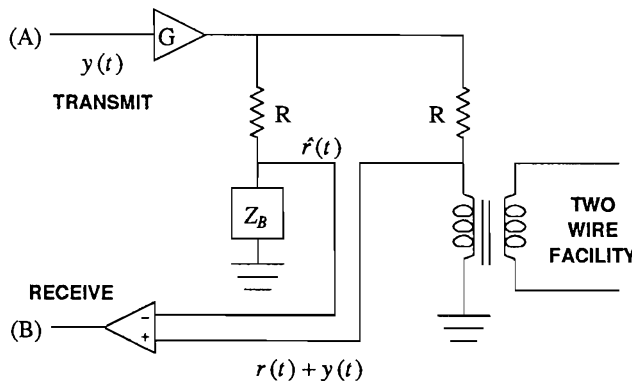


Figure 5-37. An electronic hybrid. To avoid leakage of the receive signal (A) into the transmit path (B) the impedance Z_B should exactly match the impedance of the transformer and two-wire facility.

this undesired feedthrough by constructing another voltage divider with a *balance impedance* Z_B . When $Z_B = Z_0$, the loss from transmit to receive port is infinite. In practice, a fixed compromise impedance Z_B is used, and a component of the receive signal (A) can leak through to (B) with an attenuation as small as 6 to 10 dB due to the variation in impedance of the two-wire facility.

The signal and two types of echo paths for the configuration of Figure 5-36 are shown in Figure 5-38. An *echo* is defined as a signal component that has taken any path other than the *talker speech path*. The *talker echo* is the signal that leaks through the far-end hybrid and returns to the sender (talker). The *listener echo* is the component of the talker echo that leaks through the near-end hybrid and returns again to the listener. This echo is similar to multipath propagation on radio channels (Section 5.4). The length of the telephone channel determines the round-trip echo delay. Echoes from the near end of the connection typically undergo zero to 2 msec of delay, whereas far-end echoes can have round-trip delays of 10-60 msec for terrestrial facilities, or up to 600 msec on satellite connections.

To mitigate the effects of echo on speech quality, several strategies co-exist on the network. The effect of each strategy on data signals is different. For short delays, loss is added in the talker speech path, which is advantageous because the echoes experience this loss more than once. This loss, plus the loss of the subscriber loops at each end, is the source of the attenuation that must be accommodated by data transmission; it can be as high as 40 dB (at 1004 Hz). For longer delays, devices known as *echo suppressors* and *echo cancelers* are added to the connection.

A *full-duplex* (FDX) modem is one that transmits and receives on the same telephone channel. Such a modem requires an internal two-to-four-wire conversion, as shown in Figure 5-39. Because of imperfect balance impedances of the hybrids, some of the transmitted signal echoes into the receiver and interferes with the weaker data signal from the far end. The hybrid echo loss may be as low as about 6 dB, and the received signal may have experienced as much as 40 dB loss, so the desired far-end signal may be as much as about 34 dB *below* the echo. Ways of dealing with this problem are discussed in Chapters 18 and 20.

5.5.2. Channel Capacity Compared to Practical Modems

Rough estimates of the capacity of a voiceband telephone channel indicate it is over 30,000 b/s. In Table 5-2 we summarize the bit rates achieved by existing standardized voiceband data modems. Bit rates as high as 28,800 b/s are envisioned,

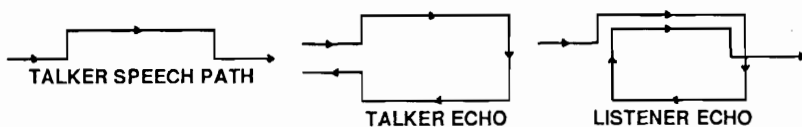


Figure 5-38. Three of many possible signal paths in a simplified telephone channel with a single two-to-four-wire conversion at each end.

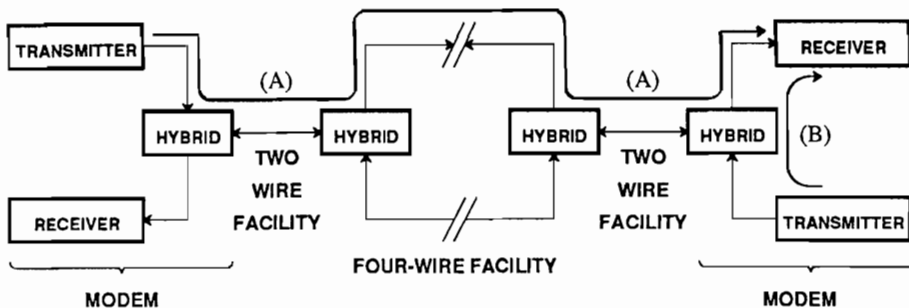


Figure 5-39. Two modems connected over a single simplified telephone channel. The receiver on the right must be able to distinguish the desired signal (A) from the signal leaked by its own transmitter (B).

although the higher rates may be achievable on a smaller fraction of possible connections. Indeed, several of the higher speed modems are used exclusively with *leased lines*, which can be conditioned for guaranteed quality.

5.6. MAGNETIC RECORDING CHANNELS

Digital communication is used not only for communication over a distance (from here to there), but also for communication over time (from now to then). The latter application is called *digital storage* or *recording*, and is usually accomplished using a magnetic medium in the form of a tape or disk. More recently, particularly in the context of read-only applications, optical storage media have been used as well.

Example 5-28.

The compact disk ROM, an offshoot of a similar consumer audio technology, allows 600 megabytes of data to be stored on a single plastic disk 12 cm in diameter [26]. The bits are stored as small pits in the surface, and are read by spinning the disk, shining a laser diode on the surface, and detecting the reflected light with an optical pickup. □

Digital recording is of course used extensively in computing systems, but is increasingly used in addition for the storage of music [27,28] or voice.

Example 5-29.

The compact disk digital audio system, which is a great commercial success, records music digitally using a similar technology to the compact disk ROM. The music is converted to digital using 16 bits per sample at a sampling rate of 44.1 kHz for each of two channels, for a total bit rate of about 1.4 Mb/s. Up to 70 minutes of material can be recorded on a single disk. □

speed (b/s)	symbol rate	duplex (method)	CCITT std.	modulation
≤ 300	≤ 300	full(FDM)	V.21	2-FSK
1200	1200	half	V.23	2-FSK
1200	600	full(FDM)	V.22	4-PSK
2400	1200	half	V.26	4-PSK
2400	600	full(FDM)	V.22bis	16-QAM
2400	1200	full(EC)	V.26ter	4-PSK
4800	1600	half	V.27	8-PSK
4800	2400	full(EC)	V.32	4-QPSK
9600	2400	half	V.29	16-AM/PM
9600	2400	full(EC)	V.32	32-QAM+TC
14,400	2400	full(EC)	V.32bis	128-QAM+TC
≤ 28,800	≤ 3429	full(EC)	V.fast(V.34)	1024-QAM+TC

Table 5-2. Important standardized voiceband data modems are summarized here. The "duplex" column indicates whether a single channel is shared for both directions of transmission (full) or separate channels must be used for each direction (half). For full duplex modems, it also indicates whether frequency division multiplexing (FDM) or echo cancellation (EC) is used for multiple access (Chapter 18). The "CCITT std" column identifies the international standard that applies to this type of transmission. Finally, the "modulation" column identifies the type of modulation, which are discussed in Chapters 6 and 14. The numbers indicate the number of symbols in the alphabet. The "TC" in the V.32 and V.33 refers to trellis coding (Chapter 14).

Example 5-30.

Digital storage on disk drives is used in speech store-and-forward systems, which are essentially the functional replacement for telephone answering systems, except that they serve a number of customers. □

Digital recording offers some of the same advantages over analog recording as we discussed earlier for transmission. The principle advantage again is the *regenerative effect*, in which the recording does not deteriorate with time (except for the introduction of random errors which can be eliminated by coding techniques) or with multiple recordings and re-recordings. An additional advantage is the compatibility of digital recording with digital signal processing, which offers very powerful capabilities.

Magnetic tape or disk can be considered as a transmission medium in much the same manner as other media such as wires and fibers [29,30]. We will now briefly discuss the properties of that medium.

5.6.1. Writing and Reading

In the writing process, a magnetic field is generated in an electromagnet called a *head* as it passes at high speed over a ferric oxide magnetic medium, thereby orienting the direction of magnetization along a track in a nearby magnetic medium on the disk or tape [31]. On reading, when the oriented magnetic pattern passes under that same

head, it produces a voltage that can be sensed and amplified.

There are two basic types of recording. *Saturation recording* is almost always used for digital recording, in which the magnetization is saturated in one direction or the other. Thus, in saturation recording, the medium is constrained to be used for binary transmission; that is, only two levels are allowed. This is in contrast to wire and coaxial media in which multi-level transmission can be considered. The other form of magnetic recording is *a.c. bias recording*, in which the signal is accompanied by a much larger and higher frequency bias sinusoid for the purpose of linearizing the channel. A.c. bias recording is necessarily used in analog recording, where linearity is important, but has not been applied to digital recording because of the deterioration in signal-to-noise ratio and the fact that saturation recording is appropriate for binary modulation and demodulation techniques.

The magnetic recording process is qualitatively illustrated in Figure 5-40. For saturation recording, the voltage applied to the write head assumes one positive and one negative value corresponding to the two directions of desired magnetization. In Figure 5-40a it is assumed that a square wave corresponding to the binary sequence "1101" is applied to the write head. This waveform correspondence to a bit sequence is called *non-return to zero*, or *NRZ*. The bit stream is recorded on linear (tape) or circular (disk) tracks on the magnetic medium, and one track is shown in Figure 5-40b. Note the two directions of magnetization, schematically indicated by the arrows. The voltage on the read head (which is physically the same as the write head) during a read operation is shown in Figure 5-40c. As long as the magnetization is constant, no voltage is induced in the read head coil, but upon a *change* in magnetization there is a voltage induced (recall that the voltage induced in a coil is proportional to the *derivative* of the magnetic field). The polarity of that voltage is determined by the *direction of change* in magnetization.

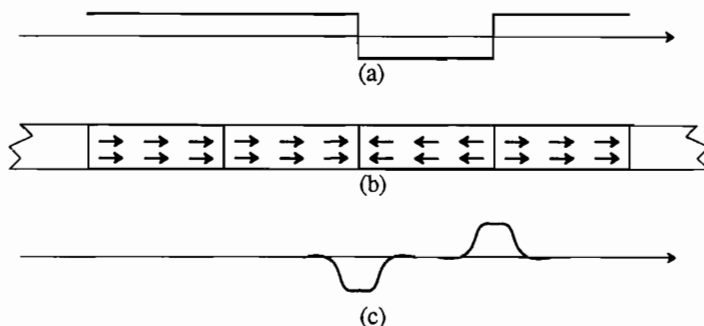


Figure 5-40. Illustration of magnetic recording. a. The NRZ waveform applied to the record head corresponding to bit sequence "1101". The abscissa is time, but this is proportional to distance on the medium for constant velocity of the head. b. The magnetization of one track after saturation recording. c. The voltage on the read head coil corresponding to position of the read head, which at constant velocity is the same as time.

This write-read magnetic recording process can be viewed as a communication channel if we observe only the input and output voltage waveforms in Figure 5-40a and Figure 5-40c and ignore the physical medium of Figure 5-40b. Both of these waveforms represent signals in time, just like in communications, although there is a conceptually insignificant and indeterminate time delay between the write and read operations. Viewed as a communication channel, we see that the magnetic recording channel of Figure 5-40 inherently includes a differentiation operation. Another way of looking at this is that the channel is sensitive to only the *transitions* in the input waveform rather than its polarity. Therefore, from a digital communication point of view, we want to map the input bits into transitions in the input waveform rather than absolute polarity. The way in which this can be done will be considered in Chapter 6.

5.6.2. Linearity of the Magnetic Channel

The magnetic channel can be made linear in a special sense to be specified now. This linearity is a very desirable feature, in that it will greatly simplify system design.

The view of Figure 5-40 is oversimplified in that it assumes that the magnetization is in either one direction or the other. In fact, the tape medium contains a multiplicity of tiny magnetic particles, and each particle must indeed be magnetized in one direction or the other. The total net magnetization can assume almost a continuum of values, depending on the number of particles magnetized in each direction. Unfortunately this continuum of magnetization depends nonlinearly on the applied magnetic field, and displays hysteresis, and therefore the write process is highly nonlinear. On the other hand, the read process is very linear, in that the voltage induced on the read head is a linear function of the magnetization.

If the applied field to the recording head is strong enough and held long enough so that the medium is fully saturated, then the output of the read head displays a form of superposition. This is because this saturation destroys the memory of the hysteresis. This form of superposition is illustrated in Figure 5-41. If the response to a positive transition at time t is $h(t)$, and the response to a negative transition at time $t + \Delta$ is $-h(t + \Delta)$, then the response to the positive followed by negative transition obeys superposition, and is

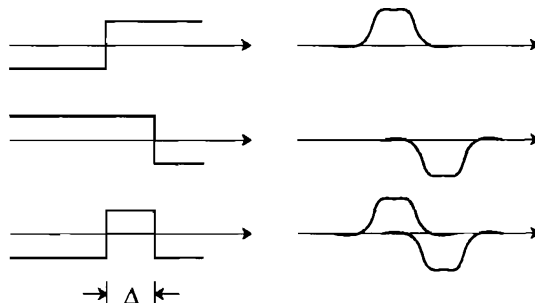


Figure 5-41. Superposition in the reading process of magnetic recording.

$$h(t) - h(t + \Delta) . \quad (5.81)$$

This is true with great accuracy *as long as* the time between transitions Δ is larger than some threshold Δ_0 . This threshold is determined by the time to achieve full saturation of the medium in one direction or the other since the last transition, and depends on the design of the write head as well as the medium.

5.6.3. Noise on the Magnetic Channel

The noise impairments are very complicated on the magnetic channel, consisting of additive and multiplicative noise components. A major source of noise is due to the granularity of the medium. The total response of the head is the superposition of the responses to a multiplicity of magnetic particles. This discrete nature of the signal is similar to the quantum nature of the optical detection process (Section 5.3) with one important distinction. In optical detection we have only photons (or photoelectrons) or the absence of same, whereas in magnetics there are both positively and negatively magnetized particles. Thus, in optical detection, when there is no signal incoming there is also no quantum noise (neglecting dark current). In the magnetic reading process the particles are present whether or not there is a signal, or putting it another way the absence of a signal is represented by an equal number of positively and negatively magnetized particles. Hence, the *granular noise* in magnetic recording is present independent of the signal, and is therefore truly an additive noise phenomenon. Its spectrum is not white because it is filtered by the read head response, and in fact its power spectrum tends to be similar to the spectrum of the read signal.

Zero crossing jitter results from variations in the composition of the medium and the distance between the write head and the medium. The effect is a small jitter in the position of the read pulses. Another phenomenon is *amplitude modulation* of the received signal, a multiplicative noise phenomenon due to medium density fluctuations. An extreme form of amplitude modulation is the tape dropout, in which the signal level gets too small for reliable detection. Since dropouts are a reproducible effect, depending on position on the medium, they are often flagged in disk files so that these areas are not used for recording. Another phenomenon is interference from adjacent tracks, which is similar to the crosstalk experienced in multi-wire-pair cables and the interference between radio systems.

5.7. FURTHER READING

The literature on communication media is vast and scattered. We offer here some suggestions that may help the reader get started. The basic theory of transmission lines is covered in [1]. There are a number of books devoted to optical fiber devices [32,6,33,34,35,36,37,38] and a smaller number that concentrate on the noise and system issues of primary interest here [39,13,14]. A special issue of *IEEE Journal on Selected Areas in Communications* (November, 1984) is devoted to undersea lightwave communication. It contains numerous useful articles describing the special problems that arise in this hostile environment. Another issue (November, 1985) covers fiber optics for local communication, and concentrates on networking issues. Yet

another issue (December, 1986) is devoted to terrestrial fiber optics, and includes papers on reliability, economics, and networking issues. Finally, the Optical Society of America's *Journal of Lightwave Technology* is a good source of information.

There are available books on satellite [18] and mobile radio [21] design. Special issues of the *IEEE Journal on Selected Areas in Communications* in July 1984, June 1987, and January 1989 are devoted to mobile radio communication. Many of the papers propose modulation schemes that are robust in the presence of multipath fading. More specifically directed to multipath fading channels is another special issue (February 1987). Another issue (April 1987) is devoted to point-to-point digital radio, and yet another (January 1985) to broadcasting satellites.

Further information about characteristics of the telephone channel is best obtained by going directly to the published line surveys [22,23,24]. Special issues of *IEEE Journal on Selected Areas in Communications* (September 1984, and August and December 1989) are devoted to modulation and coding for the telephone channel.

A special issue of *IEEE Journal on Selected Areas in Communications* in January 1992 is devoted to recent results on magnetic recording channels.

PROBLEMS

- 5-1.** Show that for a terminated transmission line with real-valued characteristic impedance, the maximum power to the load is obtained in Figure 5-6b when $Z_S = Z_L = Z_0$.
- 5-2.** For a transmission line, derive the relation

$$\lambda f = v \quad (5.82)$$

where f is the frequency of a propagating wave in Hz, λ is the wavelength in meters, and v is the velocity of the wave in meters/sec.

- 5-3.** In subscriber loop wire-pair cables, it is common in some countries to have *bridged taps*, which are *open circuited* wire-pairs bridged in parallel on the main pair. Assume that a source has impedance equal to the wire-pair characteristic impedance, the wire-pair is terminated at the other end by its characteristic impedance, and that the wire-pair has a single bridged tap. Let the distance from source to tap be L_1 , from tap to termination L_2 , and let the length of the bridged tap be L_3 .
- (a) Find an expression for the transfer function of the wire-pair including bridged tap. Be sure to take advantage of the simplifications due to the terminations with the characteristic impedance.
 - (b) Show that when the bridged tap is very long, it causes a fixed attenuation at all frequencies. What is that attenuation?
 - (c) State intuitively what you would expect the response at the termination to be to a single transmitted pulse as a function of the length of the bridged tap.
 - (d) Discuss what happens intuitively when the bridged tap approaches zero length.
- 5-4.** Use Snell's law to show that in Figure 5-12 a ray will be captured by the fiber as long as the incident angle obeys

$$\sin(\theta_1) < (n_1^2 - n_2^2)^{1/2}. \quad (5.83)$$

This confirms that rays incident at small angles are captured, and those at larger angles are not.

- 5-5.** Let the length of the fiber be L .
- Show that the path length for a ray is equal to $L \sec(\theta_2)$.
 - Show that the path length varies from L to $n_1^2 L / n_2^2$. Thus, the larger the difference in index of refraction of core to cladding, the larger the range of captured angles, but also the larger the variation in the transit time of rays through the length of the fiber.
- 5-6.** Assuming that the chromatic dispersion in a single mode fiber is 0.15 psec/km-GHz, evaluate numerically (5.30). Sketch the curve of repeater spacing vs. bit rate in the range of repeater spacings between 1 and 1000 km as limited by dispersion.
- 5-7.** In an optical fiber receiver, assume the received optical power is P , the bit rate is R bits/sec.
- Find the number of received photons per bit.
 - Show that for a constant number of photons per bit, the required received optical power is proportional to the bit rate.
 - Find the received optical power necessary to receive 100 photons per bit at a wavelength of 1.5 μmeter and a bit rate of 1 Gb/s.
 - For the same conditions as c., assume you can launch one mwatt power into the fiber, and that the fiber loss at that wavelength is 0.2 dB per km. What is the distance that we can transmit?
- 5-8.** A typical direct detection optical receiver requires about $N = 2000$ photons per bit in the notation of Problem 5-7.
- Derive the following formula [9] for the required received power at an optical detector at a wavelength of 1.5 μmeter for this value of N ,
- $$P_{dBm} = -65.8 + \log_{10} R_{Mb} \quad (5.84)$$
- where P_{dBm} is the received power in dBm required and R_{Mb} is the bit rate in Mb/s. Note how the required power increases as the bit rate increases. In particular, each order of magnitude increase in bit rate increases the required power by only one dB.
- Assuming 0 dBm launched power into the fiber, and 0.2 dB per km loss in the fiber, what is the allowable distance between repeaters at bit rates of 100 and 1000 Mb/s? You can assume that loss is the dominant impairment limiting repeater spacing.
- 5-9.** Change the assumptions in Problem 5-8 to those that might better reflect fundamental limits [9]: A launched signal power of 20 dBm and 20 photons per bit required at the receiver.
- 5-10.** Suppose we have a system requirement that a total bit rate of R_T must be transmitted over a distance of L_T using a set of parallel repeatered transmission lines (wire cable or fiber). In each repeater span we have as design parameters the bit rate B and repeater spacing L . Show that the total number of repeaters is minimized when the quantity $B \cdot L$ is maximized for the given transmission technology. Thus, if the repeaters are the dominant transmission cost, we want to maximize the product of the bit rate and the distance for each technology.
- 5-11.**
- Derive the following relationship between repeater spacing and bit rate, using the assumptions of Problem 5-8, and assuming a fiber loss of γ_0 dB/km:
- $$L = \frac{65.8 - \log_{10} R_{Mb}}{\gamma_0}. \quad (5.85)$$
- You can assume that the number of received photons per bit is held constant and the transmit power is held constant at 0 dBm.
- Sketch this relation for the range of bit rates between 1 Mb/s and 10,000 Mb/s and a fiber loss of 0.2 dB/km and verify that Figure 5-16 is qualitatively correct in predicting this loss-limited region.
 - Using the results of Problem 5-10, argue that it will be best to increase the bit rate until dispersion becomes the controlling impairment, if the criterion is to minimize the number of

repeaters.

- 5-12.** The available thermal noise power in a bandwidth B Hz is kT_nB . For a resistor generating thermal noise, the noise source can be modeled as either a series voltage source or a parallel current source. Show that the voltage source has mean-squared voltage $4kT_nRB$ and the current source has mean-squared current $4kT_nB/R$ within bandwidth B for a resistance of R ohms.
- 5-13.** At 6 GHz, what is the diameter of a circular aperture antenna that has an antenna gain of 40 dB with a 70% efficiency?
- 5-14.** A radio channel with bandwidth 30 MHz is centered at 6 GHz. What is the difference in decibels in the path loss between the high and low end of this channel? At which end is the loss the minimum? (CAUTION: The antenna gains are a function of frequency.)
- 5-15.** Compare the tradeoff between repeater spacing d and transmitted power P_T , assuming that the received power P_R is held constant for the following two media:
- Metallic cable or fiber optics with loss γ_0 dB per km.
 - A microwave radio system.
 - For which medium does the transmitted power have the most impact?
- 5-16.** Develop the following formula which relates the free-space loss between isotropic radiators in dB, the distance d_{km} between radiators in km, and the frequency f_{GHz} in GHz,
- $$\text{Loss(dB)} = 92.4 + 20\log_{10}d_{\text{km}} + 20\log_{10}f_{\text{GHz}}. \quad (5.86)$$
- Note the dependence of this loss on distance and frequency.
- 5-17.** In this problem we will determine how to combine noise sources in a radio receiver with different noise temperatures to yield a single equivalent noise source. For the configuration of Figure 5-42 where the noise temperature of the three noise sources $n_i(t)$ are T_i , find the relationship between these noise temperatures such that the two systems will have the same SNR. The parameter G is the power gain of an amplifier, i.e., the ratio of input to output power.
- 5-18.** Use the results of Problem 5-17 to find the equivalent noise temperature at the input to the

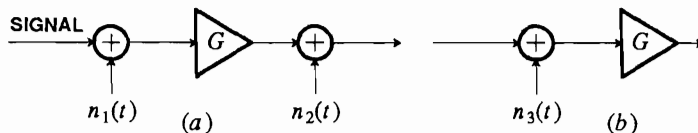


Figure 5-42. Illustration of the combination of two noise sources into a single equivalent noise source referenced to the input of the system.

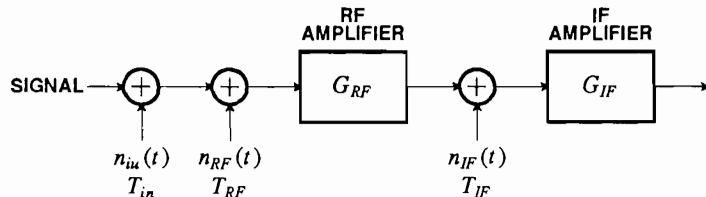


Figure 5-43. Several noise sources introduced at the input and internally to a receiver.

receiver of Figure 5-43, where each of the circuit elements is assumed to be noiseless with an associated noise source with associated noise temperature.

- 5-19. Estimate the delay spread for the two-path ground-reflection model of Exercise 5-3 for a spacing of antennas by 3 km and antenna height of 50 meters. What is the approximate baseband bandwidth over which the narrowband model is applicable?
- 5-20. Suppose the incoming power in a Rayleigh fading scenario does not arrive at a moving vehicle uniformly spread over all angles. Describe qualitatively how you would expect the power spectrum of Figure 5-32 to be affected under the following conditions:
 - (a) The vehicle is driving toward the transmitter, and more power is arriving from the direction of the transmitter than other directions.
 - (b) A lot of power is reflecting off a nearby mountain, so that more power is arriving at the vehicle from the side (relative to the direction of motion) than any other direction.
- 5-21. Consider a SSB analog voice transmission system embedded in the telephone network. Suppose that the carrier frequency f_c is nominally 1 MHz. In practice, the transmitter and receiver will be designed with components that yield modulating and demodulating frequencies that are slightly off. Component manufacturers often express the accuracy of precision parts in *parts per million*, instead of percent (which is *parts per hundred*). How accurate (in parts per million) do the modulating and demodulating oscillator frequencies have to be to guarantee less than 3 Hz frequency offset?
- 5-22. Suppose that a data signal

$$x(t) = \operatorname{Re}\{ s(t)e^{j\omega_0 t} \} \quad (5.87)$$

is transmitted over a telephone channel with frequency offset ω_0 and sinusoidal phase jitter with frequency ω_p and amplitude a . Assume there are no other impairments. Give an expression for the received signal.

REFERENCES

1. G. C. Temes and J. W. LaPatra, *Introduction to Circuit Synthesis and Design*, McGraw-Hill, New York (1967).
2. Bell Laboratories Members of Technical Staff, *Transmission Systems for Communications*, Western Electric Co., Winston-Salem N.C. (1970).
3. P. Bylanski and D. G. W. Ingram, *Digital Transmission Systems*, Peter Peregrinus Ltd., Stevenage England (1976).
4. S. V. Ahamed, P. P. Bohn, and N. L. Gottfried, "A Tutorial on Two-Wire Digital Transmission in the Loop Plant," *IEEE Trans. on Communications COM-29*(Nov. 1981).
5. K. C. Kao and G. A. Hockham, "Dielectric-Fiber Surface Waveguides for Optical Frequencies," *Proc. IEE* 113 p. 1151 (July 1966).
6. D. B. Keck, "Fundamentals of Optical Waveguide Fibers," *IEEE Communications* 23(5)(May 1985).
7. J. T. Verdeyen, *Laser Electronics*, Prentice Hall, Englewood Cliffs N.J. (1981).
8. D. B. Keck, "Single-Mode Fibers Outperform Multimode Cables," *IEEE Spectrum* 20(3) p. 30 (March 1983).
9. J. E. Midwinter, "Performance Boundaries for Optical Fibre Systems," *NATO Advanced Study Institute*, (July 1986).

10. P. S. Henry, "Introduction to Lightwave Transmission," *IEEE Communications* **23**(5)(May 1985).
11. T.Li, "Structures, Parameters, and Transmission Properties of Optical Fibers," *Proc. IEEE* **68**(10) p. 1175 (Oct. 1980).
12. S. R. Forrest, "Optical Detectors: Three Contenders," *IEEE Spectrum* **23**(5) p. 76 (May 1986).
13. S. D. Personick, *Optical Fiber Transmission Systems*, Plenum Press, New York (1981).
14. S. D. Personick, *Fiber Optics Technology and Applications*, Plenum Press, New York (1985).
15. D. Taylor and P. Hartmann, "Telecommunications by Microwave Digital Radio," *IEEE Communications Magazine* **24**(8) p. 11 (Aug. 1986).
16. J. Mikulski, "DynaT*A*C Cellular Portable Radiotelephone System Experience in the U.S. and the U.K.," *IEEE Communications Mag.* **24**(2) p. 40 (Feb. 1986).
17. V. MacDonald, "The Cellular Concept," *BSTJ* **58**(1)(Jan. 1979).
18. T. Pratt and C. W. Bostian, *Satellite Communications*, John Wiley, New York (1986).
19. W. Rummler, R. Coutts, and M. Liniger, "Multipath Fading Channel Models for Microwave Digital Radio," *IEEE Communications Mag.*, (11) p. 30 (Nov. 1986).
20. J. Chamberlain, F. Clayton, H. Sari, and P. Vandamme, "Receiver Techniques for Microwave Digital Radio," *IEEE Communications Mag.* **24**(11) p. 43 (Nov. 1986).
21. W.C. Jakes, Jr, *Microwave Mobile Communications*, Wiley-Interscience, New York (1974).
22. F. P. Duffy and T. W. Thatcher, Jr., "1969-70 Connection Survey: Analog Transmission Performance on the Switched Telecommunications Network," *BSTJ* **50**(4) pp. 1311-47 (April 1971).
23. M. B. Carey, H.-T. Chen, A. Descloux, J. F. Ingle, and K. I. Park, "1982/83 End Office Connection Study: Analog Voice and Voiceband Data Transmission Performance Characterization of the Public Switched Network," *AT&T Bell Lab. Tech. J.* **63**(9)(Nov. 1984).
24. D. V. Batorsky and M. E. Burke, "1980 Bell System Noise Survey of the Loop Plant," *AT&T Bell Lab. Tech. J.* **63**(5) pp. 775-818 (May-June 1984).
25. B. R. Saltzberg and J.-D. Wang, "Second-order statistics of logarithmic quantization noise in QAM data communication," *IEEE Transactions on Communications* **39**(10) pp. 1465-72 (Oct. 1991).
26. P. Chen, "The Compact Disk ROM: How It Works," *IEEE Spectrum* **23**(4) p. 44 (April 1986).
27. S. Miyaoka, "Digital Audio is Compact and Rugged," *IEEE Spectrum* **21**(3) p. 35 (March 1984).
28. P. J. Bloom, "High-Quality Digital Audio in the Entertainment Industry," *IEEE ASSP Magazine* **2**(4) p. 2 (Oct. 1985).
29. J. C. Mallinson, "A Unified View of High Density Digital Recording Theory," *IEEE Trans. on Magnetics* **MAG-11** p. 1166 (Sep. 1975).
30. H. Kobayashi, "A Survey of Coding Schemes for Transmission or Recording of Digital Data," *IEEE Trans. on Communications* **COM-19** p. 1087 (Dec. 1971).
31. H. Bertram, "Fundamentals of the Magnetic Recording Process," *IEEE Proceedings* **74**(11) p. 1494 (Nov. 1986).
32. D. Marcuse, *Light Transmission Optics*, Van Nostrand Reinhold, Princeton, N.J. (1972).
33. D. Marcuse, *Theory of Dielectric Optical Waveguides*, Academic Press, New York (1974).
34. D. Gloge, *Optical Fiber Technology*, IEEE Press, New York (1976).
35. H. H. Unger, *Planar Optical Fibers for Transmission*, Clarendon Press, Oxford (1977).
36. J. E. Midwinter, *Optical Fibers for Transmission*, Wiley, New York (1979).

37. S. E. Miller and A.G. Chynoweth, *Optical Fiber Telecommunications*, Academic Press, New York (1979).
38. H. F. Taylor, *Fiber Optics Communications*, Artech House, Dedham, Mass. (1983).
39. M. K. Barnoski, *Fundamentals of Optical Fiber Communications*, Academic Press, New York (1976).